CO-HYDROCRACKING OF POLYOLEFINIC WASTE PLASTIC WITH AN INTERMEDIATE STREAM OF REFINERY

FRANCISCO JAVIER VELA DÍAZ

eman ta zabal zazu

Universidad del País Vasco

Euskal Herriko Unibertsitatea

ZIENTZIA ETA TEKNOLOGIA FAKULTATEA

FACULTAD DE CIENCIA Y TECNOLOGÍA

OCTUBRE 2021

eman ta zabal zazu
Universidad del País Vasco
Euskal Herriko Unibertsitatea
NAZIOARTEKO BIKAINTASUN CAMPUSA
CAMPUS DE EXCELENCIA INTERNACIONAL

FACULTAD DE CIENCIA Y TECNOLOGÍA

DEPARTAMENTO DE INGENIERÍA QUÍMICA

CO-HYDROCRACKING OF POLYOLEFINIC WASTE PLASTIC WITH AN INTERMEDIATE STREAM OF REFINERY

TESIS DOCTORAL

Francisco Javier Vela Díaz
Leioa, Octubre 2021

eman ta zabal zazu
Universidad del País Vasco
Euskal Herriko Unibertsitatea
NAZIOARTEKO BIKAINTASUN CAMPUSA
CAMPUS DE EXCELENCIA INTERNACIONAL

FACULTAD DE CIENCIA Y TECNOLOGÍA

DEPARTAMENTO DE INGENIERÍA QUÍMICA

CO-HYDROCRACKING OF POLYOLEFINIC WASTE PLASTIC WITH AN INTERMEDIATE STREAM OF REFINERY

MEMORIA

Que para optar al grado de Doctor en Ingeniería Química
Presenta

Francisco Javier Vela Díaz

Leioa, Octubre 2021

Tenemos que disipar las tinieblas de
la ignorancia mediante el estudio, el
conocimiento y la razón.

Gaspar Melchor de Jovellanos

Estoy profundamente agradecido, de forma sincera, de la oportunidad que se me ha dado para realizar esta tesis doctoral. Esta ha significado vivir numerosas experiencias tanto personales como profesionales a lo largo de estos años y que mediante las cuales he podido obtener valiosos aprendizajes y por ende un crecimiento. Solo es cuando te tomas un tiempo de quietud y te paras a pensar, cuando se toma consciencia del proceso de transformación que se ha vivido y que ha sido en pos de alcanzar o al menos acercarme la eudaimonía. En todo este camino he estado acompañado por valiosísimas personas a las cuales me gustaría agradecer su ayuda y apoyo que me han dado tanto en el ámbito científico como personal.

Primeramente me gustaría dar las gracias a mis directores por la oportunidad que me han dado, por creer en mí, por su apoyo ante las vicisitudes que han acontecido a lo largo de la tesis y por el gran grupo de trabajo formado. Al Dr. José María Arandes le agradezco su liderazgo ejemplar en la dirección de esta tesis así como su cercanía y total disponibilidad respaldándome ante mis intrépidas aventuras en la investigación, haciendo posible mis estancias en Oxford como en KFUPM. A la Dra. Alazne Gutiérrez le agradezco su entrega y su dedicación para que la tesis llegue a buen puerto y la comprensividad mostrada en las etapas finales de la misma.

Quiero agradecer al Dr. Javier Bilbao la implicación personal que ha tenido en la tesis y destacar su capacidad de abstracción sin la cual no se habrían alcanzado razonamientos avanzados a los resultados obtenidos en la tesis. Siendo además para mí admiración la capacidad de trabajo y compromiso que tiene en aquello que hace. No es menos mi gratitud hacia el Dr. Andrés Aguayo por todo lo que me ha ayudado y enseñado respecto al "*cacharreo*" en el laboratorio. Aguayo, eres una enciclopedia abierta y haces que las cosas funcionen cuando nada funciona sacándote una inesperada "*Aguayada*" de la manga que ni MacGyver imaginaría. Muchas gracias al Dr. Pedro Castaño por sus explicaciones para hacerme comprender el mecanismo y las características de la sulfuración de los catalizadores. Al Dr. Gartzen por su ayuda prestada para moler los plásticos, pues le tenía bien cogido el punto al molino.

Estaré siempre muy agradecido a Elena por haberme ayudado desde mi llegada hasta que tomé autonomía en los labos, siendo siempre ante todo una buena amiga. Eva, al compartir contigo la docencia he visto que eres un ejemplo y modelo a seguir como profesora por tu gran implicación con los alumnos y por tu enseñanza innovadora. Además por ser sin duda la mejor compi de congresos que se puede tener. Naiara eres una gran científica pero no es menos tu humanidad, cuantos momentos de divagación y reflexión hemos tenido. Aunque se nos queda pendiente la semana cultural de la butifarra, grandes han sido los almuerzos al aire

libre. A Tomás por la ayuda en los entre manejes del laboratorio y por su pasión por la ciencia. Así como, gran compañero en los fines de semana, haciendo que el trabajar fuese más llevadero.

José siempre me ha asombrado todo el conocimiento que tienes y la total disponibilidad para ayudarme, gracias. Ainara, te estoy agradecido porque no importa lo ocupada que estés que siempre estas dispuesta a ayudar. A Rafa por compartir todos sus conocimientos sobre la desilicación de los catalizadores. A. Achutegui por su implicación para resolver los quebraderos de cabeza de la TGA. A Bea por tu ayuda con el GCxMasas.

Rober, David, Gontzal, Iratxe y Suní merecéis una mención especial por ser un estupendo grupo de trabajo, "El Hydrocracking Team". Sin vosotros no podrían haber salir a delante todos los proyectos en los que me he embarcado. Gontzal, gracias por todo lo que has aportado a esta tesis y en especial al modelo, ha sido un placer trabajar contigo codo con codo. Pero además por contagiarme tu pasión por el Athletic. A David por las nociones de Matlab y poner a punto el modelo. Rober, gracias por aportar ideas frescas, ayudar en las colaboraciones y echarme un cable con esos manuscritos. Así como a Jon Ander y Celia como alumnos colaboradores que contribuyeron al progreso de la tesis.

Quiero agradecer a todos mis compañeros profesores, doctores y doctorandos que han propiciado un magnífico ambiente de trabajo, inventadonos cualquier excusa para traer tortillas. A los Dres. Idoia, Mikel, Marta, A. Ochoa, A. Arandia, Pablo, Maite, Maider, Itxaso, Laura, A. Arregi, Gorka, Aingeru. A los futuros Dres. Ander, Hector, Leire, Zuria, Sergio, Sepideh, María, Enara, Irati Santi y Maira. Sois personas maravillosas y he tenido mucha suerte de coincidir con vosotros.

Thanks to the Prof. Peter Edwads and Dr. Tiancun Xiao for having received me in their research group and given me the opportunity to work under their supervision at the Department of Chemistry at Oxford University (U.K.). They have taught me a different perspective on how to research. Thank you very much to Dr. Sergio for making sure that the investigation progressed. Thanks to Dr. X. Jie and J. Zheng for their help and to colleagues and future doctors Saud, Atinuke, Naif and Sultan it was a pleasure have you as friends. Saud the flavor of your Arabian dates are amazing.

Thanks to Prof. M. Hossain for receive me in his research group, provide me all the facilities to work and life and give me the opportunity to work under your supervision at the Department of Chemical Engineering at King Fahd university of petroleum and minerals (KFUPM) (Saudi Arabia). Thanks to Dr. Hassan for incorporate me in his laboratories; it has been a pleasure to collaborate with you, learning a lot about synthesis and characterization of metal p-tert-butylcalixarenes complexes. Thanks to Dr. Shemsi for helping me to analyze the metal content in catalysts using his ICP. Thanks to Dr. Adamu and to Majid, Khaled, Ahamad for being such good colleagues and friends, I am fortunate to met you. Tareq thank you for your kind explanation about the reaction system with oil soluble catalysts. Thanks to Amanula, Masoud, Mohamed and Janzen, without your technical support the experimentation would not have been possible. Thanks to Aziz, Ibraheem and Vagif for your friendship, you have made me feel at home despite being thousands of kilometers away.

Es de destacar la labor que han realizado los técnicos del SGIKER que con su excelente trabajo han contribuido a que esta tesis haya podido llevarse a cabo.

Gracias a mi "cuadrilla" Emilio, Fran, Pablo, Nacho, Gabri, Marchena, Johana y Andrea, es un placer teneros como amigos, haciendo que en estos años tenga muchos momentos memorables, vuestro apoyo ha sido de gran ayuda en todo momento.

Gracias a mis padres, Antonio y Manoli, a quien les debo todo lo que tengo, pero también todo lo que soy. Gracias por los valores en los que me habéis educado, sin ellos esta tesis no habría sido posible. Sois para mí un ejemplo a seguir en la vida de trabajo, valores, y de amor. Gracias a Isabel Mª, mi hermana gemela. Soy dichoso de tenerte como hermana, me inspira ver cómo trabajas por tus sueños y tu espíritu luchador. A Ismael, mi amigo pero también mi hermano, gracias por estar siempre ahí, ayudarme en los momentos difíciles y también celebrar los buenos momentos juntos.

A Andrea, mi compañera de viaje, gracias por hacer que una cuarentena a miles de kilómetros sea amena; tu paciencia, ánimo y cariño en las dificultades han sido de gran ayuda, gracias por estar ahí.

INDEX

OBJECTIVES

The complex evolution of the oil market and its industry together with energy and environmental international context, have placed the refineries at a crossroad. This situation is mainly due to: (i) the progressive lower availability of oil and the lower quality of this, (ii) the quality requirements of fuels (due to the increasing severity of environmental legislation), and, (iii) the progressively increasing use of alternative energies, from fossil (natural gas, coal) or renewable sources, or even nuclear energy (in some geographical). Besides, the increase in the cost of CO_2 emission rights is another factor that plays against the current refinery model. On the other hand, the demand for fuels and raw materials for petrochemical synthesis is growing. In this scenario, the waste refinery aims to mitigate or solve several of the aforementioned issues by producing fuels and chemicals while recovering waste from the consumer society, specially plastics, tires and biomass. In this way, the environmental issues of this waste mismanagement can be also avoided.

The refineries are slowly adapting to the present situation due to the high volume of this industrial sector, the costs associated with initiatives for new fixed assets and market uncertainties. However, if in their depreciate units is co-feed new feedstocks, such as heavy crude oils derived from tar sands, biomass and a fraction of waste from consumer society they can accelerate their adaptation and even take advantages. Among the already installed and amortized units of the current refineries, the catalytic cracking (FCC) and hydroprocessing units are the most suitable ones to process this new fedstocks due to their versatility and high capacity. That is why they are the subject of important updating and technological innovation efforts, defining new refinery concepts such as the Biorefinery and the Waste Refinery. The incorporation of waste feeds into the refinery's conversion units it does not require from changes in these units while the waste streams are co-fed in a moderate proportion together with the current feedstocks of the units.

Furthermore, including the refining industry in recycling policies is really interesting from an economical point of view. Both tires and plastics are produced from raw materials derived from oil, and therefore it is logical that their recovery is carried out within the framework of a refinery (Waste Refinery), which is the philosophy of the Research Group and of this Doctoral Thesis. In this sense, valuing the synergy between waste recovery technologies (such as pyrolysis) and refinery units is a rational strategy. Two approaches can be combined: i) the fast pyrolysis of waste in a delocalized way, through versatile, simple and environmentally friendly units, which can be installed at waste collection and sorting points to produce plastic pyrolysis oil (PO) and then sent to refinery and ii) classification of waste according to the type of plastic (PE, PP, PS, …) and shipment to refineries. In this way, refineries can deal with homogeneous feeds at large-scale which can be

standardized and, on the other hand, the products would be incorporated together with the intermediate streams and sent to separation units to obtain commercial products.

In order to contribute to the knowledge and development of the Waste Refinery, the overall aim of this Thesis has been to explore the capacity of the hydrocracking units for direct recovery of polyolefinic plastics (HDPE and PP) as well as their pyrolysis liquid oil (PO), blended with the common feedstock of this unit (vacuum gas oil, VGO). Furthermore, the experiments are focused in obtaining information about all the elements of a catalytic process: catalyst deactivation, operating conditions, product quality and kinetic modeling.

Some specific aims have been established to fulfill the main objective, which allow successive milestones to be reached in the progress towards what could be a trial in a pilot plant unit or even on an industrial scale:

i) Create a standard criteria based on (i) some reaction index such as conversions, yields and selectivity to fuels and (ii) the quality of those fuels that allows evaluating the extent of the hydrocracking reaction.

ii) A discrimination of proposed bifunctional hydroprocessing catalysts with bimetallic function (NiMo, CoMo, NiW and PtPd will be tested) and with different meso and microporous supports (alumina, silica-alumina, HY zeolite and MCM-41), which allow obtaining high fuel yields (gasoline and diesel fractions), with low content of S and aromatics (avoiding polyaromatics) from VGO.

iii) A second screening of the most promising catalysts (NiW/HY and PtPd/HY) in the hydrotreating of a mixtures of plastic (HDPE, PP) and VGO. The reaction conditions to carry out both catalytic discriminations have been chosen based on previous works in the research group [1–3] and on the literature review.

iv) Study the feasibility of incorporating alternative feedstocks in the Waste Refinery (PO/VGO, HDPE/VGO, PP/VGO and PO/HDPE/VGO) using the most promising catalysts found in the screening section. Evaluate the impact on the results of the co-feeding regarding the neat VGO hydrocracking.

v) Enhance the catalyst performance increasing its selectivity to fuel through desilication. This technique has two positive effects on the support: (i) it increases the mesoporosity, reducing the mass transfer limitation of zeolites and (ii) it moderates the acidity of the catalyst to reduce the overcracking.

vi) Carrt out a parametric study using HDPE/VGO as feedstock and the selected catalyst in the screening section for determining the effect of time, temperature, catalyst to feed ratio and pressure.

vii) Propose a kinetic scheme for the HDPE/VGO hydrocracking and progress in the methodology of lumps kinetic modeling of hydroprocessing reactions. Obtain the kinetic equations that quantify the extent of the reactions involved to calculate the concentrations of the lumps in a wide range of operating conditions.

This information is necessary in order to have an accurate and realistic vision of the possibilities of these alternative feedstocks valorization through hydrocracking, to obtain fuels (with reduced carbon-footprint) and raw materials. This information allows to achieve a wide perspective and knowledge to be applied in forthcoming research and in the scaleing-up of the process.

CHAPTER 1

INTRODUCTION

1 INTRODUCTION

1.1 WASTE ISSUE

1.1.1 Generation

Given the non-biodegradability of plastics and tires and their contribution to the total amount of wastes disposed in landfills, their increasing generation is becoming a serious problem. The production of plastics has increased steadily since their first appearance in the market in the 1930s, reaching 359 million tons produced worldwide in 2018 (348 million tons in 2017). Asia is the region that produces the largest amount of plastics, 51% of the total amount (30% China, 4% Japan), whereas North America and the EU produce 18% and 17%, respectively [4]. This historical development is explained by their low manufacturing costs and their excellent properties for multiple applications in different areas. Postconsumer waste plastics come from five big sectors: agriculture, automotive, building and construction, distribution and packaging [5,6]. A more detailed study shows that agriculture, automotive, building and construction, and distribution sectors account for the generation of 40% of the waste plastic, whereas the remaining 60% derives from the packaging sector [6]. The latter is one of the main plastic fractions found within municipal solid waste (MSW). The average MSW composition in EU is detailed in Figure 1.1, where it can be seen that plastics only account for 7 wt% of the trash. Among these plastics, polyolefins (PP, HDPE, LDPE, and LLDPE) are the main plastic types (>60 wt%) and PVC, PS, and PET also appear in considerable concentrations [7].

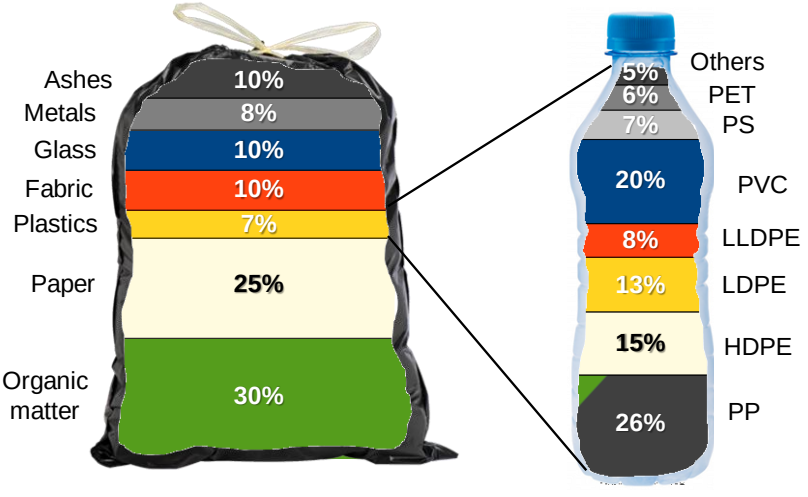

Figure 1.1 Municipal solid waste (MSW) composition and plastics found in it.

However, because of their low density, the volume contribution of the plastics to the MSW increases to 20 vol%. Accordingly, on the basis of 1.35 kg of municipal waste generated per person and day, around 19 million tons of the 270 million tons

of MSW collected in the EU in 2019 are plastics [4]. Moreover, a fact to be highlighted is the huge increase in the use of health care materials, personal protective equipment, and single-use plastics in 2020 due to the COVID-19 pandemic, which undoubtedly will contribute to increasing the generation of waste plastics [8].

1.1.2 Management

Although only 8% of the oil consumed worldwide can be attributed to the plastics production industry [9], the high oil consumed volume make relevant this percentage. The interest in their recycling is based on the need to reduce their disposal in landfills and to use as a source of fuels and raw materials for petrochemical industry. In addition, if waste plastics are recycled properly, the damage to the environment given their properties (low biodegradability and long lifespan) will be avoided [10].

Gayer et al. [11] estimated that the worldwide waste plastics production up to 2015 accounted for 6300 million tons, of which 9% have been recycled, 12% incinerated, and the remaining 79% accumulated in landfills or in natural environments. These authors also estimated that, without significant recycling efforts, 12 000 million tons of waste plastics might be disposed by the year 2050. Furthermore, the waste plastics disposed in landfills undergo gradual fragmentation into microplastics (MPs, particles of <5 mm diameter) through mechanical and microbial decomposition, weathering, photolysis, and abrasion. This phenomenon, together with the release of manufactured MPs contained in various consumer goods (micro beads, capsules, fibers, or pellets in cosmetics, personal care products, cleaning agents, paints, and coatings) are the main contributors to the 243 000 tons of MPs afloat in the oceans [12]. The high surface area and hydrophobicity of these materials ease their ingestion by living organisms and promote the risk of adsorption and desorption of toxic chemicals and pathogens in water. Accordingly, it is well established that the presence of MPs in aquatic organisms has negative health effects, such as growth and development inhibition, neurotoxic responses, metabolic disorders, and genotoxicity [13,14]. Likewise, the presence of MPs in the soil also affects its properties, plant performance, and microbial activities [15]. Moreover, the inhalation of smaller MPs (nanoplastics, NPs) and the ingestion of MP/NP-containing foodstuffs by human beings (ultimate consumers in the food chain) may involve potential risks, whose dependency on the composition and concentration of MPs/NPs is still under study [16].

Apart from being deposited in landfills, waste plastics can undergo through primary and secondary recycling process, which can avoid the aforementioned problems derived from their disposal. These are physical processes which consist of separation, cleaning, extrusion and pelletizing, molding, etc. Nevertheless, during the life cycle, the plastic products are harmed by UV light, reagents, mechanical damage, etc., which harm the polymers. Besides, every time waste plastics are extruded and processed to produce recycled pellets and plastic end products affect the mechanical properties of plastic after 10 - 30 cycles [17]. For these reasons, these recycling techniques have a limited scope.

Waste plastics can be also incinerated in order to produce energy (energy recovery) or recycled to recover the monomers that they contain, which is known as tertiary recycling. These disposal methods were of low significance before 1980. From 1980 and 1990 onward, incineration and tertiary recycling rates have increased an average of 0.7% per year, reaching average values of 28.3% and 19.3%, respectively, in 2019 [11,18]. However, these rates greatly change depending on the country or region [19]. Incineration of waste plastics is the main disposal method in some countries. Thus, Japan, Sweden, and Denmark incinerate 56, 81.7, and 57.1 wt% of the plastics, respectively, with the aim of recovering energy. This activity is carried out by taking severe measures to control emissions.

As plastics are final petroleum products [9], it seems logical to associate their recycling with the petrochemical industry and the production of chemicals and fuels. Although waste plastics could be reintroduced in different manufacturing stages, by means of primary, secondary (mechanical), or tertiary (chemical) recycling, thermochemical routes of tertiary recycling have the highest prospects to be implemented on a large scale. These routes allow the production of fuels and the recovery of the monomers, which may be converted into the original material from which they came. Furthermore, thermochemical routes solve the maximum cycle number issue mentioned above. Different reviews of these thermochemical routes have already been reported focusing on the initiatives associated with pyrolysis [20], gasification [5] and hydrocracking [21] of waste plastics.

1.2 THE PETROLEUM INDUSTRY

Petroleum is a heterogeneous mixture of organic compounds that contains mainly hydrocarbons. Its composition can change greatly depending on where the deposits are located geographically, so it does its heteroatom content. These heteroatoms are S, N, O and metals (V, Ni, etc.), so the crude can be classified according to its sulfur content from sweet (lower sulfur content) to bitter (higher sulfur content). Petroleum can also be classified according to its density (light, API > 31; Medium, 22 < API < 31; heavy, 10 < API < 22; and extra-heavy, API < 10) [22].

Based on these two classifications, the most traded and demanded oils are those with low sulfur content and high API density (the sweetest and lightest ones). These oils have low extraction costs and few technical complications since they do not require large investments in infrastructure to improve the quality of the products to fulfill the strict policy standards. However, the scarce of these oils is increasing, having to switch to use heavier oils with a greater amount of heteroatoms [23]. These oils require greater efforts both for their extraction and further development of refining technologies, requiring higher costs in processing and treatment units in refineries [24,25]. In general, the heavier the crude, the greater content of heteroatoms. The Maya crude oil, for example, has an API density of 20.9 and a sulfur content of 3.4 wt% [26] or the bituminous sands have a density of less than 10 API and the S content can reach 5 wt% [27].

1.2.1 Oil market in numbers

According to the International Energy Agency (IEA), the oil demand has grown since 1983 with annual increase of almost 1.7%, establishing the demand in 2019 at 4474 million tons as shown in Figure 1.2 [28].

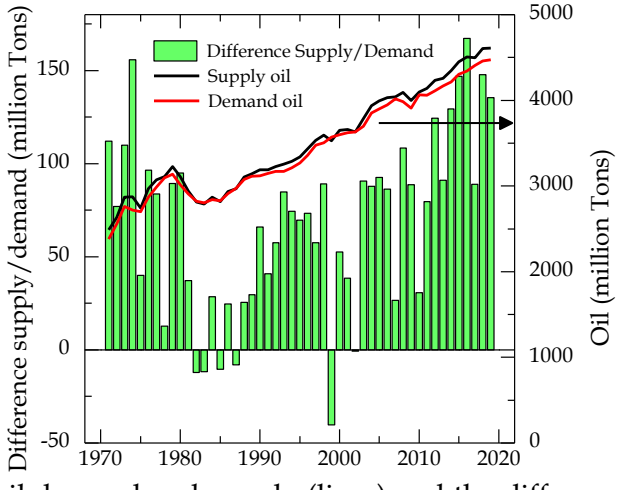

Figure 1.2 World oil demand and supply (lines) and the difference between supply and demand (columns), according to the data provided by IEA [28].

There are great inequalities in consumption by country and by continents. In Figure 1.3 [29] is shown the oil consumption in terawatt-hours (TW-h) equivalent per year, in 2019, according to the data provided by BP report [30] and collected by the University of Oxford.

United States (US) is the country with the largest oil consumption, with a consumption of 10314 TWh, which means 19.3% of total world consumption. In this geographical area, far from US, there are Canada and Mexico with 1328 and 899 TWh, respectively (2.5 and 1.6%, respectively).

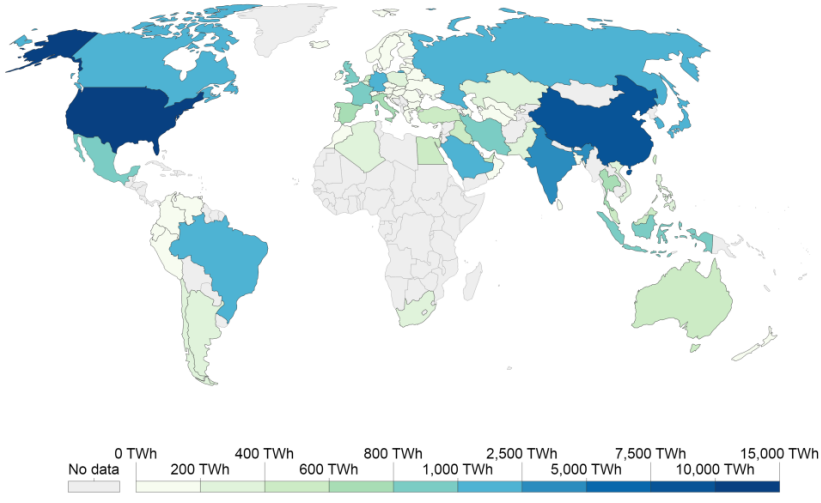

Figure 1.3 Oil consumption in TWh in 2019. Our world in data [29].

The second main oil consumer in the world is China (7760 TWh, corresponding to 14.5% of world oil consumption) which is located in the Asia-Pacific region. This area is the one with the highest oil consumption (19631 TWh), exceeding 36% of world demand. In this area are located the countries with the highest growth in their economies in recent decades, which together with its huge population leads to a large oil consumption: India has a oil consumption of 2774 TWh (5.2 % of oil world consumption), followed by Japan and South Korea with consumptions of 2034 and 1435 TWh, respectively (3.8 and 2.7% of oil world consumption), respectively. With these values, India is placed as the 3rd and Japan as the 4th oil consumer.

The oil consumption of the European Union is 6437 TWh, which is the 12% of world oil consumption. The countries with the highest consumption inside this region are Germany, France, the United Kingdom, Spain and Italy (1296, 873, 856, 749 and 709 TWh, respectively), representing the 2.4, 1.6, 1.4 and 1.3% of world oil consumption, respectively.

In the area occupied by the Commonwealth International States (CIS), Russia is by far the largest consumer with 1866 TWh, which implies the 3.5% of world oil consumption. This country is followed far behind by Kazakhstan with a consumption of 212 TWh.

In the Middle East, the area with the largest oil reserves, 4732 TWh of oil were consumed in 2019, 8.9% of the world oil consumption. In this area, the country that reported the highest consumption was Saudi Arabia with 1852 TWh, followed by Iran and Turkey with 918 and 557 TWh, respectively. In recent years, the major exporting countries (placed in this area) have increased the efficiency in the use of oil in order to reduce their consumption and therefore increase their export capacity.

In Central and South America, Brazil is the largest consumer followed by Argentina, with 1336 and 319 TWh, respectively. It should be noted that in these two areas there is no information regarding to oil consumption from many countries such as Nicaragua, Panama or Bolivia, among others.

Africa is the continent with the lowest oil consumption. However, regarding to the date, it is also the region with the largest number of countries whose consumption is unknown. Of those countries that report the data, South Africa is the one with the highest consumption followed by Algeria with 326 and 237 TWh, respectively.

Unfortunately, as it is well known, 2020 has not been an easy year due to the global pandemic caused by SAR-COV-2. As a result of the different measures established by the countries to curb the effects of the virus, oil consumption fell worldwide to 48259 TWh, which represents a decrease of more than 10% regarding 2019. On the other hand, it should be noted that as Figure 1.4 displays, although China was the epicenter of the COVID-19 pandemic, it was the only country whose consumption, at the end of 2020, not only decreased but also increased compared to 2019 consumption rate. By the end of 2020, China reported a consumption of 7916 TWh, which represents a growth of 2% compared to the previous year.

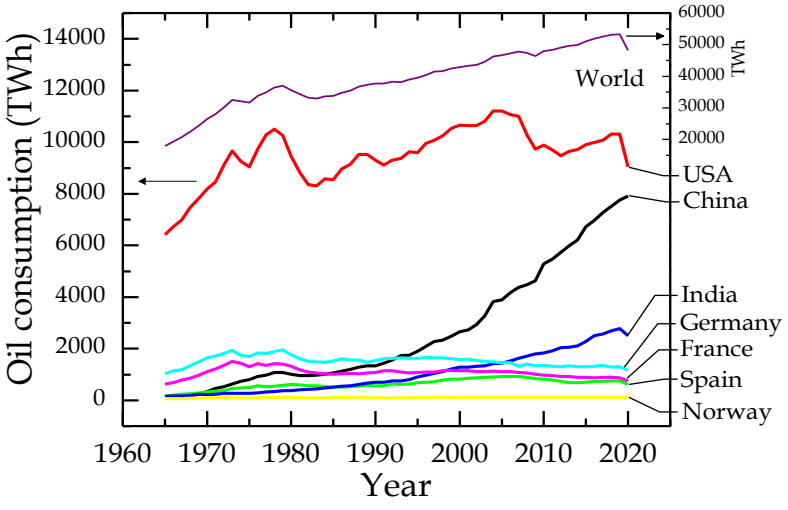

Figure 1.4 The oil consumption of different counties from 1965 up to 2020. Based on the data from statistical review of world energy [31].

However, due to the rapid recovery of the economy, by the end of 2022 the oil demand will exceed pre-pandemic levels [32], reaching approximately 100 million barrels/day (more than 53310 TWh), as it can be seen in Figure 1.5. In this Figure oil consumption forecast before and after the pandemic are compared revealing that, despite the dramatic decrease of 2019, the demand will resume the upward path.

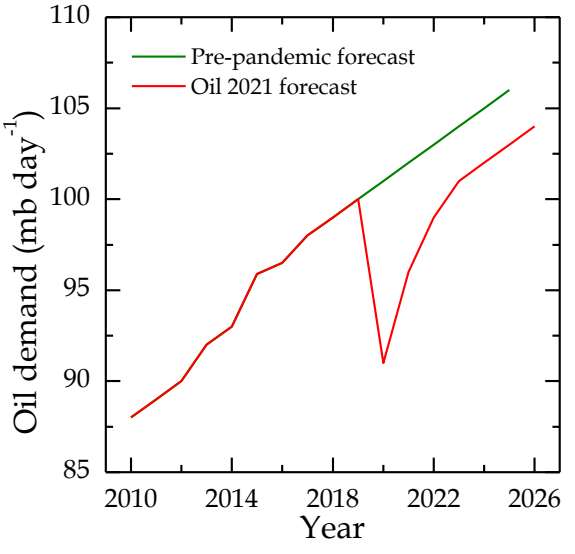

Figure 1.5 Change in the oil consumption forecast before and after the pandemic up to 2026.

On the other side, the prospection of new oil reserves is also important to support the upwards demand. Figure 1.6 shows the new reserves of conventional oil found in the last century (from 1930 to 2012) [33].

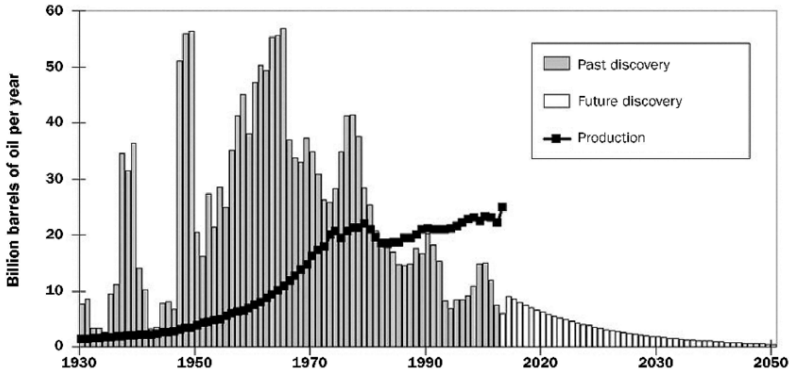

Figure 1.6 Conventional oil reservoirs discovered worldwide in the last century. Adapted from Day et al. (2009) [33].

Anyway, public data about oil reserves is strikingly inconsistent and potentially unreliable for legal, commercial, historical and sometimes political reasons. Moreover, there is no standard terminology to define reservoir and we speak of reservoir 'proved', 'probable', 'possible', 'recoverable', 'reasonable certainty', which adds more uncertainty to the topic.

As can be seen in Figure 1.6, after the maximums reached in the 60s, the trend, although with certain variations, is decreasing since then. It is estimated that in the reservoirs there are currently around 1.6×10^{12} barrels of oil in the world, enough to satisfy the demand for 50 years. Figure 1.7 (data extracted from BP Statistical Review of World Energy [30]) shows the evolution of proven oil reserves, also including the oil sands of Canada and the Orinoco Belt field of Venezuela that are barely being exploited. To satisfy the increasing demand it will be necessary to use the unconventional oil reserves (heavy oils, oil sands and bituminous sands). As a drawback, these heavy oils produce low distillate yields in atmospheric column, requiring downstream deep conversion refining systems, such as hydrotreating (HT) and hydrocracking (HC). These technologies could work simultaneously, increasing the naphtha and light cycle oil (LCO) fractions as well as removing the heteroatoms content and promoting the aromatic ring opening.

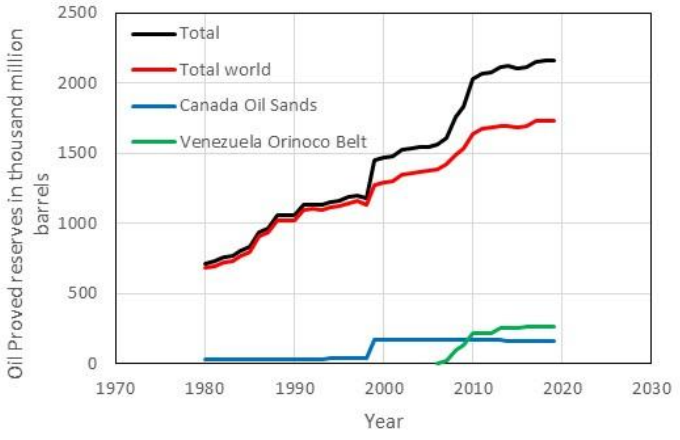

Figure 1.7 Oil proven reserves around the world [30].

1.2.2 Regulations for fuel commercialization

At the same time that refineries are forced to use heavier oils with more heteroatom content, the concern about the environment and the air quality is increasingly growing, so the policies regarding the quality of automotive fuels and ship fuel oil, is increasingly restrictive, reducing sulfur and aromatic content and increasing RON and cetane index, among others.

The maximum sulfur limit in on-road diesel for each country is shown in Figure 1.8 [34]. In the last years, despite COVID-19 pandemic, there are many countries from the Asia-Pacific region (India, Russia, China, etc.) that diminished the sulfur levels of diesel up to 10 - 15 ppm equating their levels to more developed countries like US, Canada or the EU.

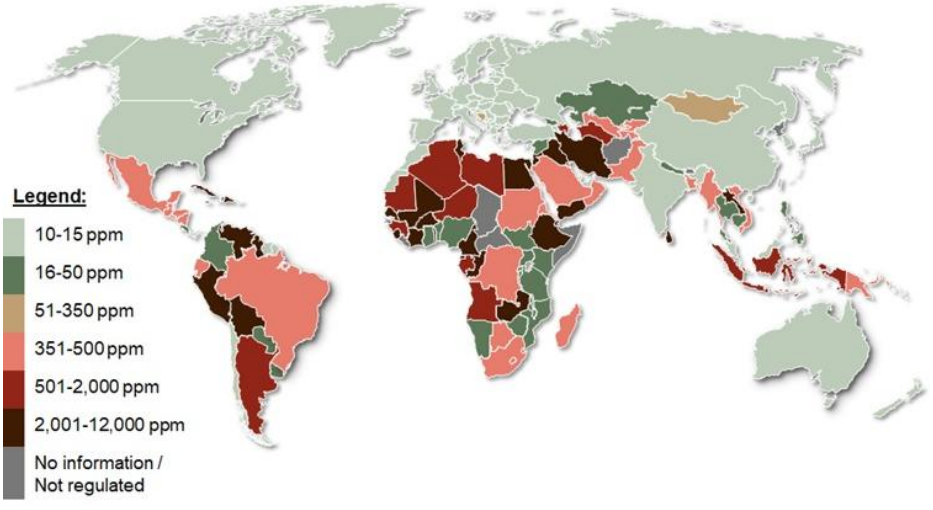

Figure 1.8 Maximum sulfur limit in on-road diesel in 2021. From Stratas Advisor (2021) [34].

The legislation also limits the emission of other compounds such as CO, NO_x, HC (hydrocarbons) and PM (solid particles) after the combustion of fuel in the engine, which implies that engine manufacturers also have to make an effort to improve their engines to ensure a good combustion. In addition, to fulfill the established emission limits, manufacturers recognize the importance of fuel quality and its relationship with emissions, hence recommend using high-quality fuels. Europe is one of the regions where regulations for engines are most advanced. Euro 6 (for engines) is in force since 2014, which establishes the NO_X emission levels for diesel at 0.08 g Km^{-1} [35]. Tier 3 and LEV III normative limit the emissions of combustion engines of passenger cars and light duty vehicles in US, new post long-term regulation in Japan, while 6a limits in China or L7 in Brazil. These legislations have different levels for the above mentioned emissions.

In Europe, the directive 2009/30/EC emended the Directive 98/70/EC regarding the specifications of naphtha, diesel and gas oil. This directive set a European standard for fuels sold in the euro-zone to protect human health and environment. Some of these requirements are summarized in Table 1.1 for petrol (naphtha) and in Table 1.2 for diesel.

Table 1.1 Naphtha requirements established by Directive 2009/30/EC.

Parameter	Limits	
	Minimum	Maximum
Research octane number (RON)	95	–
Motor octane number (MON)	85	–
Vapor pressure, summer period (kPa)	–	60.0
Distillation:		
% evaporated at 100 °C (% v/v)	46	–
% evaporated at 150 °C (% v/v)	75	–
Hydrocarbon analysis:		
olefins (% v/v)	–	18
aromatics (% v/v)	–	35
benzene (% v/v)	–	1
Oxygen content (% m/m)		3.7
Methanol (% v/v)		3
Sulfur content (mg/kg)	–	10
Lead content (g/l)	–	0.005

Table 1.2 Diesel requirements establish by Directive 2009/30/EC**.**

Parameter	Limits	
	Minimum	Maximum
Cetane number	51	—
Density at 15 °C (kg/m^3)	—	845
Distillation:		
95 % v/v recovered (°C)	—	360
PAHs (% m/m)	—	8
Sulfur content (mg/kg)	—	10
FAME content — EN 14078 (% v/v)	—	7.0

1.3 WASTE REFINERY

The decrease in the quality of oil and the difficulty of finding new reserves together with the need to increase the capacity of the installed units and to improve the quality of the fuels has placed the refineries in a crossroad. But perhaps the most important challenge is the need to sustain itself economically in the complex energy market, given the race that is being imposed to achieve energy decarbonization in an accelerated way, in order to revert the "climate change".

To Face with this situation, the activity of the refineries is expanding towards new initiatives, in particular towards the integration of new feeds in refinery units, mainly streams derived from vegetable biomass (including vegetable oils, algae biomass and lignocellulosic biomass), wastes from consumer society (end-of-life tires, waste plastics, sewage sludge, etc.), and streams derived from other fossil sources (such as CH_4 from natural gas in reforming units to obtain the called "blue hydrogen"), as well as secondary refinery streams now undergoing to new conversion processes.

In this context, has emerged the Sustainable Refinery, a research platform for fuel production processes from these unconventional feeds, but using conventional technologies or technologies similar to those of the oil industry. This platform is formed by Biorefinery and Waste Refinery. Thus, the recovery of plant biomass is studied in the well-known Biorefinery platform while, the valorization of waste from consumer society and intermediate refinery streams is carried out in the Waste Refinery. This new concept can be defined as "a plant that integrates conversion processes with units for the production of fuels, energy, and chemicals, either from wastes and their derivatives or from intermediate refinery streams" [6]. The Waste Refinery tries to integrate refinery processes together with environmental remediation [36,37]. The specific configuration of the Waste Refinery will be shaped by the nature of the several features: input feedstock; process technologies; platforms (intermediate substances like platform chemicals); and the output products that are required. Currently, the main objective of the Waste Refinery is obtaining fuels from waste which comes from fossil feedstocks.

1.3.1 Biofuels

To reduce the carbon footprint and the emission of greenhouse gases due to fossil fuels produced in refineries, alternatives of renewable energy sources are being sought to obtain clean fuels.

In 2018, the International Energy Agency reported that total CO_2 emissions due to fuels was 33,513 million tons, of which 13,978 tons were due to the

production of electricity and heat and 8,258 tons to transportation [38,39]. Hari et al. [40] reported that CO_2 emissions due to transport would increase by up to 80% by 2030. That is why they are working to find new alternative energy sources with acceptable effects on the environment. Among them, biofuels are considered as an efficient alternative due to their low greenhouse gas emissions, their biodegradability and their non-toxicity [41].

Biofuels can be obtained mainly from lignocellulosic biomass, plants with a high content of sugars, vegetable oils and organic waste of different types from municipal waste to sewage sludge. Of these four types of raw material, the most versatile are lignocellulosic biomass and vegetable oils.

The first generation of biofuels was obtained by fermentation or transesterification to obtain bio-ethanol and biodiesel as final products [42]. These biofuels have a number of drawbacks. Thus, FAME (Free Fatty Acids Methyl Esters) biodiesel, obtained by transesterification of vegetable oils (sunflower, monkfish, soy, jatropha, etc.) has raised economic, environmental and social implications due to the fact that it is about edible vegetable oils, presence of difficult to sell by-products (glycerol), and fuel quality characteristics [43–45]. Similar limitations are also reported for the first-generation ethanol. This gave rise to second and third generation biofuels, obtained from other different processes where the raw material was lignocellulosic biomass, non-edible vegetable oils and residues from different sources (2^{nd} generation biofuels) [46,47] or algal biomass (3^{rd} generation biofuels) [48].

1.3.1.1 Lignocellulosic biomass

Lignocellulosic biomass is made up of wood, wood by-products (such as sawdust) and agroforestry residues. It is of special interest, since it is outside the agri-food chain and its availability is universal. Its recovery has several disadvantages [49]: relocation of collection points, cost of collection and transport, heterogeneity of its composition, storage costs and, pre-treatment costs before its recovery.

It presents several possible large-scale recovery routes: fermentation, gasification, pyrolysis, hydrothermal-liquefaction (HTL) and thermal or catalytic depolymerization. Each route tends to obtain a certain product: thus, fermentation produces bio-alcohols (mainly bio-ethanol), gasification produces bio-gas or synthesis gas, and pyrolysis, hydrothermal-liquefaction and thermal or catalytic depolymerization produce different types of bio-oil. From these products, fuels, raw materials for synthesis and derivatives can be obtained, all of them usually

obtained from petroleum. Figure 1.9 shows a simplified scheme of the possible use of lignocellulosic biomass, based on the reference by Littlejohns et al. [50].

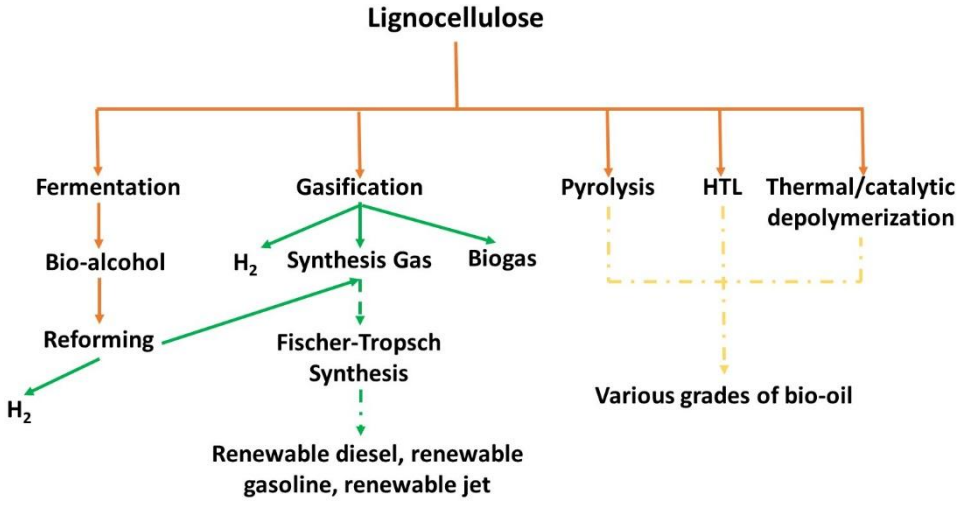

Figure 1.9 Pathways for production of bio-fuels from lignocellulosic materials adapted from Littlejohns et al. [50].

Bio-oil is produced mainly from fast pyrolysis. It is a process with reduced environmental impact that can be carried out in a delocalized way with small equipments at the collection points, thus reducing transportation costs. Depending on feedstock type, biomass may require drying prior to pyrolysis, as water increases the heat requirements. Fast pyrolysis is oriented to maximize bio-oil yield, which requires to adjust time and temperature [51–54], being able to reach up to 75% bio-oil [55]. Bio-oil contains a complex mixture of organic compounds including alcohols, aldehydes, ketones, phenols, furans, ethers, etc. Currently, it is used mainly as a fuel for heating systems, as well as a feedstock for both fragrances and food flavors [50]. Its direct combustion presents drawbacks due to the high water content (and therefore low calorific value), low cetane number, high viscosity and high acidity.

The valorization of bio-oil with catalytic processes can be carried out following different alternatives, such as those shown in Figure 1.10, [56].The recovery of bio-oil can be aimed at obtaining green hydrogen by reforming or obtaining liquid biofuels for transportation.

The reforming can be done with steam or CO_2. Each process has its advantages and disadvantages. Recovery by steam reforming has the advantage of not requiring dehydration of the bio-oil.

In the case of liquid biofuels, the objective is to reduce the hydrogen to carbon ratio (H/C) while reducing the carbon to oxygen ratio (C/O) to improve the energy

density of bio-fuels. Such techniques include transesterification, emulsification, thermal cracking, hydrocracking, and catalytic cracking [51,55,57].

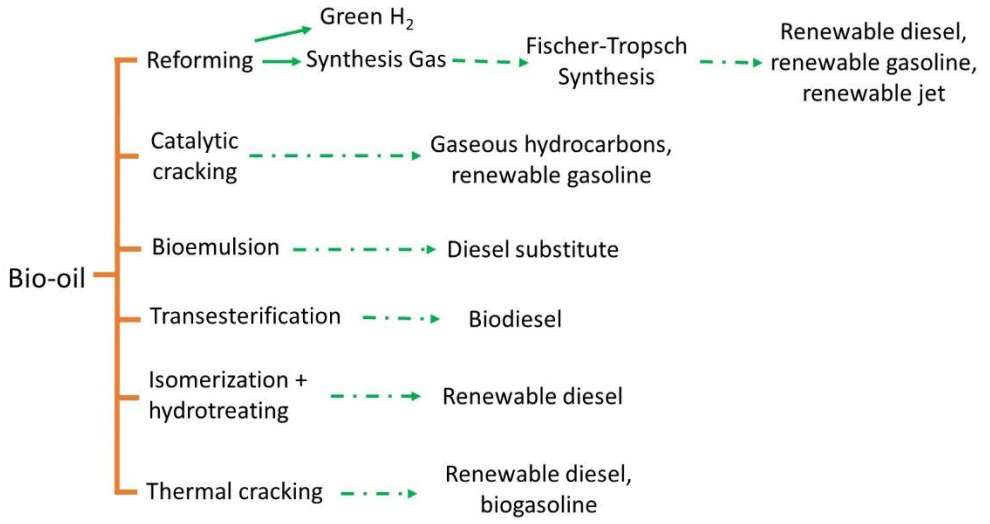

Figure 1.10 Pathways for bio-fuels production from bio-oil**.** Adapted from Isa and Ganda [56].

The transesterification process has been very successful commercially. In it, biomass derived oils are used in combination with an alcohol in the presence of homogeneous basic catalyst (NaOH, KOH). The process has limitations related to the quality of the raw material, the saponification that decreases the yield and generates low-quality bio-diesel, the increase in NO_x emissions produced by the bio-diesel, the use of non-renewable methanol from petroleum, and finally the problems associated with the separation of the catalyst and its environmental management [57,58].

Catalytic cracking and hydrocracking have the advantages of lower separation and purification costs when using heterogeneous catalysts. Catalytic cracking offers advantages over hydrocracking since it does not need to consume hydrogen and it is a process at atmospheric pressure. Oxygenated organic compounds undergo dehydration, decarboxylation, cracking, aromatization, alkylation, condensation, and polymerization reactions. These processes are compatible with the already existing infrastructure in the petroleum processing industry [59–66].

Bio-emulsion is one of the techniques used when mixing a fuel with another with a hygroscopic nature. It is an alternative to reduce pollutants in the diesel engine as well as to reduce fuel consumption. The emulsion reduces the viscosity of the bio-oil to use it as fuel, improving the fuel and flow properties [56].

Hydrotreating produces long-chain paraffins, which are the desired compounds in diesel. It is a process at high temperatures and pressures in the presence of hydrogen. In contrast, cracking gives shorter chain hydrocarbons that are more closely matched to the composition of gasoline. The choice of the route will depend on the desired product. It must be taken into account that these conversion processes can give rise to a multitude of products that can be obtained at different stages of the process.

The recovery of bio-oil to liquid biofuels through catalytic processes presents many options in terms of catalysts depending on the route. Aluminosilicates have been used [67,68], metallic oxides [69,70], metals [71] although the most used catalysts have been zeolites and especially HZSM-5 due to its selectivity and its easy modificability.

Finally, it should be noted that almost all these bio-oil recovery processes can be carried out by designing new processes and specific reactors for each objective or by taking advantage of existing refinery facilities and co-processing the bio-oil with refinery streams to obtain hybrid fuels. In this sense, Van Dyk et al. [60] studied the use of these facilities following a hypothetical refinery like the one shown in Figure 1.11.

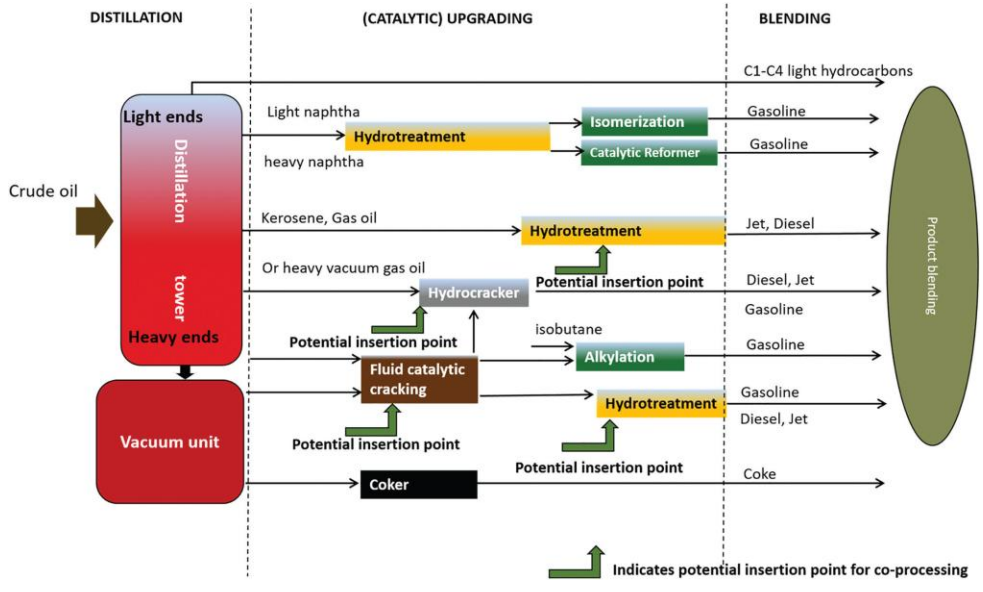

Figure 1.11 Simplified scheme of an oil refinery with potential insertion points of bio-oils. Adapted from Van Dyk et al. [60].

Figure 1.11 shows the potential points where the bio-oil can be inserted. For a well integration of refineries with bio-base intermediates, two characteristics are needed: i) that they have processes that can crack large molecules into smaller ones

(cracking, with or without hydrogen), and ii) have processes that can eliminate oxygen, especially by hydrotreating [72].

The FCC unit is characterized by its versatility and ability to co-feed heavy streams from other refinery units. These characteristics make it suitable for co-feeding raw bio-oil (with water) together with standard feeds (vacuum diesel, coker diesel, etc.) [73,74]). The studies carried out [62,75,76] have shown the existence of favorable synergies for the joint cracking of the oxygenates of bio-oil with hydrocarbons. In addition, the presence of the water in the bio-oil limits the condensation of the aromatics of the coke towards polyaromatic structures, attenuating the deactivation of the catalyst [77].

Hydrotreating is often used to remove heteroatoms from petroleum product streams. Hydrotreating reactions take place in the following order: metal removal, olefin saturation, sulfur removal, nitrogen removal, oxygen removal, and finally halide removal [78]. Hydrotreating is exothermic, the generation of heat being proportional to the consumption of hydrogen. The removal of oxygen generates a lot of heat and the temperature must be controlled to avoid unwanted reactions. Therefore, the cooling systems will have to be modified [79,80] since while the concentrations of sulfur and nitrogen in the refinery streams are small (few ppm), the oxygen concentration is very high in bio-oil. Therefore, although the sulfur, nitrogen and oxygen removal processes are similar, the operating conditions will have to be modified, requiring more hydrogen (more oxygen concentration) and the catalysts may have to be modified since they may not be effective to remove oxygen and they can also be deactivated due to the presence of CO and CO_2 that will be formed by decarboxylation and decarbonylation reactions.

Hydrocracking is similar to hydrotreating and also cracks large molecules. Although it is an expensive process (it requires pressures of more than 100 atm and consumes a lot of hydrogen), the products require fewer treatments before becoming final products. The reactor is not suitable for feeds containing oxygen or other impurities and it is a very sensitive process to any contamination, especially with noble metal catalysts such as Pt and Pd. Van Dyk et al. [60] recommend this unit as a second stage in the recovery of bio-oil.

1.3.1.2 Vegetable oils

The characteristics of these oils are very suitable to produce biofuels. Thus, water content of most vegetable oils is low, between 0.03 wt% and 0.47 wt%, much lower than that of bio-oil (15 – 30 wt%) [81]. Acid number of vegetable oils (0.20–27.2 mg_{KOH} g^{-1}) is also lower than that of bio-oils since some of the triglycerides

present in the vegetable oils are decomposed to free fatty acids. Viscosity of vegetable oil is high due to its long carbon chain and large molecules with oxygen atoms, similar to the bio-oils viscosity [81]. The density of vegetable oils ranged between 0.84 and 0.97 g/mL [81]. The higher heating value of vegetable oils is high, ranging from 37.1 to 40.6 MJ/kg (16 - 19 MJ/kg for bio-oils) [81]. The H/C molar ratio of vegetable oils ranges from 1.64 to 2.37, higher than the H/C ratio of bio-oils (0.92 - 1.53 for bio-oils) and their oxygen content ranges from 10.5% to 14.5%, much lower than that of bio-oils (28 - 40%) [81]. Furthermore, vegetable oils have proven to be valuable resource in the production of biofuels with both edible and non-edible oils having successful trials and implementation in the sector.

The processes of harnessing to obtain biofuels are the same as those shown in Figure 1.10. The vegetable oils most used to obtain first-generation biofuels by transesterification were palm oil, rape-seed oil, soybean oil and sunflower oil. Those vegetable oils have also been used as feedstocks in the other processes shown in Figure 1.10, especially in catalytic cracking and hydrotreating processes. The aforementioned problems associated with first generation biofuels have shifted the interest to 2nd and 3rd generation biofuels. These second and third generation fuels are based on non-edible vegetable oils such as jatropha, canola oil and algae oil. The major benefit of algal biomass is its ability to be cultivated in either saltwater or on land, without posing a challenge to global food and freshwater supply [82]. Biofuels can be derived from algal biomass by biochemical or thermochemical pathways, obtaining biodiesel (transesterification), biogas (anaerobic digestion), bio-alcohols (fermentation), syngas (gasification), bio-oil (pyrolysis). Syngas and bio-oil can undergo the same treatments shown in Figure 1.10 in order to obtain biofuels, such as green hydrogen, gasoline, diesel or kerosene.

Jatropha oil has a high content of free fatty acids (FFA), making it unsuitable for transesterification [83]. However, it has a significant potential for thermal and catalytic cracking as conversion routes, which can operate on various feedstock.

Canola oil has a profile of fatty acids similar than algae oil [84]. Commercialization is still far away because technical hurdles but data shows that algae will be able to produce more than 10 times the best terrestrial plant capacity per hectare which is palm oil, with a production capacity of 4000–5000 kg/ha [56].

Apart from transesterification, the most investigated conversion processes have been catalytic cracking and hydroprocessing of edible or non-edible vegetable oils.

In the catalytic cracking of vegetable oils, several reactions including decarbonylation, decarboxylation, and deoxidation take place to remove the oxygen from the triglyceride molecules [85]. Biofuels obtained by catalytic cracking of

vegetable oils include organic liquid product, gasoline and diesel oil-like hydrocarbons. Similar to bio-oil upgrading, the liquid yield during the catalytic cracking of vegetable oils was very dependent on the used catalysts and operating conditions [86]. Shape selective zeolite-based catalysts and metal oxides have been used for catalytic cracking of vegetable oils: FCC catalyst, HZSM-5, MCM-41. SBA-15, Zn/Na-ZSM-5, etc., obtaining conversions higher than 95 wt% [85]. However, some zeolite based catalysts are plagued by catalyst deactivation, short lifetime, and product contamination [85].

There are two pathways during biomass hydroprocessing: i) hydrodeoxygenation in which 1 triglyceride molecule consumes 12 hydrogen molecules to form 3 normal hydrocarbons with an even number of carbon atoms, e.g., n-octadecane (n-$C_{18}H_{38}$), and ii) hydrodecarboxylation in which 1 triglyceride molecule consumes 3 hydrogen molecules to form 3 normal hydrocarbons with an odd number of carbon atoms, e.g., n-heptadecane (n-$C_{17}H_{36}$) (Figure 1.12, [87]). The main products for hydrogenation of triglycerides are n-alkanes and by-products as propane, water, CO and CO_2 [88]. The yields and properties of the organic liquid phase depend on operating conditions, type of catalyst and vegetable oil.

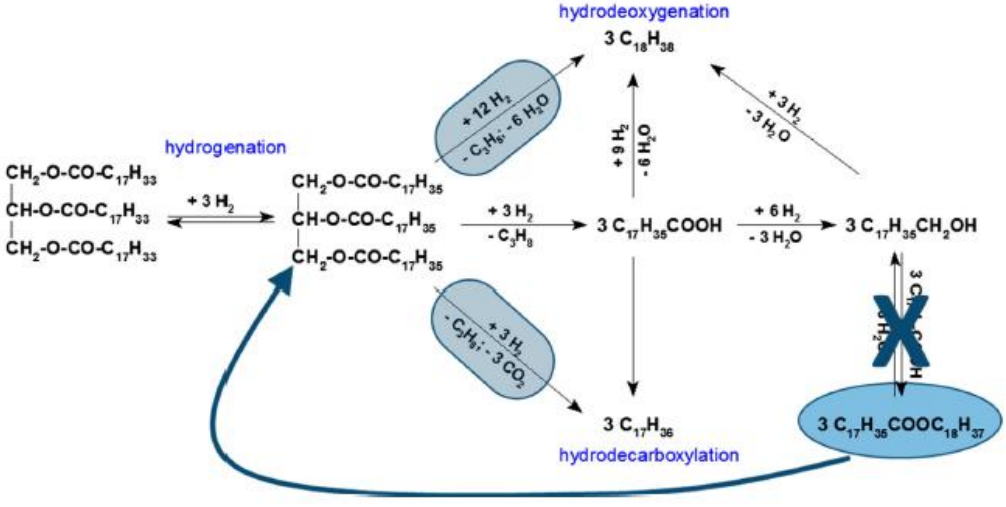

Figure 1.12 Pathways of tryglycerides hydroprocessing [87].

Hydrogen pressures ranges from 20 to 110 bars. Pressure affect the extent of the major (hydrodeoxygenation, decarboxylation and decarbonylation) and secondary reactions (strongly exothermic methanation and endothermic reverse water-gas-shift reaction), influencing the selectivity. The reaction pressure also affects the yields of the final products [89]. An increase in pressure, increases the conversion of vegetable oils [45,90,91] and it is advantageous for HDO reactions [92].

Most hydrotreatment units operate between 290 and 400 °C. The increase in temperature increases the conversion and yields of organic liquid product [87,89]. On the contrary, Bezergianni and Dimitriadis [93] say that an increase in temperature favors the elimination of heteroatoms without affecting the conversion. In general, it can be said that temperatures above 340 °C improve the conversion and yield of organic liquid products, especially if the vegetable oil is co-processed with an oil stream.

At low space velocities, saturation reactions are favored without affecting heteroatom removal, conversion, or diesel yield [94]. However, other authors indicate that when the space velocity decreases, the conversion increases but cracking is favored by increasing the gas yield [45,89,92,95]. Due to these effects, it seems evident that there is an optimal space velocity given the other operating conditions and the vegetable oil.

The catalysts used for vegetable oil hydroprocessing have been mainly Al_2O_3-based catalysts, with high surface area and acidity [96,97]. In addition, some zeolites have been investigated because their larger mesopores may facilitate the transport of bulky vegetable oil molecules to catalyst active sites [98]. The most common metals used have been Ni, CoMo, NiMo and NiW on the before mentioned supports, although catalysts with noble metals such as Pt and Pd have also been used.

As in the case of lignocellulosic biomass, these recovery processes of vegetable oils and algal biomass can be carried out by designing new processes and specific reactors for each objective or by taking advantage of existing refinery facilities and co-processing the oils with refinery streams to obtain hybrid fuels. Bezergianni et al. [59] studied the use of the facilities of a hypothetical refinery. These authors conclude that co-processing either via hydroprocessing or FCC-processing is a very promising technique to integrate bio-based feedstocks in a petroleum refinery for hybrid fuels production, which in some cases already has found its practical realization. The benefits for a refinery are plenty, not only in reducing the associated GHG emissions, but also in enabling the gradual independence from fossil sources, rendering low-carbon-highly-sustainable fuels.

1.3.2 End of life tires and waste plastics

The most important advances have been made in the technologies for tertiary recycling of waste plastics and EOL (End Of Life) tires, with emphasis being placed in the development of pyrolysis technology for the production of fuels and the recovery of monomers. Nonetheless, there is no industrial initiative for the valorization of these wastes with the required capacity to solve the current

mismanagement. This situation is strongly affected by the following drawbacks: (i) a big economic investment is required for the implementation of the units required for the integral valorization of these wastes at large scale; (ii) the obtained products must fulfill severe quality standards established by current legislation; (iii) this new and alternative industry will have to compete with the well-established oil industry. Consequently, the situation suggests the promotion of a large-scale waste valorization industry (waste refinery) by integrating primary waste valorization units within current refineries. Accordingly, primary units will produce low-quality streams that will be converted into fuels and commodities (light olefins and aromatics) in the large-scale secondary treatment units available in refineries.

The oil industry is immersed in a big dilemma given the change in the energy model that society is demanding and the fluctuations in the availability, quality, and price of crude oil [99]. Within this scenario, the involvement of the refineries in waste recycling maybe would be boosted by economic incentives and subsidies provided by public administration, which will undoubtedly help to finance the revamping of the FCC and hydroprocessing units. Moreover, global emissions of CO_2 will be notably reduced entailing a reduction in the carbon taxes of the corresponding country. Furthermore, the contribution of the oil industry to resolve an urgent environmental issue such as the uncontrolled disposal of these wastes would help to improve the image and projection of oil refineries.

The numerous activities that a waste refinery brings together can be divided into two series of interrelated actions shown in Figure 1.13. The first series corresponds to the initiatives of the petroleum industry itself, as it generates intermediate refinery streams as byproducts of distillation and reaction units. The processing of these side streams follows an increasing trend in refineries in order to intensify the valorization of heavier oil by means of increasing the yield of commercial products. Indeed, the FCC unit plays a key role in the co-feeding of vacuum residue [100] and of visbreaker and coker heavy naphthas [101–105]. Equally, hydroprocessing units can be appropriate for the co-feeding of aromatic streams, such as the pyrolysis gasoline obtained in steam cracker units [106] or the light cycle oil (LCO) obtained in FCC units [107–109], with the aim of producing naphtha and medium distillates or BTX aromatics [110]. The second series of actions of the waste refinery, which constitutes the interest of this thesis, focuses on the recycling of consumer society wastes, for example, waste plastics and EOL tires. Recycling activities relate refinery units with other additional units, which will develop the ecoindustry. Among the required additional units, the one for pyrolysis is the key for the conversion of waste solids into liquid streams that can be fed into refinery units, either as they are produced or blended with common feeds.

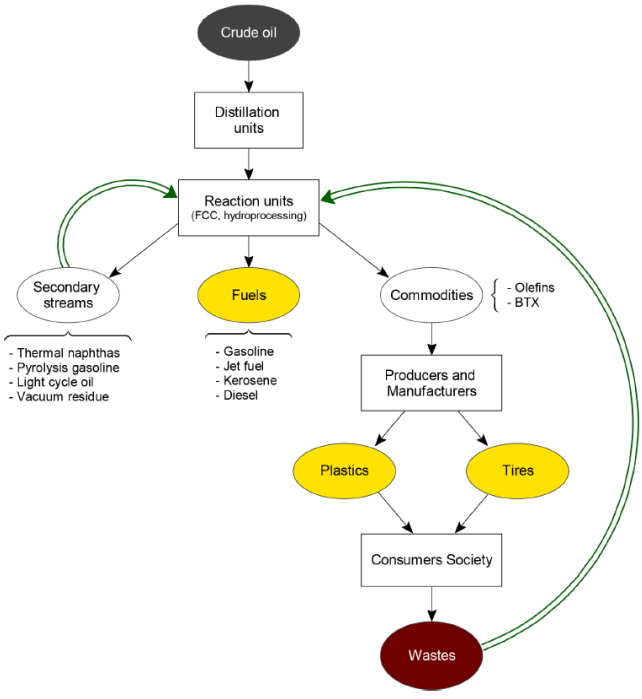

Figure 1.13 Waste refinery concept [6].

The EOL tires can only be treated in the refinery units through their conversion to pyrolysis oil. However, there are different approaches to upgrade waste plastic to environmental favorable automotive fuels range products. These different approaches have consisted on studying the hydrocracking of different blends made of plastic, plastic pyrolysis oil (PO) and refinery streams (like VGO, current feedstock of hydrocracking units) according to different strategies that the industry and refineries could follow. One of the approaches consists on the direct valorization of plastics dissolved in the refinery stream: after its classification, the waste plastics would be sent directly to refinery where it will be blended and treated in the conversion units. The second strategy is based on a decentralized model of the waste plastics, in which the collected waste plastics would be treated in a pyrolysis oil plant. The plastic pyrolysis oil obtained would be afterwards sent to refinery where it would be blended with a refinery feedstock (secondary or not) to be treated together in a refinery unit. Furthermore, the ternary mixture of plastic, its pyrolysis oil and refinery stream can be studied, being this approach a result of the combination of the previous two strategies. A possible advantage of the ternary mixture is the enhancement of plastic conversion due to a better dissolution of plastic in the reaction media.

Furthermore, oil refineries may save an important amount of crude oil by recycling the waste plastics and EOL tires. Figure 1.14 computes the total amount of hydrocarbons that can be obtained from these wastes in the EU.

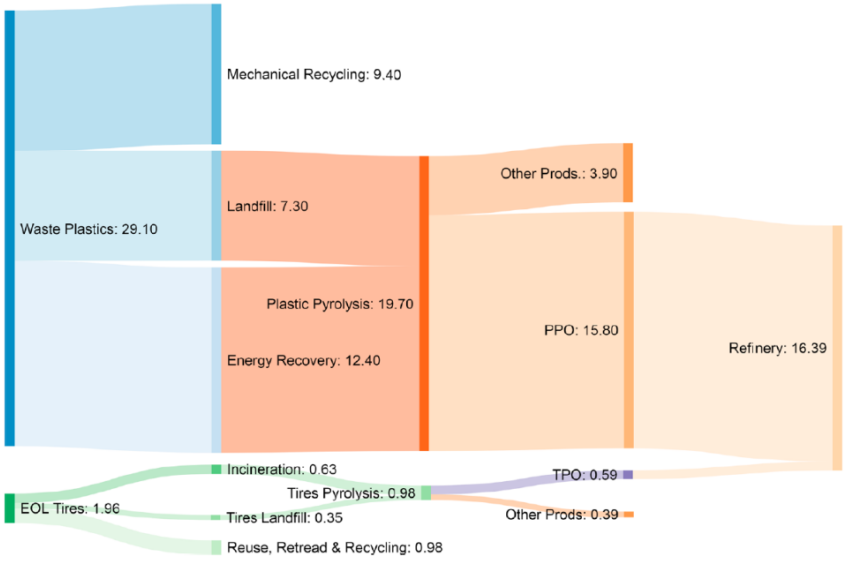

Figure 1.14 End of life plastic and tires (million tons) [6].

Therefore, analyzing first the case of waste plastics, 29.1 million tons were generated in 2018 in the EU [4]. From this amount, 9.4 million tons were mechanically recycled, whereas the remaining 19.7 million tons were landfilled or burned for energy recovery. Thus, assuming that neither landfilling nor combustion are the optimal management routes, these wastes may have been pyrolyzed. Taking into account that waste plastic pyrolysis might lead to liquid yields of 80 wt% [111], an amount of 15.8 million tons of plastic pyrolysis oil (PPO) suitable for being treated in refinery units might have been produced. Note that from the total amount of PPO produced, two-thirds approximately correspond to the PPO obtained from polyolefins. Likewise, the same analysis can be performed for the EOL tires. Thus, 1.96 million tons of EOL tires were produced in the EU in 2018. Half of these were incinerated (0.63 million tons) or landfilled (0.35 million tons). If the 0.98 million tons of mismanaged EOL tires had been submitted to a pyrolysis stage, 0.59 million tons of scrap tire pyrolysis oil (STPO) would have been produced assuming a liquid yield of 60 wt% [112]. Consequently, a total amount of 16.39 million tons of hydrocarbons would have been available for European refineries, which means an important source of raw materials considering that 740 million tons of crude oil are processed on average in the EU [113].

Based on their versatility, the refinery units with higher prospects for managing these feeds (raw plastics, waste plastic pyrolysis oil, and EOL tire pyrolysis oil) are the following ones: catalytic cracking (FCC), hydroprocessing, steam cracking, and coker units [100,114,115]. Moreover, taking into account their capacity and technological development, the refinery units that forge ahead in the implementation of the waste refinery are the FCC unit (in the short term, using already depreciated units) and the hydroprocessing unit (in the long term, given its

higher complexity and lower implementation). Furthermore, a refinery is equipped with separation, purification, and other units appropriate for the integral valorization of the remaining streams of products obtained in the pyrolysis of waste plastics and EOL tires, such as light olefins and BTX aromatics. Finally, the conclusions about the points of the refinery where feedstock streams from waste plastic can be inserted are the same as those obtained when exposing the waste refinery in relation to biofuels (Figure 1.11). The results obtained from the recovery of waste plastic in the catalytic cracking (FCC) and hydrotreating units will be presented below.

1.3.2.1 The fluid catalytic cracking (FCC) units

FCC units, which are available in most of the petroleum refineries worldwide, are used to produce high octane gasoline and light olefins from heavy streams obtained in the distillation of crude oil. They are composed of four sections [25]: (i) the pneumatic transport reactor (riser); (ii) the stripper; (iii) the gas−solid separator; (iv) the regenerator. The process starts when the preheated feedstock, commonly vacuum gas oil (VGO) with a boiling point above 344 °C, is steam-atomized at 350 - 425 °C. Afterward, the atomized feedstock is mixed at the base of the riser reactor with the catalyst stream that comes from the regenerator at 650 - 720 °C. Note that, based on the different temperatures of the feedstock and the catalyst, the mixture ends with an average temperature of 530 - 560 °C. The steam-atomized feedstock sweeps the catalyst throughout the riser, which has a length of 25 - 40 m and a diameter of 0.6 − 1.2 m. Because of the cracking reactions, the gas stream expands, reaching velocities of 5 − 15 m s^{-1}. The flow regime corresponds to a dense-phase pneumatic conveying system due to the high catalyst to oil ratio (4 − 9 g_{cat} g_{feed}^{-1}) and residence time of the gas and catalyst (1 − 5 s).

In the upper part of the reactor, cracking reactions reach their end but, in order to avoid undesired secondary reactions, the catalyst is separated from the products by high efficiency (99.995 %) cyclones. Products exit through the reactor head and go to fractionation and concentration systems, with the average fractions being commonly as follows: dry gases (C_1−C_2) 3 - 5 wt%; liquefied petroleum gases (LPG, C_3−C_4) 8 − 20 wt%; naphtha (C_5−C_{12}) 36 − 60 wt%; light cycle oil (LCO, C_{13}−C_{21}) 12 − 20 wt%; heavy cycle oil (HCO, C_{21+}) 10 − 15 wt%; coke 3 − 8 wt% [25]. The deactivated catalyst goes to the stripping section, where interstitial and adsorbed hydrocarbons are removed from the catalyst by a countercurrent stream of steam (about 2.5 kg of steam per ton of catalyst). Once they have been separated, the hydrocarbons go to a fractionation column, whereas the catalyst goes to the bubbling-bed regenerator (10 − 15 m in diameter).

The catalyst inventory of an average FCC unit, which treats ca. 50 000 barrels per day (bpd), is 270 − 300 tons. FCC units perform between 100 and 400 cycles per day, and in each cycle, the catalyst spends most of the time in the regenerator (6 − 11 min), and only a few seconds in the riser reactor. The content of coke at the entrance of the regenerator is 0.4 − 2.5 wt%, and it is removed by combustion at a temperature of 650 − 720 °C with an air velocity of 0.6 − 1.2 m s^{-1}. This way, the catalyst is reactivated and acquires the sensitive heat required to satisfy the thermal requirements of the unit [116]. Furthermore, the combustion gases that leave the regenerator drag the particles produced by the attrition phenomenon, and they must be retained and replaced by a stream of fresh catalyst.

The direct co-feeding of plastics dissolved in conventional refinery streams (vacuum gasoil, VGO) has the advantage of not requiring additional pyrolysis facilities. However, this direct strategy can be conducted successfully if: (i) a rigorous separation of polyolefinic plastics has been carried out in municipal solid waste collection and segregation points; (ii) plastics must be transported to the refineries, which is not an easy task given their low density; (iii) plastics must be dissolved in refinery streams.

The first reference in the literature about catalytic cracking in a fixed bed MAT type reactor by feeding VGO blended with HDPE (5 and 10 wt%) at 510 °C reports a substantial production of gasoline from the HDPE plastic contained in the feed (10 wt%) [117]. Later, the cracking of polyolefins and polyaromatics under conditions similar to those of the industrial unit was studied on a riser simulator reactor with different types of catalysts: (i) equilibrated commercial FCC catalysts [118,119]; (ii) commercial fresh catalysts and other in-house synthesized HY zeolite-based catalysts with different porous structures and acidities [120,121]; and (iii) catalysts prepared in the laboratory using HZSM-5 zeolites as additives [120]. The solvents used in these studies for dissolving the plastic were VGO, which is the current FCC unit feed, and light cycle oil (LCO), which is a product stream of the FCC unit with a high content of aromatics.

The co-feeding of polyolefins with LCO increased the yield of gasoline and reduced that of coke. The content of aromatics was reduced in the gasoline fraction, at the same time as the contents of isoparaffins and olefins were increased, thereby leading to an increase in the quality of the gasoline fraction obtained. Moreover, the RON increased with temperature from 98.1 to 99.0 when 10 wt% PE was in the feed [118]. The results obtained by co-feeding PP were quite similar. Furthermore, the use of HZSM-5 zeolite as an additive of the catalyst significantly affected product distribution. A notable increase in the yield of olefins was obtained, whereas the yields of aromatics, paraffins, and coke were reduced [120]. These results were later on ratified by Marcilla et al. [122] in a sand fluidized bed reactor and by Odjo et al.

[123,124] in a FCC pilot plant. Therefore, the viability of co-feeding polyolefins with VGO without affecting the yields and quality of the product streams is evident.

When 10 wt% PS was co-fed with LCO, the conversion surpassed that obtained with pure LCO, the yield of gasoline increased to the detriment of that of dry gases, and the fraction of LPG was mostly olefinic, with propylene and isobutene being the main compounds. Additionally, it should be highlighted that 50 wt% of the styrene in the PS was recovered. The RON of the gasoline, between 97.2 and 95.4, was lower than that obtained in the cracking of pure LCO. This drop is a consequence of the lower content of isoparaffins and olefins. The results obtained by co-feeding PS-BD were qualitatively similar, even though the yield of the gasoline fraction obtained was 2 wt% lower [118].

Recently, the extensive study of HDPE/VGO cracking (10 wt% of HDPE) has been carried out revealing interesting result. An increase in the catalyst to oil (C/O) ratio and, especially in temperature, allowed reaching higher conversions in the cracking of the blend. With the highest C/O ratio, the conversion of the blend was higher than the achieved by neat VGO. Under these conditions, the co-feeding of HDPE promoted the formation of LPG and gasoline fractions, to the detriment of dry gas and coke [125].

A previous step of pyrolysis of waste plastics would make much easier their valorization in refinery units. Plastics could be locally converted into liquid or waxy hydrocarbons in small pyrolysis units located near the municipal solid waste collection and sorting points. Accordingly, the subsequent transport of pyrolysis derivatives to the refinery would be easier as a small fleet of tanker trucks would be sufficient to collect all the products of medium-large geographical areas. Furthermore, this feed could be stored and mixed in the refinery oil terminals in order to attain a standard formulation prior to their treatment in the corresponding units.

Iribarren et al. [126] determined by life cycle analysis that the combined strategy of pyrolysis and catalytic treatment is the most sustainable management strategy when the perspectives involving energy and environment are considered. Based on these positive points, various authors have approached the catalytic cracking of plastic pyrolysis waxes, either neat [127,128] or dissolved [129,130].

Rodriguez et al. studied the catalytic cracking of neat HDPE pyrolysis waxes in different works [127,128]. First, the authors studied the suitability of the FCC unit for the production of fuels from the HDPE pyrolysis waxes with a parametric study. Overall, HDPE pyrolysis waxes were less reactive than VGO. Temperatures above 550 °C and C/O ratios of 7 g_{cat} g_{feed}^{-1} were required to obtain higher conversions with the waxes [127]. Then, these authors tested different FCC

equilibrated catalyst with this feedstock. In fact, catalysts with low acidity promoted the formation of gasoline with low content of aromatics, suitable to be marketed after a mild hydrotreatment stage, whereas highly acid catalysts were appropriate for the production of commodities, such as C_5 and C_6 olefins [128]. Afterward, Rodríguez et al. [130] investigated the co-cracking of HDPE pyrolysis waxes and VGO in a riser simulator reactor. They determined that the co-feeding of the HDPE pyrolysis waxes had remarkable effects on the process. Thus, the co-feeding inhibited the secondary cracking reactions, which promoted the formation of the dry gas fraction, and increased the yields of LPG and gasoline fractions. Moreover, a reduction in the content of coke was observed because of the higher H/C ratio of the blend. In addition, a higher quality gasoline fraction was obtained, with values of the RON being about 103.

According to the STPO (scrap tires pyrolysis oil), Rodríguez et al. have studied the cracking of pure STPO obtained in a conical spouted bed reactor [131,132], the cracking of STPO dissolved in VGO [133], and the nature and location of the coke formed in this process [134]. Initially [131], these researchers studied the effect of operating conditions, that is, temperature, C/O ratio, and contact time. Accordingly, they used a riser simulator reactor and an equilibrated FCC catalyst in order to perform the testing at industrial conditions. These authors observed that high temperatures promoted cracking reactions leading to the formation of light compounds within LPG and gasoline fractions. Moreover, they also verified that olefin cyclization reactions and C−C bond cracking reactions from aromatics were boosted at high temperatures, while hydrogen-transfer reactions were inhibited. Consequently, the content of olefins increased in the dry gas and LPG fractions and the content of aromatics and paraffins in the gasoline fraction. Furthermore, higher values of C/O ratios and longer contact times boosted cracking, hydrogen-transfer, and condensation reactions, promoting the paraffinicity and aromaticity of the reaction products. Later, they assessed the effects that catalyst properties have on the conversion, distribution, and composition of the reaction products [132]. Three different equilibrated FCC catalysts supplied by industrial providers were tested in the work. They concluded that the properties of the catalyst are highly influential. Thus, high total acidity and acid strength of the catalyst promoted the extent of the cracking reactions. Moreover, the textural properties of the matrix (meso- and macropores of the catalyst) play a significant role in the diffusivity of the bulky molecules.

Afterward, Rodríguez et al. [133] tried a more realistic approach, as they studied the co-cracking of STPO with the conventional FCC unit feedstock, VGO. Furthermore, they compared the results obtained with the STPO/VGO blend with those obtained in the cracking of the pure feeds separately. They report that there are various synergistic effects when the blend is fed. Thus, the addition of 20 wt%

STPO to the blend promoted the cracking of the HCO fraction, as its extent is closer to that obtained with pure STPO than with pure VGO. Furthermore, overcracking reactions that commonly lead to the formation of gas products were inhibited, as the lowest yields of dry gas and LPG fractions were obtained with the blend. Consequently, the blending promoted the formation of naphtha and LCO fractions, improving the results obtained for the VGO.

1.3.2.2 Hydroprocessing units

Hydroprocessing units are commonly available in refineries for low severity or mild hydrotreatment with the aim of removing heteroatoms and hydrogenate compounds from the feeds. Afterward, these streams can either be sent to another unit or be marketed as fuels. Nevertheless, the presence of hydrocracking units (capable of reducing drastically the presence of aromatics and generating linear hydrocarbon chains) is not so common, and they can only be found in innovative refineries [135,136]. The availability of these hydrocracking units is a key factor to face the increasingly restrictive environmental rules and the possible inclusion of new feeds (bio-oil or waste derivatives, such as those of plastics and EOL tires) and also to deal with non-conventional oils as mentioned in section 1.2.1.

The main challenges that refineries need to face with regard to hydroprocessing units are [137,138]: (i) the adaptation of the product streams to legislation concerning emissions when burning the fuels and (ii) the upgrading of intermediate refinery streams, which, due to their content of heavy molecules, aromatics, or heteroatoms, cannot be fed into other catalytic processes.

Regarding to hydroprocessing of heavy and secondary streams, Gutiérrez et al. [1,107,139] used bifunctional catalysts composed by noble metals (Pt and Pd) over different acid supports to upgrade LCO in a fixed bed reactor. One of the most promising catalysts was PtPd (1.12 and 0.46 wt%) over zeolite Y, which showed different benefits such as the highest conversion and great level of desulfuration in the pseudostable state. Besides, the composition of the middle distillates revealed a good quality fuel. Then, a wide range of operating conditions were studied by these authors to assess the effect of the process variables (temperature, pressure and space velocity) [140–142]. However, these catalysts show an appreciate decrease of the activity due to deactivation pathways by sulfur compounds in LCO and the coke formed [107,108,143]. To address this problem, the process was splitted in two steps: i) first hydrodesulfuration of the feedstock employing hydrogenation catalyst and mild conditions and ii) subsequent hydrocracking of the previously hydrotreated feedstock alone or co-processing it together with any alternative feedstock (wate plastics, EOL tires, etc.).

Regarding the first stage, there are some works in our research group which study the hydroprocessing of alternative feeds, such as scrap tires pyrolysis oil (STPO) [144–146], rich in heteroatoms like sulfur compounds, and raw bio-oil, rich in oxygenated compounds [147,148]. A secondary refinery stream, LCO was also hydrotreated in the first stage, using commercial bifunctional catalysts, made of transition metals (Co, Mo, Ni and W) over different acid supports (ASA, Al and HY) [3,109], and an in-house-prepared catalyst of NiMoP over some acidic supports (FCC, MCM41 and SBA15) [149]. The experiments were carried out in a fixed-bed reactor at 320-400 ^{o}C, 80 bar H_2, time on stream (TOS) 8 h, space time of 0.2-0.5 g_{cat} h g^{-1}_{LCO} and 1000 H_2/Feed ratio. The NiMoP/FCC achieved good results, removing 87.2 wt% of sulfur compounds. However, it cannot outperform the numbers obtained from CoMo/Al and NiW/HY, which were higher than 99 wt%. Furthermore, the second one produced higher yield to naphtha fraction, getting better results in accordance to the hydrocracking conversion.

In the second stage, where this thesis is framed, there are some previous works where the production of fuels from hydrotreated feedstocks has been studied. Hita et al. [150] used hydrotreated STPO (HT-STPO) from a previous work [144] as a feed to fuel production in a fixed-bed reactor at 440-500 ^{o}C, 65 bar H_2 and a space time of 0.16 h, using PtPd/SiO_2-Al_2O_3 catalyst. Results showed that the production of ultra low sulfur diesel (ULSD) is possible for low TOS, and after 2 hours, the activity of the catalyst decreased due to coke deposition in both metallic and acidic phase.

The plastic co-processing together with oil refinery streams in a batch reactor has aroused interest since years ago. Joo et al. [151] studied the catalytic behavior of a blend of plastic (PET, PS and LDPE) with petroleum residues or/and coal in a 20cm^3 stainless steel batch reactor at 430 ^{o}C for 60 min with 83 bar of H_2 and stirrer speed 450 rpm. Results display that the conversion was higher for plastic/coal/ petroleum resid than for the blend of plastic/coal where conversion upper than 70 wt% were reached, since the chemistry reactions was well matched, showing the feasibility of upgrading these residues together.

Karagöz et al. [152,153] co-feed LDPE or HDPE with VGO in a 100 mL stainless steel stirred batch reactor at 425-450 ^{o}C, 65 bar of H_2 for 120 min, with Cobalt over active carbon, CoNi/HZSM-5 catalyst and DHC-8 catalyst (a commercial catalyst based on NiMo over silica alumina that is used in hydrotreating and hydrocracking reactions in refinery). Obtained results describe that CoNi/HZSM-5 achieved more liquid amount at lower temperature. However, gas yield rises until more than 50 wt% at 450 ^{o}C when the temperature increases. To sum up, they point out that both acidic properties and temperature play an important role in the upgrading process of the blends.

Recently, Siddiqui and Redhwi [154] have studied the decomposition of different plastics with light Arabian crude oil residue. Experiments were carried out at 400 − 430 ºC, 500 − 1200 psi H_2 pressure and 30 − 120 min using different acid catalysts. NiMo/γ-Al achieved the best result in plastic conversion and, hence, it was used later for a parametric study. Increasing the pressure reduces the gas fraction and promotions both the conversion and the fraction of soluble products on Xylene. Kohli et al. [155] studied thermal hydrocracking of a blend of waste plastic and heavy oil or two vacuum residue at 420 ºC, 60 bar and 120 min. They obtained interesting results such as blends increase the middle distillate fraction and they also reduce the coke formation.

In addition, our research group also studied how the addition of an alternative feedstock free from heteroatoms (HDPE) affects to the hydrotreating and hydrocracking conversion pathways. The experiments were conducted in a stirred batch reactor at 320 − 400 ºC, 80 H_2 bar, stirring rate 1500 rpm and 3 h length [156]. After studying the behavior of CoMo/Al, NiMo/SiAl and NiW/HY catalysts in LCO hydrotreating, the first one achieved the more promising result and, therefore, it was used in the hydroprocessing of HDPE/LCO (10 wt%) blend. The hydrodesulfuration conversion obtained was higher adding HDPE than hydrotreating neat LCO under the same experimental conditions, keeping a very similar composition of the liquid products. Nevertheless, the HDPE conversion was slightly higher than 30 wt% at the maximum temperature (400 ºC). This low conversion of HDPE could be related with the temperatures at which the reactions have been carried out, that were not higher enough.

1.4 HYDROPROCESSING

Hydroprocessing is a refinery stage in which petroleum-derived oils are upgraded under high pressures of H_2 and high temperature. Its aims toward the adaptation of liquid fuels to environmental requirements by means of (i) the hydrogenation of the unsaturated compounds, especially aromatics, (ii) the removal of impurities (N, S, O, and metals), and (iii) the cracking of heavy compounds improving the yields of gasoline and diesel fractions [157,158]. This process is carried out under a broad range of operating conditions, and therefore hydroprocessing units are denoted as (i) hydrotreating (HDT) and (ii) hydrocracking (HYC) units.

HDT units are commonly used to reduce the content of heteroatoms. Thus, hydrodesulfurization (HDS), hydrodenitrogenation (HDN), hydrodeoxygenation (HDO), and hydrodearomatization (HDA) reactions occur in the processing of light and medium distillation fractions. When heavier streams are processed, together with the aforementioned reactions hydrodemetallization (HDM) and hydrodeasphaltenization take also place. On the other hand, HYC units aim to convert heavy fractions, such as vacuum, coker, or atmospheric gas oil, into lighter fractions, that is, gasoline and diesel. HYC units may be classified into two subgroups depending on the severity of the treatment; thus, mild hydrocracking (MHYC) and standard hydrocracking units (HYC) are available in refineries. Table 1.3 shows the ranges of operating conditions of different hydroprocessing units.

Table 1.3 Hydrotreating and hydrocracking conditions.

Conditions	Hydrotreatment (HDT)	Mild-Hydrocracking (MHYC)	Hydrocracking (HYC)
Temperature (^oC)	270−400	320−440	380−450
Pressure (bar)	25−50	35−70	90−210
H_2/Feed (m^3/m^3)	300−500	300−700	1000−2000
LHSV (h^{-1})	2−4.0	0.3−1.5	0.4−2.0

These types of units are quite extended within modern refineries. Indeed, at least three hydroprocessing units are usually installed [159,160]: (i) one for naphtha, (ii) one or two for light gas oil, and (iii) one or two for heavy or vacuum gas oil (mild-hydrocracking). The units used for hydrocracking purposes are less numerous than those for hydrotreating, but the installation of hydrocracking units has increased in recent times in order to fulfill environmental policy requirements for fuels. Furthermore, the uses of oils with lower API gravity increase the flows from vacuum distillation tower that need to be cracked and/or hydrocracked in refineries.

1.4.1 Hydrotreating (HDT)

When a feed undergoes through a hydroprocessing treatment, the H_2 pressure in these units not only removes the heteroatoms but also olefins and aromatics are hydrogenated. In fact, the hydrogenation reactions are faster than, for example, remove the sulfur from some compounds if an appropriated catalyst and reaction conditions are used [109]. Furthermore, when hydrogenation reactions take place, remove the heteroatoms is easier since the stability that the double bonds provide to the compounds disappears.

Generally, hydrogenation reactions are reversible and exothermic. These reactions consist of introducing hydrogen in π-bond of C since is a weaker bond and requires less energy in comparison with σ-bond to be break. Hydrogenation reactions depend on the molecular weight since occur faster in light olefins than heavier ones [161]. Olefins are very reactive compounds and hydrogenation reaction is even at atmospheric pressure. However, it is difficult the hydrogenation of aromatics under this condition. These reactions require high H_2 pressure to take place. This happens due to the resonance of double bonds in aromatic compounds.

On the other hand, the heteroatoms removal requires to break σ-bonds of C-X, where X can be C, S, N, O or metal, introducing hydrogen. The name of these hydrotreating reactions have been introduced above (HDS, HDN, HDO, HDM and HDA). It has to be mentioned that HDS, HDN, HDA and HDM are the most common reactions that take place in hydrotreating crude oil derivates and STPO whereas HDO is common in hydrotreating oils from biomass.

In HDS reaction, the sulfur removed from the compounds is released as H_2S. Obviously, not all molecules react in the same way. As a general rule, paraffins are the compounds that have a higher reactivity, followed by naphthenes and lastly the aromatics [162]. Furthermore, thiophenes desulfuration is easier compare to benzothiophenes and dibenzothiophenes. There are two mechanism pathways to remove sulfur from aromatic compounds. When the HDS is first and then the HDA, the reaction pathway is called direct hydrodesulfuration. However, when the reaction take place in the reverse order (first the hydrogenation and then the hydrogenolysis), the reaction pathway is named indirect hydrodesulfuration [163–166]. These reactions are depicted in Figure 1.15 using dibenzothiophene as model compound.

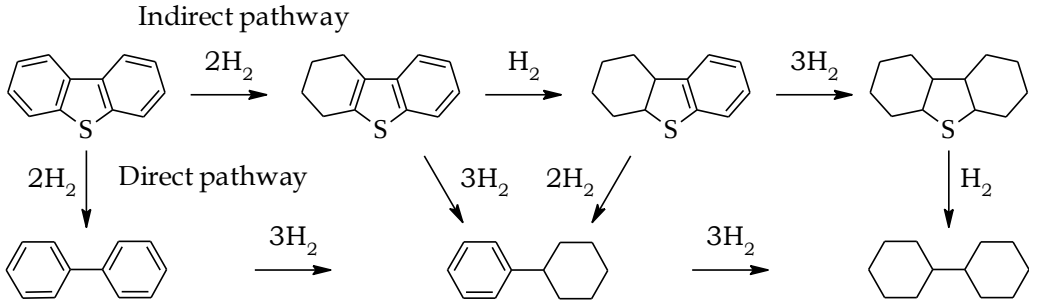

Figure 1.15 Hydrodesulfuration and hydrodearomatization of dibenzothiophene.

The direct pathway is more efficient since uses less H_2 in sulfur removal. Nonetheless, the resonance of double bond of aromatics reduces the reactivity of the molecule. By contrast, the aromatic compound hydrogenation reduces the bound energy of C-S, easing the scission. The H_2 pressure is a key factor, conditioning the equilibrium of the reactions. When there is low H_2 pressure and high temperature, the dehydrogenation reactions are promoted [167]. Furthermore, the activity of the catalyst also plays an important role due to a low activity impact on the reaction pathways.

In crude oil, the nitrogen can be found as part of two types of aromatic compounds: i) basic compounds (quinoline, acridine and pyridine); and, ii) non-basic compounds (benzothiazole, indole, pyrrole and carbazole) [168]. The nitrogen is linked to the aromatic compound by three bounds, thus the N-compounds have to be hydrogenated before remove the nitrogen and release ammonia [169]. Unlike sulfur compounds that can be desulfurized directly, nitrogen compounds rarely do so. Therefore, a previous hydrogenation of the ring which contains the nitrogen is required. Figure 1.16 shows the HDS and HDN of benzothiazol, releasing H_2S and NH_3.

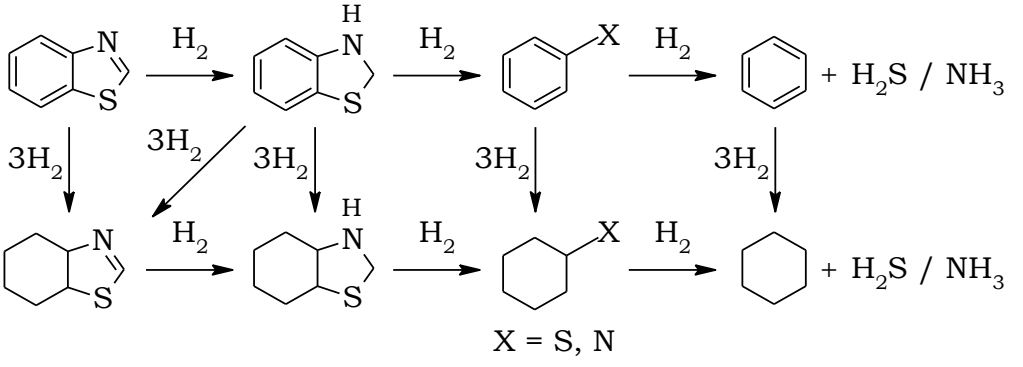

Figure 1.16 Scheme of benzothiazol hydrodenitrogenation.

HDA consists of both the hydrogenation of an aromatic ring to give a naphthenic compound and the subsequent opening of the naphthene ring to an alkane [170]. The more polar is the compound the greater is attracted by the acid site [171,172]. Therefore, the polyaromatics and diaromatics react easier than monoaromatics. Nevertheless, the HDA of monoaromatics is a difficult task. Such an example, Figure 1.17 shows the dearomatization of toluene up to naphthenic ring and methane. First and one by one, the double bounds are saturated until obtain a methyl-naphthenic compound and finally, the de-alkylation takes place.

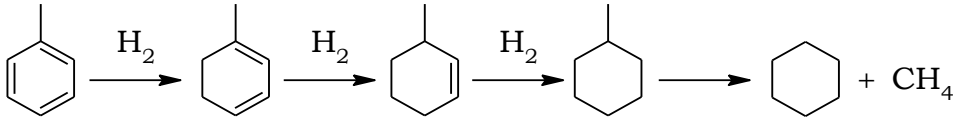

Figure 1.17 Scheme of toluene hydrodearomatization.

HDM has been studied in the literature [173–175], taking metal-tetraphenylporphyrin as the standard molecule (MTPP), with Ni or V as metal (the most abundant in crude oil). The scheme is depicted in Figure 1.18. There it has been checked a series mechanism with two reversible hydrogenation steps and one irreversible hydrogenolysis, resulting in a deposit of metal sulfide. Rana et al. [176] have evaluated the effect of the presence of H_2S in HDM reactions observing that it has a promoter effect. Its presence favors the adsorption of the ring metal-porphyrin in the Brønsted-type acid sites. There takes place the first step, where entails its conversion into the metal-chlorine structure, facilitating the subsequent stage of hydrogenolysis, which by breaking the metal-N bond gives rise to the removal of metal from the structure as metal-sulfide deposit.

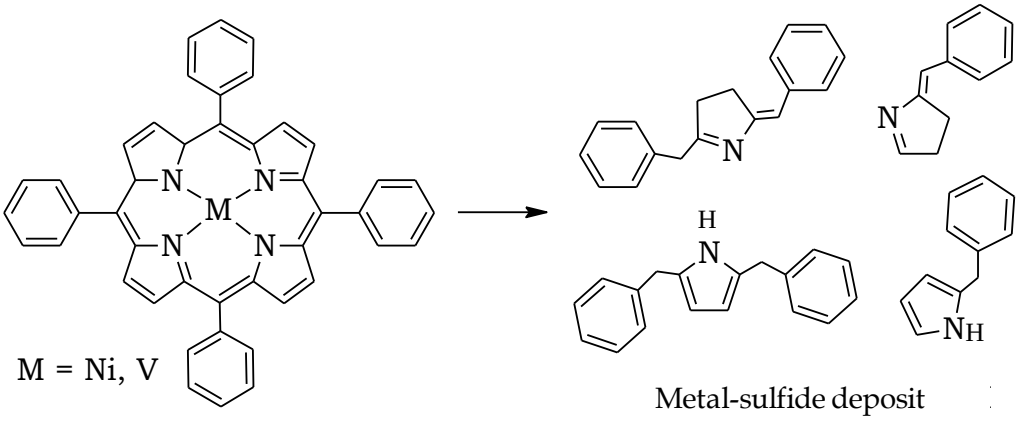

Figure 1.18 Scheme of metal-tetraphenylporphyrin hydrodemetallization.

1.4.2 Hydrocracking (HYC)

The reactions that involve the hydrocracking are the same that are involved in the hydrotreating together with the reactions that provoke the reduction of carbon atoms number of hydrocarbons. When the aim is the hydrocracking of a feedstock, bifunctional catalysts with strong acid sites are used. Furthermore, the reaction conditions also are more severe than for HDT as depicts Table 1.3.

The hydrocracking mechanism was deeply studied by Weitkamp et al. [114]. They proposed a kinetic scheme using a carbenium-ion as intermediate in the reaction and where the C-C bond is broken through β-scission on the Brønsted acid site. Besides, there are some reactions that take place in the metal site (hydrogenation/dehydrogenation) and others that involve the acid sites (skeletal rearrangement and β-scission). Figure 1.19 summarizes the hydrocracking reaction mechanism of a n-paraffin.

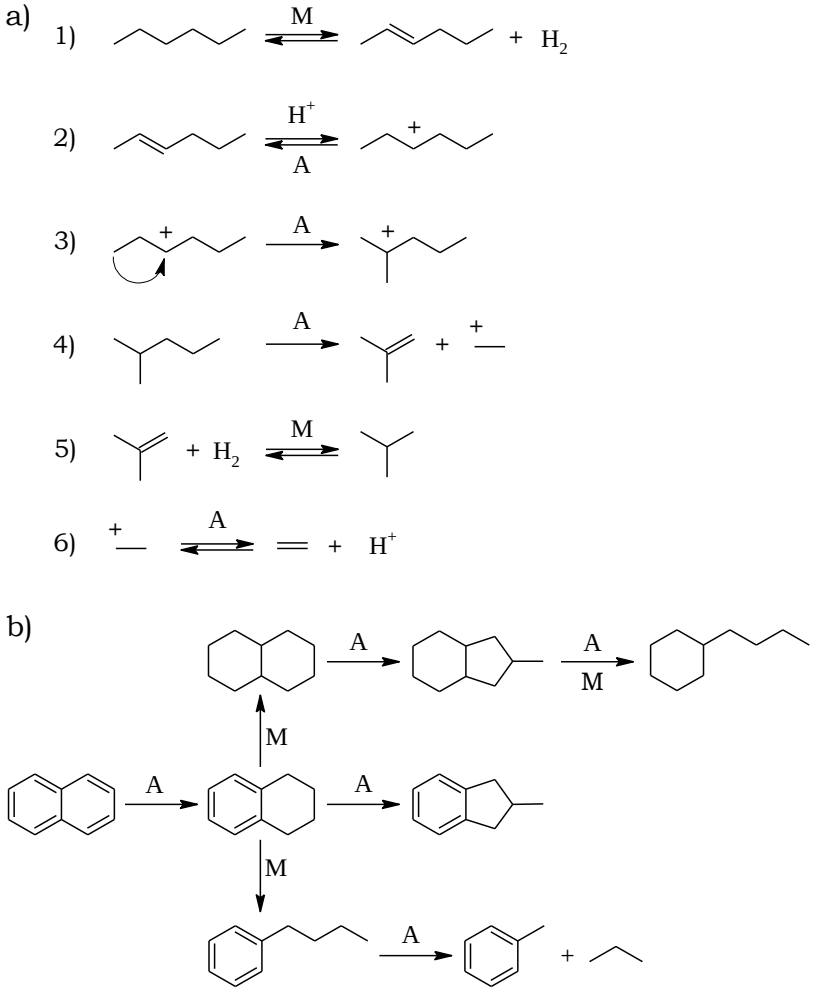

Figure 1.19 Mechanism scheme hydrocracking.

In the step 1 of Figure 1.19a, after the adsorption of n-paraffin into a metal site, the formation of an olefin takes place. In the step 2, the desorbed olefin is adsorbed on a close Brønsted acid site and the carbenium-ion is formed but the β-scission cannot happen yet since the reaction is not thermodynamically favorable. In step 3 is where the carbenium-ion changes to alkylcarbenium-ion through skeletal rearrangement. Furthermore, step 3 can be repeated increasing the number of isomerizations. In fact, the greater the number of isomerizations, the higher the probability that β-scission will occur. In the step 4, the β-scission takes place producing an olefin and a smaller carbenium-ion. The olefin can either undergo further cracking on an acid site (starting the process from step 2), or it can be saturated in a metal site to form an i-paraffin (step 5). On the other side, the carbenium ion from step 4 can also be converted into paraffin by deprotonation (step 6).

The hydrocracking of naphthalene is summarized in Figure 1.19b according to Ardakani and Smith [177]. The first step is the formation of tetralin through hydrogenation. Then, the tetralin can follow three pathways. The hydrogenation can go further, hydrodearomatizing the other ring, followed by isomerization and saturated ring opening producing finally an alkyl-ciclohexane. On the other hand, the two remaining pathways have an isomerization from the tetralin or saturated ring opening and dealkylation. The product can be a monoaromatic or a monoaromatic and paraffin, respectively.

1.4.3 Side reactions

There are several reactions in HDT and HYC that take place simultaneously, among of which the most relevant ones are product recombination, catalytic poisoning with compounds from heteroatoms removal (NH_3 or H_2S) and coke formation. Catalyst poisoning occurs when some heteroatoms of the feed (S, N, Ni and V) modify the nature of the metallic and/or acidic phase of the catalyst and block the porous structure and the access to active sites by condensation of heavy hydrocarbons with low H/C ratio (coke) [108,178].

For example, in sulfur removal reactions with enough contact time, unwanted recombination between an olefin and the released sulfide maybe occur to form a mercaptane. To solve this problem, an amount of hydrotreating catalyst can be added or even an adsorbent with high selectivity for mercaptanes to increase the life-time of catalyst.

Coke formation during the HYC and HDT of heavy and complex feedstock is due to the direct deposition of the heavier molecules of the feed, what is known as Conradson coke, or due to the formation of hydrocarbons with low H/C ratio

which deactivate the metallic or acidic sites. Nevertheless, the term "coke" includes all the carbonaceous materials that remain adsorbed on the catalysts. The general expression of coke is $(CH_X)_n$, where the "x" value is close to 2 for undeveloped coke (also called coke precursor) and near to 0 for very developed or condensed coke [179]. The nature of the coke deposition depends on the catalyst properties, as are: (i) porous structure, (ii) total acidity and (iii) acidic strength of the sites [108]. Although the total acidity is beneficial in terms of HYC performance, it is also causing a more rapid deactivation with a more developed coke due to polymerization and aromatic condensation reactions taking place faster.

Another cause of catalytic deactivation, especially in HYC, is the sinterization of the metal phase [180]. This is the deterioration of the catalyst materials (migration and agglomeration of the metal crystals to form bigger metal particles and aging of acid sites) due to the high temperature.

In general, as the catalyst is deactivated, a common practice to "overcome" this problem and maintain the conversion is to increase the temperature. But this is a short-term solution, since it promotes the formation of more coke and also the sintering, deactivating the catalyst even faster.

1.4.4 Catalysts

Metal/acid bifunctional catalysts are used in hydroprocessing. The metal function is responsible for the hydrogenation and hydrogen-transfer reactions. On the other side, the acid function carries out the hydrocracking of C-C bonds from the hydrocarbon skeletal. Nevertheless, there are relevant synergistic effects between both functions [181]. Hence, the metallic function, apart from boosting hydrogenation reactions, promotes the cracking activity of the acid function by forming an intermediate olefin by dehydrogenation. Furthermore, the acid strength of the acid sites is a key parameter, as the ring opening reactions of aromatic compounds require very strong acid sites [182,183]. The challenge in the preparation of hydroprocessing catalysts is that fuels obtained satisfy the legal requirements mentioned in section 1.2.2 reaching the ultra-low sulfur diesel (ULSD) standard. In Table 1.4 it can be found the more common metallic and acid phases used in different hydrotreating processes.

Table 1.4 Catalysts commonly used in hydrotreating and hydrocracking reactions.

Catalyst	Use	Catalytic activity
Metallic Functions		
CoMo	HDS	moderate
NiMo	HDN, MHYC	high
NiW	HDN, MHYC	very high
PtPd	HDA, HYC	high
Support		
γ-Al_2O_3	HDA	low
Amorphous SiO_2/Al_2O_3	MHYC	high
HY and HZSM-5 zeolites	HYC	very high

1.4.4.1 Metallic function

As it can be seen in Table 1.4, two metals or more are usually used to impregnate a support. The most common metals are within two groups [184]: (i) non-noble metals of the groups VI A (Mo, W) and VIII A (Co, Ni), or combinations of these metals based on the synergic effects that are created between them; and (ii) noble metals (Pt, Pd, Ir, among others). The activation method of catalysts which contains transition metals are the sulfidation and for noble metals the reduction of their metallic species. As it is shown in Table 1.4, the more common non-noble metals are CoMo, NiMo and NiW whereas the most employed noble metals in tandem are PtPd. Some of the non-noble metals can be used for both HDT and HYC. However, the noble metals are more used in the HYC of feedstocks with low concentration of heteroatom since they are very sensitive to heteroatom poisoning and subsequent deactivation. CoMo catalysts have a good performance in HDS, but are less active for HDN and hydrogenation of aromatic compounds. NiMo catalysts, on the other hand, are excellent at HDN and MHYC of aromatics. NiW catalysts present a very high aromatics hydrogenating activity, but their use has been limited due to their higher cost [185]. The concentration of the metals is usually 1-4 wt% for Co and Ni, 8-16 wt% for Mo and 12-25 wt% for W. Meanwhile, the concentration of noble metals is a much lower, 0.25-1.5 wt% for each metal [186].

1.4.4.2 Supports

As in the case of metals, there are supports with a more appropriate performance for the HDT and others better for the HYC and they are selected based on the desired conversion achieved and depending on the feedstock. Some of the HDT supports, however, are sometimes used for the HYC. The supports used for

HDT consist of a porous structure with low or medium acidity, whereas support used in HYC consist of a medium and high acidic porous structure. The most common active supports for HYC are microporous materials what means a faster and undesired deactivation by coke. Therefore, to overcome this situation the supports are made of microporous material and another material with lower acidity and higher meso- and macropore area which enhance the diffusional limitations. In that way, the supports used for HDT have low acidity to avoid the coke formation and maximum porosity to enhance metallic exposure, whereas the HYC catalyst would have similar features and additional acidity to promote cracking reactions.

The most commonly used HDT supports are γ-Al_2O_3 and amorphous SiO_2-Al_2O_3 (ASA) [187]. Nevertheless, to enhance the catalytic behavior different studies have been carried out to develop new supports which are: Al_2O_3-TiO_2 [188–191], Al_2O_3-ZrO_2 [192] or Al_2O_3-MgO [193]. There are alternative ways to add the metal to the support from the physical mixture to the wet impregnation. The latter enhances the interaction of the metal with the support [182,183,194,195].

As it has been mentioned previously for HYC catalysts, the support needs to have medium or high activity, with strong acidic sites that promotes the cracking functionality [181,183]. Consequently, zeolites like HZSM-5, HY, or Hβ have been widely used alone [186,196–200] or blended with another material or even steamed to enhance the diffusivity and stabilize the activity over time. A common binder is an amorphous acidic support as γ-Al_2O_3 (in less than a 3 wt%) having an important effect in the catalyst activity and selectivity [201,202]. Moreover, boehmite (AlOOH) is also used in greater extent (70 wt%) with zeolites and recrystallized zeolites [203–205].

There are some authors that reported good results for the zeolite desilication treatment in order to change their acidity and create mesoporous structure. After that, catalysts show a greater stability in fixed-bed reactor for long-term runs (several hours or even days), maintaining higher conversion, good selectivity and less coke content than parent catalyst. Those tests have been conducted with different reactions: (i) methanol to aromatics [206], (ii) methanol to hydrocarbons [207] and (iii) hydrocracking of n-C_{16} [208]. However, if the reaction time is increased enough to appreciate a decreases in the conversion on desilicated catalyst, the deactivation found on these catalysts end up accumulating a higher coke content given the increase in the mesoporous surface [209,210]. Furthermore, they observed that for the parent catalyst the major coke deposit is in the micropores (internal coke), meanwhile for desilicated catalysts the coke is mainly sited in the meso- and macropores (external coke). On the other hand, for the catalytic cracking of bio-oil, other authors have observed higher coke yield for the desilicated catalysts than for the parent catalysts at the same reaction time [211].

Silica-based mesoporous materials represent an expanding research area of catalytic supports for HDT and HYC feedstocks. The researches show a high interest with MCM-41 and SBA-15 for HDT and MHYC applications [212–214]. These materials have a mesoporous structure with a narrow pore size distribution, displaying a good behavior in HDT process [215–219]. Furthermore, there are some innovations including P, Ti or Zr to SBA-15 support to enhance its performance changing the morphological properties, providing a better metal dispersion [215–222] and reporting better results in HDT [223–226].

There are also interesting studies that use active carbon (AC) as a support for HDT and HYC reactions. Some of its advantages are the high surface area and customizable porous and acidic features [227]. The activation of AC is the modification of the acidity of AC through acidic treatment with H_3PO_4 [228,229]. After the activation, the added phosphorus creates new thermally stable complexes on the surface which enhance the acidic properties. As with P-complexes, other functional groups can be added/created such as carboxyls, lactones and phenols by air-oxidation [230] and chemical treatment with different acids like HNO_3 [231,232] or H_2SO_4 [233]. On the other side, the carbon atoms located on the surface of the AC crystallites act as active sites where elements like O, H, N or S are chemisorbed. Those elements form complexes in the surface which are responsible for the most of the physical-chemical properties of the solid material, being the oxygen complexes the most important ones [234]. This type of supports have been studied in the hydrotreatment of heavy and complex feedstocks [235–237], also in the form of carbon nanofibers [238,239], and subjected to modifications with zeolites [240].

1.5 HYDROCRACKING KINETIC MODELS

The design of the hydroprocessing reactor as well as the design of the catalysts requires kinetic models for the economic and industrial viability of the process. When working with hydrocarbon feeds, the complexity of the process modeling increases exponentially since it requires defining a huge network of interconnected reactions and sophisticated analytical and numerical techniques for their resolution due to it contains a wide range of different compounds [241]. Although numerous works have been published on hydrocracking kinetic models for this process, most of them have been done using model compounds or using simplified reaction schemes to reduce the complexity.

The proposed models can be classified into two broad categories: i) both discrete and continuous lumps and ii) mechanistic, molecular and single-event. These models have different degrees of approach to reality. Since the thesis does not address kinetic modeling using mechanistic, molecular or single-event models, no further reference will be make to them.

Discrete lumps kinetic modeling is the traditional method that considers the species involved in the reaction as groups according to a common characteristic such as the boiling point range. In this way, the reaction scheme is formed by a reduced number of reaction stages. The progress of the reaction is quantified by potential kinetic equations referred to the concentrations of the different lumps or by Langmuir-Hinshelwood/Hougen-Watson type equations that take into account the role of the active sites in the reaction mechanism.

Since it is very practical, the discrete grouping lumps technique is one of the most widely used techniques [242].This method has been widely used to model the reactions involved in the catalytic conversion of petroleum fractions like: (i) catalytic cracking, (ii) hydrotreating or (iii) hydrocracking [243,244]. In this methodology, the lumps are perfectly defined as pseudospecies that allow the monitoring of the course of the reaction [245].

The main advantages of this method are: (a) it facilitates the programming of the mathematical equations of the model, since a reduced number of mathematical equations and experimental data are required; (b) it makes it possible to predict properties of the mixture, such as density, molecular weight, viscosity, etc., and (c) it requires a reduced number of parameters to be estimated [245]. It must be taken into account that the greater the number of pseudocomponents, the better the approximation of the hydrocracking reactions. Nevertheless, the number of parameters to be estimated also increases considerably as the number of lumps increases [244,245]. Furthermore, sometimes, using a large number of parameters in the lumps model can lead to results that lack physical meaning [246].

In this thesis, it has projected to obtain the kinetic model for the co-processing of a blend of HDPE and VGO. In the literature, a specific reaction scheme for the hydrocracking of this mixture is not defined, and therefore, a literature review of the models proposed for both components separately will be carried out.

1.5.1 Discrete lumps models

1.5.1.1 VGO reaction scheme

The kinetic of gas oil hydrocracking was studied for the first time by Qader et al. [247], proposing a first order kinetic with concerning the concentration of gas oil (Figure 1.20a). Later, more complex models were proposed. Callejas et al. [248] proposed a simple three-lumps model for the hydrocracking of a residue (Figure 1.20b). Yui et al. [249] proposed another different kinetic model of 3 lumps in the range 350 – 400 ^{o}C (Figure 1.20c). Aboul-Geit [250] as well as Orochko [251] determined the hydrocracking kinetics of VGO proposing a 4-lumps model (Figure 1.20d, e, respectively). Botchwey et al. [252] proposed another kinetic model (Figure 1.20f) for the hydrocracking of gas oil from bitumen, with 4 lumps: A (500 – 600 ^{o}C), B (400 – 500 ^{o}C), C (300 – 400 ^{o}C), D (IP – 300 ^{o}C). Han et al. [253] proposed a similar 4-lumps model for VGO hydrocracking of mixtures from Iranian and Saudi crudes.

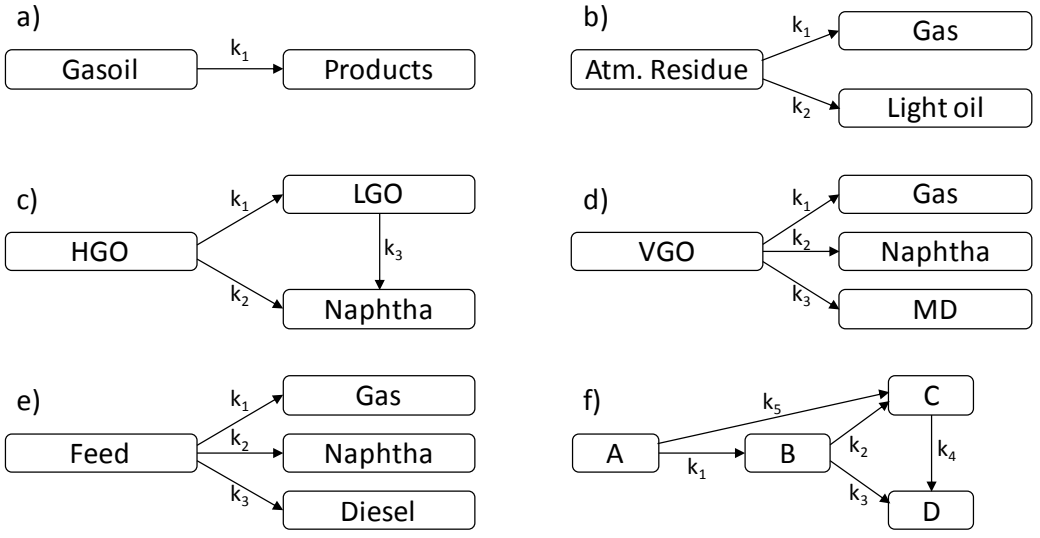

Figure 1.20 Proposed reaction schemes for hydrocracking.

In those early years, similar models to these were also used for the hydrocracking of different feeds: fluorine [254], long chain alkylbenzenes [255], middle distillates [256], asphaltenes [257], bitumen [258], polynuclear aromatics [259], n-paraffins [260], tetralin [261], or Fischer-Tropsch waxes [262].

However, most authors have proposed kinetic models of lumps that include series-parallel reactions regarding the VGO. For example, Valavarasu et al. [263] proposed a 4-lumps model that included cascade reactions for the hydrocracking of a desulfurized VGO using Ni-Mo/USY as a catalyst at 100 bar and 380 - 410 °C. This can be seen in Figure 1.21.

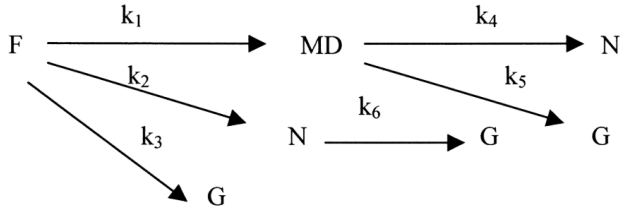

Figure 1.21 Reaction scheme for VGO hydrocracking proposed byValavarasu et al. [263].

The same model was proposed by Faraji et al. [243] for VGO hydrocracking at 171 bar and 375 - 395 °C using a commercial catalyst based on zeolite. With the same argument of the cascade reactions, other authors have proposed models of a greater number of lumps (6-9) for VGO hydrocracking [241,264,265].

Botchwey et al. [266] proposed another kinetic model for the hydrocracking of gas oil (Figure 1.22) where they distinguished between hydrogenation reactions (solid lines) and cracking reactions (broken lines), which allowed applying the model under different conditions: hydrotreating (reactions 1-7) at temperatures between 340-390 °C, and mild hydrocracking (reactions 1-9) between 390-420 °C.

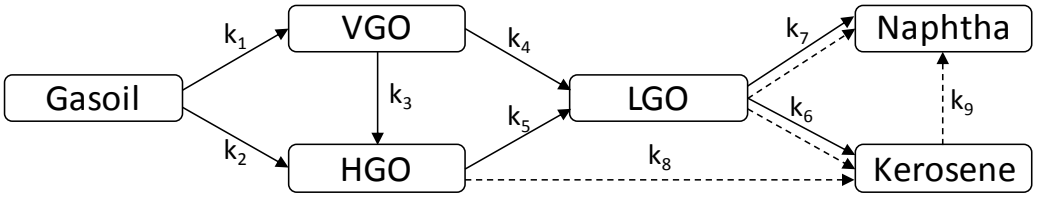

Figure 1.22 Reaction scheme of Botchwey et al. [266].

Ayasse et al. [258] studied the hydrocracking kinetics of residues using a modification of the kinetic model proposed by Mosby et al. [267]. They proposed the 7-lumps kinetic model shown in Figure 1.23.

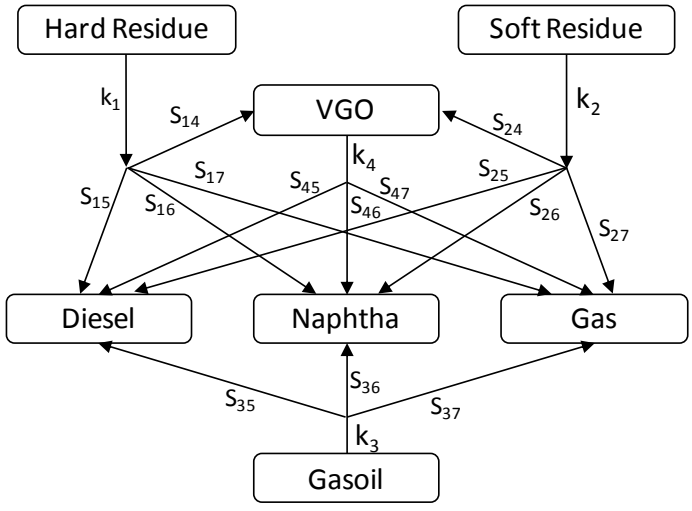

Figure 1.23 Reaction scheme proposed by Ayasse et al. [258] for the joint hydrocracking of residue and VGO.

The most widely used model for the hydrocracking of heavy oil fractions was a scheme of cascade reactions proposed by Sánchez et al. [268]. The scheme comprise serial and parallel reactions from heavier to lighter products grouped in 5 lumps and connected by 10 reactions as shown in Figure 1.24. The model was used for the kinetic modeling of vacuum residue hydrocracking of Maya crude oil in a fixed bed reactor at 70 bar and 380 - 420 ^{o}C using a commercial Ni-Mo catalyst.

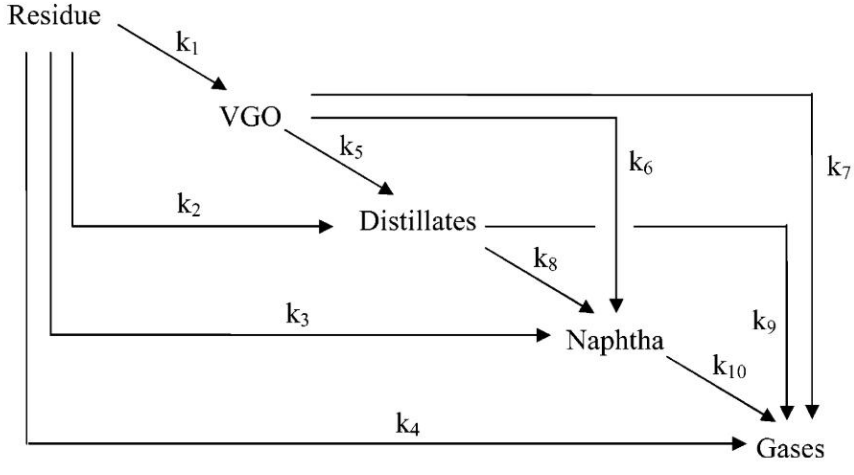

Figure 1.24 Reaction scheme for vacuum residue hydrocracking from Maya crude oil, adapted from Sanchez et al. [268].

This model has been used by a large number of authors in the literature to carry out kinetic studies under similar [245,269–271] and different operating conditions and also with different feedstocks, which supports its great versatility.

In fact, although the catalytic and thermal reactions follow different mechanisms, the same kinetic model was used to represent the non-catalytic hydrocracking of an atmospheric residue of a Maya crude oil in a pilot-scale fixed-bed reactor unit operating at 100 bar and 380 - 420 ^{o}C by Ramírez et al. [272]. Huang et al. [273] presented the same 5-lumps model to describe the hydrocracking of an Iranian heavy crude at 90 bar and 405 - 435 ^{o}C in a CSTR reactor using oil dispersed catalysts. A similar approach was followed by Loria et al. [274], who proposed a 5-lumps kinetic model for the hydroprocessing of an Athabasca bitumen carried out in a pilot plant with a plug-flow reactor at 27 bar and 320 - 380 ^{o}C, using oil ultra-dispersed catalysts.

More examples of this model can be found in the literature. Álvarez et al. [275] proposed the same 5-lumps kinetic model for the hydrocracking of an atmospheric residue of a light Arabia crude and a vacuum residue of a Safaniya crude in a semi-discontinuous CSTR reactor at 150 bar and 420 - 440 °C. Garcia et al. [276] also presented the same 5-lumps model for the hydrocracking of a Maya vacuum residue in a CSTR at 100 bar and 350 - 370 ^{o}C using a liquid catalyst. Pham et al. [277,278] have used this 5-lumps model for the slurry phase hydrocracking of vacuum residue and for kinetic modeling of asphaltene placed in a batch reactor with a commercial slurry-phase catalyst. Umana et al. [279] also used a similar model for hydrocracking of vacuum residue, and Martínez and Ancheyta [270] for hydrocracking of atmospheric residue. Chen et al. [280] used a similar 5-lumps model for coal tar hydrocracking. On the other hand, Félix and Ancheyta [281] based on the original model of Sanchez et al. [268], simplified the model by eliminating the gases lump and they used it to predict the yields of the mild hydrocracking of a vacuum residue of a Maya crude at 39 bar and 360 - 400 ^{o}C, as observed in Figure 1.25(a).

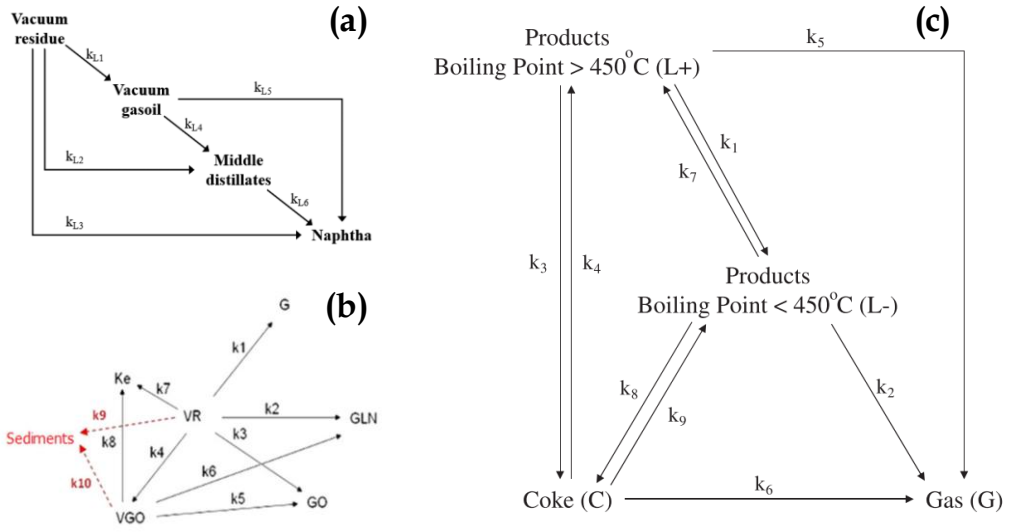

Figure 1.25 Reaction scheme for vacuum residue hydrocracking proposed by Félix and Ancheyta [281]; (b) Manek and Haydary [282]; and (c) Puron et al. [244].

Since coke is a sub-product of great importance in the evolution of hydrocracking reactions, several authors have considered it in the reaction scheme. For example, Manek and Haydary [282] included a sediment lump in which coke is encompassed, as shown in Figure 1.25 (b). In addition, Quitian and Ancheyta [245] highlighted the validity of the model proposed by Sánchez et al. [268], shown in Figure 1.24, for those reactions where there is a large formation of coke. As is known, coke is formed mainly by the polymerization of polyaromatic hydrocarbons (PAHs) on the surface of the catalyst.

Additionally, Puron et al. [244] highlighted that there is a continuous mass transfer between coke and the liquid phase and consequently, they proposed that it is formed by a non-reactive part that is strongly adsorbed on the acid sites (also known as *hard coke*) and on the other hand, it can be desorbed (called *soft coke*). That is why, in their model of 2 liquid lumps plus coke and gas, Puron et al. [244] proposed reversible reactions between coke and liquid lumps, as shown in Figure 1.25 (c). Thus, k_3 and k_8 reactions of this model take into account the formation of both types of coke from the liquid, while k_4 and k_9 reactions represent the desorption of *soft coke*. Furthermore, from the results obtained in the aforementioned reference (k_6, k_8 and k_9 are 0), it was concluded that the coke exclusively interacted in a reversible way with the heavy fraction of the liquid and that no gas was generated from coke.

In line with the previous discussion, several authors concluded that coke was only produced from the heaviest lumps. For example, Asaee et al. [246] proposed a 6-lumps model for the hydroconversion of a vacuum residue in a batch reactor at 70 bar and 390 - 435 °C using a dispersed catalyst. This model is shown in Figure 1.26,

there coke was produced starting from the heaviest lumps (atmospheric gas oil, VGO and vacuum residue), and after mathematical adjustment, it was determined that it was only produced from VGO and VR. Even experiments carried out with only VGO have reached the same conclusion, establishing that the contribution in the formation of coke of light products such as distillates, naphtha and gases is negligible [242,283,284].

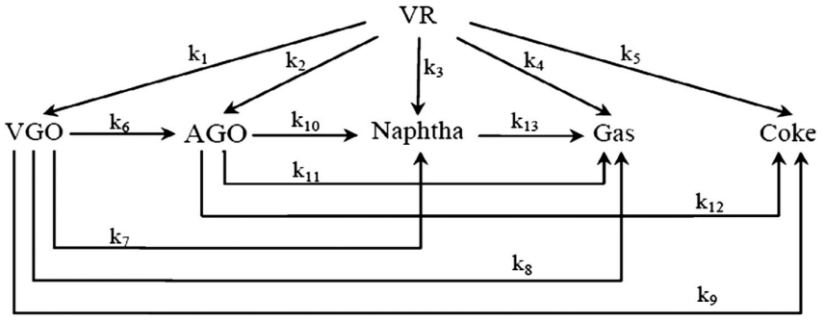

Figure 1.26 Reaction scheme for vacuum residue hydroconversion from vacuum residue proposed by Asaee et al. [246].

Finally, the most recent models for the VGO hydrocracking have been reported by Al-Attas et al. [241], Al-Rashidy et al. [282] and Bdwi et al. [284]. These authors have studied the effect of adding an ultra-dispersed catalyst to a conventional supported catalyst in a slurry-type batch reactor. In the three references, the reactions are carried out at pressures between 80-85 bar and at temperatures of 390 - 450 ^{o}C, feeding VGO from Saudi crude. Furthermore, the proposed reaction scheme, shown in Figure 1.27, turns out to be the same. The model, with 5 lumps, includes VGO, distillates, naphtha, gases and coke, and considers that cascade reactions occur except for the production of gases from distillate. Also, the model foresees that coke formation comes only from VGO, as previously indicated.

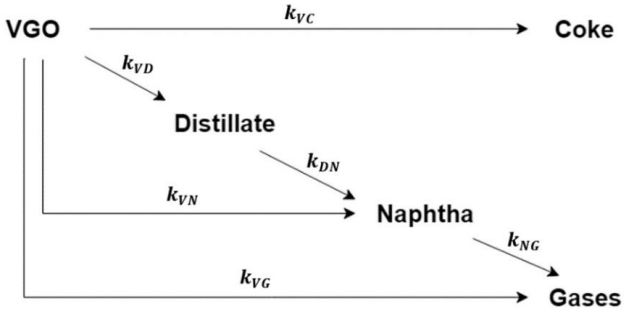

Figure 1.27 Reaction scheme for VGO hydrocracking proposed by Al-Attas et al. [242].

However, all the previously mentioned studies only take into account the catalytic reaction. Nevertheless, the thermal reactions are not negligible at the operating conditions studied. There are some authors that have studied only the thermal decomposition (without catalyst) of heavy residues under nitrogen at temperatures between 300 - 350 ºC at atmospheric pressure [285], at 430 ºC and 10 MPa [286] and also under hydrogen atmosphere between 380 - 430 ºC at 80 bar [245,277]. Besides, the last authors also compare the kinetic model of thermal and catalytic hydrocracking. De Almeida and Guirardello [287] worked in the hydroconversion of Marlin vacuum residue and proposed a 5-lumps kinetic model (Marlin crude oil, vacuum residue, gasoil, diesel and naphtha+gas) where thermal and catalytic reactions take place simultaneously. Therefore, a robust model that is closer to reality is obtained. Their reaction scheme is depicted in Figure 1.28.

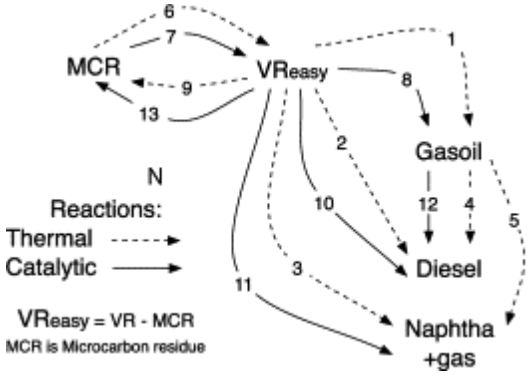

Figure 1.28 Thermal and catalytic reaction scheme proposed by De Almeida and Guirardello [287].

1.5.1.2 HDPE reaction scheme

A literature review has been carried out to learn about the application of lumps modeling to plastics hydrocracking, finding only two references [21,288]. In fact, Munir et al. [21], in their detailed review on the state of the art of plastics hydrocracking, indicated that studies of this type are practically non-existent and highlighted the kinetic study proposed by Ramdoss and Tarrer [288]. They studied the kinetics of non-catalytic thermal hydrocracking of a mixture of plastics. This blend is composed mainly of polyethylene and polypropylene with a C/H ratio of 6.17 (84.6 wt% C, 13.7 wt% H, 0.65 wt% N and 0.01 wt% S). The reactor used was a tubing-bomb type micro-reactor. It was operated in presence of H_2 at 7.9 bar and 475 - 525 °C. The proposed reaction scheme considers the plastic hydrocracking as a cascade model of 5-lumps, plastic and four pseudo-products, which are: heavy distillate (H= heavy oil), light distillate (L= light oil), gas (G) and coke (C). The light

distillate lump would encompass the LCO and naphtha fractions in one group. The model is shown in Figure 1.29.

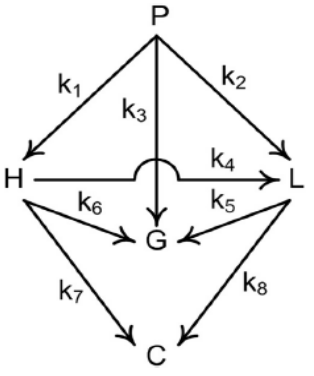

Figure 1.29 Reaction scheme for HDPE hydrocracking proposed by Ramdoss and Tarrer [288] and collected by Munir et al. [21].

The plastic cracks producing heavy distillate, light distillate and gases in parallel. The heavy distillate is cracked, in turn, to produce light distillate, gas and coke fraction. Lastly, the light distillate would produce gases and also coke. In this model it is considered that coke formation occurs from heavy distillate (H) and light distillate (L) and that it would not occur directly from plastic (P).

The results of the kinetic constants obtained showed that the most important reactions are those that generate heavy distillate (k_1) and light distillate (k_2) from plastic and to a lesser extent the generation of gases (k_3). Specifically, it is observed that the cracking of plastic to gases (k_3) depends to a greater extent on temperature, being very similar to k_2 only at higher temperatures (525 ^{o}C).

If this lumps kinetic model for plastic hydrocracking is compared with the model of VGO hydrocracking, there is a great similarity once the plastic is transformed into distillates. A cascade reaction scheme (series–parallel) is carried out from the heaviest to the lightest products. Furthermore, the plastic kinetic model contemplates that coke can be produced from both heavy and light distillate. Furthermore, this model also does not contemplate the reversibility of coke formation.

1.5.2 Continuous lumps models

Simplicity is the main advantage of the discrete lumping approach. However, increasing the number of lumps increases the number of kinetic parameters notoriously. To avoid defining a large number of *k* values, it would be more practical to define a continuous function relating the reactivity of the i-type species to one of its properties. Then, the continuum lumping assumes that the properties

of each individual component (e.g., reactivity, concentration, volatility) are described through suitable component indexes, such as the boiling point or the molecular weight: the methodology is particularly useful when the number of components is large (usually greater than twenty) [289].

Laxminarasimhan et al. [290] developed a model based on the continuous lumping theory to describe the hydrocracking of vacuum gas oil and proposed a model formulation to determine the concentration distribution of the reaction mixture at any given residence time. In this theory, the blend is considered to form a continuous blend with respect to its species type, boiling point, molecular weight, etc. The model considers properties of the reaction blend, the reaction pathways and the associated selectivity of the reactions.

The parameter that characterizes the mixture is the true distillation curve or TBP (True Boiling Point). The main concept in this formulation is that rate constant of hydrocracking is assumed as a monotonic function of the TPB, and the mass balance equations are reformulated by considering the reaction rate constant as a continuous variable. During the reaction, the distillation curve of the blend changes continuously in the reactor and with increasing residence time most of the heavier components become lighter components. A normalized TBP curve as a function of an index (θ) is used instead of the TBP curve. If C(θ,t) is the value of the concentration distribution function corresponding to a normalized TBP θ for a given time t, C(θ,t). The dθ will be a fraction of the species with a corresponding boiling point to the normalized interval TBP from θ to θ+dθ.

$$\theta = \frac{\mathrm{TBP} - \mathrm{T_{min}}}{\mathrm{T_{max}} - \mathrm{T_{min}}} \tag{1.1}$$

where TBP_{max} and TBP_{min} respectively represent the maximum and minimum possible boiling points of the blend corresponding to the lightest and heaviest components present in the reaction media.

Now, it is required to define the transformation function from the normalized TBP, θ, and the species reactivity, k (the reaction rate constant). This transformation can be described as a monotonic power law type [290]:

$$\frac{\mathrm{k}}{\mathrm{k_{max}}} = \theta^{1/\alpha} \tag{1.2}$$

where k is the reactivity or rate constant, k_{max} is the reactivity of the species with the highest TBP, namely, θ = 1, and α is a model parameter.

The equations of the model are formulated as a function of reactivity according to the procedure proposed by Chou and Ho [291]. For an instant t:

$$C(\theta, t).\, d\theta = c(k, t).\, D(k).\, dk \tag{1.3}$$

To express the equation with k as the independent reactivity, a transforming operator is needed. D(k) can be considered as a species-type distribution function. D(k).dk indicates the number of species with reactivity between k and k+dk. This approach has the advantage that there is no concentration distribution function, where c(k,t) is the concentration of the component with reactivity k.

Then, the concentration distribution function C(θ,t) must pass into the functional form c(k,t). The species-type distribution function D(k) can be considered as a Jacobian transformation of coordinates i - k (where i is the index of the species) and can be represented as:

$$D(k) = \frac{di}{dk} = \frac{di}{d\theta}.\frac{d\theta}{dk} \tag{1.4}$$

By definition of the pseudocomponents with respect to θ, the species indices i are equally spaced in the *i* axis. Assuming the total number of species in the mixture is N (N → ∞), the di/dθ term can be approximated to N. In addition, the dθ/dk term can be obtained by differentiating eq (1.2). Hence, D (k) becomes:

$$D(k) = \frac{N\alpha}{k_{max}^{\alpha}} = k^{\alpha-1} \tag{1.5}$$

The core of the model is a mass balance of species with k reactivity, which can be expressed with the integrodifferential equation:

$$\frac{dc(k,t)}{dt} = -k\, c(k, t) + \int_{k}^{k_{max}} p(k, K) K\, c(K, t) D(K) dK \tag{1.6}$$

where p(k,K) is the yield distribution function that determines the amount of species formed with k reactivity from the hydrocracking of species with reactivity K. The above equation can be solved numerically if we have the function p(k,K). This function p(k,K) must satisfy the following conditions:

(i) The value of p(k,K) must be 0 at k = K, since the reactivity species k cannot be cracked to give itself. p(k,K) = 0 for k > K, since in hydrocracking there is no dimerization, etc.

(ii) p(k,K) must satisfy the following mass balance criterion:

$$\int_{0}^{K} p(k, K)\, D(k) dk = 1 \tag{1.7}$$

(iii) p(k,K) must be a finite, small value and not zero when k = 0, which is given because when a component of reactivity K cracks, even the least reactive compounds are formed, although if they are traces.

(iv) p(k,K) must always be positive.

This distribution function can be approximated in the model by a skew-Gaussian distribution function, obtained from experimental data based on the reactivity of various model compounds.

$$p(k,K) = \frac{1}{S_0\sqrt{2\pi}}\left\{\exp\left[-\left(\frac{\left(\frac{k}{K}\right)^{a_0}-0.5}{a_1}\right)^2\right] - A + B\right\} \tag{1.8}$$

where: $$A = e^{-(0.5/a_1)^2} \tag{1.9}$$

$$B = \delta\left(1-\frac{k}{K}\right) \tag{1.10}$$

Parameters a_0, a_1 y δ are specific to each system and are adjustable. The parameters a_0 and a_1 determine the location of the maximum reactivity in the interval $k \in (0,K)$. δ is another model parameter, which accounts for the fact that p(k,K) should be a finite small quantity when k = 0. The term A, defined by eq. (1.9), comes from the condition p(k,K) = 0 when k = K. The parameter S_0 defined in eq. (1.8) is estimated as follows:

$$S_0 = \frac{1}{\sqrt{2\pi}}\int_0^K \left\{\exp\left[-\left(\frac{\left(\frac{k}{K}\right)^{a_0}-0.5}{a_1}\right)^2\right] - A + B\right\} D(K)\, dk \tag{1.11}$$

The distribution function chosen satisfies the four criteria set out above. The continuous lumping model formulated above consists of five parameters: k_{max}, α, a_0, a_1, and δ. These parameters can be estimated by fitting the experimental data to the model.

The solution procedure consists of solving the integral part of the integral differential equation (eq. 1.6) and then evaluating c(k, t) in that differential equation using a technique of moving forward in time. To do this, the integral part has to be solved at each instant of time for the entire K space (that is, for each of the K species). The integration is carried out by means of a Gaussian quadrature, with some linearization of the function c(K, t).

To obtain the desirable accuracy, a large number of species (pseudo-components) should be considered ($N \to \infty$). Accordingly, the K plane is divided in N nodes (the TBP experimental data (in the range from TBP_{min} to TBP_{max}) is divided into N equally spaced divisions), and the difference equation for any i^{-th} node and a time differential δt, assuming a linear interpolation for the function c(K, t) between two successive nodes, is written as:

$$\frac{\left(c(k_i,t)-c(k_i,t-\delta t)\right)}{\delta t}=c(k_i,t)\left[-k_i+I_1(k_i,k_{i+1})\right]+\sum_{j=i+1}^{N-1}c(k_j,t).I_1(k_j,k_{j+1}) + \sum_{j=i+1}^{N-1}c(k_j,t).I_2(k_j,k_{j+1}) \tag{1.12}$$

$$I_1(k_j,k_{j+1})=\int_{k_j}^{k_{j+1}}p(k_i,K)\frac{(K-k_{j+1})}{(k_i-k_{j+1})}D(K)d(K) \tag{1.13}$$

$$I_2(k_j,k_{j+1})=\int_{k_j}^{k_{j+1}}p(k_i,K)\frac{(K-k_j)}{(k_{j+1}-k_i)}D(K)d(K) \tag{1.14}$$

The initiation of the numerical solution in this case occurs at the N-th node (the one with the highest reactivity) since these molecules only disappear, they are not formed. Then for each time increment:

$$c(k_N,t)=c(k_N,t-\delta t).e^{-k_N\delta t} \tag{1.15}$$

where $k_N = k_{max}$.

The above equation is solved for all nodes and time increments to obtain c(k,t). The solution can be integrated to find the yield of a particular fraction (given in the TBP) based on:

$$C_{1,2}(t)=\int_{k_1}^{k_2}c(k,t).D(k).dk \tag{1.16}$$

where k_1 and k_2 correspond to the reactivities at the initial and final boiling points of the cut of interest, and $C_{1,2}(t)$ is the weight fraction of the desired cut. The solution method is efficient and easy to implement.

Lababidi and AlHumaidan [292] studied the hydrocracking associated with the hydrotreatment of atmospheric residue (AR) for three types of conventional hydrotreating catalysts (hydrodesulfurization (HDS), hydrodemetalization (HDM), and hydrodenitrogenation (HDN)) at three space velocities and three operating temperatures and they developed a kinetic model based on the continuous lumping approach. The developed continuous lumping models predicted the concentration profile of the complete true boiling point (TBP) range with reasonably high accuracy.

Adam et al. [289] applied the continuum lumping methodology to the hydrocracking of Fischer–Tropsch waxes (n-paraffins). They investigated the role of the type-distribution function by employing two expressions of such function and by studying how it affects the model predictions. The results were not very

conclusive. Increasing the temperature and the residence time resulted in an increase of the error percentage between the model and experimental data, perhaps due to that the model included only hydrocracking reactions.

Elizalde and Ancheyta [293] studied the kinetics of the hydrocracking of residue and catalyst deactivation by using the continuous kinetic lumping approach. They found that the parameters of the continuous kinetic model showed dependence with time on stream and temperature, confirming the fact that these parameters are a function of catalyst activity.

Narasimhan et al. [294] and Basak et al. [295] extended the model explained above for the case of blends divided into continuous mixtures of paraffinic, naphthenic and aromatic components. In addition to the hydrocracking reactions that form compounds within the same family, this model contemplates the formation of paraffins from naphthenes, of paraffins from aromatics, and of naphthenes from aromatics. The models require the definition of a concentration function, a reactivity function, and a species distribution function for each family of compounds, as well as 6 different product distribution functions.

Recently, Becker et al. [296] have proposed a continuous lumps model, with distinction between three families (paraffins/naphthenes/aromatics, PNA). The hydrocarbon mixture is also considered as continuous distribution of true boiling point (TBP). The network of continuous lumping model with PNA families, in addition to the hydrocracking reactions that form compounds within the same family, contemplates also the formation of paraffins from naphthenes and of naphthenes from aromatics. The model is similar to that proposed by Laxminarasimhan et al. [290] but with two important improvements: i) several chemical families as paraffins, naphthenes and aromatics are taken into account, and ii) inhibitors effects such as nitrogen and the partial pressure of ammonium are taken into account. The distribution of paraffins, naphthenes, and aromatics with TBP is required as input for the model. They measured the PNA content of predefined cuts (<150, 150–250, 250–370, and >370 ^{o}C) and this allowed the distillation curves of the three families to be reconstructed by fitting a Weibull distribution to the data [297]. In total, this model requires 28 empirical parameters to be identified.

CHAPTER 2

EXPERIMENTAL

2 EXPERIMENTAL

2.1 FEEDS

2.1.1 Vacuum gasoil (VGO)

The VGO (Vacuum Gas Oil) has been supplied by Petronor S.A. refinery (Muskiz, Vizcaya). It is a mixture of gas oil from different refinery units, most of the VGO comes from the vacuum distillation unit but it has small amounts of gas oil from visbreaking and coking units. This gas oil has been previously desulfurized, so it has low sulfur concentration (510 ppm), which is shown in Table 2.1 together with other physicochemical properties of VGO.

2.1.2 HDPE pyrolysis oil

The pyrolysis oil from HDPE (PO) has been provided by Gaiker Technology Center. PO comes from HDPE pyrolysis in a PARR autoclave reactor model 4570 operating in a discontinuous regime. The reaction system consists of an AISI 316 stainless steel tank with a useful volume of 2 L, an electric heating jacket and an internal coil where open water system is used as a cooling system. The reactor can operate up to 500 °C and 80 bars. The PO was obtained at atmospheric pressure and 430 °C for 38 min of reaction time under N_2 atmosphere. The main physicochemical properties of PO are shown in Table 2.1.

2.1.3 High density polyethylene (HDPE)

Polyethylene is a linear homopolymer made up of ethylene olefin monomers (ethene) as depicts Figure 2.1. High-density polyethylene (HDPE) has low branching degree in comparison with low density polyethylene (LDPE) [298,299]. For the present study, the HDPE was supplied by Dow Chemical Iberica (Tarragona) in the form of pellets of approximately 4 mm. Before being used, these pellets have been grinded (d_P < 0.5 mm) under cryogenic temperature. The physicochemical properties are collected in Table 2.1.

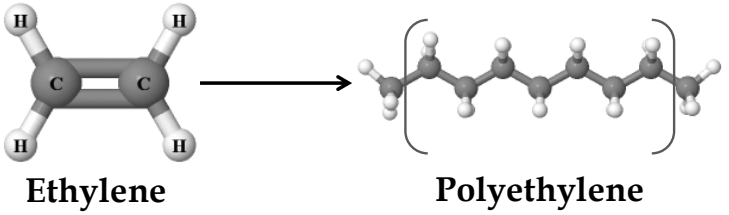

Figure 2.1 Ethylene molecule and polyethylene chain.

2.1.4 Polypropylene (PP)

Polypropylene (PP) is a polymer made up of propylene (propene) monomers (Figure 2.2). For the present study the PP was also provided by Dow Chemical Iberica (Tarragona) in pellets form of 4 mm and it was also grinded under the same conditions (d_P < 0.5 mm) before being used. This physicochemical properties are in Table 2.1.

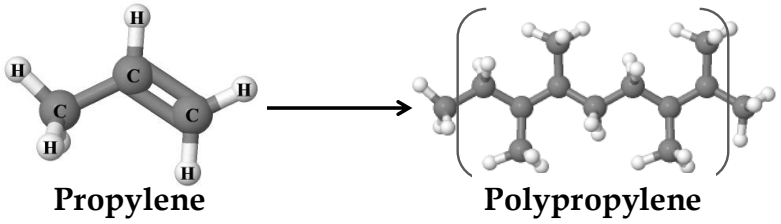

Figure 2.2 Polypropylene molecule and polypropylene chain.

2.2 FEEDS CHARACTERIZATION

Table 2.1 shows the main physicochemical properties of the feeds. The VGO and PO densities have been measured experimentally. To obtain this value, a 10 mL pycnometer was filled with the feed and weighted in a precision balance. The measure was done by tripled and the average value is depicted in Table 2.1.

Table 2.1 Main physicochemical properties of the feeds.

Properties	VGO	PO	HDPE	PP
Physical properties				
density at 25 °C (g mL^{-1})	0.89	0.82	0.94	0.89
viscosity at 37.8 °C (cSt)	34.2	2.82	–	–
av. molecular weight (g mol^{-1})	377	212	46200	50000
higher calorific value (MJ kg^{-1})	52	43	50	50
Simulated distillation (°C)				
IBP–FBP	156–519	69–513	–	–
T_{50}–T_{95}	415–491	306–479	–	–
Distillation fractions (wt%)				
naphtha (< 216 °C)	0.17	26.5	–	–
LCO (216–350 °C)	4.48	33.1	–	–
HCO (> 350 °C)	95.4	40.4	–	–
Elemental analysis (wt%)				
C	87.3	79.0	85.7	85.7
H	12.5	12.5	14.3	14.3
N	–	–	–	–
O	–	8.50	–	–
S (ppm)	510	–	–	–
Composition (wt%)				
paraffins	14.0	28.3	–	–
naphthenes	35.3	3.06	–	–
olefins	–	53.9	–	–
1–ring aromatics	20.3	6.82	–	–
2–ring aromatics	12.4	4.06	–	–
3^{+}–ring aromatics	15.8	3.82	–	–
Sulfur compounds	2.3	–	–	–

The kinematic viscosity has been obtained experimentally. For this, a Ubbelohde-Viscometer 53823 type IIC placed inside a thermal bath, was used. The sample (VGO or PO) is loaded in the viscometer and waits until reach the requiring temperature (37.8 ºC). Subsequently, the time required for the sample to pass through the viscometer is taken. This measurement has been repeated 6 times. The average of these 6 measurements is the one used to calculate the viscosity according to the eq. (2.1). In this equation, the viscosity is calculated in centistokes (cSt) and it is equal to a constant K (which depends on the capillarity of the viscometer and it is tabulated) multiplied by the difference between the average time in the speed test (the average time in seconds, *t*) and the correction factor (*υ*, in seconds) which is typical of the viscometer model and the measurement time (provided by Ubbelohde).

$$v = K(t - \upsilon) \tag{2.1}$$

The average molecular weight for VGO and PO has been calculated using the procedure for molecular weight of heavy petroleum fractions described in section 2B2.3 of the American Petroleum Institute (API) Technical Data Handbook, which allows estimating this value for a mixture of heavy hydrocarbons. As it is explained in this procedure, it is necessary to know the viscosity of the fractions at 100 and 210 ºF. Therefore, the procedure 11A4.2 in API Technical Data Handbook was used for estimating the liquid viscosity of undefined mixtures as a function of temperature at low pressure.

The higher calorific value (HCV) has been determined with the Dulong formula (eq. (2.2)) for all the feedstocks. This equation takes into account the elemental composition of the feed (Carbon, Hydrogen, Oxygen and Sulfur) to estimate the HCV.

$$HCV = 0.01\left[8.08C + 34.5\left(H - \frac{O}{8}\right) + 2240S\right] \tag{2.2}$$

where elements (C, H, O and S) are in weight percentage and HCV is obtained in kcal/kg.

2.2.1 Composition

2.2.1.1 Vacuum gas oil (VGO)

The VGO composition was determined by Repsol S.A. in Móstoles Technology Center following the ASTM D2786 standard. The analysis was performed by ionizing high voltage mass spectrometry and the results are shown in

Table 2.1. Eighteen types of compounds have been identified, which have been grouped according to their nature (14 wt% paraffins, 35.3 wt% naphthenes, 48.5 wt% aromatics and 2.3 wt% sulfur compounds).

2.2.1.2 Plastic pyrolysis oil (PO)

The HDPE pyrolysis oil (PO) composition was determined by bi-dimensional chromatography on an Agilent Technologies 7890A Gas Chromatograph coupled with an Agilent Technologies 5975C XL on-line mass spectrometer. The gas chromatograph consists of: (i) two columns: a non-polar DB-5 ms J&W 122-5532 (length 30 m; internal diameter 0.25 mm; thickness 0.25 μm) and a polar HP-INNOWAS (length 5 m; internal diameter 0.25 mm; thickness 0.15 μm), (ii) an Agilent Technologies 7683B autosampler, and (iii) a flame ionization detector (FID). The method used for the analysis is shown in Table 2.2.

Table 2.2 GC method used to analyze the HDPE pyrolysis oil (PO) composition in a GCxGC-MS.

Section	Variable	Value
Oven	T_0 (°C)	50
	t_0 (min)	1
	R_1 (°C min^{-1})	2
	T_1 (°C)	260
	t_1 (min)	40
Injector	T (°C)	300
	P (bar)	1.83
	1st column flow (mL min^{-1})	0.75
	2nd column flow (mL min^{-1})	35
	Split ratio	50:1
FID	T (°C)	350
	H_2 Flow (mL min^{-1})	20
	Air Flow (mL min^{-1})	450
	Make up Flow (mL min-1)	20

Figure 2.3 shows a section of a typical bi-dimensional chromatogram for PO, where on the ordinate axis (x) the compounds from lowest to highest boiling point can be observed from left to right. On the abscissa axis (y), the compounds from the highest to the lowest polarity are shown from the lower zone to the upper zone. In such way, compounds can be separated according to their nature (paraffins, olefins, naphthenic and aromatics). Furthermore, the MS ease the identification task.

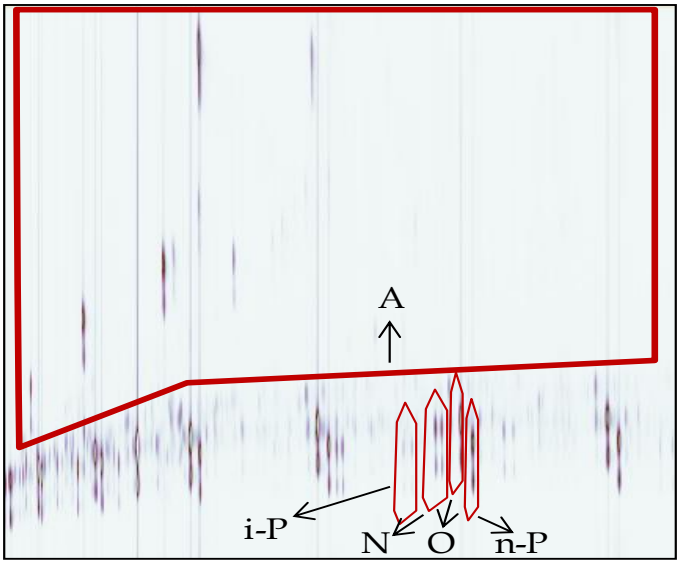

Figure 2.3 A fraction of the PO chromatogram using bi-dimensional chromatography where they can be observed i-paraffins (i-P), n-paraffins (n-P), naphthenics (N), olefins (O) and aromatics (A).

The results of the analysis are shown in Table 2.1. Most of hydrocarbons are olefins followed by paraffins, aromatics and naphthenic (53.9, 28.3, 14.7 and 3.1 wt%, respectively). The distribution is very different in comparison with VGO, which is mainly made of aromatics and naphthenes.

2.2.2 Elemental analysis

Elemental analysis has been carried out at the SGIKER service at the University of the Basque Country (UPV/EHU). A LECO apparatus with two modules has been used: (i) TruSpec CHN Macro that determines the content of C, H and N and (ii) TruSpec S for the content of S. The analysis consists of 3 stages: purge, combustion and analysis. Therefore, after the purge stage, the sample is burned in a furnace at 950 ^{o}C in oxygen atmosphere. Then, collected gases are measured via infrared (IR), H_2O detector and a thermal conductivity detector (TCD) to determine the C content, the H content and the N content in the sample. Furthermore, TruSpec S module has a high sensitivity IR-detector for SO_2 analysis. The amount of oxygen is calculated by difference and results are shown in Table 2.1.

The results from the analysis depict that the composition of both plastics are quite similar and that none of them has N nor S. The PO has the lowest C and H content, has a small amount of oxygen and also has no N or S. Finally, the VGO

displays the highest C content. Besides, 510 ppm of sulfur remains in this feedstock although it was previously hydrotreated.

2.2.3 Simulated distillation

Simulated distillation is a test that emulates a real distillation and makes it possible to know the distillation curve of a stream. Simulated distillation of VGO and PO has been performed in accordance with ASTM-D2887. The tests were performed on an Agilent 6890 Series GC System chromatograph with a flame ionization detector (FID) and a Simdis D-2887 Fast/ext column of 10 m x 0.53 mm x 0.88 μm. The analysis method is shown in Table 2.3.

Table 2.3 Conditions of the method used for simulated distillation analysis.

Section	Variable	Value
Oven	T_0 (°C)	40
	t_0 (min)	5
	R_1 (°C min^{-1})	10
	T_1 (°C)	125
	t_1 (min)	0
	R_2 (°C min^{-1})	5
	T_2 (°C)	155
	t_2 (min)	0
	R_3 (°C min^{-1})	10
	T_3 (°C)	300
	t_3 (min)	30
Injector	T (°C)	350
	P (bar)	0.078
	Column flow (mL min^{-1})	9.4
	Split ratio	2.5:1
FID	T (°C)	320
	H_2 flow (mL min^{-1})	40
	Air flow(mL min^{-1})	450
	Make up flow (mL min^{-1})	20

The VGO and PO chromatograms are shown in Figure 2.4a. It can be seen that compounds in PO appear since lower retention times while, the first peaks in VGO

arises after 20 min, denoting its heavier nature. Figure 2.4b shows the simulated distillations curves after processing the chromatographic signals; where the percentage of distillate (in mass fraction) versus the temperature is plotted. Results (collected in Table 2.1), display the percentages of naphtha (boiling range <212 ^{o}C), light cycle oil (LCO) (boiling range 212-343 ^{o}C) and heavy cycle oil (HCO) (boiling range> 343 ^{o}C).

There is a big difference between PO and VGO distillation curves, since VGO is much heavier than PO. The PO contains a greater amount of light compounds and more than 59 wt% of the distillate is obtained at temperatures below 343 ^{o}C. For VGO, however, less than 5 w% of the distillate is obtained below that temperature.

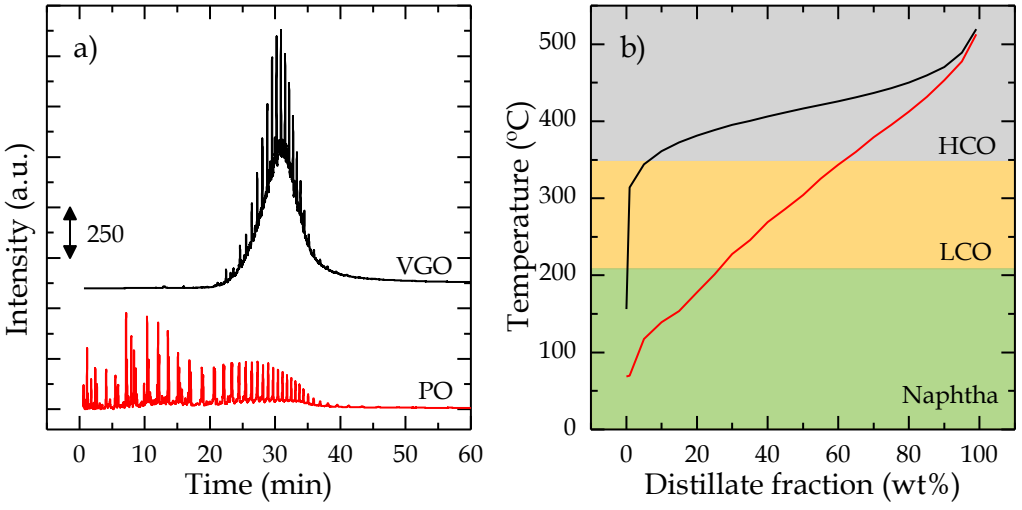

Figure 2.4 Chromatograms (a) and simulated distillation curves (b) for VGO and PO.

2.2.4 Thermogravimetric analysis (TGA)

The feedstocks were pyrolyzed at programmed temperature to study their thermal decomposition. This analysis records the mass loss when temperature rises with a programmed ramp. The equipment used is a TGA Q5000-IR TA Instruments thermobalance. After loading the sample (around 10 mg), air was purged in an inertization step passing 50 mL min^{-1} of nitrogen while the temperature was stabilized at 40 ^{o}C. Then, maintaining the nitrogen flow (50 mL min^{-1}), temperature was risen up to 800 ^{o}C (using a ramp of 5 ^{o}C min^{-1}) and held for 10 min.

Figure 2.5a shows the weight loss of the samples with temperature, thus, the temperature at which degradation of the samples begins. The PO contains volatile compounds and therefore a mass loss is seen almost from the beginning of the analysis. However, a certain temperature is required for other samples to start the

decomposition: 125, 380 and 410 ºC for VGO, PP and HDPE, respectively. So, HDPE shows the highest thermal resistance. The temperature at which each sample completes the pyrolysis is, approximately, 275 ºC for PO and VGO and around 500 ºC for PP and HDPE.

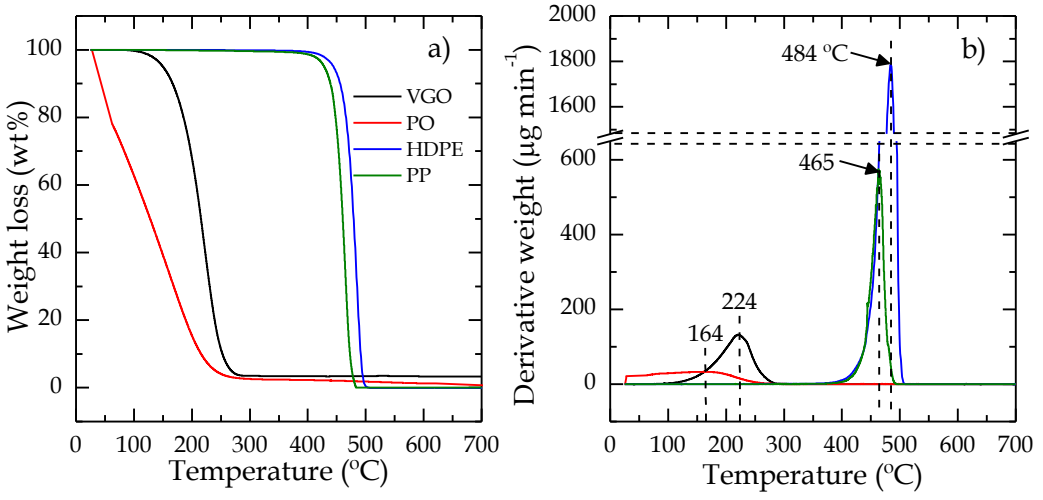

Figure 2.5 Thermogravimetric analysis (TGA) of feedstocks: (a) weight loss and (b) weight loss derivative.

Figure 2.5b displays the weight derivative signal (DTG) when temperature increases. The peak maximum in Figure 2.5b corresponds to the temperature at which the degradation rate is the highest. PO shows a broad profile due to its heterogeneous complex composition and its wide boiling point range (shown in the simulated distillation). The VGO begins to crack a temperature higher than PO. Furthermore, the derivative weight depicts a more defined peak with a maximum at 224 ºC. Nevertheless, the peak maximum take place a temperature lower than that obtained with plastics. Among plastics, PP is the first one to begin to pyrolyze. It has a narrow and sharp DTG profile with a maximum at 465 ºC. Finally, HDPE requires the highest temperature to be pyrolyzed (484 ºC) and the DTG profile is also slim and sharp.

2.3 CATALYSTS

Six catalysts have been used in the screening step that is carried out in section 3.2. Three of them are commercial catalysts: CoMo/Al, NiMo/SiAl and NiW/HY, which are commonly used in refinery process for lighten oil fractions (NiW/HY), sulfur removal (CoMo/Al) and hydrodearomatization (NiMo/SiAl catalyst) [150,300]. On the other side, a PtPd/HY catalyst has been in-house prepared via ion exchange using a ultrastable zeolite and following the procedure described in literature [108] for synthesis of the PtPd/HY catalyst and summarized in Figure 2.6. Besides, NiW/SiAl also was in-house prepared trough the synthesis of SiO_2-Al_2O_3 and a subsequent wet impregnation following the procedure explained in Figure 2.7. Furthermore, NiW/MCM-41 was in-house prepared through the wet impregnation of Ni and W on commercial MCM-41 support following the same procedure for the preparation of NiW/SiAl catalyst (Figure 2.7).

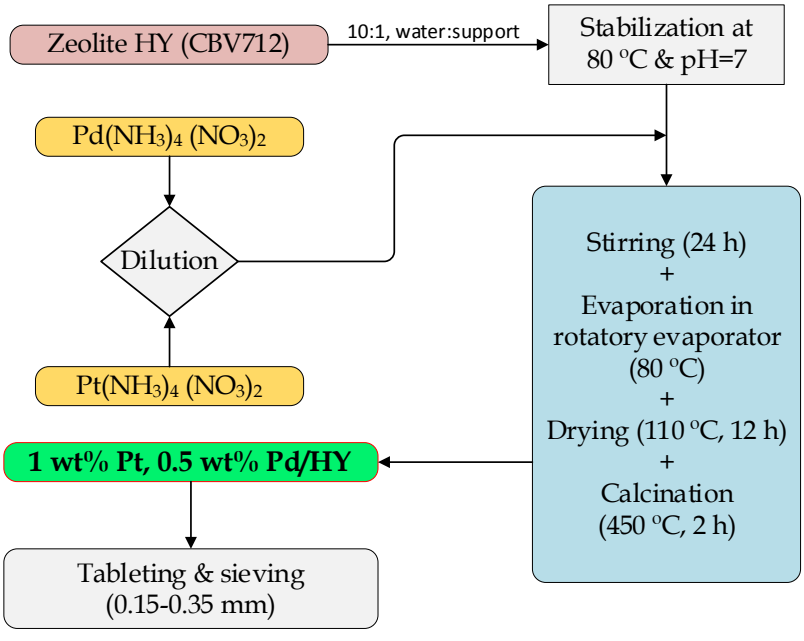

Figure 2.6 Scheme of the synthesis procedure of PtPd/HY catalyst. Adapted from Castaño et al. [140].

The zeolite HY used (ultrastable zeolite CBV712) is supplied by Zeolyst International in the ammonium form with a SiO_2/Al_2O_3 ratio of 12. Metals have been incorporated starting from two aqueous solutions, $Pt(NH_3)_4(NO_3)_2$ (Alfa Aesar) and $Pd(NH_3)_4(NO_3)_2$ (Strem Chemicals), diluted in double distilled water until obtaining a Pt and Pd concentration of 2500 ppm for each one.

Before incorporating the metals, the support has been calcined to obtain the acidic form according to the following steps: (i) 2 h at 400 °C (5 °C min^{-1}), (ii) 15 h at 500 °C (5 °C min^{-1}), and (iii) 2 h at 550 °C (5 °C min^{-1}). Then, the powder of HY

support is suspended in double distilled water (10:1 water:support) at 80 ºC. Furthermore, the pH is measured and controlled at pH = 7 by adding NH_3 or NH_4NO_3 solution drops when necessary. Subsequently, to add the desired amount of metals, the required amount of aqueous solutions is dropwise added to the diluted support. Once adsorption equilibrium has been reached (~24 h), a rotavapor removes the excess water. After that, catalyst is dried in an oven at 110ºC for 24 h and finally calcined at 450 °C for 2 h following a temperature ramp of 5 °C min^{-1}.

The synthesis of the support (SiO_2-Al_2O_3) of the NiW/SiAl catalyst and metal impregnation is depicted in Figure 2.7.

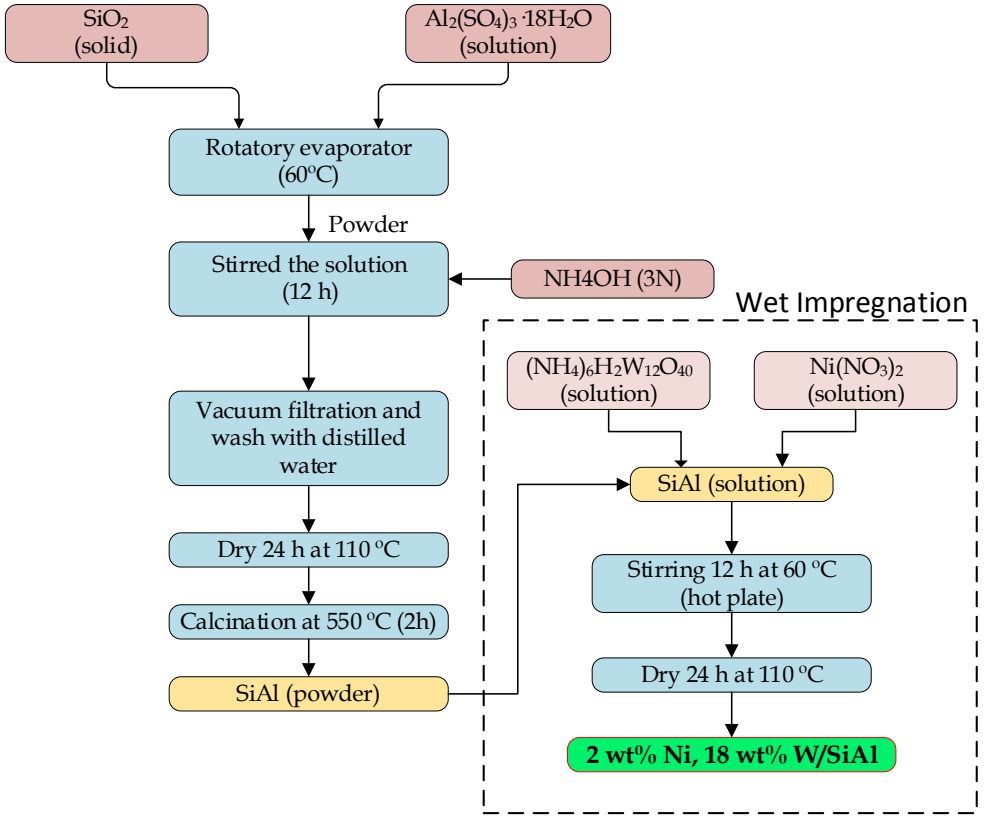

Figure 2.7 Scheme of the synthesis procedure of NiW/SiAl catalyst.

In order to obtain 300 g of SiO_2-Al_2O_3 at 15 wt% of Al_2O_3, first a solution of $Al_2(SO_4)_3 \cdot 18H_2O$ (Probus) at 10% by weight has been prepared and the silica gel 60 (Merck) has been sieved until obtaining 255 g of SiO_2 with a particle size of 0.25-0.35 mm. The SiO2 was then introduced into a 2 L balloon and connected to the rotary evaporator, while the burette was filled with the previously prepared $Al_2(SO_4)_3 \cdot 18H_2O$ solution and coupled to the inlet valve of the rotary evaporator. The rotary evaporator (60 ºC) was started and the silica gel was impregnated with the $Al_2(SO_4)_3 \cdot 18H_2O$ solution, keeping it constantly wet in order to guarantee the homogeneous impregnation of the solid. Once all the solution has been added and

evaporated, in order to extract the Al^{3+} that has not managed to penetrate the structure of the silica gel, it has been immersed in a solution of NH_4OH (3 N) in which these ions precipitate in the form of $Al(OH)_3$. To guarantee its elimination, the solution was stirred for 12 h. After 12 h, it was filtered under vacuum and washed with abundant distilled water until the conductivity of the solid was less than 50 μS; then it was dried 24 h in an oven at 110 ºC and calcined for 2 h in a muffle at 550 ºC. Finally, the 2 wt% of Ni and 18 wt% of W addition was through wet impregnation. Two solutions from $Ni(NO_3)_2$ and $(NH_4)_6H_2W_{12}O_{40}$ were prepared and added to SiAl in a beaker which was heated at 60 ºC and stirred in a hot plate. After 12 h, the powder was dry in an oven at 110 ºC during 24 h, and the catalyst is ready to tableting and sieving.

2.3.1 Catalysts characterization

2.3.1.1 Adsorption-desorption isotherms of N_2

The textural properties of the catalysts (specific surface, pore volume and pore size distribution) have been determined from the adsorption-desorption isotherms of N_2 at -196 ºC, using a Micromeritics ASAP 2010 apparatus. The experimental methodology implies a pretreatment where the sample is degassed at 150 ºC for 8 h under vacuum conditions (2 10^{-3} mmHg), to eliminate any impurities, followed by the adsorption-desorption of N_2 (99.9995 % purity) in multiple equilibrium stages of relative pressure from 0.01 to 1, until the sample reaches the saturation point at cryogenic temperature (liquid N_2).

The specific surface area (S_{BET}) is calculated according to the BET equation (Brunauer-Emmett-Teller) in the range of relative pressures (P/P_0) between 0.01 and 0.2. The micropore area (S_{micro}) has been determined by the t-method, which is based on the Harkins-Jura equation. Finally, the mesopore surface (S_{meso}) was determined by the difference of S_{BET} and S_{micro}. The pore volume distribution is calculated by applying the BJH method to the N_2 adsorption branch. The total pore volume was calculated by t-plot method [301].

2.3.1.2 Inductively coupled plasma with atomic emission spectroscopy (ICP-AES)

The metal content of the catalysts has been measured by inductively coupled plasma with atomic emission spectroscopy (ICP-AES) on the Geology Department of the Faculty of Science and Technology of the University of the Basque Country (UPV/EHU). It was used an X7-II Thermo quadrupole mass spectrometer (Q-ICP-MS) from Perkin Elmer, equipped with an Xt interface, shielded torch and

concentric nebulizer. The equipment calibration was carried out by using multielemental solutions of 100 ppm. Furthermore, for the control of instrumental drift, a Rh solution has been used as an internal standard, which is added online.

A mixture of HNO_3:HF was added to about 50 mg of sample in closed containers of PFA (Savillex) for 24 hours at 90 °C. During the evaporation of the solution obtained, $HClO_4$ is added to avoid the formation of insoluble fluorides. The residue is taken up in HCl and heated overnight at 90 °C, then is dried and finally taken up in HNO_3. The solution obtained has been diluted to a factor of 1:450 in double distilled water for the determination of the metal content.

2.3.1.3 Temperature-programmed-desorption of tert-butylamine ($TPD_{t\text{-}BA}$)

The acidity properties of the fresh catalysts (total acidity and acid strength) have been determined by adsorption and TPD/cracking profile of t-butylamine (t-BA), which is a suitable technique for the characterization of catalysts with low and medium acidity. Furthermore, t-BA has the ability of characterize strongly acid sites, with heats of adsorption greater than 200 kJ mol^{-1} [302]. The adsorption and TPD tests have been carried out in a Setaram TG-DSC 111 calorimeter, connected in line with a ThermoStar mass spectrophotometer (Balzers Instruments). Besides, the t-BA is injected in the system using a Harvard pump. The total acidity is quantified from the amount of chemisorbed base at 100 °C, in $mmol_{t\text{-}BA}\ g_{cat}^{-1}$, while the acid strength is defined as the heat released during the adsorption of the base, kJ $mmol_{t\text{-}BA}^{-1}$.

The experimental procedure to carry out the differential scanning calorimetry of t-BA consists of the following steps: i) the sample is pretreated to eliminate water and possible impurities by means of sweeping with He (160 mL min^{-1}) at 550 °C for 30 min; ii) stabilization of temperature at 100 °C with a He flowrate of 20 mL min^{-1}; iii) saturation of the sample by continuous injection of t-BA (150 µL min^{-1}) at 100 °C; iv) sweep with He (20 mL min^{-1}) at 100 °C to remove the physisorbed adsorbate; and v) TPD/cracking of chemisorbed t-BA through heating ramp. To follow both the t-BA and the cracked butene, the spectroscopic lines m/e=58 and m/e=56 were used, respectively. Therefore, the higher the acid strength of the active sites, the lower the cracking temperature of t-BA [303].

2.3.1.4 Fourier-transform infrared spectroscopy (FTIR) of adsorbed pyridine

The nature of the acidic sites (Brønsted or Lewis) has been determined by Fourier-transform infrared spectroscopy (FTIR) of adsorbed pyridine. The analysis

has been carried out in a Thermo Nicolet 6700 apparatus, which has a Specac transmission catalytic chamber.

The procedure is as follows: i) a pill from catalyst powder (~20 mg) is introduced into the chamber; ii) the chamber is heated up to 380 °C with a heating rate of 5 °C min^{-1} under vacuum (0.75 bar) for 30 min to remove possible impurities from the catalyst surface; iii) temperature is stabilized at 150 °C; iv) a pyridine pulse is injected, subsequently the pill is subjected to vacuum at 150 °C for 15 min to eliminate physisorbed pyridine and FTIR spectrum is recorded with a frequency of 2 cm^{-1}, repeating the cycle until the spectrum of the sample displays a saturation.

To identify the nature of the acidic sites is necessary to analyze the bands related to the bonded pyridine which appears at wavelengths between 1400–1600 cm^{-1} in the spectra. Specifically, Brønsted acidic sites protonate the pyridine to form pyridinium ions that display C–C stretching vibrational frequencies (and the consequent peak) at 1545 and 1634 cm^{-1}. On the other hand, pyridine can be detected by the stretching of C–C bond molecularly coordinated in Lewis acid sites, which appears at 1455 and 1610 cm^{-1} [304]. Then, the spectrum taken is deconvoluted to know the area of these peaks (Brønsted and Lewis), which can be correlated with the number of micromoles of pyridine per gram of sample adsorbed according to Pieta et al. [305]. It has to be pointed out that for those computations, it is necessary to know the coefficients of molar extinction (Ø) of both IR bands, being 1.67 and 2.22 cm μmol^{-1} for Brønsted and Lewis acidic sites, respectively [306].

2.3.1.5 X-Ray Diffraction (XRD)

X-ray diffraction (XRD) analysis was also performed to characterize the crystalline structure of the catalysts. This non-destructive technique provides information on crystallographic orientation, phase identification, crystal size and even the Si/Al ratio in the crystal structure, among others. These analyses were carried out on the SGIker service at the University of the Basque Country (UPV/EHU) using a PANalytical Xpert PRO diffractometer, equipped with copper tube ($\lambda Cu_{K\alpha average}$=1.5418 Å, $\lambda Cu_{K\alpha1}$=1.54060 Å and $\lambda Cu_{K\alpha2}$= 1.54439 Å), vertical goniometer (Bragg-Brentano geometry), programmable divergence slit, automatic sample exchanger, graphite secondary monochromator and PixCel detector. The analyses were carried out at 40 KV and 40 mA collecting the data from 5 to 80º 2theta.

2.3.1.6 X-Ray Fluorescence (XRF)

The composition of the catalysts (Si/Al atomic ratio and total metal charge) has been measured on the SGIker service at the University of the Basque Country (UPV/EHU) using wavelength dispersion X-ray fluorescence spectrometry (WDXRF). A borated glass bead is prepared from the powdered catalyst sample by melting it in a micro-induction furnace. Merck's Spectromelt A12 flux and samples were mixed in a ratio of approximately 20:1. Chemical analysis of the borated beads was carried out under vacuum using a PANalytical Axios model spectrometer equipped with an Rh anode and three detectors: gas flow, scintillation and Xe seal. The calibration curves were established with international standards of rocks and minerals.

2.3.1.7 X-Ray Photoelectron Spectroscopy (XPS)

The X-ray photoelectron spectroscopy (XPS) is used to analyze the catalysts surface and provide qualitative and semi-quantitative elemental composition of the surface. In this case, the XPS analyses were conducted on the SGIKER service at the University of the Basque Country (UPV/EHU) with a SPECS system equipped with Phoibos 150 1D-DLD analyzer and Al Kα (1486.6 eV) monochromatic radiation source. Before the analysis, the apparatus was calibrated using Ag 3d 5/2 peak (368.28 eV). The analysis procedure starts with a wide scan of the sample: step energy 1 eV, dwell time 0.1 s, pass energy 40 eV. After that, a detailed analysis of the detected elements was performed under the following conditions: step energy 0.1 eV, dwell time 0.1 s, pass energy 20 eV with an electron outcome angle of 90°. Finally, the collected data were processed using CasaXPS 2.3.16 software that deconvoluted the peaks according to Gauss-Lorentzian contributions after subtracting the background.

2.3.1.8 Transmission Electron Microscopy (TEM)

The transmission electron microscopy (TEM) analyses have been performed on the SGIker service at the University of the Basque Country (UPV/EHU) using a SuperTwin CM200 Philips microscope (acceleration voltage, 200 kV; resolution, 0.235 nm) equipped with a lanthanum hexaboride filament and EDX microanalysis system. Before the analysis the sample preparation began by i) dispersion in hexanol; followed by ii) deposition and extension of a drop of the solution on a 300 mesh copper grid; iii) coating with a porous carbon film; and, iv) drying of the sample under vacuum.

2.3.1.9 Temperature Programmed Reduction (TPR)

Temperature programmed reduction (TPR) has been carried out to determine the reduction temperature of the different metallic phases on the catalysts and identify possible interactions between the metallic phases and the support. This technique expose the catalysts to a reducing gas flow, generally H_2, diluted in inert gas, with a linear ramp of temperature. The consumption of H_2 is continuously measured and therefore the reduction rate of metallic species is determined. In addition, the TPR analysis complemented with the XRD technique allows identifying the possible species of reducible metals present in each catalyst. TPR tests were performed on an AutoChem II 2920 from Micromeritics equipped with a thermal conductivity detector (TCD).

With the aim of eliminating water or any impurity, an initial sweep of the catalyst sample is carried out with a stream of He, heating the sample up to 200 ^oC with a rate of 10 $^oC\ min^{-1}$ and maintaining it for 30 min. Once the sample is stabilized, it is exposed to a stream of 10 vol% H_2 in Ar (50 $cm^3\ min^{-1}$) and heated from room temperature to 900 °C (heating rate 5 °C min^{-1}), continuously recording the TCD detector signal and temperature. Besides, a 1-propanol/N_2 (liq.) cold trap located between the sample and the detector is used to retain the H_2O that is formed during reduction to avoid interference in the TCD signal.

2.3.1.10 Temperature Programmed Desorption of H_2S (TPD-H_2S)

To obtain information on the nature and strength of the metal-sulfur interactions with the support, the temperature programmed desorption of H_2S (TPD-H_2S) [307] has been carried out in an AutoChem II 2920 from Micromeritics. A pretreatment of the sample is conducted to remove any impurities from the catalyst surface. Initially, the sample is swept with a stream of He while temperature is raised up to 300 °C (heating rate 20 °C min^{-1}) and held 60 min. Afterwards, the temperature of the sample is stabilized at 50 °C and a flow of 50 $cm^3\ min^{-1}$ of a mixture of H_2S/H_2 (10/90 % vol.) is injected with a Harvard pump until saturation (stabilization of the TCD signal). Following this adsorption step, the physisorbed H_2S on the catalyst is removed with a flow of He at 50 ^oC until the TCD baseline stabilizes. Finally, under a He flow, desorption (TPD) is carried out by heating the sample from the adsorption temperature (50 ^oC) up to 650 ^oC (heating rate 10 $^oC\ min^{-1}$). The signal from the TCD detector and the temperature are continuously recorded. Furthermore, a 1-propanol/N_2 (liq.) cold trap located between the sample and the detector is used to retain the H_2O that may be released during desorption and to avoid interference in the TCD signal.

2.4 REACTION EQUIPMENTS

2.4.1 Reactor for catalysts activation (sulfuration or reduction)

Prior to the reaction, the metallic phase of bifunctional catalysts must be activated. The activation is carried out ex-situ in a fixed-bed reactor system that consist of: (i) three rotameter in parallel (one for N_2 at 99.9995 % of purity from Carburos Metálicos, the second one for H_2 at 99.999 % of purity from Air Liquide and the third one for a mixture of H_2S/H_2 (10/90 % by volume from Air Liquide); (ii) a heating jacket with temperature controlled by TOHO TTM-005 controller; (iii) a stainless steel fixed bed reactor; and (iv) a gas washing bottle with 0.1 M NaOH solution to remove the H_2S before vent valve.

The procedure used, based on previous works, is as follows:

(i) *Loading the catalyst into the fixed-bed reactor*. An excess amount of catalysts is weighed and mixed with carborundum (CSi, d_P = 0.5 mm) in 1:1 ratio. Carborundum is a material that avoids the formation of gas-flow preferential routes in the catalyst bed. Furthermore, two layers of 20 mm of carborundum (above and below the catalyst bed) are used to keep the catalyst from being dragged by the gas.

(ii) *Catalyst activation.* A flow of activating gas is passed to reduce or to sulfide the bifunctional catalysts (50 mL min^{-1} of H_2S/H_2 for transition metal catalysts sulfidation; and 30 mL min^{-1} H_2 and 50 mL min^{-1} N_2 for PtPd catalyst reduction). Besides, temperature is raised up to 400 °C following a 5 °C min^{-1} ramp and held for 4 h.

(iii) *Cooling.* After activation, the heater is switched off and temperature is cooled down up to room temperature maintaining the previous flow rates.

(iv) *Sieving (d_P = 0.15-0.30 μm).* Once the catalyst is cooled, it is separated from the carborundum sieving the mixture using a mesh size of 400 μm because the carborundum used has a particle size d_P > 500 μm. After, the catalyst is loaded to the batch reactor.

2.4.2 Hydrocracking reactor and procedure

2.4.2.1 Hydrocracking unit

The hydrocracking reactions have been carried out in a laboratory-scale semi-batch stirred micro-reactor from PID Engineering & Tech. It allows working at pressures and temperatures up to 150 bar and 440 °C. The equipment is completely automatized and data acquisition and equipment control is conducted by means of Process@ software. The equipment scheme is shown in Figure 2.8 and can be

divided into six parts: (i) gas supply, (ii) product sampling lines, (iii) reactor, (iv) condenser, (v) refrigeration and (vi) stirring system.

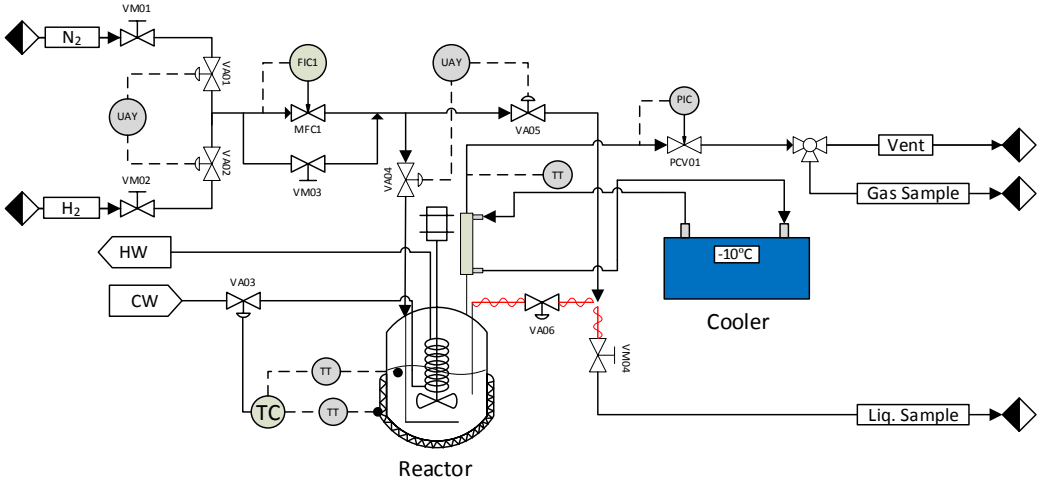

Figure 2.8 Reaction system scheme.

(i) Gas feeding: there are two gas lines to feed the reactor, which are controlled by a mass-flow from Bronkhorst (maximum flow rate of 250 mL min^{-1} under normal conditions). There is also a manual by-pass to faster pressurize the reactor. The gases used are:

- Gas 1, nitrogen (99.9995 wt%) up to 240 bar from Carburos Metálicos used to inertize the reactor atmosphere.
- Gas 2, hydrogen (99.999 wt%) up to 240 bar from Airliquide used to generate a reducing atmosphere prior to the experiment and as a reagent during hydrotreating reactions.

(ii) Product sampling lines: the reaction equipment have a liquid and gaseous sampling lines. This will make it possible to study the variation in the composition of both phases during the reaction.

- Gas line: the gases leave the reactor passing through a condenser. As it can be seen in Figure 2.8, the thermocouple TT measure the temperature of gases leaving the condenser, which is kept below than -5 ^{o}C, preventing any drag of compounds with higher boiling point than butane.
- Liquid sample line: the automatic valve VA06 must be activated to take a sample from the reactor, then, the sample is collected in a bottle acting manually over VM04 valve.

(iii) Reactor: the reactor was made by Parker Autoclave Engineering, model E010SS and customized by PID Engineering & Technologies. It is a stirred batch reactor with a maximum useful volume of 100 mL. It operates in a semi-continuous regime, since the gas can pass continuously while the liquid and solid remain

in the batch reactor. It is made of 316ss stainless steel and the internal dimensions are 46.23 mm diameter and 69.8 mm deep plus the curved bottom. A deflector is located inside the reactor, to promote turbulent flow and to guarantee the homogeneity of the reaction system. Furthermore, there is a coil inside the reactor used in cooling step.

(iv) Condenser: it is set up in the beginning of gas outlet line from the reactor to prevent the leaks of > C_5 compounds. It is a stainless steel double tube exchanger with an internal diameter of 3/8 " and 65 cm long. A Julabo model F32-HE cryo-thermostat is connected to this exchanger operating in counter-flow. Furthermore, the antifreeze coolant allows working at temperatures below than -10 ^{o}C throughout the condenser.

(v) Cooling: the cooling of the reactor is carried out with a coil located inside the reactor. This coil is connected to an open water system.

(vi) Stirring system: it is a magnetic stirrer from the Autoclave Engineers brand, model MAG075. This technology avoids the need for maintenance (greasing) and avoids thermal problems as indicated by the manufacturer. It allows reaching a maximum stirring speed of 1350 rpm. It consists of an external magnet that rotates when coupled to a rotating electric motor by means of a transmission belt. This external magnet acts on an internal magnet fixed to the shaft where the paddle agitator is located. The stirring system consists of a shaft with 6 paddles located on the bottom. The material of construction of both the shaft and the paddles is stainless steel.

2.4.2.2 Reaction procedure

Using the Process@ software is possible to schedule stages (also called sessions) to carry out experiments in automatic mode. Once the catalyst is activated (section 2.4.1), it is loaded into the reactor together with the feedstock. Then, the reactor system is closed, screws are tightened with a torque wrench and a heating jacket is settled. The reactions are carried out using the following sessions scheduling:

Session 1. *Inertization*. The first session is employed to remove the air from the reactor. For that, 250 mL min^{-1} of nitrogen is introduced in the reactor during 5 min while the pressure valve is completely open. Then, the pressure valve is closed and pressure of nitrogen raises up to 8 bar. This session is repeated twice.

Session 2. *Leak test*. The reactor is pressurized with N_2 using the by-pass valve (VM03) up to the reaction pressure set point and is held for 30 min. If there is not leakage, the nitrogen is vented and a second pressure test with H_2 is carried out.

Session 3. In this session H_2 is fed at 250 mL min^{-1} during 5 min and then pressurized up to 8 bar. This session is repeated twice.

Session 4. A first pressurization stage is carried out up to 50 bars with H_2 at 250 mL min^{-1}. This pressure stage is to prevent the boiling of the feedstock when temperature rises, avoiding modifications in feedstock composition before the reaction begins.

Session 5. The reactor is heated up to the reaction temperature using a rate of 5 ^oC min^{-1}. In order to enhance the heat transfer, the reactor is stirred at 300 rpm.

Session 6. Once the reaction temperature is reached, the reactor pressure is rising until the reaction pressure. It is done through the by-pass, although the last bar is pressurized by the mass-flow controller.

Session 7. *Reaction step*. The stirrer speed is set at 1300 rpm and the temperature and the pressure are kept constant throughout the experiment length while passing 200 mL min^{-1} of H_2.

Session 8. *Cooling*. Once the reaction is finished, the hydrogen flow is stopped, the stirring speed is reduced up to 300 rpm, the heating jacket is turned off and the cooling of the reactor begins. To faster cool the reactor, valve VA03 is opened and water passes through the coil in an open cooling system.

Session 9. *Depressurization.* After cooled down, the reactor is depressurized at 4 bar min^{-1}. This task is conducted by automatic control pressure system (PCV01).

Session 10. *Safety*. Finally, all the valves and set points are changed to safety positions and values to reduce whatever risk.

2.5 REACTION PRODUCT ANALYSIS

2.5.1 Reaction products

The gases leaving the reactor are cooled after passing through a condenser and they are collected in a bag to be analyzed. The amount of gas formed in each reaction is determined by weighing the reactor before and after the reaction. Liquid products are separated from the catalyst by: i) vacuum filtration when there is no plastic in the feedstock; and ii) by solvent extraction when feeding plastics are blended with VGO. The extraction methodology, described in Figure 2.9, is carried out in order to (i) recover the liquid products, (ii) extract the unconverted plastic and (iii) recover the spent catalyst.

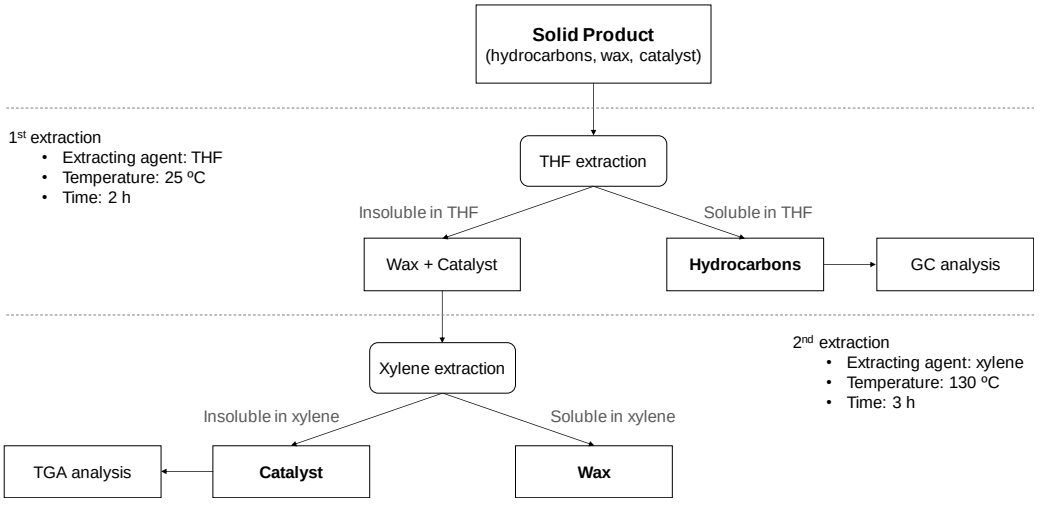

Figure 2.9 Extraction method followed in the analysis of reaction products.

In a first extraction, at room temperature with tetrahydrofuran (THF) and the subsequent vacuum filtration (d = 50 mm, Filter-Lab), the hydrocarbons (soluble in THF) are separated from the unconverted plastic (present in the form of waxes) and spent catalyst. In the second extraction, with xylene at 130 °C and subsequent vacuum filtration (0.45 μm PTFE membrane filter, Omnipore), the unconverted plastic (waxes) and the spent catalyst are separated. After this second extraction, wax and spent catalyst are dried in an oven at 130 ºC for 24 h to remove xylene.

2.5.2 Composition of gas product

Gases have been analyzed by chromatographic means in an Agilent Technologies 6890 cryogenic gas chromatograph equipped with a dimethylpolysiloxane (100%) capillary column (50 m × 0.2 mm) and a FID detector. The gas sample is taken from sample bag with 1 mL Hamilton sample-lock syringe

and is manually injected in the GC. The analytical conditions of the method are shown in Table 2.4.

Table 2.4 GC method to analyze the gas composition.

Section	Variable	Value
Oven	T_0 (°C)	-30
	t_0 (min)	5
	R_1 (°C min^{-1})	15
	T_1 (°C)	235
	t_1 (min)	1
	R_2 (°C min^{-1})	30
	T_2 (°C)	275
	t_2 (min)	0
Injector	T (°C)	300
	P (bar)	0.85
	Column flow (mL min^{-1})	0.9
	Split ratio	100:1
FID	T (°C)	320
	H_2 flow (mL min^{-1})	40
	Air flow(mL min^{-1})	450
	Make up flow (mL min^{-1})	20

2.5.3 Analysis of liquid product

2.5.3.1 Simulated distillation

The simulated distillation has been carried out according to the ASTM D2887 standard in an Agilent Technologies 6890 GC System. Liquid products (0.2 µL) are manually injected in the GC using a Hamilton 7000 syringe. The method used to conduct this analysis was summarized in Table 2.3.

2.5.3.2 Liquid composition

Liquid products composition from hydrocracking reactions was also analyzed in the same way as PO composition (section 2.2.1.2). A 1.5 mL vial with liquid sample is loaded in the autosampler (Agilent Technologies 7683B) which is equipped with a 10 µL syringe from Agilent. The analysis is carried out by bi-dimensional chromatography (Agilent Technologies 7890A GC) coupled on-line

with a mass spectrometer (Agilent Technologies 5975C XL). The syringe is cleaned with the liquid sample itself three times, throwing the sample to a waste bottle. Then, 0.2 μL of sample is injected and then the syringe is cleaned with toluene and acetone. The analysis conditions are listed in Table 2.2.

2.5.4 Coke content on spent catalysts

The amount, nature and location of coke deposited on the catalysts has been analyzed by temperature-programmed oxidation (TPO) in a TA Instruments TGA-Q 5000 thermobalance coupled in-line to a ThermoStar mass spectrometer from Balzers Instruments to trace the evolution of CO_2 during coke combustion.

The procedure followed in the TPO analysis is based on the work of Ibañez et al. [178]. The spent catalyst (~15 mg) is pretreated to remove the light organic compounds remaining in the catalyst through a temperature programmed desorption. The pretreatment process consist of, firstly, a temperature equilibration at 50 ^{o}C under 50 cm^3 min^{-1} of N_2. Then, temperature rises up to 450 ^{o}C at a ratio of 10 ^{o}C min^{-1} and this temperature is held for 10 min. Afterwards, the temperature is reduced up to 50 ^{o}C and the catalyst sample is ready to conduct the TPO analysis. The temperature is maintained at 50 ^{o}C meanwhile 50 cm^3 min^{-1} of air is fed. Henceforth, temperature rises up to 550 ^{o}C with a ramp of 5 ^{o}C min^{-1}. Moreover, to ensure the complete coke combustion, the maximum temperature is held for 60 min. Finally, the sample is cooled down at room temperature following a rate of 20 °C min^{-1}. During the whole analysis, signals of temperature, weight, and derivative weight are registered by the TGA, as wells as CO, CO_2 and H_2O signals in the mass spectrometer.

2.5.5 Reaction indexes

Different reaction indices have been computed to assess the product yields and distribution and therefore, the selectivity to fuel after the runs.

2.5.5.1 Yields

The yield of each lump (Y_i) has been defined as the relationship between its mass in the product stream and the amount of feedstock as follows:

$$Y_i = \frac{m_i}{(m_{VGO} + m_{Plastic} + m_{PO})_{initial}} \tag{2.3}$$

where m_i is the mass of lump i in the product, m_{VGO} is the initial mass of VGO fed, $m_{Plastic}$ is the mass of plastic fed and m_{PO} is the mass of plastic pyrolysis oil (PO) fed.

2.5.5.2 Hydrocracking conversions

As the main aim of this work is, on the one hand, the hydrocracking of the heaviest fraction of the VGO, that is, the HCO, to obtain lighter fractions; and, on the other hand, the plastic hydrocracking (HDPE and PP) blended with VGO and PO to obtain liquid hydrocarbons, two conversions have been defined:

$$X_{HCO} = \frac{(m_{HCO})_{initial} - (m_{HCO})_{final}}{(m_{HCO})_{initial}} \tag{2.4}$$

$$X_{Plastic} = \frac{(m_{Plastic})_{initial} - (m_{Plastic})_{final}}{(m_{Plastic})_{initial}} \tag{2.5}$$

where $(m_{HCO})_{initial}$ and $(m_{HCO})_{final}$ are the amount of HCO in the feed and in the liquid product, respectively; and $(m_{Plastic})_{initial}$ and $(m_{Plastic})_{final}$ are the amount of plastic fed (HDPE and PP) and unconverted one (waxes at the end of the reaction), respectively.

2.5.5.3 Selectivity to fuel

The selectivity to fuel parameter (S_F) has been determined in order to deep on the catalytic activity. This definition has been adapted from the dimensionless catalytic performance parameter proposed by Al-Attas et al. [308]:

$$S_F = \frac{Y_{Naphtha} + Y_{LCO}}{Y_{Gas} + Y_{HCO} + Y_{Wax} + Y_{Coke}} \tag{2.6}$$

where $Y_{Naphtha}$, Y_{LCO}, Y_{Gas}, Y_{HCO}, Y_{Wax} and Y_{Coke} are the yields of naphtha, LCO, gas, HCO, unconverted plastic and coke, respectively.

2.5.5.4 Naphtha and LCO extent (gradients)

As the characterization of PO shows (Table 2.1), around 50 wt% of this feedstock is composed by hydrocarbons whose boiling point range corresponds to naphtha and LCO lumps. Therefore, the extent of formation of each lump (ΔY_i) has

been also assessed to know its origin (from feedstock or from hydrocracking reaction). For this purpose, the difference between the yield of each lump in the products and the content of the same lump in the feedstock fed to the batch reactor has been computed:

$$\Delta Y_i = Y_i - (Y_i)_{initial} \tag{2.7}$$

where Y_i is the yield of each lump according to equation (2.6) and $(Y_i)_{initial}$ is the mass content for each lump in the feedstock.

2.5.5.5 Research octane number (RON)

The research octane number (RON) has been calculated from chromatographic data according the Anderson-Sharkey-Walsh method [309]. This method divides the naphtha lump into 31 groups of compounds, assigning to each one a value of RON. The groups are chosen in such a way that each one has a small boiling point range and contains similar chemical compounds. In fact, some of these groups are made up of a single component. According to the mass percentage reported for each group, the RON can be estimated by means of a weighted sum:

$$RON = \sum_{i=1}^{31} w_i \, RON_i \tag{2.8}$$

where w_i is the mass fraction of group i, obtained from the chromatographic analysis and RON_i is the RON of the mixture of group i, defined in the method for each group.

2.5.5.6 Cetane index

Cetane index has been calculated using the ASTM D-4737 standard. This standard estimates the cetane index as a function of density and T_{10}, T_{50} and T_{90} from simulated distillation using the following equation:

$$\begin{aligned} CI = {} & 45.2 + 170B + 0.0892 \cdot T_{10N} + (0.131 + 0.901B) T_{50N} + \\ & + (0.0523 - 0.42B) T_{90N} + 0.00049 (T_{10N}^2 - T_{90N}^2) + 60B^2 \end{aligned} \tag{2.9}$$

where B is calculated with equation (2.10):

$$B = \left[e^{-3.5\left(\rho - 0.85\right)} \right] - 1 \tag{2.10}$$

where ρ is the density of LCO (g ml^{-1}) and it has been estimated from LCO composition in GCxGC-MS according the compounds nature and its number of carbon atoms, T_{10N} is the temperature in °C at which the 10 vol% distillates minus 215, T_{50N} is the temperature in °C at which the 50 vol% distillates minus 260 and T_{90N} is the temperature in °C at which the 90 vol% distillates minus 310.

CHAPTER 3

SCREENING CATALYSTS

3 SCREENING CATALYSTS

In this chapter, different catalysts for the valorization of a blend of HDPE/VGO have been tested with the aim of finding the more promising one. The process has been divided in two steps. First of all, after in detail characterization of the catalysts (Section 3.1) using a wide set of techniques described in section 2.3.1, the hydrocracking of VGO has been carried out in section 3.2. The yields, the HCO conversion (heavier VGO fraction) and the naphtha composition have been calculated in order to assess the performance of each catalyst. Furthermore, the quality of the naphtha (RON) is also calculated. In this way, this analysis enables to discard the unpromising ones.

The operating conditions after literature review [21,156,310–314] have been:

- HDPE in de blend: 0.20 in mass
- Temperature: 420 ^{o}C
- Pressure: 80 bar H_2
- Catalyst to Feed ratio: 0.1 in mass
- Stirrer speed: 1300 rpm
- Reaction time: 120 min

In the second step (section 3.3), the two most promissing catalysts for VGO hydrocracking have been employed for HDPE/VGO hydrocracking under the previous operating conditions. The temperature, however, have been tested in a range of 400-440 ^{o}C to asses a preliminary operational study. To appraise the performance of these catalysts, conversion and yields have been calculated (Section 3.3.1). Moreover, the naphtha and diesel composition and quality (RON and cetane index) has been analyzed in section 3.3.3 and 3.3.4, respectively.

3.1 PROPERTIES OF FRESH CATALYSTS

The literature and previous work conducted in our research group reveal interesting bifunctional catalysts which, according to their properties, may be appropriate for hydrocracking and hydrotreating the HDPE/VGO blend. The catalysts chosen were: (i) cobalt and molybdenum supported on alumina (CoMo/Al), which is commonly used in hydrodesulfuration processes; (ii) nickel and molybdenum on silica-alumina (NiMo/SiAl), which stands out for its great aromatic ring opening capacity; (iii) three nickel and tungsten catalysts supported on silica-alumina (NiW/SiAl), MCM-41 (NiW/MCM41) and Y type zeolite (NiW/HY), with a good behavior removing heteroatoms but low hydrocracking activity the former and the second one and high hydrocracking and hydrotreating performance the last one; and (iv) platinum and palladium over Y type zeolite (PtPd/HY) that is a good catalyst for hydrogenation/dehydrogenation reactions with a high cracking activity. It has to be pointed out that the CoMo/Al, NiMo/SiAl and NiW/HY are commercial catalysts and the NiW/MCM41, NiW/SiAl and PtPd/HY are in-house prepared catalyst.

The more relevant physicochemical properties of the catalysts are shown in Table 3.1. For all the catalysts, the textural properties were determined by N_2 adsorption-desorption isotherms. Employing the BET method it has been calculated the surface area (S_{BET}) and the micropore area (S_{micr}), whereas the mesopore area (S_{meso}) was obtain by difference. The pore volume (V_{pore}) and average pore diameter (D_P) were calculated using BJH method. The metal content was determined by ICP-AES. Finally, the acidic properties were determined by two techniques: (i) terc-butylamine TPD to conclude the total acidity and acidic strength, and (ii) pyridine adsorption to estimate the B/L ratio.

Table 3.1 Textural properties, chemical composition and acidic properties of the fresh catalysts.

Catalyst	CoMo/Al	NiMo/SiAl	NiW/SiAl	NiW/MCM41	NiW/HY	PtPd/HY
S_{BET}, ($m^2\ g^{-1}$)	187	278	93	66	229	620
S_{micr}, ($m^2\ g^{-1}$)	33	0.00	10	11	138	543
S_{meso}, ($m^2\ g^{-1}$)	154	278	83	55	91	77
V_{Pore} ($cm^3\ g^{-1}$)	0.52	0.51	0.36	0.21	0.24	0.39
D_P (nm)	10.50	6.66	16.73	20.76	7.31	8.44
Ni (wt%)	0.1	2.98	2.22	4.26	4.54	–
W (wt%)	–	–	18.27	25.02	22.7	–
Co (wt%)	2.83	–	–	–	–	–
Mo (wt%)	12.2	7.31	–	–	–	–
Pt (wt%)	–	–	–	–	–	1.19
Pd (wt%)	–	–	–	–	–	0.53
A_T[a] ($mmol_{tba}\ g^{-1}$)	0.54	0.46	0.22	0.09	0.41	1.69
A_S[b] ($KJ\ mol_{tba}^{-1}$)	86	124	118	81	131	135
B/L ratio	2.16	2.25	1.90	0.18	2.39	1.53

a A_T is the total acidity
b A_S is the acidic strength

3.1.1 Physical and textural properties

3.1.1.1 N_2 absorption-desorption isotherm

Textural properties, pore size distribution and pore volume of the catalysts were obtained from non-destructive analysis of physisorption and desorption of N_2 over the catalyst surface. The isotherms obtained for each catalyst are depicted in Figure 3.1 and in Figure 3.2 the pore volume distributions are shown.

The isotherms in Figure 3.1 represent the amount of adsorbed N_2 volume, established by agreement in standard conditions of temperature and pressure (STP), versus the relative pressure of the adsorbate. According to the IUPAC nomenclature [315], the isotherms for NiMo/SiAl, CoMo/Al and NiW/SiAl catalysts can be classified as type IV, which implies that supports are mesoporous adsorbents. Furthermore, the isotherms for these catalysts show a hysteresis loop between the adsorption-desorption branches in the multilayer phase. This behavior is attributed to capillary condensation at the end of the process being affected by the pore geometry. For the three before mentioned catalysts, the hysteresis type can be relate with H2 type, characteristic of pores with non-uniform length and conformation with cylindrical-like shapes. In the case of NiW/MCM41 catalyst, surprisingly, the isotherm is also type IV, but the parallel and narrow branches with no clear plateau describe the H3 hysteresis more typical in macroporous materials.

Finally, NiW/HY and PtPd/HY catalysts describe hybrid isotherms type I-a and IV with a H4 hysteresis, typical in slit-shaped and with zeolites. Furthermore, the catalysts with H2 hysteresis type have a monolayer until relative pressure higher than 0.6-0.7, after that the hysteresis loop appears. For NiW/MCM41 catalyst, with H3 hysteresis, the loop appears at 0.8 being the highest value observed. On the other hand, for NiW/HY and PtPd/HY catalysts, with hysteresis H4, the monolayer is observed until relative pressure slightly upper than 0.4, showing those catalysts the lowest value for which the hysteresis loop arise.

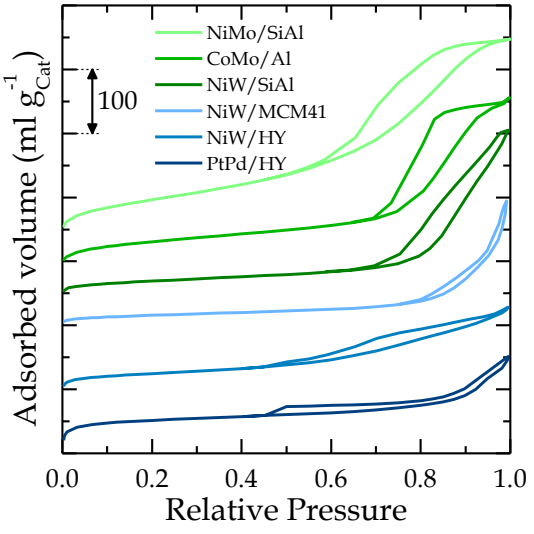

Figure 3.1 N_2 adsorption - desorption isotherms of fresh catalyst**.**

As mentioned before, the information given by the isotherms was employed to calculate the surface area by the BET method and results are sum up in Table 3.1. Generally speaking, it could be observed that catalyst based on pure zeolite (PtPd/HY catalyst) has the highest surface area followed by NiMo/SiAl catalyst. On the other hand, NiW/HY catalyst shows lower surface area than PtPD/HY catalyst ought to agglomeration possibly with an amorphous silica-alumina (ASA) support, as it is confirmed by XRD spectra. As expected, catalysts based on zeolites have the higher micropore area, corresponding the highest to the catalyst with pure zeolite (PtPd/HY > NiW/HY). CoMo/Al catalyst shows a middle surface base on mesopore area. On the other hand, NiW/SiAl catalyst has a non-hierarchy structure of aluminosilicate with low surface area and NiW/MCM41 catalyst has the lowest surface area.

The pore size distributions, shown in Figure 3.2, have been calculated from N_2 adsorption isotherm branch by BJH method described in section 2.3.1. The incremental pore volume regarding pore diameter range in logarithmic scale is depicted versus the average pore diameter. It can be seen that CoMo/Al and

NiW/SiAl catalysts have a narrow pore distribution with a maximum at 125 and 144 Å, respectively. In the case of NiMo/SiAl catalyst the maximum appears at 89 Å in a broad peak. NiW/MCM41 catalyst shows also a wide peak with a maximum at 177 Å. Catalysts based on zeolite show their peaks at 74 Å for NiW/HY catalyst and 286 Å for PtPd/HY catalyst. Nevertheless, NiW/HY and PtPd/HY catalysts not have a noticeable maximum in the signal due to they are microporous materials, which have a pore diameter less than 10 Å.

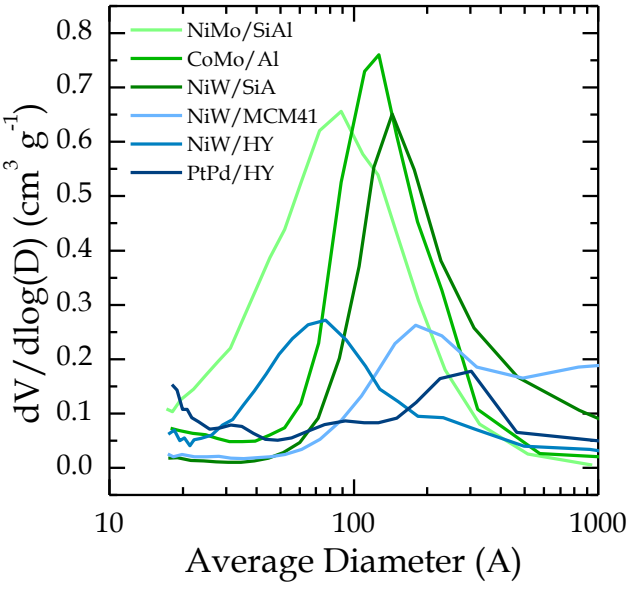

Figure 3.2 Pore diameter distribution of fresh catalysts.

3.1.1.2 Transmission electron microscopy (TEM)

The catalysts were analyzed by TEM and pictures taken are disposed in Figure 3.3. These images allow us to see the metal dispersion over the support and in the case of non-noble metal catalysts, we could also study the sulfided metal-active phase.

In general, all catalysts show a good dispersion of the metal in its active form over the support, with homogeneous distribution of the metallic phase in the catalyst particle. However, for NiMo/SiAl and NiW/SiAl catalysts (Figure 3.3b and d) zones with a high accumulation of metals can be identified in the figure (darker areas).

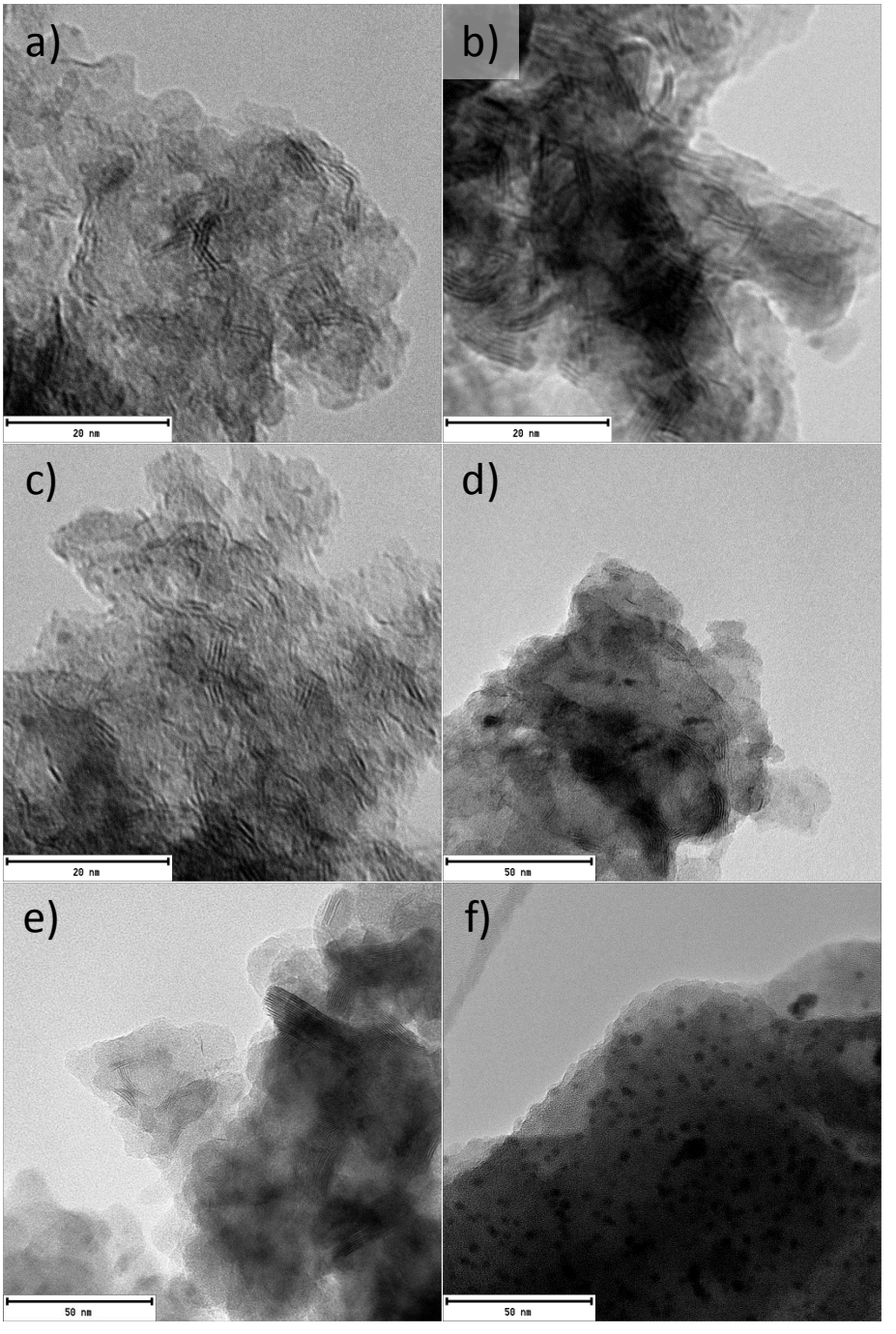

Figure 3.3 TEM images of sulfided transition metal catalyst CoMo/Al (a), NiMo/SiAl (b), NiW/HY (c), NiW/SiAl (d) and NiW/MCM41 (e) and the reduced PtPd/HY catalyst (f).

Focusing on the transition metal catalysts, the organization of the metal in staking way can be appreciated. This phenomenon is caused when MoO_3 and WO_3 metals change to sulfided form (MoS_2 and WS_2) during the catalyst activation stage described in section 2.4.1. During the activation, trigonal prisms of sulfur coordinated with Mo and W are developed creating 2-dimension layers of S-metal-

S which can be stacked multiple times [185,316]. Furthermore, these structures are highly related with the hydrotreatment activity of the catalysts [317] being the most active form [318]. Hence, TEM images are an accurate technique for analyze these structures. In them, it can be seen that the structure of the sulfided metals is heterogeneous in length and stacking degree and that is well dispersed over the support. The average of the stacking degree ($\bar{N}$) and the slab length ($\bar{L}$) were estimated according to the following equations [319] and summarized in Table 3.2.

$$\bar{L} = \frac{\sum_{i=1}^{n} n_i l_i}{\sum_{i=1}^{n} n_i} \tag{3.1}$$

$$\bar{N} = \frac{\sum_{i=1}^{n} n_i N_i}{\sum_{i=1}^{n} n_i} \tag{3.2}$$

where l_i is the length of the slab particle, N_i is the number of layers in the particle i, and n_i is the number of the particles with l_i length or N_i layers.

Table 3.2 Stacking degree and slab length of sulfided catalysts.

Catalyst	**Stacking degree, $\bar{N}$**	**Slab Length, $\bar{L}$ (nm)**
NiMo/SiAl	2.03	2.81
CoMo/Al	2.22	2.37
NiW/SiAl	3.50	5.42
NiW/MCM41	4.77	6.86
NiW/HY	2.36	4.65

The support has an important effect on the shape of active metal, thereby, in slabs length and stacking degree [320]. The composition of the support also influences the metal-support linkage, achieving higher dispersion Al than Si [321]. The NiMo/SiAl, CoMo/Al and NiW/HY catalysts show the lower stacking degree and slab length. These results denote a well dispersion of the active phase which will have better hydrotreating capability as Díaz de León et al. [322] reported. On the other hand, NiW/MCM41 catalyst obtains the highest values of length and stacking degree predicting a worsen behavior than previous one.

3.1.2 Chemical and structural properties

3.1.2.1 Acidity

The acidity properties of the fresh catalysts (total acidity, acidic strength and nature of acid sites) have been determined by two techniques, (i) adsorption and TPD/cracking profile of terc-butylamine (t-BA) and (ii) FTIR of adsorbed pyridine, both techniques explained in detail in section 2.3.1.

The results from t-BA TPD profile of each catalyst are shown in Figure 3.4, where the signal recorded from the MS corresponding to released butane after t-BA is cracked in acid sites is depicted. For all the catalysts, the temperature shows a maximum (clearly indicated in the figure), which can be related to the acidic strength of the catalysts. Keeping this in mind, the lower temperature, easier t-BA has been cracked, so, stronger is the acid site. No acid behavior is seen for NiW/MCM-41 catalyst, predicting a very low cracking activity. A similar result is also obtained when using ammonia to MCM-48 by Liu Y. [323]. It is noticeable that PtPd/HY catalyst depicted a broad peak, which is related with the different nature of the acid sites in the catalyst, although the main one is at the lowest temperature. On the other hand, the other catalysts have shown narrower peaks. Organizing the catalysts in accordance to the acidic strength, the trend is the following:

PtPd/HY > NiW/HY > NiMo/SiAl ≈ NiW/SiAl > CoMo/Al

Furthermore, the total acidity is obtained from the area below the signal and results are depicted in Table 3.1. The results show that by far, PtPd/HY catalyst has the highest total acidity being more than three times bigger than that of CoMo/Al catalyst. The trend continues with NiMo/SiAl and NiW/HY catalysts not far from the previous. NiW/SiAl catalyst is the next behind them for which the profile exhibits attenuation. Finally, as previously mentioned, a flat signal was observed for NiW/MCM-41 catalyst.

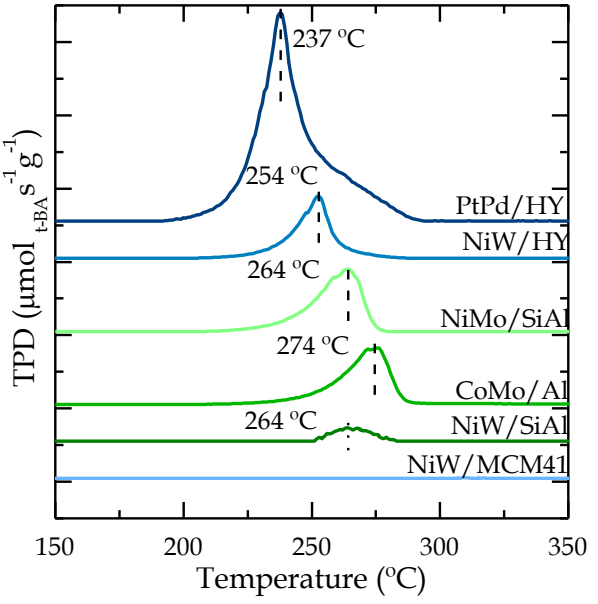

Figure 3.4 TPD of t-BA of fresh catalysts.

The FTIR of adsorbed pyridine can be used in a qualitative and quantitative way to determine the nature of acid sites as pointed out Emeis [306], being able to calculate the Brønsted and Lewis ratio from the characteristic bands that these types of acid sites have at wavelengths of 1455 and 1545 cm^{-1}, respectively. The ratio is calculated using the equations (3.3) and (3.4) based on literature [305,324].

$$n_L = \frac{A_L C_d}{\varepsilon_L m} \tag{3.3}$$

$$n_B = \frac{A_B C_d}{\varepsilon_B m} \tag{3.4}$$

where n_L and n_B are the total number of micromoles of pyridine per gram of sample adsorbed at each type of Lewis (L) or Brønsted (B) sites, A is the area below IR absorbance bands (cm^{-1}). Since pyridine can be adsorbed both at Lewis (L) or Brønsted (B) sites, C_d is the cross-sectional area (cm^2) of the catalyst pill, m is the mass (g) of the pill, and ε is the molar absorption coefficient (cm μmol^{-1}) for pyridine at Lewis (L) or Brønsted (B) sites obtained from literature [306].

The B/L ratio are gathered in Table 3.1 where NiW/HY catalyst achieved the greatest value closely followed by CoMo/Al > NiMo/SiAl> NiW/SiAl > PtPd/HY. All the catalysts mentioned have a ratio bigger than 1, which means that $n_B > n_L$. Nevertheless, once again, NiW/MCM41 catalyst has the lowest B/L ratio, and lower than 1. However, not because NiW/HY catalyst has the highest value in the B/L ratio, it is the catalyst with the highest n_B. This can be seen in Table 3.3 where

the catalyst with the highest n_B is PtPd/HY catalyst followed far by CoMo/Al > NiMo/SiAl > NiW/HY >> NiW/SiAl > NiW/MCM41.

Table 3.3 Density of Brønsted and Lewis acid sites.

Catalyst	Brønsted (μmol/g)	Lewis (μmol/g)
CoMo/Al	232	107
NiMo/SiAl	198	88
NiW/SiAl	16	8
NiW/MCM41	2	9
NiW/HY	176	74
PtPd/HY	726	476

3.1.2.2 X-ray diffraction (XRD)

The XRD technique has been conducted to study the degree of crystallinity of the supports. The results are collected in Figure 3.5, divided in non-zeolites catalysts (a) and zeolite-catalysts (b). As we can see in Figure 3.5a the NiMo/SiAl catalyst shows an elevation of signal bottom from 15-35º in 2θ positions that is related with amorphous Si-Al. Moreover, at 43-48º and 64-70º two peaks related with alumina appear, and similar results were obtained by other authors in literature [149,325]. These two peaks can also be observed for CoMo/Al catalyst. However, there is no elevation of the signal bottom since this support has not silica. On the contrary, NiW/SiAl catalyst shows only the elevation of the background due to amorphous Si-Al and no alumina signal appears. Nevertheless, some peaks were detected regarding to crystalline metal phases of $NiWO_4$ (square) and $Na_2W_2O_7$ (triangle). The diffractogram of NiW/MCM41 catalyst is very similar between 15-80º in 2θ positions although the more relevant peaks of $NiWO_4$ and $Na_2W_2O_7$ can be observed.

Regarding to XRD diffractograms of zeolite based catalysts depicted in Figure 3.5b, the NiW/HY catalyst shows a crystalline phase as expected due to the zeolite support. This technique also reveals the presence of an amorphous phase, increasing the background. Furthermore the two peaks related to alumina appear again shyly. No signal for crystalline metal phases can be seen in this case in comparison with the other NiW catalyst due to the crystal size is smaller. TEM analysis also support this statement since the low stacking degree and length evidence the strong metal-support interactions (SMSI) [326]. Finally, PtPd/HY catalyst has the more crystalline support with narrow and pointed peaks (black circle) ought to pure zeolite used in its synthesis. Some peaks of crystalline phases related to Pt and Pd metals were detected in this case (pointed with asterisks).

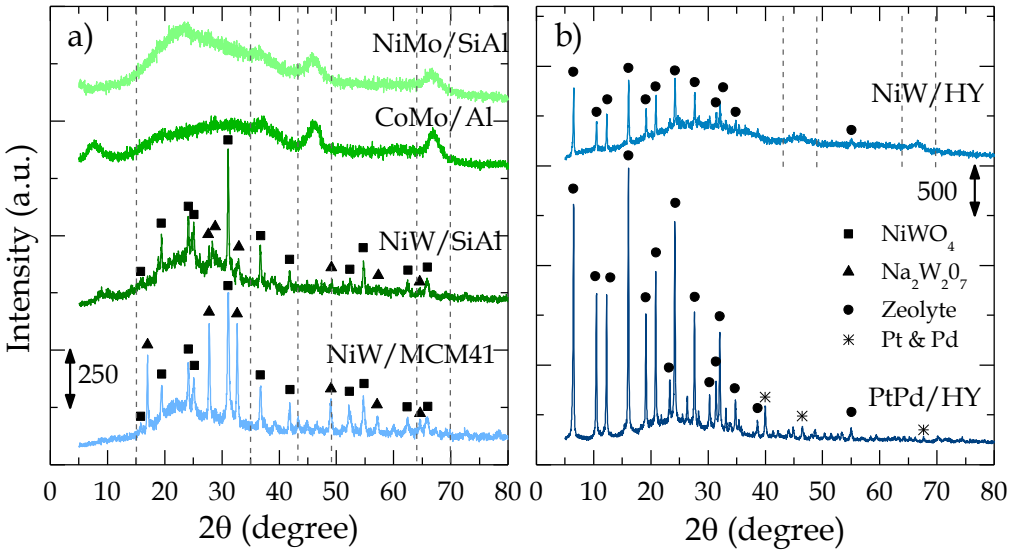

Figure 3.5 XRD of the catalysts: non-zeolites (a) and zeolites (b).

3.1.2.3 X-ray fluorescence (XRF)

The results of the chemical composition in the surface of a pearl made from the catalysts according to the procedure described in section 2.3.1 are summarized in Table 3.4. The results obtained from this technique have been compared with those obtained by ICP. It has to be pointed that Pt and Pd quantification was carried out through semi-quantitative software due to the pearl sample preparation involve the use of Pt-Pd container, thus cannot be accurate. The proportion between metals in the same catalyst is similar to those from ICP. Comparing to the results obtained by ICP, metal content in NiW/MCM41 and NiW/SiAl catalysts are very similar and slightly higher for tungsten in NiW/HY catalyst. Furthermore, the content of NiMo/SiAl and CoMo/Al catalyst was close and precise regarding ICP.

Table 3.4 Metal content by XRF analysis for fresh catalysts.

Catalysts	CoMo/Al	NiMo/SiAl	NiW/SiAl	NiW/MCM41	NiW/ZY	PtPd/ZY
Si	0.14	12.59	29.94	27.32	12.24	31.58
Al	30.50	22.69	3.22	2.42	17.43	4.95
Ni	0.18	2.74	1.74	3.35	3.53	–
W	–	–	14.49	19.84	23.15	–
Co	3.03	–	–	–	–	–
Mo	11.73	7.82	–	–	–	–
Pt	–	–	–	–	–	0.37
Pd	–	–	–	–	–	0.24

3.1.2.4 X-Ray photoelectron spectrometry (XPS)

XPS analyses have been carried out to study the chemical species exposed in the surface of the bifunctional catalysts. Figure 3.6 show the binding energy spectra obtained for each catalyst in the region of each metal (Co, Mo, Ni and W) loaded over the supports. This figure is divided into four sub-figures, according to the metals previously mentioned (a, b, c and d, respectively). It has to be mentioned that despite extensive XPS analysis has been carried out for PtPd/HY catalyst, no clear signs of metals were found due to its low metal content, as ICP-AES certified.

Figure 3.6a of Co on CoMo/Al catalyst depicts the characteristic doublet corresponding to the spin–orbit coupling profile of Co which could be deconvoluted with the curve-fitting in 4 peaks. After Shirley background subtraction, at 797.8 and 782.2 eV are the main peaks that are relate with $2p_{1/2}$ and $2p_{3/2}$ orbital of Co and at 803.9 and 787.3 eV their satellite peaks corresponding to previous mentioned orbital are identified. The difference between the main peak and his satellite peaks allows predicting that the cobalt is in tetrahedral structure. It has to be mentioned that for Co, the $2p_{3/2}$ is the most intense peak [327,328].

In the case of molybdenum, it is present in CoMo/Al and NiMo/SiAl catalysts (Figure 3.6b). Both catalysts show that Mo has the same oxidation state ($3d_{5/2}$ and $3d_{3/2}$) according to the peaks observed in their binding energy spectra after deconvolution. Then, two peaks are observed according to each spin-orbit component with maximums at 235.4 and 232.5 eV, which are related to Mo(VI) $3d_{3/2}$ and Mo(VI) $3d_{5/2}$, respectively [329–331], being the last type the highest one. The light shift of the peaks to higher values can be appreciated in NiMo/SiAl catalyst due to the strong interaction between the metal and support.

There are 4 catalysts that use Ni as one of the metals. The XPS signal regarding to Ni for all of them is collected in Figure 3.6c. In all cases, the profile describes two main bands that for NiW/SiAl and NiW/MCM41 catalysts are at 872.9 and 856.6 eV from Ni $2p_{1/2}$ and Ni $2p_{3/2}$ spin-orbital splitting of the Ni (II) species. They are also supplemented by its satellite bands at 879.4 and 861.4 eV apiece. The more relevant signal is obtained for Ni $2p_{3/2}$ with a sharp peak [332,333]. However, NiMo/SiAl and NiW/HY catalysts have the mains and satellite peaks displaced to stronger energy.

Figure 3.6d depicts the profile of W for XPS analysis. Signal shows one broad peak that, after deconvolution using Lorentzian-Gaussian method, reveals two peaks that can be identified as W(VI) $4f_{5/2}$ and W(VI) $4f_{7/2}$ at 36.2 and 35 eV, respectively, corresponding probably with WO_3 [334]. Here, the shift to left of the peaks is stronger for NiW/HY catalyst. It has to be pointed that NiW/SiAl catalyst has a smooth peak around ~40 eV which, according to literature, is related to

W $5p_{3/2}$ core level [335]. As before, the signals of some catalysts are slightly shifted due to metal interactions with the support.

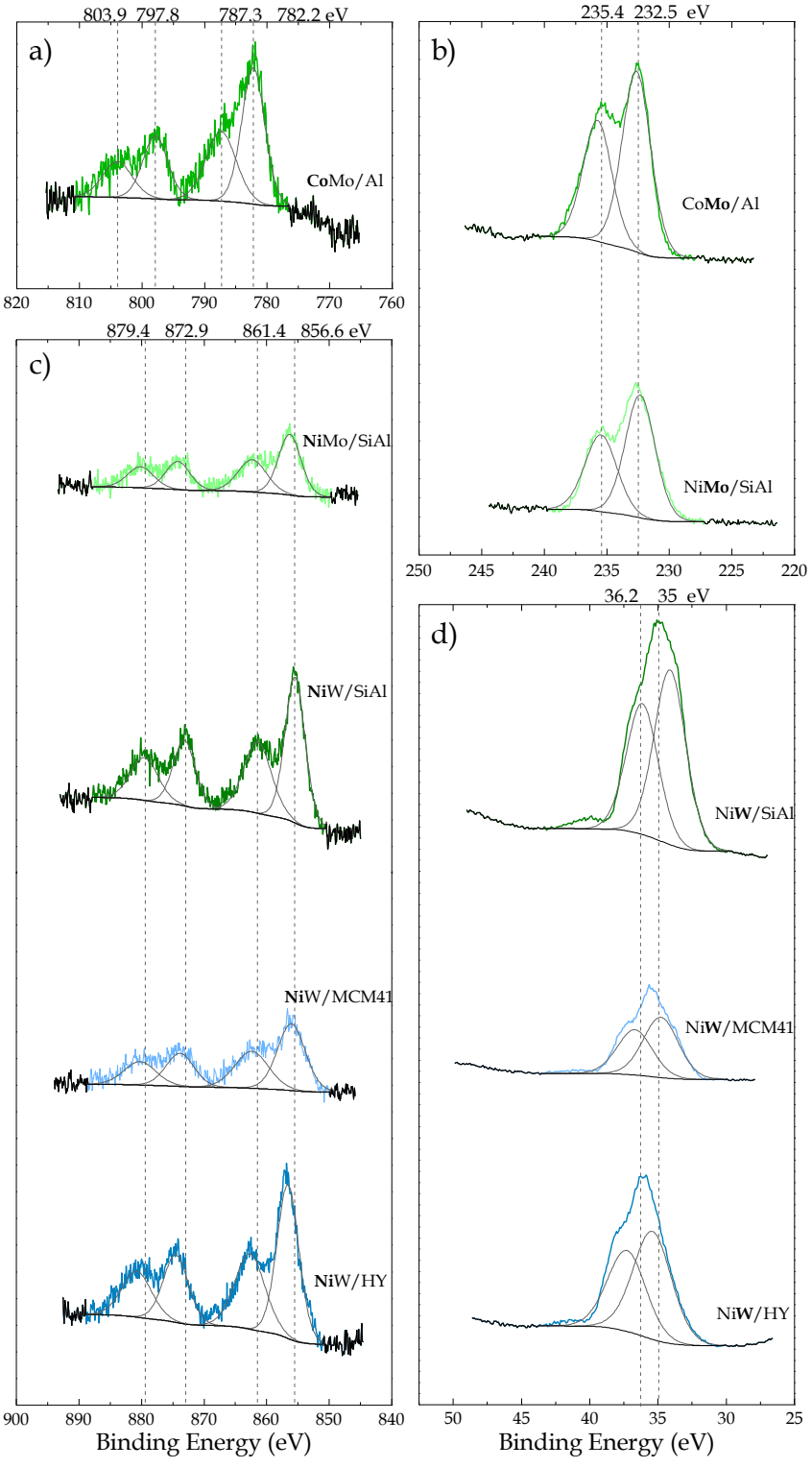

Figure 3.6 XPS spectra in the region of Co (a), Mo (b), Ni (c), and W (d) for fresh catalysts.

3.1.2.5 Temperature programmed reduction (TPR)

The reducibility of the oxidized metallic species supported in the catalysts was studied by H_2 TPR and the profiles are depicted in Figure 3.7. This technique gives us information according to the oxidation state of the metal phases and their interaction with the support.

In this figure, NiMo/SiAl catalyst shows a broad profile in the main reduction peak at 385 ºC. This maximum is associated to the partial reduction of the molybdenum species (Mo^{6+} to Mo^{4+}) [144]. After that, an abrupt drop appears in the signal at ~500 ºC, temperature at which the reduction of dispersed NiO particles that interact weakly with the support occurs [336] and after that, at 558 ºC the reduction of particles with strong interaction [337]. CoMo/Al catalyst displays also the main peak related to the reduction of the molybdenum (Mo^{6+} to Mo^{4+}) but, at this time, the peak is shifted to higher temperature (431 ºC) ought to powerful interaction with the support.

The reduction of the cobalt oxide happens in two steps: (i) below 400 ºC approximately, reduction of Co^{3+} to Co^{2+} takes place and (ii) up to 500 ºC the reduction of Co^{2+} to Co^0 metal. Therefore, the first reduction step is completed at the same time that the reduction of molybdenum. Nevertheless, the second step could be associated to the shoulder at 501 ºC [338]. It has to be pointed that the small shoulder at 284 ºC can be associated with the reduction of some particles of Co^{3+} to Co^{2+} with low interactions with γ-Al that comes from residual cobalt nitrate form used in the catalyst synthesis [339,340].

The bimetallic NiW catalysts depict a similar behavior. The TPR profiles show a peak at 501 ºC which, as previously commented, indicates the reduction of NiO particles. This peak appears at lower temperature (487 ºC) for NiW/MCM41 catalyst, meaning that the interaction with the support is weaker. Furthermore, NiW/HY catalyst has two peaks at lower temperature (225 and 284 ºC) attributed to NiO reduction to metallic nickel which is well-dispersed and has non or low interaction with Brønsted sites of the support, respectively. Besides, this peak is displaced to lower temperature when metal amount increases [341,342]. Lastly, the peaks at 558 and 582 ºC, respectively, are related with the reduction of Ni-W-O phases [343]. It has to be pointed that comparing the peaks of NiW catalysts, NiW/HY catalyst has the most defined ones, specially the two last ones which are related to most active metal phase for hydrogenation. In addition, comparing NiO (at 487 and 501 ºC) versus Ni-W-O peak (558 ºC), the former is almost at the same height that the second one for NiW/SiAl and NiW/MCM41 catalysts, whereas for NiW/HY catalyst the second one is higher than the former. For that reason, the last catalyst is more likely to achieve better performance because has strong metal support interactions (SMSI).

Finally, the reduction of PtPd/HY catalyst shows the flattest profile. The intensity of the signal is related with the metal content, so the results agree with those obtained by ICP-AES. This catalyst shows three reduction peaks in his H_2 TPR profile. Literature reports that particles of PdO are reduced to β-PdH in hydrogen atmosphere at 25 ºC [344], hence it cannot be detected with this analysis. On the other hand, Bhogeswararao and Srinivas [345], who worked with Pt/Al catalysts, observed two peaks in TPR profile, as it is seen in Figure 3.7 (145 ºC and 300 ºC). These peaks are related to the reduction of PtO to Pt^0 species which have weakly or medium interaction with the support. Finally the reduction of Pt-Pd particles to metal takes place at 525 ºC, being an intense and broad peak which means a strong metal-support interaction [326,346].

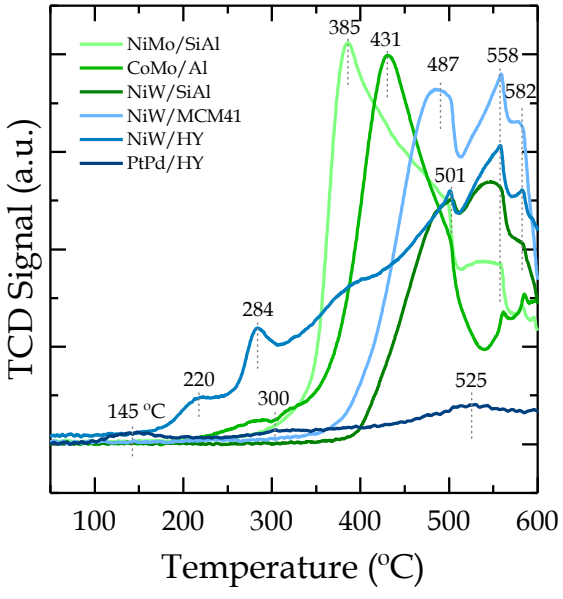

Figure 3.7 Temperature programmed reduction (TPR) of the fresh catalysts.

3.1.2.6 Temperature programmed desorption of H_2S (TPD-H_2S)

The analysis of the stability of sulfur species has been carried out by H_2S temperature-programmed desorption and the results are shown in Figure 3.8. This technique discloses how sulfur interacts with the catalyst and its strength. The higher temperature the sulfur is released, the stronger the interaction will be. Surprisingly the interaction not only depends on metal (or metals) selected but it also is influenced by dispersion of the metal and the support acidic properties [185].

The NiW/SiAl and NiW/MCM41 catalysts display one main peak at 100 ºC, although some authors associate that sulfur released at low temperatures to sulfur

interaction with the support [347] as TEM analysis reveal that these catalysts have a high interaction sulfur-metal. Thus, in this case this peak could be related with loss of sulfur from sulfided metals-like structures which also correlates this result with the low acidity of the support as mention Burch and Collins [348].

On the other hand, the other three catalysts with transition metals (NiMo/SiAl, CoMo/Al and NiW/HY catalyst) show two desorption peaks at 185 and 450 ºC; 100 and 380 ºC; and 160 and 420 ºC for each catalyst, respectively. The peak corresponding to lower temperature is related with weak interactions with the support [349]. The second peak involves interactions with Brønsted sites and appears at 450 ºC, 380 ºC and 420 ºC, respectively. These temperatures are closed to the reaction conditions which catalyst test take place. It is worth mentioning that this may lead to think that the Brønsted sites disappear due to H_2S adsorption but nothing could be further from the truth because Tøpsoe et al. [350], verified their existence in sulfided Mo/Al catalysts under temperature at which reactions were carried out. They used pyridine as base molecule adsorbed at 150 ºC to detect the acid sites by FTIR technique on the sulfided catalysts.

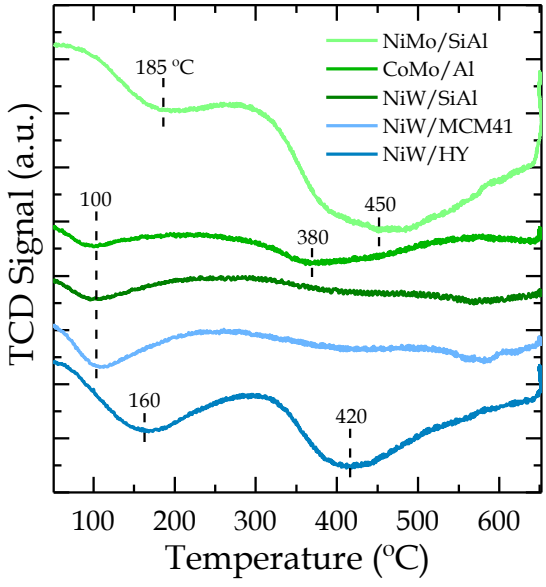

Figure 3.8 TPS of fresh transition metal catalysts.

3.2 VGO HYDROCRACKING

The conversion of the blend (HDPE/VGO) requires catalysts not only with a good hydrotreating performance [144,146] but also with high cracking activity to promote the breakage of long hydrocarbon chains from HDPE and poly-aromatics hydrocarbons (PAH) from VGO into fuel range products. For that reason, this preliminary study will focus on the catalytic conversion of the heavier fraction of VGO feedstock, i.e. heavy cycle oil (HCO), which implies more than 90 wt% of the VGO.

3.2.1 Hydrocracking yields and conversion

Figure 3.9 collects all the results regarding product yield (left axis) and conversion (right axis) using the equations in section 2.5.5. Furthermore, the product distribution of VGO fed is depicted on the first column. NiW/SiAl and NiW/MCM41 catalysts obtained similar conversions (31.6 and 27.4 wt%, respectively) comparable to thermal reaction (28.1 wt%). That is why since the conversion achieved by these reactions is in essence radical mechanism, in spite of reactions with catalysts which are acidic enough to perform β-scission reactions. Moreover, they have similar product distribution, being HCO the most abundant fraction, representing ~70 wt% in three cases and followed by far by LCO fraction (~16 wt%). In those runs, naphtha and gas fractions shown low yields with small differences between them, being both yields ~7 wt%, respectively, for thermal cracking (Th) and NiW/MCM41 catalyst, and 9 and 10 wt%, respectively, for NiW/SiAl catalyst. These results are closely related with catalyst properties: (i) textural and particularly (ii) acidic properties, as other authors saw [135,351]. In this case, the key factor was the low total acidity and the weakness of the acidic sites, together with the low surface area of both catalysts. Thus, the activity of these catalysts can be associated with thermal reactions. These poor results discourage the use of these catalysts in HDPE/VGO hydrocracking.

CoMo/Al and NiMo/SiAl catalysts, which both are good hydrotreating catalysts [146], exhibit an improvement concerning thermal reaction and previous catalysts, which can be attributed to their higher total acidity and also with more Brønsted sites. For both catalysts the conversion increases up to ~50 wt%. LCO and naphtha yields also increase, achieving ~25 and ~15 wt% with a small amount of gas fraction (~10 wt%). As they show similar acid properties, density of Brønsted acid sites have shown to be more important in the conversion than total acidity [352].

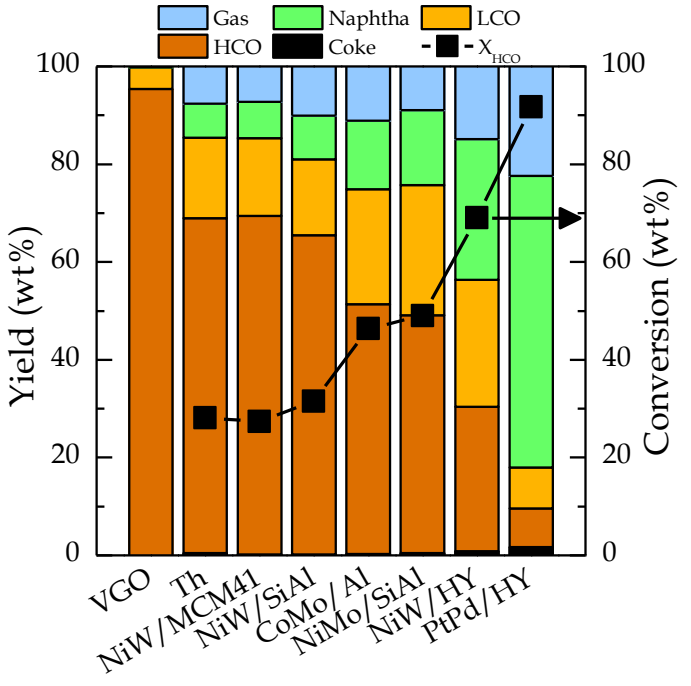

Figure 3.9 Product distribution (bars) and conversion (black square) of HCO with different catalysts. Reaction conditions: feed, VGO; 420 °C; 80 bar; C/F ratio, 0.1; and reaction time, 120 min.

Finally, NiW/HY and PtPd/HY catalysts obtain the best performance. In the case of NiW/HY catalyst, despite neither its textural properties or total acidity are outstanding, surprisingly, this catalyst displays a conversion of 69 wt% with 29 and 26 wt% of yields to naphtha and LCO respectively, keeping a good balance between hydrotreating and hydrocracking activity. However, this catalyst has good metal dispersion and greater number of Brønsted sites since has the highest B/L ratio. Furthermore, this catalyst has SMSI of the most active metal phase (Ni-W-O), which is corroborated by three events: (i) low stacking degree and short length of the sulfided metal particles, (ii) the absence of peaks of the metal phases in XRD and (iii) the highest intensity of the peaks that are related to Ni-W-O species in TPR analysis. On the other hand, PtPd/HY catalyst achieves the highest conversion (91 wt%) with the largest naphtha yield (59 wt%) but the lowest LCO fraction (8 wt%). The prominent behavior of this catalyst involves in addition a higher production of gas (22 wt%). The outstanding hydrocracking activity of this catalyst is due to its higher total acidity and BET surface area.

To sum up, NiW/HY and PtPd/HY catalysts achieve promising results, being appropriate for different approaches in the VGO hydroprocessing: PtPd/HY catalyst is an interesting alternative when pursuing the production of a stream suitable to be added to the commercial gasoline pool, whereas NiW/HY catalyst

may be suitable to produce an adequate stream to be mixed with commercial diesel blending.

To study in deep the performance of the catalysts according their properties, Figure 3.10 depicts two correlations. If we study the correlations of both BET surface and total acidity versus conversion (Figure 3.10a and b, respectively), the results are enlightening. There are good linear correlations for almost all the catalysts in both figures, in such a way, the higher the property value, the higher conversion is achieved. The strength of this correlation is measured with Pearson regression coefficient, which is commonly used to correlate lineally two variables. In that case, the resultant coefficient is 0.989 and 0.984, for correlation in Figure 3.10a and b, respectively. So, these properties are good at explaining the throughput. However, NiW/HY catalyst is out of this trend, not being able to explain the conversion results by any of these correlations. This behavior is due to the strong interaction of Ni-W-O species (as shown in XRD and TPR) that leads to low stacking degree with shorter length when catalyst is sulfided. These attributes together with the highest B/L ratio are stronger linked to hydrogenation and dehydrogenation reactions, which are the key factors for his outstanding results. By contrast, CoMo/Al and NiMo/SiAl catalysts have compensated BET surface area and total acidity, nevertheless, the TPR not shows prominent peaks at high temperature where SMSI appears. On the other hand, NiW/SiAl and NiW/MCM41 catalysts have good metal candidates; nonetheless, their poor textural and acid properties not promote the formation of small crystal size of metal and the formation of SMSI structures.

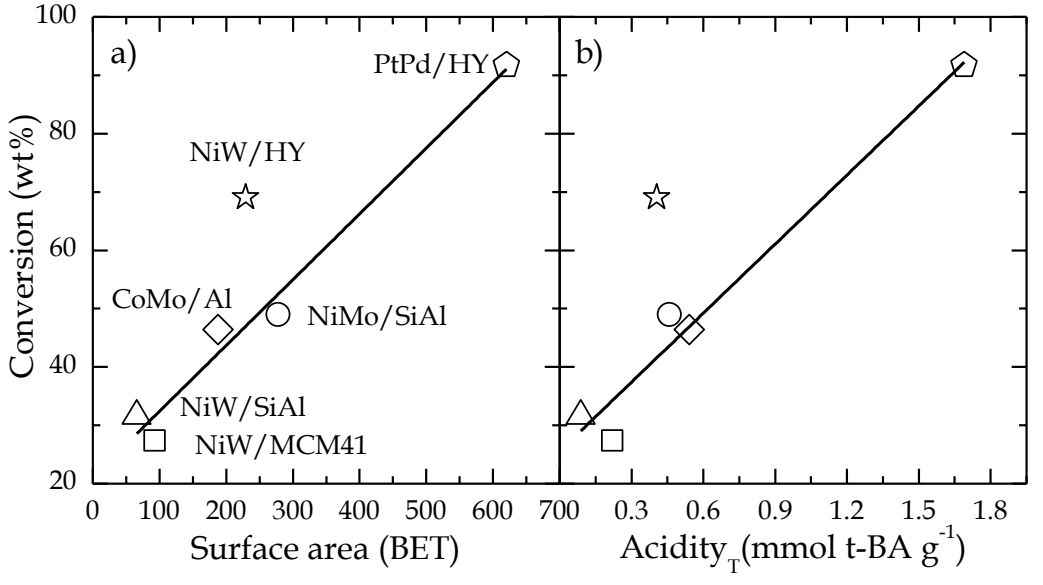

Figure 3.10 Correlation between (a) BET surface and (b) conversion and total acidity and conversion.

So, the different behavior of the catalysts reveals the importance of two facts: (i) the balance between the hydrogenation and dehydrogenation activity of the metallic function of the catalyst and the ring opening/cracking activity of the acidic function of the support, as well as (ii) the diffusivity of the reaction intermediates in the porous structure. Weitkamp [353] highlights that this balance is the key in the conversion and product distribution.

The quality of the hydrocracking has been measured trough the selectivity to fuel index in Figure 3.11. This index, described in depth in section 2.5.5, takes into account the naphtha and LCO produced (dividend) and places the sub-products and unconverted feed as a drawback (divisor), resulting a dimensionless index. When desired products are in larger amount than the value of divisor, this index is larger than 1 ($S_F > 1$) and the higher the value the better. Values of S_F lower than 1 suggest that reaction does not make sense due to either low hydrocracking activity or high selectivity to undesired products. This parameter was applied previously in literature by Li et al. [354,355] to study catalytic activity and selectivity and also to analyze the reaction conditions [308]. As we can see in Figure 3.10, the trend of this index is very similar to that shown by the conversion. Hence, NiW/SiAl and NiW/MCM41 catalysts have an index similar to thermal hydrocracking, CoMo/Al and NiMo/SiAl catalysts have a higher index, although neither reach the value $S_F = 1$. Finally, NiW/HY and PtPd/HY catalysts are the most worthwhile. The values achieved by these catalysts are 1.2 and 2.1 respectively, being both bigger than 1.

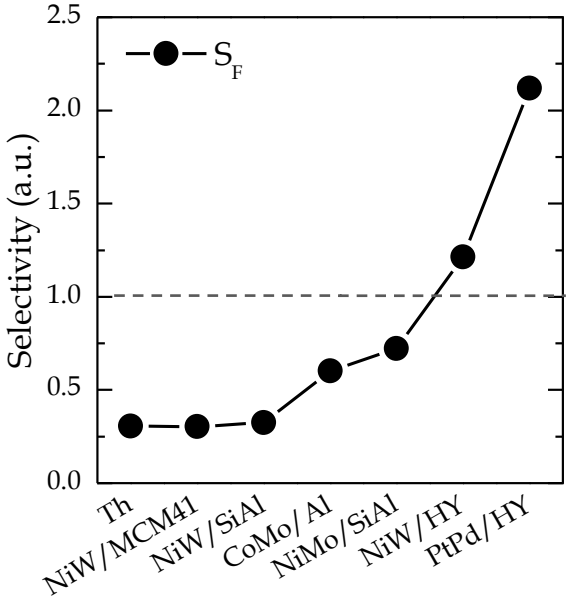

Figure 3.11 Selectivity to fuel index. Reaction conditions: feed, VGO; 420 ºC; 80 bar; C/F ratio, 0.1; reaction time, 120 min.

3.2.2 Gas composition

The composition of the gas obtained in thermal and catalytic runs is depicted in Figure 3.12. The main components in thermal runs (first column) were n-butane and i-butane (~55 wt%) followed by an interesting fraction of propane (20 wt%). Small amount of olefins (as propene) appears also (6 wt%). Although hydrogen pressure was used during the reaction, olefins are reaction intermediates and is common find them due to the absence of metal-hydrogen transfer centers increase its life span [114,135]. These gases constitute the liquified petroleum gas (LPG) fraction (~80 wt%), which have a great economic interest since some of them are platform compounds to synthesize other interesting products such as polyolefin plastics or synthetic fuels by means of oligomerization [356]. Methane and ethane fraction was 10 and 8 wt% respectively and constitute the less interesting dry gas fraction (DG). This fraction is often used in refinery boilers as fuel, helping to reduce the CO_2 footprint since DG produces less CO_2 emissions than other fuels such as gasoil.

The composition obtained for CoMo/Al, NiMo/SiAl and NiW/SiAl catalysts are too similar between them. Comparing with thermal hydrocracking, a reduction of a ~15 wt% in LPG fraction takes place. The main fraction was n-propane with ~30 wt% followed by n-butane (~25 wt%). On the other hand, i-butane fraction (~9 wt%) does not change too much in comparison with thermal hydrocracking. Thus, methane and ethane yields increase, being ~17 and ~20 wt% respectively. It is remarkable that NiW/MCM41 catalyst was the only catalyst generating olefins; this fact denoting low activity of the catalyst. Despite this, the composition of gases was similar to the previous.

Finally, NiW/HY and PtPd/HY catalysts show the best performance since they achieve more LPG than the others. LPG fraction accounted ~80 wt%, as happens in thermal reaction. However, the reduction of n-butane (12 and 19 wt%) occurs while increasing i-butane (32 and 28 wt%) and maintaining high yield to n-propane (~38 wt% in both cases). The DG fraction was ~16 wt%, being ethane the ~10 wt%. Bearing these results in mind, the isomerization activity of these catalysts is another key point, since it indicates a remarkable activity of the acid sites [114]. Furthermore, the absence of olefins reveals a proper behavior of metallic function, which is responsible for hydrogenation-dehydrogenation reactions.

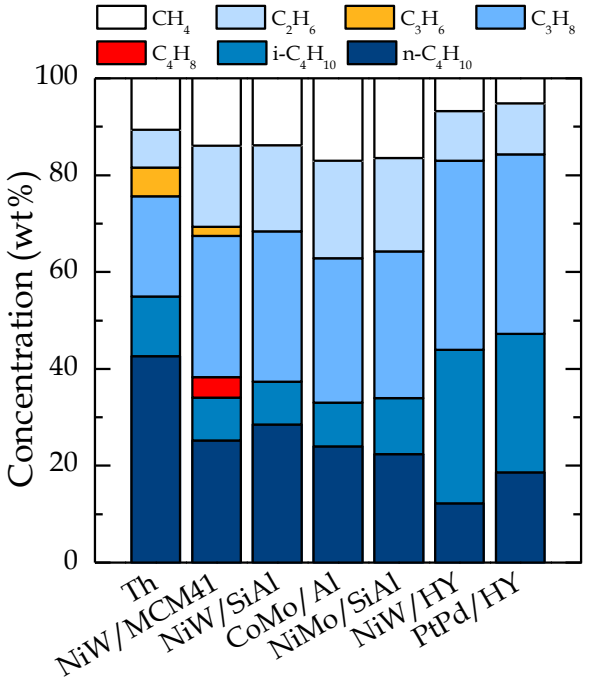

Figure 3.12 Composition of gas fraction. Reaction conditions: feed, VGO; 420 ^{o}C; 80 bar; C/F ratio, 0.1; and reaction time, 120 min.

3.2.3 Naphtha composition

The naphtha compositions for both the thermal hydrocracking and six catalysts are depicted in Figure 3.13. The composition obtained for thermal hydrocracking and when NiW/MCM41 and NiW/SiAl catalysts are used was quiet similar, since the activity of the catalysts was too low. Hence, radical mechanism was the predominant one, which corresponds to thermal cracking. Naphtha from NiW/MCM41 and NiW/SiAl catalysts are slightly more paraffinic, less aromatic and with a similar amount of naphthenic compounds than Th: n-P 34 wt%, i-P 26 wt%, N 12 wt%, A_1 17 wt% and A_2 10 wt%for both catalysts, versus , n-P 33 wt%, i-P 22 wt%, N 12 wt%, A_1 22 wt% and A_2 and 10 wt%, for thermal hydrocracking. The olefin content was negligible in all the cases. According to the previous, the acidity of the support is a key factor in the hydrocracking reactions [139,143,357], when support is not acid enough the main mechanism is the thermal one.

The composition of Th and those catalysts are similar to that obtained by different authors using dispersed catalysts, because although the reaction medium is different the mechanism whereby C-C bonds are broken down is the same. Du et al. [358] run their experiments for three different feedstocks in a stirred batch reactor at 8.0 MPa and 420 ^{o}C during 1 hour using MoS_2 at 300 μg g^{-1} as dispersed catalyst. For all the feedstocks used, naphtha composition showed more aliphatic

than aromatic compounds. The low aromatic content reported may be due to the fact that they were in lower concentration in their feedstock than in our VGO. However, they obtain some alkenes in naphtha. So, the non existence of alkenes in our naphtha could be related to greater performance of our catalyst.

On the other hand, naphtha from CoMo/Al catalyst displays a reduction in n-P and an increase in i-P compared with thermal hydrocracking. However, naphthenic compounds increase up to 15.9 wt% while aromatics are slightly reduced, especially A_2. Although the use of NiMo/SiAl catalyst provides a high yield to naphtha, its composition is highly aromatic under the reaction conditions. A_1 and A_2 imply 26.5 and 11 wt% respectively, in detriment of n-P and i-P (25 and 21.3 wt%, respectively). Naphthenic compounds remained similar to CoMo/Al (15.9 wt%).Finally, naphtha from NiW/HY and PtPd/HY catalysts show the less n-P (~14 wt%) and higher i-P (26.7 and 23.8 wt%, respectively) concentration. Beside, as mentioned in literature [159], NiW/HY catalyst denotes better behavior in HDA in comparison with PtPd/HY catalyst reducing the total aromatic content (XX and XX wt%, respectively) where the main ones are A_1 28.6 and 44.6 wt% respectively. Nevertheless, PtPd/HY shows lower concentration of A3 than NiW/HY (3.3 vs. 7.4 wt% respectively).

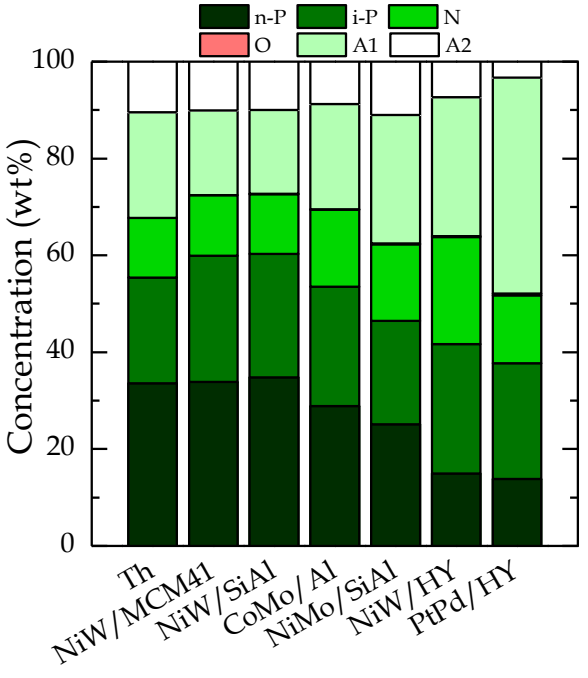

Figure 3.13 Composition of the naphtha. Reaction conditions: feed, VGO; 420 ^{o}C; 80 bar; C/F ratio, 0.1; and reaction time, 120 min.

In Figure 3.14, compounds are grouped by the total number of carbon atoms to study their distribution in naphtha fraction. Under the same reaction conditions, NiW/MCM41 and NiW/SiAl catalysts continue showing a similar distribution

profile to thermal hydrocracking. For these three ones, about 60 wt% is composed by C_9-C_{12} (heavy naphtha). When increasing acidity (CoMo/Al and NiMo/SiAl catalysts), although C_9 is still the main fraction, the compounds with more than 9 carbon atoms diminish, i.e. C_{10} and $C_{11\text{-}12}$ compounds, while C_6-C_8 compounds increase. Finally, NiW/HY and PtPd/HY catalysts achieve the lighter naphtha, being C_7-C_8 the main compounds while the distribution takes a bell-shape. Hence, as a consequence of acidic properties and the subsequence cleavage of heaviest molecules, the lowest C_{10} and $C_{11\text{-}12}$ amount is achieved, especially for PtPd/HY catalyst.

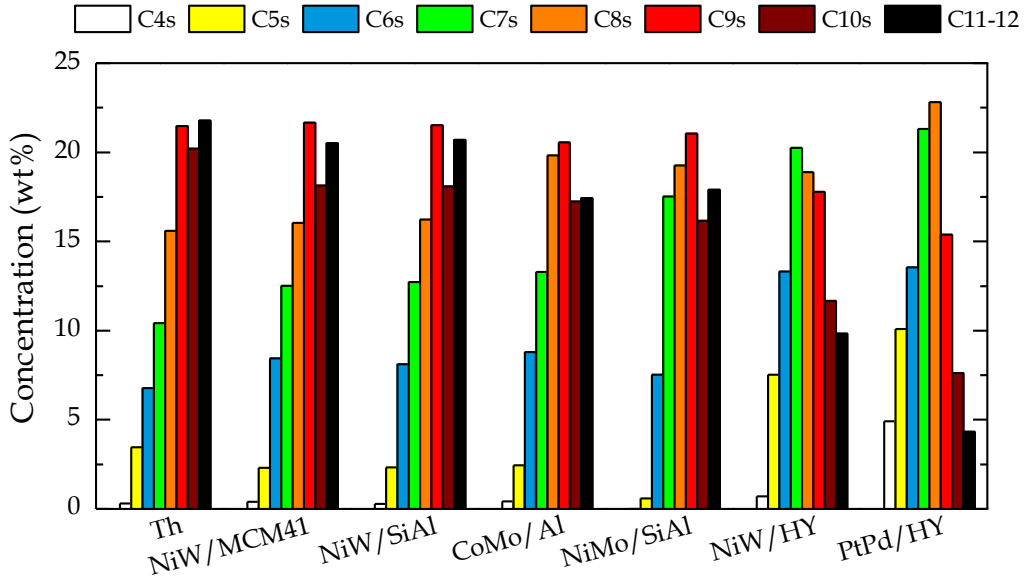

Figure 3.14 Carbon atoms distribution in naphtha fraction. Reaction conditions: feed, VGO; 420 ^{o}C; 80 bar; C/F ratio, 0.1; and reaction time, 120 min.

Something really important that could be a compelling reason in order to choose the best catalyst is not only the quantity of the product but also its quality. With this aim, the research octane number (RON) has been calculated for naphtha fraction and depicted in Figure 3.15. The RON is based on chromatographic information and calculated using the Anderson-Sharkey-Walsh method [309] (explained in detail on section 2.5.5).

The RON obtained with NiW/MCM41 and NiW/SiAl catalysts are slightly lower than that obtained by thermal hydrocracking (76.6, 76.1 and 79, respectively). In thermal hydrocracking, more aromatics are produced increasing the RON. Naphtha from NiMo/SiAl catalyst has a better composition in comparison with previous reactions and RON is 79.9 due to the decrease on n-P and increase in aromatics concentration. On the other hand, although naphtha from CoMo/Al catalyst has less aromatic compounds than that from NiW/MCM41 and NiW/SiAl catalysts, the increase of i-P was a key factor to push RON until 81.3. NiW/HY and

PtPd/HY catalysts show a remarkable upgrade in this parameter, being 86 and 91.4, respectively. Naphtha from these catalysts is more isoparaffinic and aromatic, which enhances the RON. Beside, most compounds are in the C_6-C_9 range. The quality achieved by naphtha coming from PtPd/HY catalyst is comparable to that obtained by Lappas et al. [359], who achieved a RON of 93 in the catalytic cracking of VGO, using a commercial catalyst in a fluidized bed reactor. As well, the result is closed to the values obtained by a CREC RISER simulator reactor during the catalyst cracking of VGO [125]. To sum up and as this screening step shown, the acidity of the catalyst is tightly related with RON obtained by naphtha [360].

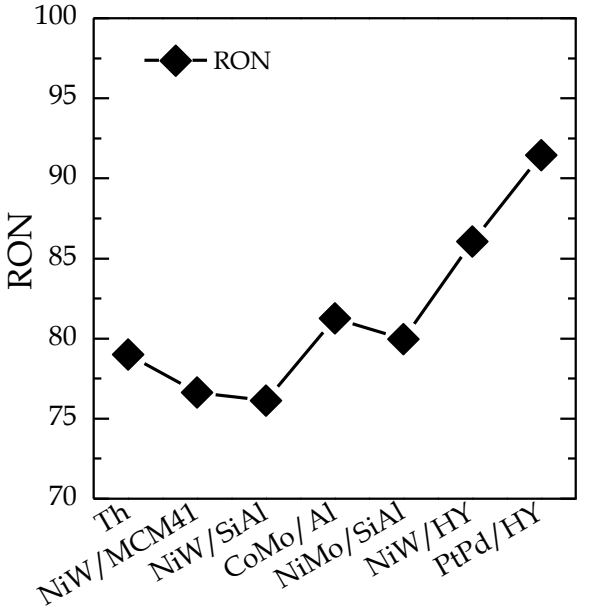

Figure 3.15 Research octane number (RON) of naphtha from different catalysts.

3.3 HYDROCRACKING A BLEND OF HDPE/VGO

After the previous catalyst screening, the hydrocracking of HDPE/VGO blends will be carried out using the most promising catalysts, i.e. NiW/HY and PtPd/HY. The aim of this preliminary study is to assess the prospects of this process for plastic valorization, studying the effect of the addition of HDPE on the conversion and product distribution. Furthermore, this study unveil the more suitable catalyst and appropriate temperature to maximize the production of automotive-like fuels, i.e., gasoline and diesel.

3.3.1 Hydrocracking yields and conversion

The effect of temperature on the hydrocracking conversion of both VGO and HDPE/VGO blend using NiW/HY and PtPd/HY catalysts has been depicted in Figure 3.16.

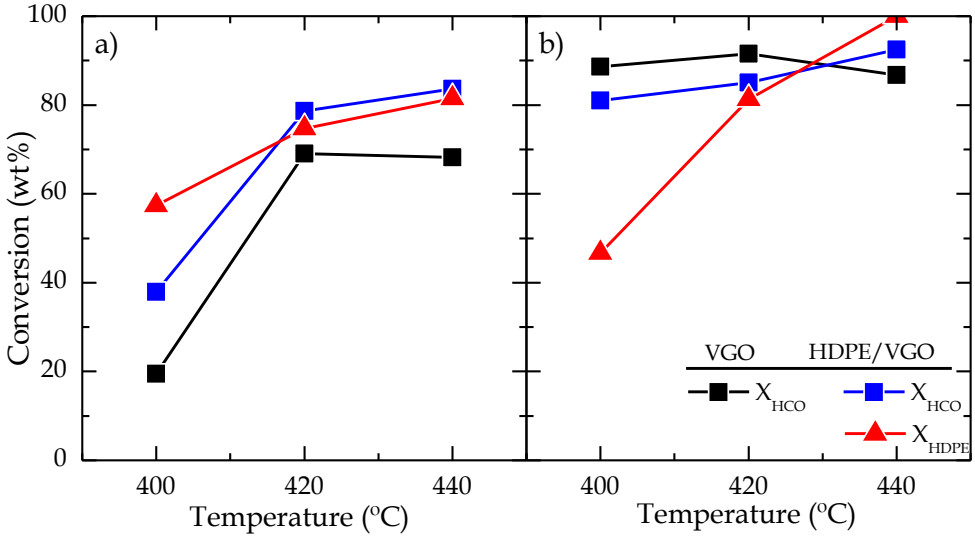

Figure 3.16 Effect of temperature on the conversion of VGO and HDPE in the hydrocracking of VGO and HDPE/VGO blend for NiW/HY (a) and PtPd/HY (b) catalysts. Reaction conditions: 80 bar; C/F ratio, 0.1; reaction time, 120 min.

Comparing the results obtained with both feedstocks, the incorporation of HDPE to the reaction medium has a positive effect on the apparent conversion of HCO for NiW/HY catalyst (Figure 3.16a), for the whole studied temperature range. This result can be attributed to the activity of the strong acidic (Brønsted) sites of this catalyst that activate the carbocationic cracking mechanism of the dissolved HDPE chains above 400 °C, which is the first stage of the hydrocracking mechanism of polyolefins [310]. On the other hand, for PtPd/HY catalyst (Figure 3.16b), the

conversion of HCO is lower for HDPE/VGO blend at 400 and 420 ºC, but higher at 440 ºC. This result can be attributed to the high microporosity of this catalyst that hinders the access of large molecules to the active sites. Therefore, at 400 ºC partially activate the carbocationic cracking mechanism of the dissolved polyolefins. However, above 420 ºC, it is remarkable the increase in the rate of protonation of the olefinic chains, which will presumably be formed by means of the well established free radical mechanism characteristic of non-catalytic cracking. The global tendency of the conversion of HCO is to increase with temperature when the HDPE/VGO blend is fed.

Likewise, the conversion of HDPE rises when temperature is increased for both catalysts, reaching a conversion of HDPE of 81.4 wt% at 440 ºC with NiW/HY catalyst. On the other hand, PtPd/HY catalyst achieves approximately the same HDPE conversion than NiW/HY catalyst but at 420 ºC. However, when the temperature has been increased up to 440 ºC, the total conversion of HDPE has been obtained for PtPd/HY catalyst.

An explanation to the higher HCO conversion in the blend compared to the neat VGO can be found in the synergy between the cracking mechanisms of VGO and the dissolved HDPE. The mechanism of the main hydrocarbon compounds of VGO is well established in the literature [114,361]. Thus, alkanes are hydrogenated in the metallic sites to alkenes, which desorb from the metallic sites and are protonated in the Brønsted sites of the acid function to secondary alkylcarbenium ions. These are the active intermediates of sequential reactions of skeletal rearrangements (different routes) and C-C bond breakage (β-scission), with the subsequent formation of a smaller alkylcarbenium ion and an alkene explained in detail in section 1.4.2. In this mechanism, the alkenes are hydrogenated in the metallic sites to the corresponding alkanes. The aromatics (mainly in the VGO) are hydrogenated in the metallic sites to their corresponding naphthenes (polynaphthenes in the case of PAHs), whose ring opening leads to olefins, which are hydrogenated to paraffins in the metallic sites. This synergy of the stages displaces the thermodynamic equilibrium of the hydrogenation reactions. The co-feeding of HDPE together with the VGO will lead to the fast formation of the secondary alkylcarbenium ions by protonation of the free radicals formed from the HDPE chains [310], activating the aforementioned mechanism for hydrocracking the components of VGO.

The results collected in Figure 3.17 expose that under the investigated conditions high naphtha yield or balanced naphtha and LCO yields can be obtained selecting the proper catalyst and temperature. However, a notorious effect co-feeding HDPE has been observed, which influences the product distribution. Hence, it is more relevant chose the appropriate catalyst given the established aims.

This way, in general, with the NiW/HY catalyst (Figure 3.17a) a temperature higher than420 ºC are required in order to obtain high yields of naphtha and LCO fractions. Besides, the naphtha and LCO yields obtained at 440 ºC are higher for the blend than those obtained in the hydrocracking of VGO. This way, the yield of naphtha is 24.8 wt% (24.4 wt% for the VGO) and the yield of the LCO is 28.1 wt% (24.4 wt% for the VGO). The yield of gases is lower than that obtained with the PtPd/HY catalyst (Figure 3.17b) as a lower overcracking of the naphtha and LCO fractions takes place. Comparing the gas yield for NiW/HY at 440 ºC between both feedstocks, higher yield is obtained when the HDPE/VGO blend is fed (26.5 wt%) compared to that obtained with the VGO (19.5 wt%). Moreover, the gases obtained in the hydrocracking of the blend are composed of lighter compounds (Figure 3.19). It should be noted that the amount of coke deposited on the catalyst is similar for the blend and for the VGO (0.9 and 1.0 wt%, respectively), which indicates that the addition of HDPE to the feedstock has a low impact on the coke formation.

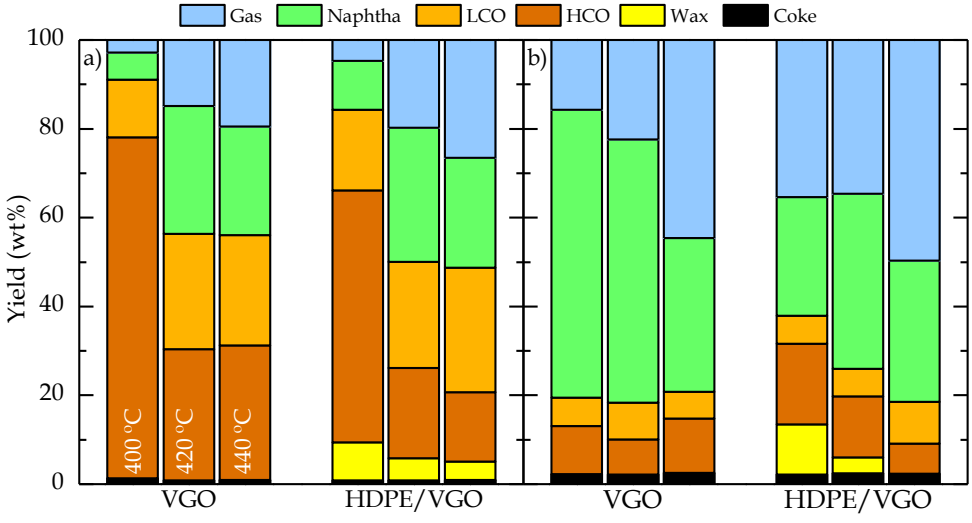

Figure 3.17 Yields (wt%) in the hydrocracking of VGO and HDPE/VGO blend for NiW/HY (a) and PtPd/HY (b) catalysts at different temperatures. Reaction conditions: 80 bar; C/F ratio, 0.1; reaction time, 120 min.

On the other hand, with PtPd/HY catalyst (Figure 3.17b) an excessive overcracking has been obtained when feeding the blend, which led to a high yield of gases and to a subsequent reduction of naphtha and LCO yields. The results obtained at 440 ºC do not follow this trend, as an increase of the yield of the LCO fraction has been obtained in the co-feeding (9.4 wt% for the blend and 6.1 wt% for the VGO) and total conversion of HDPE has been attained, i.e. non wax was detected. Furthermore, a high yield of the naphtha fraction has been obtained (31.8 wt%), even though lower than that obtained in the hydrocracking of VGO (34.9 wt%) because of the overcracking.

Figure 3.18 depicts the selectivity to fuel (S_F) for both catalysts using VGO and HDPE/VGO as a feed. In the case of NiW/HY (Figure 3.18a), the selectivity of VGO hydrocracking reaches a maximum of 1.21 at 420 ºC. The temperature increase beyond 420 ºC provokes a decrease of S_F because the gas yield increases decreasing the naphtha yield. When HDPE is co-fed with VGO, the behavior was similar to the previous one, not interfering positively or negatively in this parameter. Besides, at the highest temperature at which the reactions have been carried out, S_F gets a closer value compared to the best one (1.12). On the other hand, Figure 3.18b collects the results for the PtPd/HY catalyst. Hitherto, this catalyst achieves the best result for this index hydrocracking VGO. However, an abrupt decrease takes place when the temperature increases. Nevertheless, the trend change completely when the blend is hydrocracked. Although results show a maximum at 420 ºC, the selectivity was lower than 1 for all the temperatures in spite of Figure 3.17b shows higher conversions. This fact is due to the large gas yields is the main lump. In this case, it will be interesting to study other operating conditions which reduce the gas yield and maintain good yields to desirable products.

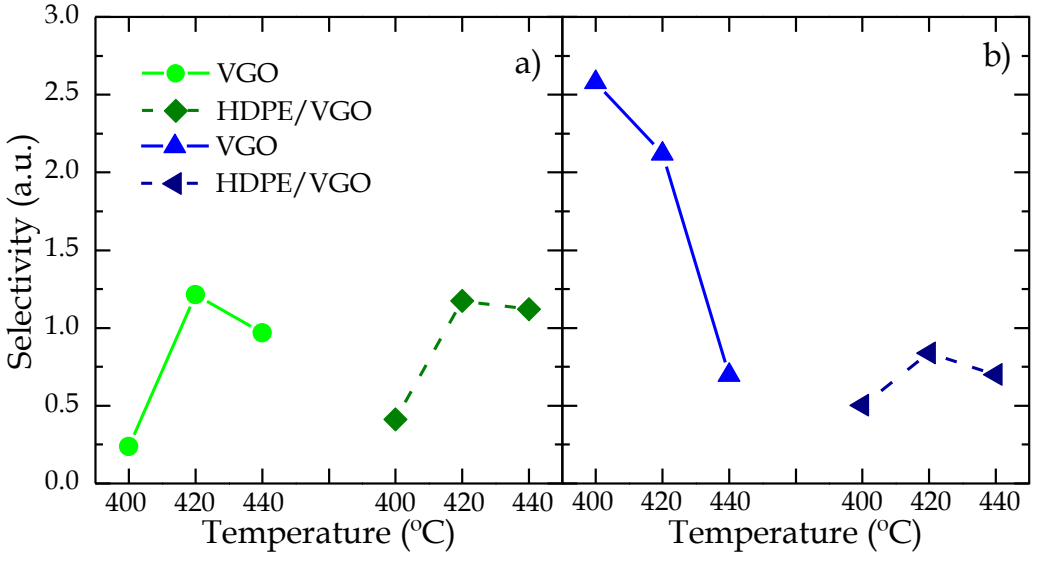

Figure 3.18 Fuel selectivity for NiW/HY (a) and PtPd/HY (b) catalysts at different temperatures. Reaction conditions: 80 bar; C/F ratio, 10; reaction time, 120 min.

3.3.2 Gas composition

As shown in Figure 3.19, in the hydrocracking of VGO and HDPE/VGO, and for both catalysts, the gas fraction is formed by methane, ethane, propane and *iso*-butane. For the NiW/HY catalyst (Figure 3.19a), the addition of HDPE to VGO produced an increase in the yields of propane and *iso*-butane at all temperatures, with values of 48.4 and 25.6 wt%, respectively, at 440 ºC. At the same time, the

yields of the other compounds decreased, with values of 16.3 wt% for ethane and 9.7 wt% for methane. Hence, at low temperatures, the co-feeding of HDPE favors the isomerization reactions, as well as the β-scission reactions of branched hydrocarbons [362]. Furthermore, similar behaviors have been observed with this catalyst in the hydrocracking of VGO at the same temperatures.

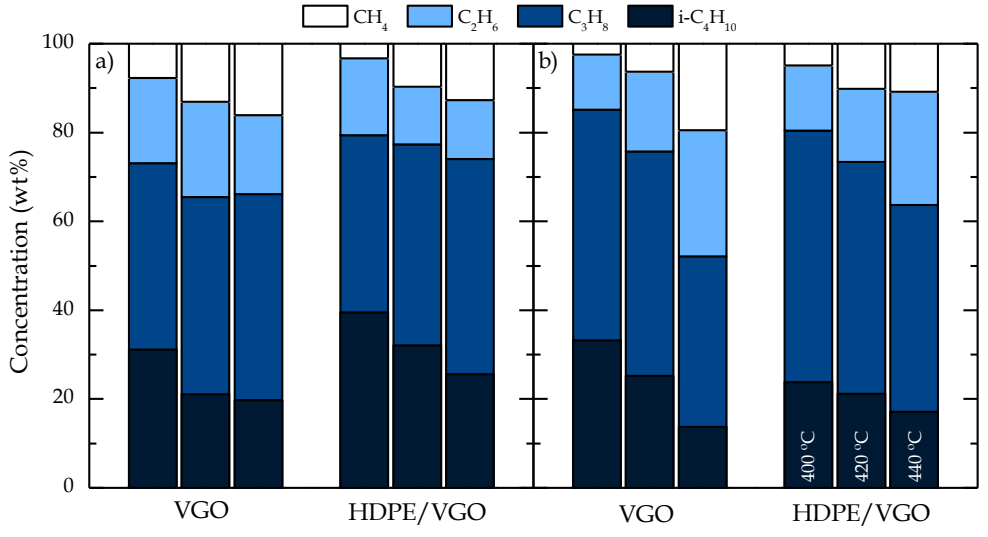

Figure 3.19 Effect of temperature on gas composition in VGO and HDPE/VGO hydrocracking over NiW/HY (a) and PtPd/HY (b) catalysts. Reaction conditions: 80 bar, C/F ratio, 0.1; reaction time, 120 min.

For PtPd/HY catalyst (Figure 3.19b) the same trends for both feedstocks are observed when increasing temperature, thermal cracking reactions are boosted and the yields of methane and ethane raised, whereas the of propane and *iso*-butane yields decreased. However, for this catalyst the concentration of *iso*-butane is lower than that obtained with the NiW/HY catalyst, while the concentration of methane is similar and the concentration of ethane and propane is higher, since the high acidity of the catalyst (Table 3.1) produces the cracking towards lighter compounds.

In the hydrocracking of the HDPE/VGO blend, also higher temperatures favor the production of lighter fractions, increasing the yields of methane and ethane from 4.9 and 14.7 wt% at 400 ºC to 10.8 and 25.5 wt% at 440 ºC, respectively. The yield of propane is reduced with the increase of temperature from 56.6 to 46.5 wt%, as well as the yield of *iso*-butane from 23.8 to 17.2 wt%. It is noticeable that none of the catalysts produce olefins, even at 440 ºC, due to the promotion of hydrogen-transfer reactions that take place on the acid sites available (Table 3.1), particularly by those of high acidic strength [363].

3.3.3 Naphtha composition and RON

The composition of the naphtha fraction obtained with NiW/HY and PtPd/HY catalysts is depicted in Figure 3.20. With NiW/HY catalyst (Figure 3.20a), the naphtha is slightly more olefinic and paraffinic and less aromatic when the HDPE is co-fed. However, temperature has not a marked effect on the composition of the naphtha fraction obtained with both feedstocks, as similar concentrations of all the compounds, i.e. paraffins, naphthenes, olefins and aromatics, have been obtained. Attending to the effect of temperature, it can be seen that the formation of paraffins is boosted at higher temperature, while decreasing the concentration of the rest of compounds.

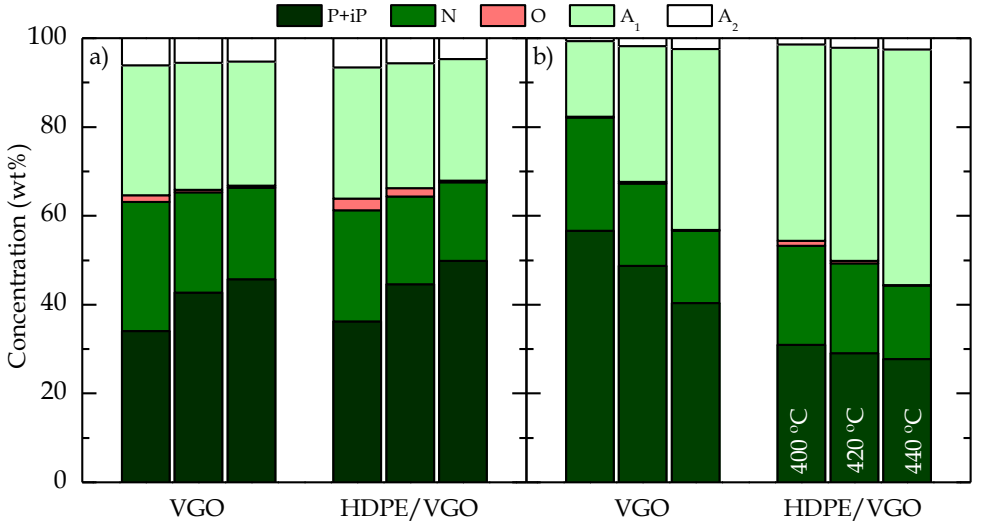

Figure 3.20 Effect of temperature on naphtha composition obtained in the hydrocracking of VGO and HDPE/VGO blend with NiW/HY (a) and PtPd/HY (b) catalysts. Reaction conditions: 80 bar; C/F ratio, 0.1; reaction time, 120 min.

On the other hand, with PtPd/HY catalyst (Figure 3.20b), the co-feeding of HDPE causes the decrease of the paraffin fraction and favors the presence of aromatic compounds, increasing at the same time the RON [364], due to the lower B/L ratio (lower density of Brønsted sites) and consequent lower cracking activity of the support that displaces unfavorably the thermodynamic equilibrium of the first stage of hydrogenation and dehydrogenation reaction. The naphtha obtained at 400 ºC is much more aromatic (45.7 wt%) than that obtained with VGO (17.6 wt%). In the same way, the concentration of paraffins and naphthenes is also smaller (30.9 and 22.2 wt%, respectively).

Furthermore, a small concentration of olefins (1.1 wt%) has been obtained. With an increase of the temperature from 400 to 420 ºC, the concentration of paraffins remains almost constant, whereas the concentration of naphthenes and olefins decrease to 20.2 and 0.6 wt%, respectively. The concentrations of mono- and

di-aromatics increased to 47.9 and 2.15 wt%, respectively, due to the thermodynamic limitation of the hydrogenation. When increasing the temperature up to 440 ºC, the aromatic fraction increased to 55.58 wt%, reducing the concentration of the saturated fraction (naphthenes, 16.58 wt% and paraffins, 27.7 wt%). Finally, the concentration of olefins in the naphtha fraction decreased to 0.1 wt%, as their stability is reduced and their cracking to gaseous products is boosted.

The research octane number (RON) is depicted in Figure 3.21 to assess the quality of the naphtha fraction. In this way, we can see the effect of temperature and compare it between catalysts and how the HDPE addition influences the naphtha RON. The points on the scatter plot are the experimental data and each data group is also accompanied by tendency lines (continuous for VGO and dot lines for HDPE/VGO). Results show that the naphtha RON for VGO hydrocracking with NiW/HY catalyst (Figure 3.21a) decrease when the temperature rises. This catalyst achieves the maximum RON at 400 ºC, which it is 89, and then decreases. This behavior can be related to the increase of the paraffinic fraction and decrease of aromatics.

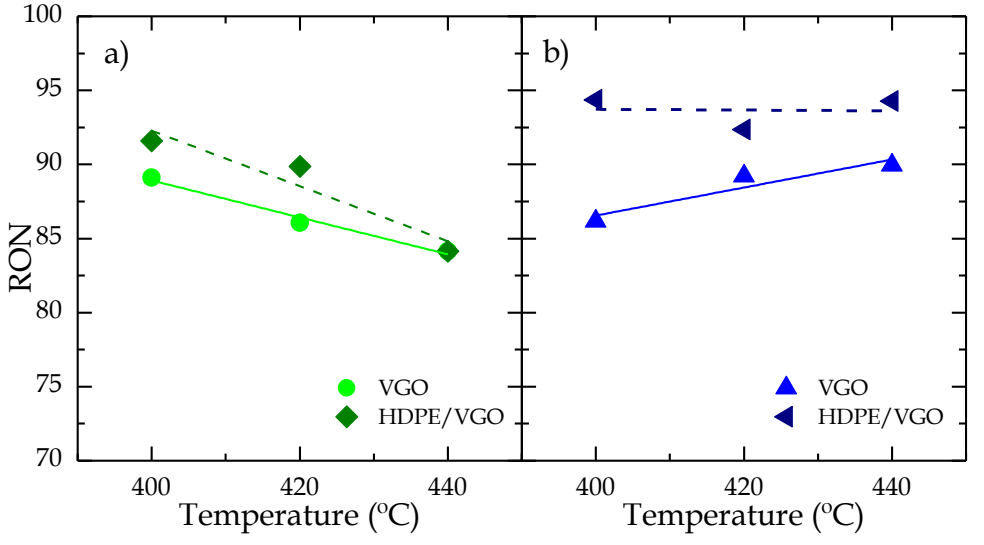

Figure 3.21 Research octane umber (RON) of naphtha vs. temperature for NiW/HY (a) and PtPd/HY (b) catalysts hydrocracking VGO and HDPE/VGO. Reaction conditions: 80 bar; C/F ratio, 0.1; reaction time, 120 min.

On the other hand, PtPd/HY (Figure 3.21b) has an opposite performance. This catalyst enhances the RON when increase the temperature, attaining its maximum value of 90 at 440 ºC. The reason that explain that performance is the push of aromatics when increase the temperature. When HDPE is co-fed, in general, although shows a flat tendency, the obtained RON was higher compared to the RON from the VGO hydrocracking. The PtPd/HY catalyst (Figure 3.21b)

returns the best result of RON for all the temperatures, being 94 the maximum value at 440 ºC. In spite of the different behavior, both catalysts produce naphthas which are feasible to be added in a refinery naphtha pool.

3.3.4 LCO composition and cetane index

The composition of the LCO fraction obtained in the hydrocracking of VGO and HDPE/VGO with NiW/HY and PtPd/HY catalysts is shown in Figure 3.22 to assess that if could be added to diesel pool.

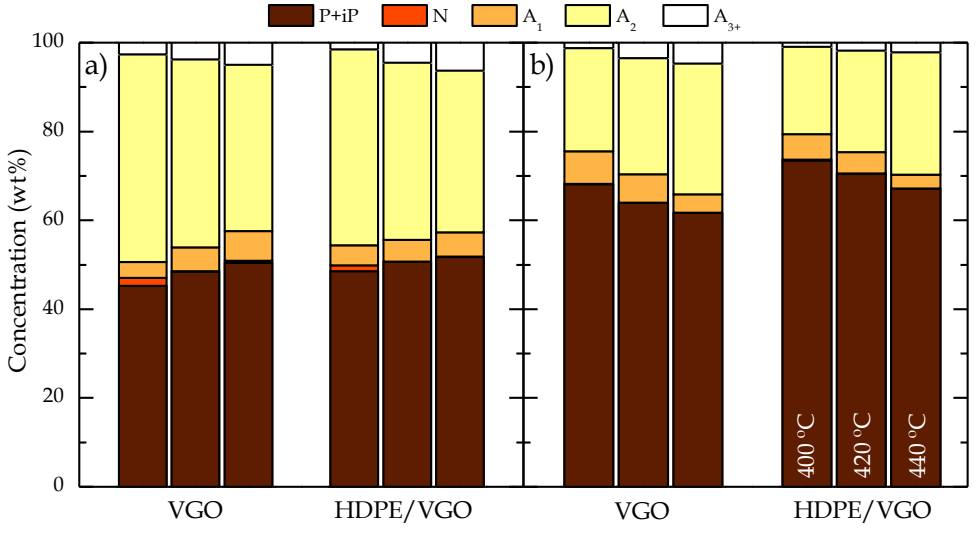

Figure 3.22 Effect of temperature on LCO composition obtained in the hydrocracking of VGO and HDPE/VGO blend with NiW/Y (a) and PtPd/Y (b) catalysts. Reaction conditions: 80 bar; C/F ratio, 0.1; reaction time, 120 min.

NiW/HY catalyst (Figure 3.22a) depicts a more paraffinic LCO in the hydrocracking of the blend than that obtained in the hydrocracking of VGO. At 400 ºC, the LCO composition from VGO hydrocracking is: 48.5 wt% of paraffins, 1.3 wt% of naphthenes, 4.5 wt% of mono-aromatics, 44.2 wt% of di-aromatics and 1.5 wt% of poly aromatics. When increasing the temperature to 420 ºC, the concentration of paraffins increased until 50.7 wt% due to the major extent of the cracking reactions and it remained almost constant at higher temperatures. The concentration of naphthenes becomes negligible at 420 ºC, due to the greater extent of the dehydrogenation reactions to aromatics. In that way, the concentration of poly-aromatics increased with temperature from 4.6 wt% at 420 ºC to 6.3 wt% at 440 ºC. Thus, the concentration of di-aromatics decreased, since they condensed to form poly-aromatics. Moreover, the mono-aromatics slightly increased when temperature was increased to 420 ºC and to 440 ºC (4.9 wt% and 5.4 wt%,

respectively), since they are obtained in the cracking of di-aromatics or from hydrodearomatization of naphthenic compounds.

The results for the hydrocracking of both VGO and HDPE/VGO over PtPd/HY catalyst are shown in Figure 3.22b. Due to the highest activity of the metallic sites of this catalyst, which hydrogenates the aromatics and shifts the equilibrium of the cracking reactions and because most of the HDPE cracks to > C_{16} compounds, the obtained LCO is more paraffinic, less aromatic and no naphthenic fraction has been detected for all the temperature range and both feedstocks. The addition of HDPE to VGO provokes an increase in the concentration of paraffins in the LCO fraction. At 400 ºC, the concentration of paraffins (73.5 wt%) is higher than that obtained in the hydrocracking of VGO (68.1 wt%), while the concentration of mono-, di- and poly-aromatics is lower (5.8, 19.6 and 1.0 wt%, respectively). When increasing the temperature, the hydrogenation reactions are disadvantaged, increasing the concentration of the di- and poly-aromatics while decreasing the concentration of mono-aromatics as well as that of paraffins.

The cetane index is a well know parameter to estimate the quality of the diesel fraction, which is applicable to our LCO fraction. The method followed to estimate this parameter were the ATSM D4737 standard, which are described in detail in section 2.5.5. Figure 3.23 shows with light color symbols with their continuous tendency lines the data from VGO hydrocracking whereas the dark colors with their dot lines are from the HDPE/VGO hydrocracking.

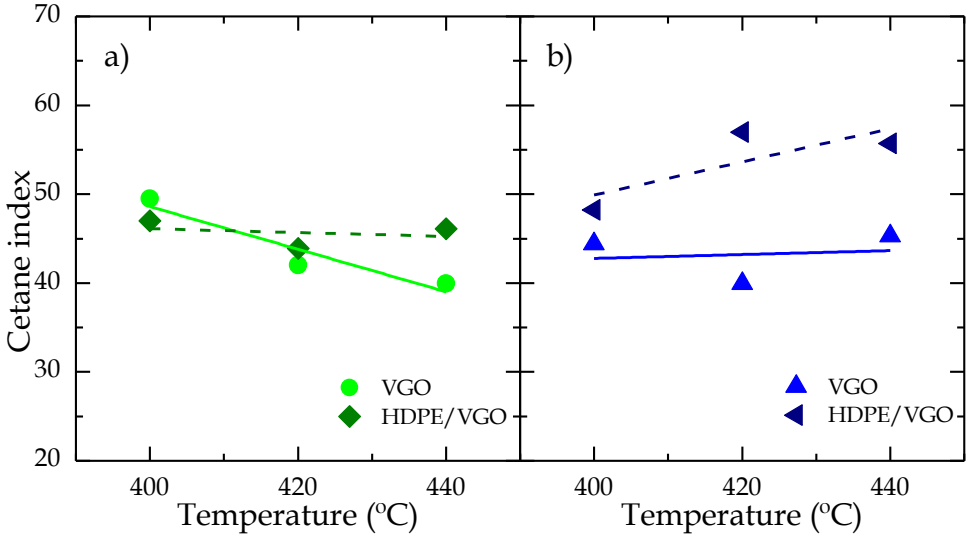

Figure 3.23 Cetane index of LCO fraction vs. temperature for NiW/HY (a) and PtPd/HY (b) catalysts hydrocracking VGO and HDPE/VGO. Reaction conditions: 80 bar; C/F ratio, 0.1; reaction time, 120 min.

The increase of temperature reduces the cetane index of LCO from 50 to 40 when VGO is hydrocracked using NiW/HY catalyst in Figure 3.23a. While on the contrary in Figure 3.23b, the PtPd/HY catalyst illustrates a small but positive slope, achieving 45 at the maximum temperature. So 420 ºC is a inflexion point in this case where the NiW/HY catalyst comes from behaving better at lower temperatures but the situation flips and the PtPd/HY catalyst underscores at higher temperatures. The addition of HDPE to VGO reveals an improvement for both catalysts in comparison with the obtained in LCO from neat VGO hydrocracking. In the case of the NiW/HY catalyst (Figure 3.23a), it reduces drastically the influence of temperature in the cetane index keeping it almost constant at 45. On the other hand, hydrocracking the blend with the PtPd/HY catalyst (Figure 3.23b) produces a LCO whose CI increases when temperature rises.

CHAPTER 4

CO-HYDROCRACKING OF DIFFERENT WASTE PLASTIC AND VGO

4 CO-HYDROCRACKING OF DIFFERENT WASTE PLASTIC AND VGO

In this chapter it has been studied the suitability of different approaches to upgrade waste plastic to automotive fuels range hydrocarbons. These approaches have consisted on the hydrocracking of different blends made of plastics (HDPE and PP), plastic pyrolysis oil (PO) and vacuum gasoil (VGO, current hydrocracking unit feedstock) according to different strategies.

One of the approaches consists on the valorization of a blend of PO and VGO. This strategy is based on a decentralized waste plastics management model, in which the polyolefinic plastics (2/3 of plastics in municipal solid waste (MSW)) would be treated in a fast pyrolysis plant located in the proximity of the MSW collection and classification points, and the PO obtained would be afterwards sent to refinery for its centralized upgrading to fuels. The PO studied is the one corresponding to the pyrolysis of HDPE. The PO content in the blend (20 wt%) has been established based on the results of the catalytic cracking study under FCC conditions [127–130] and the hydrocracking PO [365–367].

The second strategy is the direct valorization of the polyolefins (HDPE or PP in our case) dissolved in VGO. This dilution with 20 wt% of plastic, regarding the results in the catalytic cracking [117,119,123,125] and in hydrocracking of HDPE or LDPE blends with LCO and VGO [152,153,156],can be done in either at the sorting points or at the refinery itself. Furthermore, the hydrocracking of a ternary mixture of HDPE, PO and VGO has been studied, being this approach the combination of the previous two strategies, with the possible advantage respect to the valorization of the HDPE/VGO blend with a better dissolution of HDPE in the reaction media. Besides, neat VGO and PO have been also hydrocracked in order to quantify the influence of blending in the results.

To facilitate the monitoring of the results, the blend of PO/VGO, HDPE/VGO, PO/HDPE/VGO and PP/VGO will be identified with the key Blend 1, Blend 2, Blend 3 and Blend 4, respectively. The reaction conditions will be the following:

- Temperature: 400 - 440 ^{o}C
- Pressure: 80 bar H_2
- Catalyst to feed ratio: 0.1 (in mass)
- Stirrer speed: 1300 rpm
- Reaction time: 120 min

The reactions are carried out with a NiW/HY catalyst (section 4.1), since it is an active catalyst with a commitment production of naphtha and LCO (diesel)

fractions as it has been previously proven (in section 3.3), and with a PtPd/HY catalyst (section 4.2), as it achieves high naphtha rates and full conversion of HDPE [368]. Furthermore, in both sections, the gas and liquid fractions have been analyzed as well as it has been calculated the selectivity index which has allowed performing a proper analysis of the hydrocracking quality as well as evaluating the suitability of the products for their integration into the refineries' fuel pools.

Thereafter, in general, it has been found along this Thesis that the PtPd/HY catalyst causes overcracking of most feedstocks and especially with PO, PO/VGO (Blend 1) and HDPE/VGO (Blend 2). In the case of PO, this overcracking is justified given that it contains low boiling point compounds (into naphtha range). This behavior also takes place even with the NiW/HY catalyst. However, this argument is not applicable to the HDPE/VGO blend. PtPd/HY catalyst has high acidity but place the main one in the micropore of the zeolite, there HDPE molecules has a difficult access to the micropore of the zeolite and overcracking the liquid fraction (VGO). Therefore, two possible alternatives have been proposed to face the overcracking of PtPd/HY with HDPE/VGO: (i) modify the acidic and textural properties of the catalyst through alkaline desilication (carried out in section 4.3) and (ii) study the effect of operating conditions on product distribution and conversions in order to minimize the undesired products (gas and coke) and maximize the naphtha and LCO lumps (Chapter 5). Consequently, in section 4.3.3 the results of HDPE/VGO hydrocracking at 440 ^{o}C, 80 bar, 120 min with the parent PtPd/HY catalyst (called, Cat-A) are shown in comparison with two other catalysts synthesized from Cat-A with different alkaline treatments (Cat-B and Cat -C).

4.1 NiW/HY CATALYST

4.1.1 Hydrocracking yields and conversion

Figure 4.1 shows the effect of temperature on product distribution (yields) and the HCO and plastic conversions (X_{HCO} and $X_{plastic}$, respectively) obtained for each batch. Reaction products have been lumped in six lumps (gas, naphtha, LCO, HCO, wax and coke). This way, at 400 °C moderate values of X_{HCO} have been obtained with all the blends (X_{HCO} < 26 wt%) except for Blend 4 (X_{HCO} = 33 wt%). Indeed, the lowest value has been obtained for the VGO (19.1 wt%) followed by PO (21 wt%), meaning that either binaries or ternary blends promote the conversion of heavy compounds into lighter ones. This asseveration is ratified by the conversion obtained with PO/VGO (Blend 1), higher than that obtained in the hydrocracking of neat VGO or PO.

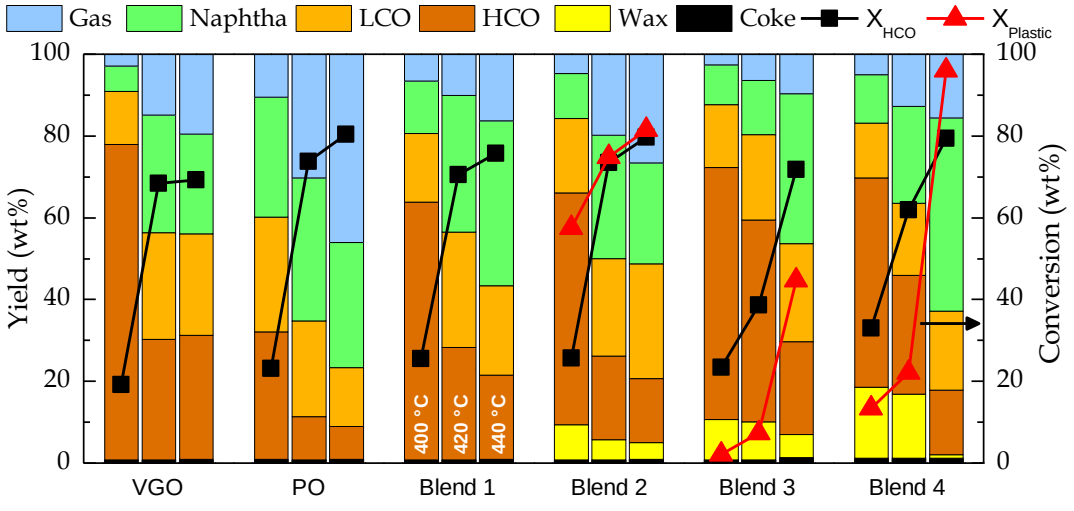

Figure 4.1 Effect of temperature on the yields and conversions for different feedstocks. Reaction conditions: NiW/HY catalyst; 80 bar; C/F ratio, 0.1; reaction time, 120 min. Key: Blend 1, PO/VGO; Blend 2, HDPE/VGO; Blend 3, PO/HDPE/VGO; Blend 4, PP/VGO. The data of neat VGO and HDPE/VGO hydrocracking (Blend 2) have been obtained from section 3.3.

The higher X_{HCO} with all binary mixtures may be due to: (i) the higher hydrocracking reactivity of HDPE, PP and PO compounds comparing to VGO, and; (ii) the synergistic effects between the cracking mechanisms of VGO and dissolved HDPE, PP or PO. However, the low PP conversion denies these two statements for all the feedstocks. Hence, the fact of the high HCO conversion with PP/VGO can be because of the low reactivity of PP and the only reactions of VGO molecules.

The mechanism of the main hydrocarbon compounds of VGO has been deeply studied in literature [114,361,369]. Therefore, Figure 4.2 depicts how alkanes

are dehydrogenated to alkenes in the metallic sites, and that is why the metal plays an important role being relevant its hydrogenation and dehydrogenation capacity (Figure 4.2a).

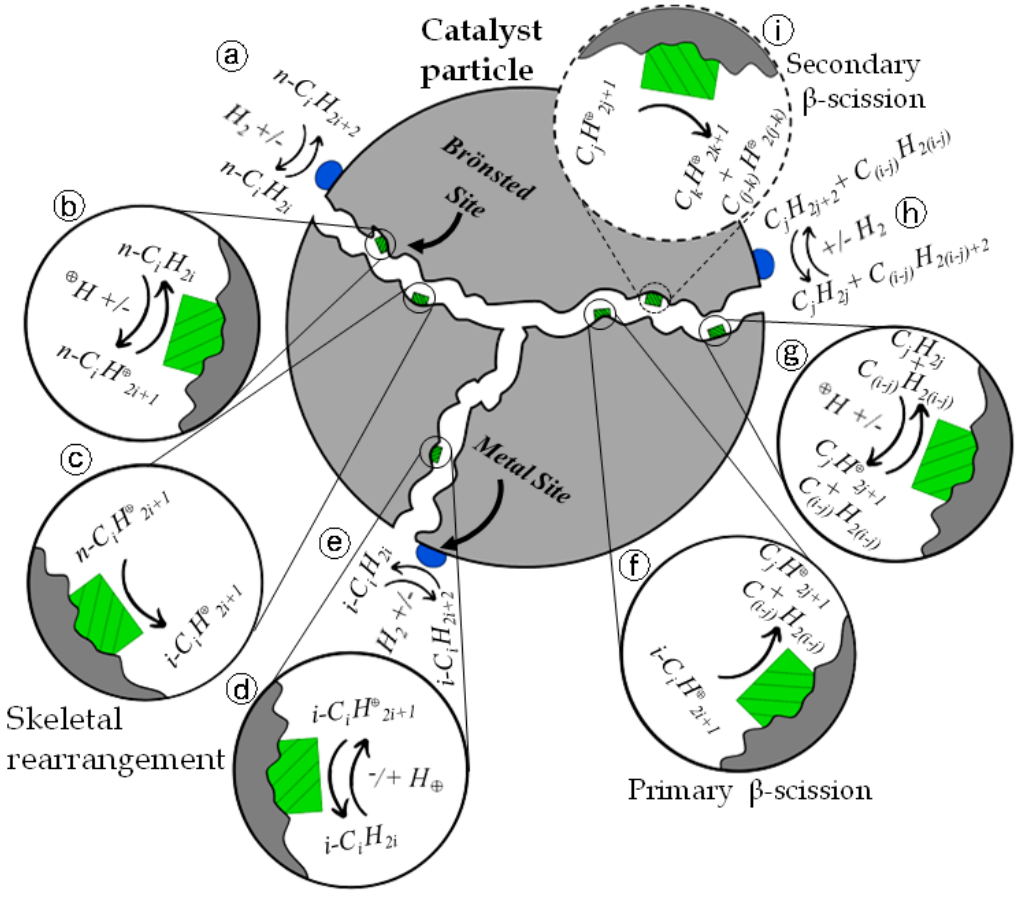

Figure 4.2 Hydrocracking and isomerization mechanism scheme from alkanes in both metal and Brønsted acid sites.

The formed alkenes desorb from the metal sites and migrate to Brønsted acid sites to be protonated to secondary alkylcarbenium ions (Figure 4.2b). The β-scission of the secondary alkylcarbenium ions, in which a smaller alkylcarbenium ion and an alkene are formed (Figure 4.2f), rarely occurs because the by-product of the reaction is energetically unfavorable. However, it is remarkable that the likelihood of β-scissions take place increases as long as the branching degree in the secondary alkylcarbenium ion increases. Thus, the most likely route is the skeletal rearrangement to mono-branched alkylcarbenium ions (Figure 4.2c), which desorb from the acid sites as i-alkenes after being deprotonated (Figure 4.2d) and diffuse to metal sites where they are hydrogenated to the corresponding iso-paraffins (Figure 4.2 e). As the conversion moves forward, mono-branched paraffins are promoted to di-branched paraffins and so on. After that, when di-branched paraffins come to Brønsted acid sites, is highly probable that primary β-scissions take place (Figure

4.2f). Then the new alkylcarbenium ion and ($C_j H^{\oplus}_{2j+1}$) is deprotonated in the same or other Brønsted active site (Figure 4.2g) and in metal active site both alkenes are hydrogenated (Figure 4.2h). There is the possibility that a second β-scission occurs when the new alkylcarbenium ion is long enough and has branches (Figure 4.2i), giving rise to another alkylcarbenium ion and another alkene. These new molecules would later follow the procedure already described giving new shorter chain alkanes (Figure 4.2g and h).

On the other hand, aromatics (major compounds in VGO) also are hydrogenated in the metal sites to their corresponding naphthenes (or polynaphthenes in the case of PAHs). The ring opening reactions of the naphthenes that form olefins is thermodynamically favored, which are, in turn, hydrogenated on the metallic sites into paraffins. The synergy of the two stages, hydrogenation and subsequent cracking, displaces the thermodynamic equilibrium of the hydrogenation reactions. So, taking into account the composition of the waste plastic-derived feeds, the co-feeding of HDPE, PP or PO together with VGO will lead to the rapid formation of secondary alkylcarbenium ions by protonation of the free radicals which, although are neutral charge molecules, they are highly reactive, as Shabtai et al. [310] notice from HPDE chains and PO olefins, activating the aforementioned mechanism for the hydrocracking of VGO components.

As was evaluated in Section 3.3, Blend 2 achieves a surprisingly high valor de $X_{plastic}$ (57.4 wt%), which almost doubles the conversion obtained (31.0 wt%) by Palos et al. [156] in the hydrotreating of a HDPE/LCO blend under similar operating conditions. This difference is a consequence of the higher reactivity of the components of the VGO regarding to the LCO ones, which is a highly refractory refinery stream. However, the $X_{plastic}$ obtained with the PO/HDPE/VGO (Blend 3) (2 wt%) is much lower than that obtained with binary mixtures. Furthermore, the lowest X_{HCO} corresponding to the blends is also obtained with PO/HDPE/VGO (Blend 3) (23.2 wt%), which clearly exposes that, PO and HDPE molecules are competing for being adsorbed on the active sites. This is strongly affected by the preferential adsorption of some compounds due to their different chemical structure, and hence, their polar nature is the key factor. The adsorption order of the molecules on hydrocracking catalysts is [171]: aromatics > naphthenes > alkanes. The composition of PO is mainly alkenes (more than 50 wt%) which are slightly more polar molecules than alkanes. Moreover, the diffusivity of molecules in the pores of the catalyst is strongly affected by his molecular weight. This way, the suppression of the conversion of diluted HDPE macromolecules because of both the preferential adsorption and easier diffusion of PO components can explain the obtained result.

Furthermore, concerning to the preparation of some feeds, two different types of polyolefin plastics have been used: HDPE and PP. Although in somehow those plastics are considered semi-crystalline with low short branching degree, have different properties like density, melting point or organic solvent resistance among others. Thus, as a consequence of the fact that PP has higher resistance to chemicals and organic solvents, is stiffer and has higher melting point in comparison to HDPE, it makes PP a harder plastic to be attacked. However, in spite of PP TGA shows its pyrolysis at lower temperature than HDPE (maximum of DTG at 465 and 484 ^{o}C, respectively), it still above enough in comparison with the reaction temperature achieved in some reaction conditions, thus, the conversion of PP into like-fuel products is more difficult. Hence, at temperatures lower than 420 ^{o}C PP achieves poorer outcomes in comparison to HDPE. However, at maximum temperature, the resistances depicted previously according to their different nature seems to fade away down and therefore PP conversion in Blend 4 overcome the extent achieved by HDPE in Blend 2 at the same operating conditions. These better results from Blend 4 may be due to the fact that when the PP is broken into medium-sized chains, the natural branches in this chains can promote the secondary β-scission (Figure 4.2i), which push the conversion and yields to light compounds in the naphtha range.

Attending to the products distribution, it can be seen that higher temperatures than 400 °C are required to further hydrocrack HCO lump into lighter lumps. This way, the highest and lowest yields of HCO lumps have been obtained in the hydrocracking of VGO and PO (77.1 and 31.1 wt%, respectively), which is in concordance with their composition (Table 2.1). Therefore, these feedstocks achieve a X_{HCO} of 19.1 and 23 wt%, respectively. However, the yields of desired products (naphtha and LCO) are 6.2 and 13 wt%, respectively, in the case of the VGO and 29.3 and 28 wt%, respectively, for PO. Such difference comes from the starting composition as mentioned before, where the compounds in PO produce more gases in its hydrocracking than VGO (10.5 and 2.8, respectively). In blends hydrocracking, the presence of PO, PP or HDPE with the VGO promotes the X_{HCO}. Furthermore, PO/VGO (Blend 1) and neat PO are the feedstock that are greatly converted into gas products, given their lighter composition (Table 2.1) and its higher tendency to overcrack. The yield of naphtha and LCO, which are the most interesting products, is quite similar for all the blends. In the case of naphtha, yields vary from 9.8 wt% for Blend 3 to 12.8 wt% for Blend 1 and for LCO, its yield changes from 13.4 wt% for Blend 4 to 18.1 for Blend 2. Finally, the yield of coke deposited on the catalyst, is slightly higher in the hydrocracking of PP/VGO (Blend 4) (1.2 wt%) than for the rest of the feedstocks (c.a. 0.85 wt%). Overall, similar results have been obtained by Karayildirim et al. [311] in the hydrocracking of VGO, LDPE and the blend thereof.

According to X_{HCO}, differences between feeds are not too big. While with Blend 3 is obtained the poorer conversion (23.3 wt%), with Blend 4 the greatest one is achieved (32.8 wt%) and with Blend 1 and 2 the X_{HCO} values are similar (~25.6 wt%). However, the values of $X_{Plastic}$ await big differences with different feedstocks. While with Blend 2 is attained the greatest conversion (53.4 wt%), the results with Blend 3 and 4 (regarding HDPE and PP conversion, respectively) are kept very far (2 and 13.3 wt%, respectively). The poor results obtained by Blend 3 seem to be a problem of compatibility between the feeds, since Blend 2, which also contains HDPE, is the one that has obtained the highest conversion. On the other hand, although the addition of plastic alone seems to work well for HDPE, this does not happen for PP. The reasons why a good performance is not achieved lies in the difference of its properties regarding to HDPE mentioned above. PP has properties that make it harder and resistant to be attacked, which is the reason why it is more difficult to convert.

An increase of the temperature up to 420 °C has a significant effect on both conversions (X_{HCO} and X_{HDPE}) and product distribution, with the exception of the PO/HDPE/VGO (Blend 3) for which it is less noticeable. Naphtha and LCO yields reach good levels from neat feed. Naphtha yields are 28.8 and 35 wt% for VGO and PO, respectively, whilst LCO yields are 26.1 and 23.3 wt%, respectively. However, with some blends are achieved better targets in naphtha yield than that shown by VGO and close to neat PO. Thus, the hydrocracking of Blend 1 and 2 exhibits similar naphtha yields (33.5 and 30.1 wt%, respectively). Nevertheless, the highest value of LCO yield is obtained for Blend 1 (28.2 wt%) while the LCO yield corresponding to Blend 2 hydrocracking is comparable to neat feedstock hydrocracking (23.8 wt%). Behind those results, there are the yields of Blend 4. This blend produces 23.7 wt% of naphtha and 17.5 wt% of LCO. Those lesser results can be due to the lower reactivity of PP. Finally, Blend 3 hydrocracking report the lowest naphtha yield (13.4 wt%) and low LCO yield (20.8 wt%), which are even lower than neat feedstock hydrocracking. This way, it seems that there are good synergies observed in Blend 1, Blend 2 and also Blend 4 which are binary mixtures. However, for ternary mixtures (Blend 3) the competition for the active sites remains as an important drawback.

Concerning X_{HCO}, the hydrocracking of VGO offers once again the lowest value (68.3 wt%), whereas the highest ones have been obtained with both PO and HDPE/VGO (Blend 2), with c.a. 73.5 wt%. The highest X_{HCO} of the PO is directly attributed to the lighter composition of this feedstock (Table 2.1), while from HDPE/VGO (Blend 2) can be attributed to the hydrogen donor character of the HDPE [155]. The hydrocracking of PO/VGO (Blend 1), in turn, offers a satisfactory value of X_{HCO} of 70.3 wt%, slightly lower than that obtained with the other feedstocks, meaning that the conversion boosting effects of this blend observed at

400 °C are attenuated when temperature is increased. On the other side, the X_{HCO} of Blend 4 is lower (61.8 wt%) and much lower for Blend 3 (38.5 wt%). On the other side, the $X_{plastic}$ obtained with HDPE/VGO (Blend 2) increases notoriously with temperature, reaching a value of 74.7 wt% at 420 °C. The conversion is promoted by the greatest number of free radicals which appear when temperature is raised [21]. Free radicals are formed by thermal hydrocracking owing to thermolytic process in the medium or by hydrogen abstraction reaction that occurs in the catalyst weak acid sites [152]. On the contrary, both Blend 3 and 4 display poor $X_{plastic}$. In spite of the high $X_{plastic}$ in the hydrocracking of Blend 2, this conversion in Blend 3 is stuck at 7.3 wt% due to a bad synergy in which the competition for acid sites blocks the adsorption of larger alkanes from HDPE. Finally, although the competition for active sites is not the problem in the case of PP conversion in Blend 4 (22.1 wt%), this value is explained by the intrinsic resistance of this polymer for being cracked.

As expected, the values of the X_{HCO} and $X_{plastic}$ have increased with temperature, reaching its maximum values at 440 °C (Figure 4.1), even for the blend PO/HDPE/VGO (Blend 3). However, this not implies an improvement in the products distribution, because the gas yield increases drastically at this reaction temperature; in the case of hydrocracking of VGO, this yield arises to 19.5 wt% from 2.8 wt% at 400 ^{o}C. But this increase is not comparable to that achieved by PO hydrocracking, for which the highest gas yield is obtained at 440 ^{o}C (45.9 wt%). These increases in the gas yield impact the yield of desired products. This way, naphtha and LCO yields are lower than at lower temperature, being 24.4 and 24.8 wt%, respectively, for VGO, and 30.6 and 14.5 wt%, respectively, for PO. On the other hand, co-feeding polyolefins with VGO have led to mitigate or enhance the yield of products lumps. For Blend 1, Blend 3 and Blend 4, the gas yields are lower than obtained by neat feeds (16.2, 9.6 and 15.5 wt%, respectively). So, the blends have meant an improvement reducing the overcracking issue. In the particular case of Blend 4, which contains PP, this plastic contains one branch in its monomeric structure. Therefore, the cracked fragments from long PP chain have various branches which, according to Weitkamp [114], promote the primary and secondary β-scission, then reducing the amount of gas.

Based on these results, an interesting distribution of products is obtained for the hydrocracking of the Blends at 440 ^{o}C, with a naphtha yield of 40.4, 36.7 and 47.2 wt% for Blend 1, Blend 3 and Blend 4, respectively. It has to be pointed how the performance changes from PO to Blend 1 (PO/VGO) where the overcracking of naphtha to gas has lessened. Furthermore, in the hydrocracking of Blend 4, the greatest naphtha yield is obtained as a result of the push received by the β-scission of fragments from PP chain. The LCO yield when hydrocracking these feeds (Blend 1, Blend 3 and Blend 4), not overcomes the values achieved by VGO hydrocracking but are similar (21.7, 23.9 and 19.4 wt%, respectively). Only from Blend 2 has

slightly larger gas yield (26.5 wt%) than from VGO, with also a slightly higher naphtha yield (24.8 wt%). However, the LCO yield (28.1 wt%) overcomes the LCO yield achieved by VGO, and is the largest value obtained for all feedstocks. Finally, it should be noted that the coke yield increases slightly when increasing the reaction temperature for all the feedstocks. This result is explained because the condensation and dehydrogenation reactions of the components of the reaction medium (particularly the heavier ones) are favored to form the polyaromatic structures of coke. This effect becomes more important than the hydrocracking reactions of the coke precursors.

The values of X_{HCO} in the hydrocracking of neat VGO and PO achieve the minimum (69.1 wt%) and the maximum (80.3 wt%) values, respectively, at 440 ºC. This way, for the ternary mixture (Blend 3) X_{HCO} achieves a higher value (71.7 wt%) than for the VGO, whereas Blend 1 is located in the middle of the range with 75.6 wt%. Finally, the X_{HCO} values for Blend 2 and 4 are closer to achieved by neat PO, being 79.5 and 79.3 wt%, respectively. Therefore, although PO hydrocracking attains the maximum HCO conversion due to its light composition, the binary mixtures PP/VGO (Blend 4) and HDPE/VGO (Blend 2) show better results of desired products with a lower gas yield. Hence, the aforementioned results indicate that at 440 ºC direct plastic addition to VGO has greater advantages than the PO addition, in both X_{HCO} and product distribution.

In accordance with the strategies to convert polyolefins from waste plastic, it should be noted that at 440 ºC, better results are obtained with the binary plastic blends (Blend 2 and 4) than with the ternary blend. Although it is observed that the $X_{plastic}$ obtained for PO/HDPE/VGO (Blend 3) has increased substantially at 440 ºC respect at 420 °C (44.5 vs. 7.3 wt%) due to the extent of radical mechanism is favored, results still so far from the obtained with HDPE/VGO (81.4 wt%) and PP/VGO (95.9 wt%). Therefore, as conversions denotes, there is no advantages in the hydrocracking of ternary Blend (PO/HDPE/VGO) in comparison with binary ones (PO/VGO, HDPE/VGO and PP/VGO), even when PP (less reactive plastic) is fed. However, attending to products distribution, PO/HDPE/VGO (Blend 3) offers the smallest yield to gas products, thus resulting in a high yield of desired products (60.6 wt%). With PO/VGO and HDPE/VGO Blends, at 400 ºC, is remarkable the formation of gas by overcracking [312] since the high reactivity of PO or HDPE. It has to be highlighted that in the hydrocracking of Blend 4 (PP/VGO), very interesting results are obtained. This blend reported a high conversion of PP (95 wt%) with low gas yield and hence, maximizing the yields of desired products (naphtha and LCO) (66.6 wt%). These good results in the hydrocracking of PP mixed with VGO are consistent with those obtained by Jumah et al. [370] from hydrocracking post-consumer PP at 330 ºC and 20 bar of initial H_2 pressure. It is interesting that this good result at 440 ºC can be attributed to the fact that PP begins

to decompose thermally at this temperature, because it is closer to the peak of DTG (465 ºC), at which the maximum thermal decomposition takes place in compliance with the results shown in Section 2.2.4.

Analyzing the afore mentioned results for the 400-440 ºC range, the hydrocracking of PO produces the highest gas yield, 45.9 wt% at 440 °C. This tremendous gas formation, which is in line with the results obtained by Lee [365] in the catalytic cracking of pyrolysis wax oil at 450 °C using zeolite-based catalysts, can be mitigated by reducing the temperature to values below 350 °C [366,367]. However, this temperature is out of the conventional range used in the hydrocracking of VGO (350−425 °C) and this action will only be valid for the hydrocracking of pure PO. A practical solution to make the co-feeding feasible has been proposed by Singh et al. [371] and consists of a previous distillation of the PO to adapt its boiling point range to the distillation curve of VGO. This way, the fraction of light compounds in the PO will be reduced and, consequently, the overcracking is inhibited, which allows to operate at temperatures above 350 °C. Presumably, this step of distillation probably even helps to improve the less interesting results obtained hydrocracking PO/HDPE/VGO (Blend 3).

On the other side, the blends hydrocracking achieve important reductions of gas yield, increasing naphtha and LCO yields as depicted the discussed results. Furthermore, both HCO and HDPE conversion improves with temperature obtaining interesting results. PO/HDPE/VGO is clearly in disadvantage regarding to the performance shown by binary blends. Although you have to be careful since higher conversion is not always the best. Thus, the yields of the desired products (naphtha and LCO) in the hydrocracking of the binary blends are greater than the maximums for PO. Finally, comparing the $X_{plastic}$ values for the HDPE/VGO and PP/VGO blends, the higher reactivity of HDPE is observed at low temperature and, on the contrary, at 440 ºC (temperature close to the maximum cracking of PP) PP depicts a higher conversion in hydrocracking.

The results of selectivity to fuel index (S_F) in Figure 4.3 offer interesting information of which hydrocracked feedstock maximize the desired products: naphtha and LCO lumps. The highest value at 400 °C is obtained by far hydrocracking PO (1.37), because of its composition (Table 2.1). Furthermore, it's the only one that overcome $S_F = 1$ (marked with dashed line), being this milestone important because means that desired products are in larger amount than sub-products and feed. At 420 °C, the hydrocracking of PO/VGO blend offers the best result (1.61), whereas the values obtained with PO, VGO and HDPE/VGO blend (1.40, 1.21 and 1.17, respectively) are quite interesting too. However, the values of S_F for PO/HDPE/VGO and PP/VGO blends are very poor at this temperature (0.52 and 0.7, respectively), still under the break point. At 440 °C, the best value of the

selectivity is achieved by PP/VGO (1.99), in second place PO/VGO (1.64) and closely followed by PO/HDPE/VGO blend (1.54). The value obtained with HDPE/VGO blend has decreased a bit from that obtained at 420 °C (1.12), being still quite promising. Finally, the selectivity to fuel obtained in the hydrocracking of the VGO and the PO at 440 °C is very poor (0.97 and 0.82, respectively), being also worsen than at 420 ºC.

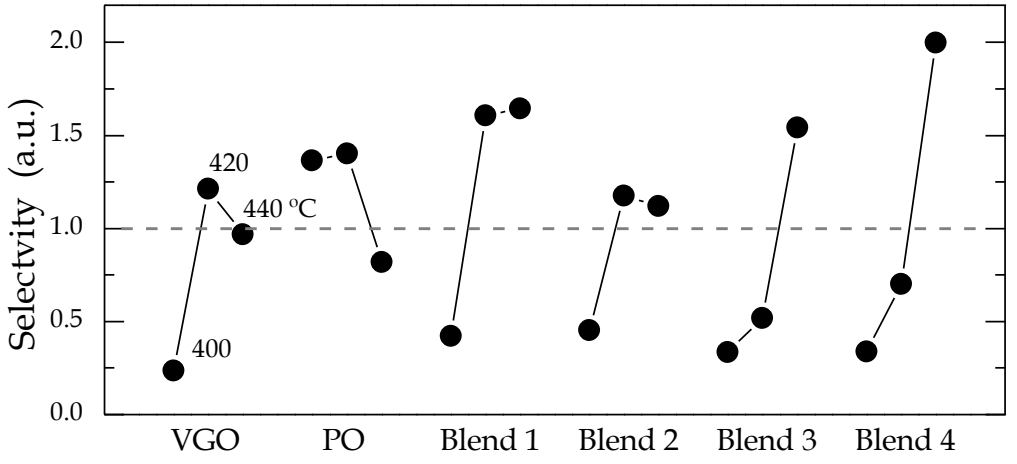

Figure 4.3 Effect of temperature on the selectivity to fuel index for different feedstocks. Reaction conditions: NiW/HY catalyst; 80 bar; C/F ratio, 0.1; reaction time, 120 min. Key: Blend 1, PO/VGO; Blend 2, HDPE/VGO; Blend 3, PO/HDPE/VGO; Blend 4, PP/VGO. The data of the hydrocracking of neat VGO and HDPE/VGO (Blend 2) have been obtained from section 3.3.

It is well known that desired products of a hydrocracking process are those within naphtha and LCO lumps, as they can be assimilated into commercial gasoline and diesel fuels, respectively. Thus, the results collected in Figure 4.1 offer a good description of products distribution and attained conversions and Figure 4.3 establish for each feed which temperature maximize them. However, as the contents of naphtha and LCO lumps are different on each feedstock (Table 2.1), a direct comparison of obtained results with each feedstock could be a little tricky. In this context, the use of the extent of formation index for both naphtha and LCO lumps ($\Delta Y_{Naphtha}$ and ΔY_{LCO}, respectively) helps to provide a more accurate picture of the hydrocracking results. The values obtained for these indices at the different temperatures have been collected in Table 4.1.

Attending to the formation of naphtha ($\Delta Y_{Naphtha}$), it is observed that the increase of the temperature from 400 to 420 °C causes an important increase of the values obtained, especially for VGO (from 5.98 to 28.6 wt%), PO/VGO blend (from 7.33 to 28.0 wt%), HDPE/VGO blend (from 12.9 to 30.0 wt%) and PP/VGO blend (11.75 to 23.55 wt%). On the contrary, a moderate increase has been obtained for the

ternary blend (PO/HDPE/VGO blend) (from 6.99 to 10.6 wt%) and for PO (from 3.05 to 8.55 wt%). In the case of the hydrocracking of PO it is a consequence of its high content of naphtha (Table 2.1), whereas the low formation of naphtha obtained for the PO/HDPE/VGO blend can be attributed to the aforementioned competitive adsorption for the active sites which limits the speed of the reactions involved. However, a further increase of the temperature to 440 °C is not positive for all the feedstocks. This way, for the VGO, PO and HDPE/VGO blend the value of the $\Delta Y_{Naphtha}$ obtained at 440 °C is lower than that at 420 °C, due to some overcracking degree. On the contrary, the values obtained for PO/VGO and, especially, PP/VGO blend and PO/HDPE/VGO blends are higher at 440 °C than at 420 °C. The PP/VGO achieves, by far, the maximum formation index for naphtha (47.12 wt%).

Table 4.1. Effect of temperature on the reaction index for different feedstocks, in wt%. Reaction conditions: NiW/HY; 80 bar; C/F ratio, 0.1; reaction time, 120 min. Key: Blend 1, PO/VGO; Blend 2, HDPE/VGO; Blend 3, PO/HDPE/VGO; Blend 4, PP/VGO. The data of neat VGO and HDPE/VGO hydrocracking (Blend 2) have been obtained from section 3.3.

Reaction index	400 °C	420 °C	440 °C
$\Delta Y_{Naphtha}$			
VGO	5.9	28.6	24.2
PO	3.1	8.6	4.2
PO/VGO	7.3	28.0	35.0
HDPE/VGO	12.9	30.0	24.6
PO/HDPE/VGO	6.9	10.6	33.9
PP/VGO	11.8	23.6	47.1
ΔY_{LCO}			
VGO	8.5	21.6	20.3
PO	−4.9	−9.7	−18.6
PO/VGO	6.7	18.0	11.6
HDPE/VGO	14.5	20.3	24.5
PO/HDPE/VGO	8.4	13.9	17.1
PP/VGO	9.8	13.9	15.8

Regarding to the formation of LCO (ΔY_{LCO}), the hydrocracking of PO offers a singular result with negative values of ΔY_{LCO} for all the temperatures. It means that the content of LCO decreases and in a greater extent at high temperature. The values of ΔY_{LCO} obtained with VGO and PO/VGO blend, in turn, increase with temperature, but they reach a maximum value at 420 °C (21.6 and 18.0 wt%, respectively). Once again, the overcracking suffered by these feedstocks causes a reduction of the ΔY_{LCO} at 440 °C (20.3 and 11.6 for the VGO and PO/VGO blend, respectively). Finally, the ΔY_{LCO} obtained with HDPE/VGO, PP/VGO and

PO/HDPE/VGO blends increase with temperature (24.5, 15.8 and 17.1 wt%, respectively at 440 °C). Hence, it can be assumed that the different results are strongly associated to the presence of plastic in the feedstock. Therefore, that means that although HDPE and PP require higher temperatures to be converted into smaller compounds, its presence reduces the overcracking (higher values of ΔY_{LCO} and $\Delta Y_{Naphtha}$ compared with other blends).

4.1.2 Gas composition

The analysis of the gas products, depicted in Figure 4.4, exposes that gases are composed by paraffins: methane (CH_4), ethane (C_2H_6), propane (C_3H_8), i-butane (C_4H_{10}) and n-butane (C_4H_{10}). Even though PO contains a high concentration of olefins (53.9 wt%, Table 2.1), light olefins have not been detected in the gas products as they are easily hydrogenated under the studied conditions. Furthermore, the composition of the gas fraction can be used in a certain way as an indicator of the prevailing hydrocracking mechanisms. As it is well established in literature [114,272,372], gases can be obtained by catalytic or thermal reactions. The former route occurs through an intermediate carbenium ion that undergoes a number of conversions, e.g. carbon−carbon bond cleavage or skeletal rearrangements, and it is characterized by inhibiting the formation of CH_4 and C_2H_6 paraffins. Consequently, C_3H_8 and C_4 compounds will be the main products within the gas lump. However, thermal route proceeds through a chain reaction mechanism that involves radicals as intermediates, being its main products methane and ethane.

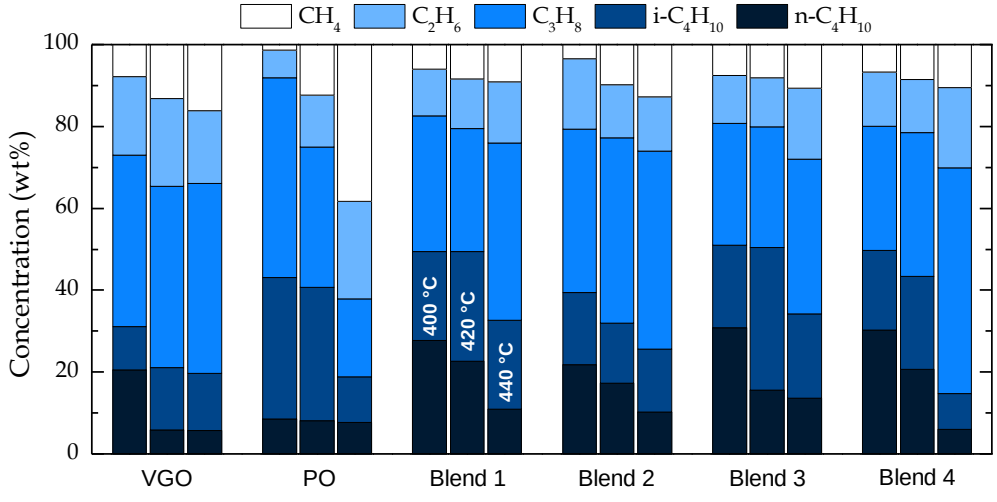

Figure 4.4 Effect of temperature on gas composition for different feedstocks. Reaction conditions: NiW/HY catalyst; 80 bar; C/F ratio, 0.1; reaction time, 120 min. Key: Blend 1, PO/VGO; Blend 2, HDPE/VGO; Blend 3, PO/HDPE/VGO; Blend 4, PP/VGO. The data of neat VGO and HDPE/VGO hydrocracking (Blend 2) have been obtained from section 3.3.

The results at 400 °C expose the predominance of the catalytic route because C_3H_8 and C_4 paraffins account for more than 70 wt% of the gas products for all the feedstocks. The concentration of these compounds is especially high with PO, as the concentration of C_3H_8 and C_4 paraffins goes over 90 wt%. With regard to the different blends, a similar overall composition of the gas products has been obtained with all of them. There is a notorious difference in the C_3H_8/C_4 ratio obtained for each feedstock, as the concentration of C_3H_8 is higher than that of C_4 just for the HDPE/VGO (Blend 2), whereas the concentration of C_4 is higher for the PO/VGO (Blend 1), PO/HDPE/VGO (Blend 3) and PP/VGO (Blend 4). Indeed, the composition obtained with HDPE/VGO (Blend 2) is more similar to that of the VGO. Thus, it can be assumed that compounds within the VGO of the blend are those that mainly contribute to the gas products.

Comparing the results obtained at 420 °C, it can be seen that thermal hydrocracking route gains relevancy for the hydrocracking of VGO, PO, HDPE/VGO (Blend 3) and PP/VGO (Blend 4). The most noticeable effect of the increase in the temperature has been suffered by the hydrocracking of PO, as the concentration of dry gas (CH_4 and C_2H_6) has been multiplied by three when increasing temperature from 400 to 420 °C (from 8.1 to 24.9 wt%, respectively). It may be a consequence of the lighter composition of the PO (Table 2.1) in which the low molecular weight compounds within naphtha range have been converted into gas phase compounds relatively easy [373]. On the contrary, for the PO/VGO (Blend 1), PO/HDPE/VGO (Blend 3) and PP/VGO (Blend 4) the importance of this route has remained steady. Furthermore, for VGO the main effect of temperature increasing is to reduce the concentration of the C_4 fraction (from 31.1 to 21 wt%).

At the highest temperature, 440 ^oC, different results have been obtained in the hydrocracking of pure feedstocks (VGO and PO) comparing with those obtained with the blends. This way, the concentration of dry gas (CH_4 and C_2H_6) is quite relevant in the hydrocracking of PO (62.1 wt%), however, it is not the case for VGO (33.82 wt%). Thus, these results expose that free radical mechanisms are the predominant ones [374] in the hydrocracking of the PO but less relevant in the case of the VGO. On the other hand, the concentration of dry gas (CH_4 and C_2H_6) has experienced an increase in a greater or lesser extent when rises the temperature in the hydrocracking of all blends but being always lower than from hydrocracking neat feedstocks. As a general trend, when temperature rises, an increase of C_1 and C_2 compounds take place in detriment of C_4 [375]. Hence, at 440 ^oC the concentration of dry gas (CH_4 and C_2H_6) in the gas phase follows the trend: PO/VGO (23.9 wt%) < HDPE/VGO (25.9 wt%) < HDPE/PO/VGO (27.9 wt%) < PP/VGO (30.1 wt%). Metecan et al. [375] also obtained a lower yield of dry gas in the hydrocracking of HDPE compared to PP, in experiments in a batch autoclave reactor after 60 min reaction length at different temperatures with and without

catalyst. This way, the presence of PO in the blends entails the inhibition of free radical mechanisms, which is positive due to dry gas (CH_4 and C_2H_6) has low interest for the industry. However, the cracking severity derived from the increase of temperature up to 440 °C has increased the concentration of C_3H_8 paraffins in the products obtained with the PO-containing feedstocks in detriment of the C_4 ones.

4.1.3 Naphtha composition and RON

The compounds of the naphtha fraction have been grouped in: n-paraffins (n-P); iso-paraffins (i-P); naphthenes (N); olefins (O); 1-ring aromatics (A_1); and 2-ring aromatics (A_2) (PIONA). Results unveiling the effect of temperature on the naphtha composition for the different feedstocks which are depicted in Figure 4.5.

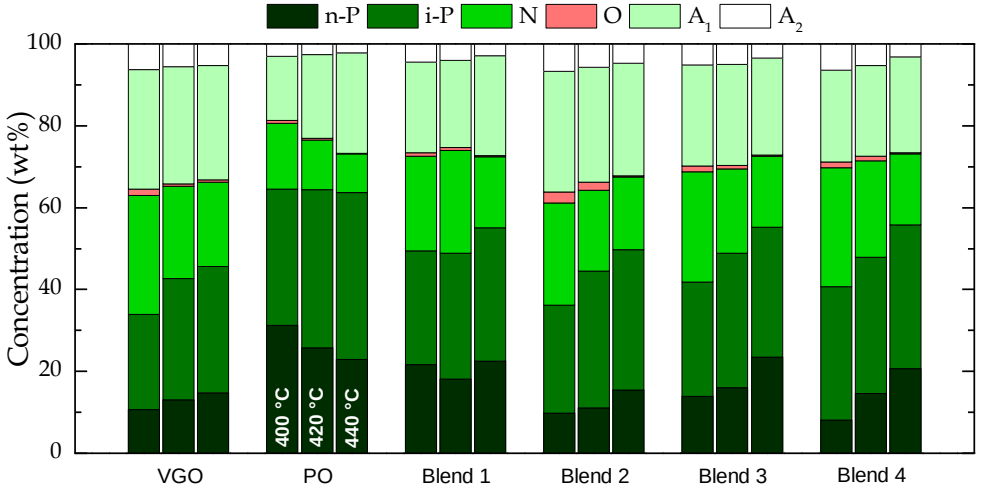

Figure 4.5 Effect of temperature on the naphtha composition for different feedstocks. Reaction conditions: NiW/HY catalyst; 80 bar; C/F ratio, 0.1; reaction time, 120 min. Key: Blend 1, PO/VGO; Blend 2, HDPE/VGO; Blend 3, PO/HDPE/VGO; Blend 4, PP/VGO. The data of neat VGO and HDPE/VGO hydrocracking (Blend 2) have been obtained from section 3.3.

As it can be seen in Figure 4.5, both the composition of the feedstock and the reaction temperature strongly affect the naphtha composition. It can be seen a similar behavior in the composition of the naphtha fraction obtained with VGO, and Blends 2-4. For these cases, an increase of temperature promotes an increase of n-paraffins and i-paraffins concentrations in detriment of aromatics, olefins and naphthene. Nonetheless, the expected trend for the aromatics should have been increasing, considering the thermodynamic limitation of the hydrogenation reactions of aromatics at ca. 380 °C [109]. Therefore, the obtained results are presumably the consequence of: (i) the displacement of the thermodynamic equilibrium of hydrogenation toward higher temperatures by cracking and ring

opening of some of the aromatic rings over the acid function of NiW/HY catalyst [140], and; (ii) the hydrocracking of side-chains of heavy aromatic compounds toward lighter aromatics (dealkylation reactions), which increases with temperature. Also, small concentrations of olefins have been detected in the reaction products, and the concentration of these compounds is also reduced when increasing temperature because of the boosting of the hydrogen-transfer reactions that convert olefins into saturated compounds.

By contrast, the results of PO hydrocracking show the opposite behavior. High temperatures involve an increase in the concentration of aromatics and olefins due to condensation reactions, as it has been previously reported by Palos et al. [109] and decrease the concentration of n-paraffins. This behavior can be due to the low concentration of aromatics in the feedstock, nevertheless, the A_2 diminish when increase the temperature simplifying the complexity of aromatics. It is noticeable that in the case of Blend 1 the effect of the dehydrogenation reaction with temperature compensates the capacity of the catalyst to displace the thermodynamic equilibrium of hydrogenation reactions. Hydrocracking Blend 1, the concentration of n-paraffins barely change increasing the temperature but i-paraffins and the monoaromatic increases in detriment of A_2, olefins and naphthenes. Thus, promoting again the reduction of the complexity of aromatics and increasing the paraffins concentration through hydrogenation and ring opening reactions. It has to be mentioned that in Blend 4 (PP/VGO) has been used other type of polyolefin (PP), less reactive than the HDPE, also obtaining naphtha with a suitable composition for its integration in the refinery pool.

Comparing the composition of the naphthas obtained with the different feedstocks, the highest concentration of aromatics has been obtained in the hydrocracking of VGO, which goes from 35.3 wt% at 400 °C up to 33.2 wt% at 440 °C. Concerning the different blends, in the hydrocracking of HDPE/VGO (Blend 2) it has been obtained the same trend but a slightly minor concentration of aromatics than that obtained with the VGO. On the other hand, in PO/VGO (Blend 1), HDPE/PO/VGO (Blend 3) and PP/VGO (Blend 4), the concentration of aromatics is notoriously reduced to values of 24.3, 23.6 and 23.4 wt%, respectively, at 440 °C. From these results it can be extracted that blend VGO with PO (either binary or ternary blended) and with PP have a direct positive effect, as the content of aromatics in the feedstock is in a certain way diluted given the different composition of the feedstocks (Table 2.1). Furthermore, the slight aromatic reduction in Blends 2-4 might come from the synergetic effect of the added aliphatic chains when plastic (HDPE or PP) is dissolved with VGO. The PIONA composition of naphtha from PP/VGO hydrocracking also depicted a lower aromatics concentration in comparison with HDPE/VGO for all temperatures studied. Similar results were found by Metecan et al. [375] comparing the naphtha composition

from HDPE and from PP hydrocracking at 425 ºC using Ni-Al as catalyst in a batch autoclave reactor. As in Blend 4 hydrocracking, they reported that naphtha from PP was less aromatic and more paraffinic (being the i-paraffins the main ones) than naphtha from HDPE hydrocracking [375].

Moreover, some positive synergies have been also observed comparing the composition of the naphtha lump obtained from PO/VGO hydrocracking than neat feedstocks (VGO and PO) hydrocracking. This is because the content of aromatics remains at levels close to those obtained from neat PO at high temperature but lower than obtained from VGO. In addition, this Blend 1 also achieves a high concentration of both types of paraffins are obtained. On the other hand, the concentration of 1-ring aromatics in naphtha is in all the cases higher that of 2-ring aromatics. Regarding the concentration of olefins in the naphtha lump, it can be seen that the higher concentrations are obtained with HDPE/VGO (Blend 2), HDPE/PO/VGO (Blend 3) and PP/VGO (Blend 4) at 400 and 420 °C, which are provided from the cracking of plastic chains.

Making a global comparison of naphtha composition, it should be mentioned that the co-feeding effect in the PO/VGO blend promote the reduction of aromatic compounds according to the hydrocracking of VGO, being an interesting feature given the continuous tightening of gasoline environmental regulations. In the same line, blending VGO with plastics, or the ternary mixture, allow to obtain naphthas with a lower aromatic concentration than that corresponding to neat VGO hydrocracking.

RON also is calculated to obtain an additional point of view concerning the naphtha quality and outcomes are displayed in Figure 4.6. In the hydrocracking of VGO this value decreases from 89.1 to 84.1 when temperature is increased from 400 to 440 ºC. This result is a consequence of the reduction in aromatics concentration and the increase in n-paraffins concentration. On the contrary, the RON of naphtha from PO hydrocracking improves when temperature rises, from 77.5 at 400 ºC up to 81.8 at 440 ºC, since aromatics and i-paraffins increase whereas n-paraffins decrease with temperature (Figure 4.4). Those RON values are lower but close to that obtained by Vasile et al. [367] and Joo and Guin [376], who hydrotreated plastic pyrolysis oil from electronic waste plastic and a mixture of plastic (HDPE, PP and PS), respectively. Both operated in different type of reactors (batch autoclave reactor and fixed bed reactor), but they obtained a similar value of RON for naphtha, i.e.: ~88 and ~87, respectively.

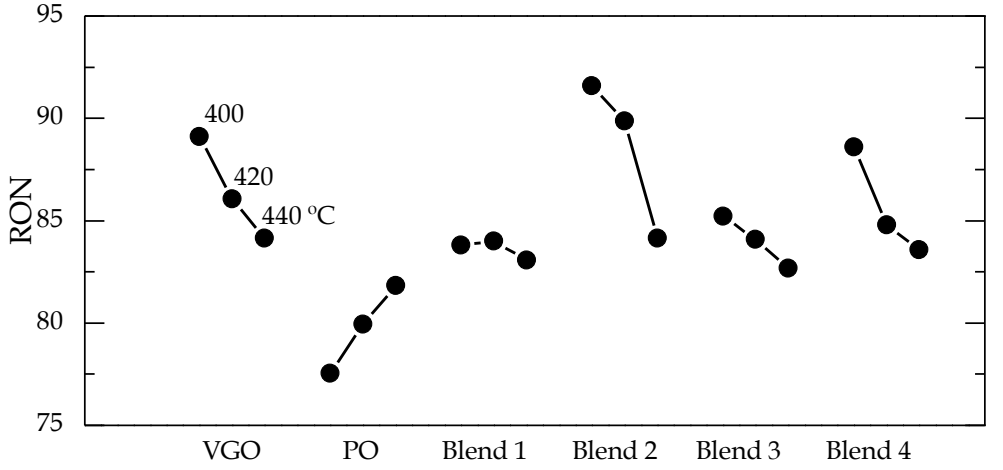

Figure 4.6 Effect of temperature in the research octane number (RON) of naphtha obtained for different feedstocks. Reaction conditions: NiW/HY catalyst; 80 bar; C/F ratio, 0.1; reaction time, 120 min. Key: Blend 1, PO/VGO; Blend 2, HDPE/VGO; Blend 3, PO/HDPE/VGO; Blend 4, PP/VGO. The data of the hydrocracking of neat VGO and HDPE/VGO (Blend 2) have been obtained from section 3.3.

A decreasing tendency in RON from naphthas obtained in blends hydrocracking is observed in Figure 4.6 when temperature rises. The best results correspond to HDPE/VGO (Blend 2). This blend apparently pushes the hydrocracking mechanism to promote compounds with higher RON, i.e. i-P. The RON achieved for Blend 3 and 4 was poorer than that obtained with neat VGO as also observed Rodriguez et al. [125] in the catalytic cracking. Finally, although RON in naphtha from PO/VGO (~84) (Blend 1) was higher than that obtained with neat PO, the values are lower than that obtained with neat VGO.

Consequently, according to the results of composition and RON of naphtha lump obtained with all the blends, they are suitable to be handled in refineries as is currently being managed the naphtha lump obtained from VGO hydrocracking. So, they can be added to naphtha pool where after its adequacy, can be marketed. It should be noted that the lower content of aromatics is an important advantage to reduce the severity in the hydroprocessing of these streams and the associated costs. In addition to the lower concentration of aromatics, the lower concentration of sulfur and nitrogen (not present in principle in plastics) is another favorable aspect of these naphthas.

4.1.4 LCO composition and cetane index

Figure 4.7 collects the composition of the LCO lump obtained with each feedstock at the studied temperatures. The compounds detected have been grouped according to PIONA analysis. The composition of this lump is less influenced by temperature than that of naphtha lump (Figure 4.5), but there are still some differences that must be highlighted.

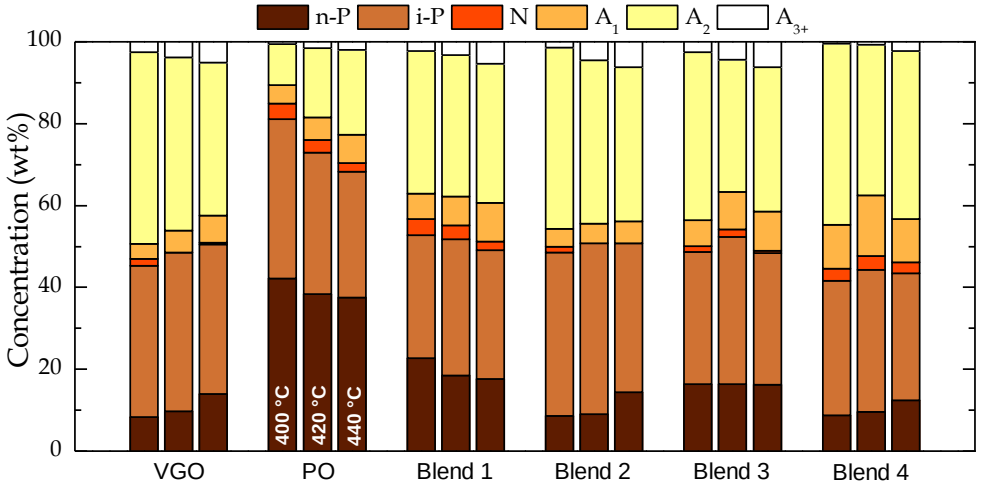

Figure 4.7 Effect of temperature on LCO composition for different feedstocks. Reaction conditions: NiW/HY catalyst; 80 bar; C/F ratio, 0.1; reaction time, 120 min. Key: Blend 1, PO/VGO; Blend 2, HDPE/VGO; Blend 3, PO/HDPE/VGO; Blend 4, PP/VGO. The data of neat VGO and HDPE/VGO hydrocracking (Blend 2) have been obtained from section 3.3.

In all the feedstocks, an increasing concentration of 3^+-ring aromatics when raising the temperature occurs. Although is interesting that the LCO product of PO hydrocracking has a low concentration in 3^+-ring aromatics due to its nature, however, PP in Blend 4 repress its formation. This increase of the polyaromatic fraction when temperature rises is in concordance with the increasing content of solid coke observed in Figure 4.1, as coke is produced by the radical polymerization of these compounds [377].

On the other hand, the total aromatics concentration does not follow the same tendency with temperature for pure feedstocks, as it decreases for the VGO (as dealkylation reactions are favored) and increases for the PO (as the condensation of the olefins is promoted) due to its low content in the feedstock. With regard to the blends, subtle modifications are observed in the aromatic concentration because of the contrary effect of the temperature in the hydrocracking of each components in the blends.

Attending to the results of the effect of hydrocracking temperature in Figure 4.7, neat feeds (VGO and PO) display opposite behaviors. For VGO hydrocracking

the total aromatic concentration in the LCO decreases when temperature rises, increasing the paraffin concentration. However, PO hydrocracking depicts a converse behavior. This different behavior can be explained by the different composition of VGO and PO (Table 2.1). When the feed has a high aromatic concentration (like VGO), this catalyst has good hydrodearomatization (HDA) performance reducing the total aromatic concentration. However, this behavior is not observed if the aromatic concentration is low (less than 15 wt% in PO). So given his low concentration and since dehydrogenation reactions are favored when the temperature increases, total aromatic concentration increases from 15.1 wt% up to 29.6 wt% at 400 and 440 ^{o}C, respectively. Nevertheless, it still far from concentrations achieved by VGO hydrocracking. For PO, both n-paraffins and i-paraffins are reduced from 42.2 to 37.5 wt% and from 38.9 to 30.7 wt% at 400 and 440 ^{o}C, respectively.

According to the results from blends hydrocracking, this catalyst, as for naphtha production, is also good for LCO production, because it supports a small variation in the composition of the different feed, maintaining a uniform composition of LCO, although with certain differences which will be discussed hereunder. Comparing the composition of the LCO lump obtained with the different blends, HDPE/VGO (Blend 2) offers a similar composition to that obtained for LCO from VGO hydrocracking, although the content of aromatics is even a bit reduced with the co-feeding of HDPE and also the impact of temperature on the composition is diminished.

In the hydrocracking of PO/VGO (Blend 1) the effect of temperature has the same trend as for neat PO although the amount of PO in the Blend 1 is less than in the VGO (20 wt%). LCO is less aromatic than obtained by neat VGO in spite of total aromatic compounds increase with temperature from 43.3 up to 49.2 wt%. Furthermore, this blend has improved the partial hydrogenation of 2-ring aromatics to 1-ring aromatics, being higher at 440 ^{o}C (9.4 wt%). In the same line, PO/HDPE/VGO (Blend 3) also pushes the 1-ring aromatic compounds in similar amount, being the maximum 9.6 wt% at 440 ^{o}C. Nevertheless, this blend seems to neutralize both type of trends notice until now, showing no clear trend of the large groups of compounds. Nonetheless, increasing temperature from 400 to 440 ^{o}C condensation reactions increase the concentration of A_{3+} compounds gradually from 2.5 up to 6.2 wt%. Furthermore, the concentration of n-paraffins almost remain constant (16.4 wt%).

On the other hand, LCO from Blend 4 shows similar levels in aromatic concentration compared to LCO from VGO. The addition of PP looks like to inhibit the formation of A_{3+} (2.2 wt% at the maximum temperature) and promotes 1-ring aromatic compounds, achieving the greatest value at 440 ^{o}C (10.6 wt%). Moreover,

the concentration of n-paraffins exhibits an increase while the i-paraffins are reduced. That happens from 8.7 to 12.5 wt% for the former and 32.8 to 30.9 wt% for the latter at 400 and 440 ºC, respectively.

Cetane index is for LCO (diesel) one of the parameters that establish the quality of this lump which is related to the auto-ignition ability of fuel in diesel engines. The lowest value allowed is 46, defined in EN-590 (standard published by the European Committee for Standardization) for all diesel fuel commercialized in Europe. Results of this parameter are depicted in Figure 4.8 for the LCO lumps obtained hydrocracking the different blends.

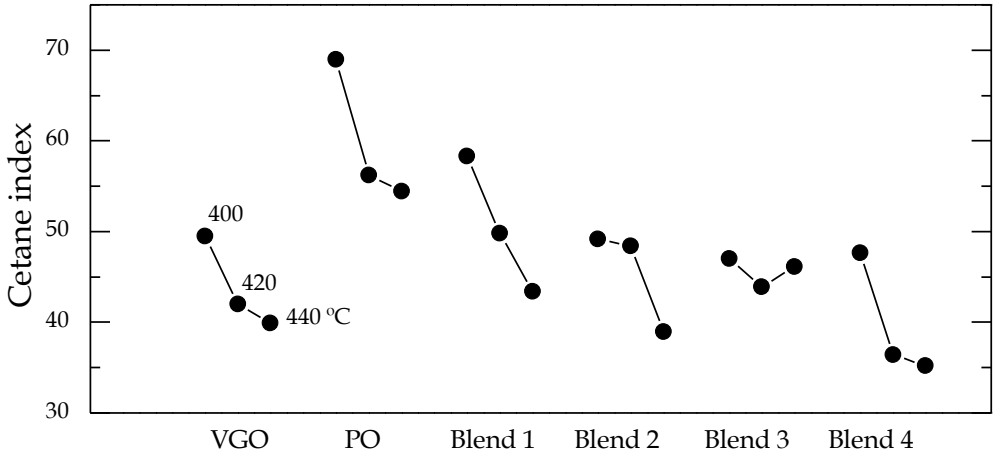

Figure 4.8 Effect of temperature on cetane index of LCO for different feedstocks. Reaction conditions: NiW/HY catalyst; 80 bar; C/F ratio, 0.1; reaction time, 120 min. Key: Blend 1, PO/VGO; Blend 2, HDPE/VGO; Blend 3, PO/HDPE/VGO; Blend 4, PP/VGO. The data of the hydrocracking of neat VGO and HDPE/VGO (Blend 2) have been obtained from section 3.3.

When temperature raises, the cetane index decreases for all feedstocks. A cetane index of 49.5 is obtained at 400 ºC for LCO from VGO hydrocracking and when the reaction temperature increases, this index downgrade up to 39.9 at 440 ºC. The LCO from pure PO hydrocracking also shows this trend, nevertheless, the cetane index is the highest for all the temperatures, 68.9 at 400 ºC and 54.4 at 440 ºC. These values are slightly higher than that obtained by other authors in the hydrotreating of postconsumer PP pyrolysis oil at 350 ºC, 70 bar of hydrogen pressure for 6 hour in a batch reactor [378]. Hydrocracking binary mixtures (PO/VGO (Blend 1), HDPE/VGO (Blend 2), and PP/VGO (Blend 4)), the downward tendency as the temperature increases is very evident. For Blend 1 is achieved the highest cetane index followed by Blend 2 and Blend 4. The values of Blend 1 are 58.3 and 43.4 obtained at 400 and 440 ºC, respectively, whilst, with Blend 2 and 4 the cetane index values are in a narrower range where the maximum are 49.2 and 47.7 and the minimum 38.9 and 35.2, respectively. Finally, for the

ternary mixture (HDPE/PO/VGO) the hydrocracking temperature has no clear effect on the cetane index, which has a value of ~ 45 for all the temperature range.

To sum up, either the composition or the cetane index of the LCO lump obtained in the hydrocracking of all the unconventional feedstocks improve, even a bit, the results obtained with the VGO. In most of cases, cetane index is greater than that established in EN-590 (46). Therefore, the incorporation of the corresponding LCO to diesel pool in the refinery should not have a negative impact either.

4.2 PtPd/HY CATALYST

4.2.1 Yields and conversion

In Figure 4.9 yields and conversion from hydrocracking different feedstocks are collected. Reaction products have been lumped in six product lumps (gas, naphtha, LCO, HCO, wax and coke) and two conversions have been estimated (X_{HCO} and $X_{Plastic}$).

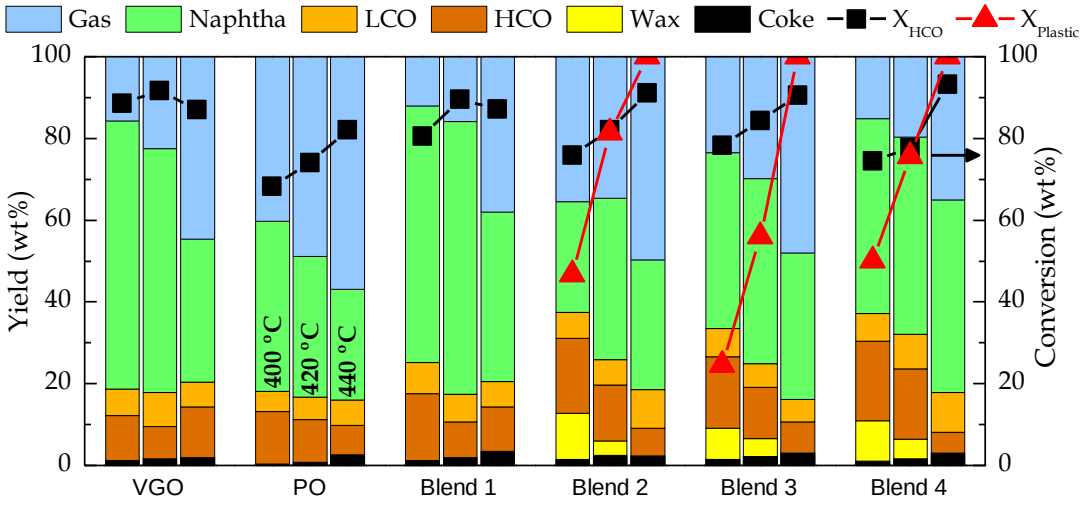

Figure 4.9 Effect of temperature on the yields and conversions for different feedstocks. Reaction conditions: PtPd/HY catalyst; 80 bar; C/F ratio, 0.1; reaction time, 120 min. Key: Blend 1, PO/VGO; Blend 2, HDPE/VGO; Blend 3, PO/HDPE/VGO; Blend 4, PP/VGO. The data of neat VGO and HDPE/VGO hydrocracking (Blend 2) have been obtained from section 3.3.

The increase in the temperature, and the consequent growth of both conversions, reflects a transition from heavier feeds to lighter ones. As general rule, with this catalyst a noticeable naphtha yield is produced and the conversions are higher than 60 wt% since 400 ºC. This outstanding performance is related with the physicochemical properties that are shown in section 3.1. According to textural properties, this catalyst exhibits a high BET surface area, which is consequence of the elevated micropore surface area. The limited mesoporosity justifies the high selectivity to naphtha at low temperature [379], but the mostly microporous structure promotes the gas production. Thus, the gas yield dramatically increases when temperature rises, due to the overcracking of the naphtha compounds [380]. On the other hand, it is well know that acid properties also play an important role in hydrocracking conversion, by favoring the extent of the cracking stage [381], favoring the displacement of the equilibrium of the hydrogenation stage [107,114,381]. This catalyst has a high total acidity with a predominance of Brønsted sites (Table 3.1), which are the most active ones in the carbenium ion mechanism in the cracking reactions [114]. As a result of good textural and acid properties, this

catalyst can achieve outstanding behavior even at lowest temperature. Although PO/HDPE/VGO get the lowest plastic conversion at temperatures below 420 ºC, with this catalyst, for HDPE/VGO, PO/HDPE/VGO and PP/VGO blends, at the maximum temperature is obtained a 100 wt% plastic conversion. Moreover, the plastic conversion has a similar behavior for HDPE and PP, and the refractivity character shown by PP with NiW/HY (Section 4.1.1) is not observed for this catalyst, that is more active. However, as with the NiW/HY catalyst, the presence of PP in the feedstock also improves the performance, minimizing gas yields.

The results at 400 ºC depicted for VGO the highest X_{HCO} (88.5 wt%), being naphtha the main product (65.6 wt%) followed far by gas (15.7 wt%) and LCO (6.4 wt%). Unexpectedly, the hydrocracking of PO, in spite of it is the lightest feedstock, shows lower values of X_{HCO} (68.2 wt%), being naphtha and gas the main lumps (41.5 and 40.2 wt%, respectively). For PO hydrocracking, LCO is the minority fraction (4.9 wt%).

On the other hand, in the case of blends, the X_{HCO} was not far between them. In the hydrocracking of HDPE/VGO (Blend 2) and PP/VGO (Blend 4) this conversion is ~75 wt% and blends which contain PO improve a little bit, being ~80 wt% for PO/VGO (Blend 1) and PO/HDPE/VGO (Blend 3). It has to be pointed that even at the lowest temperature (400 ºC) the X_{HCO} of PP/VGO is quiet similar to obtained by HDPE/VGO. This is a highlight event due to in section 4.1.1 the result was closer to Blend 3. The highest $X_{plastic}$ is obtained for the PP/VGO hydrocracking followed by the conversions obtained for HDPE/VGO and PO/HDPE/VGO (50.1, 46.7 and 24.5 wt%, respectively). In the hydrocracking of the ternary mixture (Blend 3), the HDPE conversion is low due to a competitive adsorption of PO in the catalyst active sites, persisting even with this catalyst the same problem than with the NiW/HY catalyst. Concerning the yields, in the hydrocracking of PO/VGO is achieved the best naphtha yield (62.7 wt%), decreasing for the other blends with the following trend:

PP/VGO (47.7 wt%) > PO/HDPE/VGO (42.9 wt%) > HDPE/VGO (27.1 wt%)

Furthermore, PO/VGO achieves the lowest gas fraction whereas the highest one is for HDPE/VGO, 12 and 35.3 wt%, respectively. It has to be said that for PP/VGO hydrocracking the gas yield is only 15 wt%. Consequently, both plastics denote different behaviors in gas production since the lowest temperature. This is because as is mentioned, PP contains branches along the structure. Thus, these branches boost β-scission, leading to a better composition of naphtha (branched molecules) compared to HDPE hydrocracking, and reducing the overcracking. It should be noted that the LCO yield is small for all the blends (~6.5 wt%) with this catalyst.

When the reaction temperature increases from 400 up to 420 ºC, for neat feeds, the naphtha yield decreases. In the hydrocracking of VGO, naphtha is the prevailing lump followed by gas, although there is a slight reduction in naphtha with this increase in temperature. For PO, the naphtha yield is reduced from 41.5 to 34.4 wt% and gas yield is increased from 40.2 to 48.8 wt%, being now the gas fraction the main one. The increase of temperature has a positive effect in $X_{HCO,}$ reaching 74 wt% at 420 ºC, but continues being less than that obtained by VGO.

In the case of blends, in the hydrocracking of PO/VGO is achieved a X_{HCO} of 89.6 wt%, where naphtha yield increases up to 66.8 wt%, maintaining a low gas yield (15.8 wt%). HDPE/VGO and PO/HDPE/VGO have a similar X_{HCO} (~83 wt%), while $X_{plastic}$ is very different between them (81.3 and 56 wt%, respectively). Besides the increase of the conversions as the temperature rise and naphtha is larger than gas yield. For PO/HDPE/VGO these yields are 45.2 and 29.8 wt%, respectively, and for HDPE/VGO 39.4 and 34.6 wt%, respectively. It is observed that with the ternary mixture the speed of the hydrocracking reactions is reduced, due to competition for active sites, obtaining less conversion and then lower overcracking. The overall effect is that the formation of naphtha is favored and the gas yield decreases.

Finally, the hydrocracking of PP/VGO shows a similar behavior as well. The X_{PP} is high (75.6 wt%) but lower than HDPE/VGO, though X_{HCO} (77.7 wt%) is slightly improved when raises the temperature to 420 ºC. For this feed, the naphtha is the main lump (48.2 wt%) and gas yield, as in the hydrocracking de PO/VGO, not overcome 20 wt%. LCO lump remains low at 420 ºC, for all the feedstocks, though heavier fractions diminish when temperature increases from 400 ºC. Thus, this fraction seems to be an intermediate that as it is formed from heavy ones, rapidly is hydrocracked to generate lighter compounds when PtPd/HY catalyst is used.

At the highest temperature (440 ºC), in general, gas becomes the main fraction. When neat VGO is fed, a dramatic increase of gas production was detected in detriment of naphtha fraction (44.6 and 34.9 wt%, respectively) in comparison with lower temperatures. For the hydrocracking of PO, although the X_{HCO} is very high (82.1 wt%), gas yield is the more benefitted of this advance (56.8 wt%), whereas naphtha yield is reduced till 27.1 wt%. This distribution of the yields denotes that the overcracking has been produced in an excessive way at this temperature and for this feedstock. Coke is the minority fraction of the products that should not be underestimated, as it reveals important information for reaction/regeneration cycles. In the case of VGO hydrocracking, the coke yield is 1.3 wt% at 400 ºC increasing with temperature up to 1.9 wt% at 440 ºC. In contrast, for PO hydrocracking, the coke yield was the lowest (0.4 wt% at 400 ºC). But at

440 ºC, the coke yield drastically increases to 2.68 wt%, overcoming that produced by hydrocracking VGO.

In the case of blends hydrocracking, at 440 ºC the X_{HCO} overcomes more than 90 wt% in comparison with neat VGO or PO. PP/VGO blend achieves the highest HCO conversion (93.3 wt%). It is noticeable that is the only feed for which at this temperature although the gas yield has increased considerably (34.9 wt%) is lower than naphtha, which continues being the main lump (47.1 wt%). Consequently, the addition of PP clearly improves the performance. The presence of PP boosts the carbocationic mechanism, limiting the gas formation, which is an interesting behavior at high temperatures. For this feed, the coke yield starts with 1.1 wt% at 400 ºC and increases up to 3.1 wt% at 440 ºC, which is a higher coke yield than for both neat feedstocks.

HDPE/VGO hydrocracking obtained close results: it has the second largest X_{HCO} (91.2 wt%) but the gap with the yields is higher, especially because of high gas yield. Thus, the gas yield was the largest one at 440 ºC (49.6 wt%) with a high impact in naphtha yield (31.8 wt%). The coke yield obtained with this feedstock is the highest reported (1.6 wt%) for all blends at low temperature (400 ºC). However, at 440 ºC, the result is the opposite, being the 2.4 wt% the lowest coke yield obtained for blends hydrocracking under these conditions.

The ternary mixture (PO/HDPE/VGO) hydrocracking has higher X_{HCO} than neat feedstocks (VGO and PO) (90.5 wt%) and, opposite to with NiW/HY catalyst, the total plastics conversion is achieved. Furthermore, the apparent inhibition effect slightly improves the yields respect to HDPE/VGO hydrocracking, reducing gas yield and enhancing the naphtha yield (47.9 and 35.8 wt%, respectively). Regarding LCO yield, the changes in this lump are almost imperceptible for all the blends when temperature increases from 400 to 440 ºC, reaching the lowest values for PO/HDPE/VGO and the highest one for PP/VGO hydrocracking of 5.5 and 9.8 wt%, respectively. The coke yield at 400 ºC is 1.5 wt% and at the highest temperature (440 ºC) the coke yield (3.1 wt%) is the same to the reported by PP/VGO blend.

At the end, PO/VGO hydrocracking obtained the lowest X_{HCO} of all the blends (87.1 wt%). However, it has surprisingly a low gas yield (38 wt%) with similar naphtha production to that obtained by PP/VGO (46.1 wt%). The coke yield for this feedstock comes from 1.2 wt% at 400 ºC up to 3.5 wt% at 440 ºC, being the latter the highest obtained for any feedstock tested. This coke yield reduces the catalyst activity and therefore, it would explain why a lower conversion is obtained at 440 ºC in comparison with 420 ºC for this feedstock.

PtPd/HY catalyst is more active than NiW/HY catalyst in the hydrocracking of different feedstocks due to its physicochemical properties, achieving higher conversions (X_{HCO} and $X_{Plastic}$) at 400 ºC. Generally, the X_{HCO} is higher than 70 wt% for all the feedstocks when PtPd/HY is used.

Regarding plastic conversion, appreciable differences are also observed between both catalysts since for PtPd/HY catalyst at 400 ºC the lower plastic conversion is 22 wt% for the ternary mixture and at 440 ºC the complete conversion (100 wt%) is reached for all feeds. On the other hand, the NiW/HY catalyst at 400 ºC, the lower $X_{Plastic}$ is 3 wt% also for the ternary mixture and none of the feedstocks at 440 ºC achieves the complete conversion of plastic.

But not all are positive results for the PtPd/HY catalyst. The yields analysis shows that the higher activity also has negative consequences. This catalyst overcracks the desired products to gas yield, thus reducing the naphtha and LCO yields. In addition, this higher activity entails a greater production of coke which would shorten the catalyst activity and therefore it will have to be regenerated more frequently in a hypothetical continuous process. Conversely, the NiW/HY catalyst, with a more moderate activity, reduces those problems with the aforementioned consequent reduction in HCO and plastic conversions.However PtPd/HY catalyst reported promising result which could be enhanced optimizing the operating conditions or moderating its physicochemical properties.

After analyzing lump yields and conversions, it is important to analyze the selectivity to fuels (S_F) achieved for each feed with this catalyst. This complementary information improves the knowledge about the performance of this hydrocracking catalyst at different temperatures. Results are shown in Figure 4.10 and are argued below.

In the hydrocracking of VGO, the S_F index decreases with temperature, going from 2.6 at 440 ºC to 0.7 at 440ºC. According to product distribution, the exponential increase of gas causes this fall. In the case of PO hydrocracking, the overcracking trend, already shown, together with the higher activity of this catalyst, leads to have a low S_F index even at low temperatures. For this feed, S_F shows a low variation with a decreasing trend (0.9 and 0.5 at 400 and 440 ºC, respectively). On the contrary, in the hydrocracking of blends a maximum of S_F at 420 ºC is obtained in all of them. In the case of Blend 1, the best value of S_F for all the temperature range is achieved at 420 ºC (S_F = 2.8). Nevertheless, Blend 3, which also contains PO, has much lower S_F, being its maximum value 1.0 at 420 ºC. It should be noted that for these feeds, at 440 ºC, S_F is even lower than at 400 ºC, being 0.9 and 0.7 respectively, due to the increased gas yield. When HDPE is co-fed with VGO (Blend 2), the selectivity is very poor, similar to that obtained for PO. The maximum value of S_F is 0.8 at 420 ºC. Surprisingly, the S_F of the PP/VGO (Blend 4) hydrocracking

has an increasing trend with temperature and denotes to be the third best mark. Nonetheless, results are far from those obtained with Blend 1. For this feed, the maximum S_F is 1.3, achieved at 440 ºC.

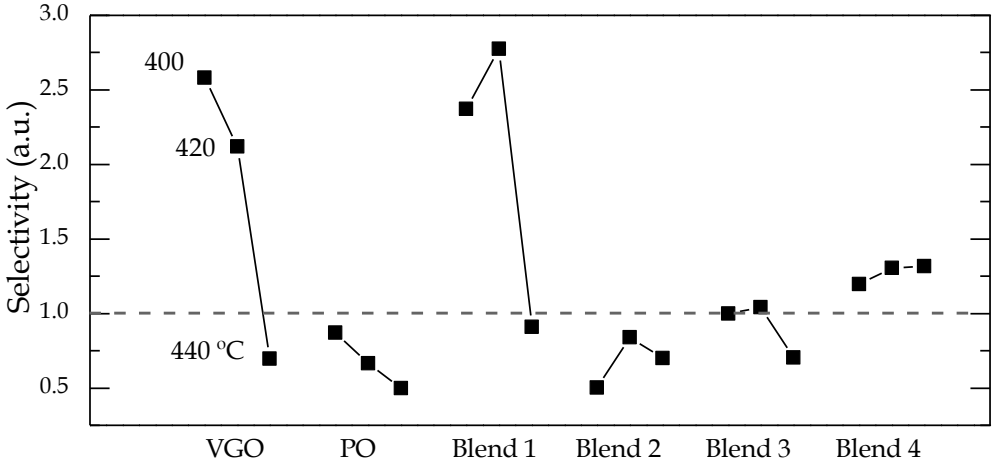

Figure 4.10 Effect of temperature on selectivity to fuel index for different feedstocks. Reaction conditions: PtPd/HY catalyst; 80 bar; C/F ratio, 0.1; reaction time, 120 min. Key: Blend 1, PO/VGO; Blend 2, HDPE/VGO; Blend 3, PO/HDPE/VGO; Blend 4, PP/VGO. The data of the hydrocracking of neat VGO and HDPE/VGO (Blend 2) have been obtained from section 3.3.

The extents of desires product (naphtha and LCO lumps) are calculated to assess if they came from the feedstock or are produced in the hydrocracking reactions. The results for the increment of naphtha and LCO yields ($\Delta Y_{Naphtha}$ and ΔY_{LCO}, respectively) are collected in Table 4.2. Production of naphtha ($\Delta Y_{Naphtha}$) from neat VGO achieves its maximum at 400 ºC (65.5 wt%). The increase of temperature produces a reduction of this value (34.8 wt% at 440 ºC). Since PO is mainly formed by naphtha, at 400 ºC only 15.1 wt% of naphtha comes from hydrocracking and this value is reduced to 0.6 wt% at 440 ºC. As a result, the amount of naphtha obtained at 440ºC is almost the same (but with different composition) that it is present in the feed. In the case of blends hydrocracking, all of them depict a maximum of $\Delta Y_{Naphtha}$ at 420 ºC. The highest index is obtained for PO/VGO at 420 ºC (61.4) and is very close to that obtained with VGO hydrocracking at 400 ºC (the highest one). The order in naphtha production ($\Delta Y_{Naphtha}$) continues as follows:

PP/VGO (47.7 wt%) > PO/HDPE/VGO (42.4 wt%) > HDPE/VGO (39.2 wt%)

It has to be pointed that for PP/VGO (Blend 4) a very low variation of naphtha fraction (less than 1 wt%) is observed when temperature is increased.

Table 4.2 Effect of temperature on the reaction index for different feedstocks, in wt%. Reaction conditions: PtPd/HY catalyst; 80 bar; C/F ratio, 0.1; reaction time, 120 min. Key: Blend 1, PO/VGO; Blend 2, HDPE/VGO; Blend 3, PO/HDPE/VGO; Blend 4, PP/VGO. The data of neat VGO and HDPE/VGO hydrocracking (Blend 2) have been obtained from section 3.3.

Reaction index	400 °C	420 °C	440 °C
$\Delta Y_{Naphtha}$			
VGO	65. 5	59.5	34.8
PO	15.1	7. 9	0.6
PO/VGO	57.2	61.4	36.0
HDPE/VGO	26.9	39.2	31.7
PO/HDPE/VGO	40.2	42.4	33.1
PP/VGO	47.6	47.7	46.9
ΔY_{LCO}			
VGO	1.9	3.8	1.6
PO	-28.1	-27.6	-26.9
PO/VGO	-2.5	-3.5	-4.1
HDPE/VGO	2.7	2.6	5.8
PO/HDPE/VGO	0.1	-1.1	-1.4
PP/VGO	3.1	4.9	6.2

On the other side, for this catalyst the production of LCO is very low. So, the increments of this fraction (ΔY_{LCO}) are very low or even negative. In the VGO hydrocracking, ΔY_{LCO} has a maximum value of 3.8 wt% at 420 ºC, whereas for PO has a negative balance which is less negative when increases the temperature. This fact reinforces the assumption that this catalyst turns the LCO fraction to lighter ones and is also linked to the increase in naphtha and especially gas fractions.

On the other hand, when co-feeding plastics with VGO, ΔY_{LCO} increases with temperature, achieving the highest value for PP/VGO and HDPE/VGO at 440 ºC (6.2 and 5.8 wt%, respectively). Conversely, as it happens for hydrocraking of neat PO, blends with PO produce negative values for ΔY_{LCO}. The 10 wt% of PO contained in the ternary mixture (PO/HDPE/VGO) is enough to push the increment of LCO index to negative values at 420 and 440 ºC (-1.1 and -1.4 wt%, respectively). So, when increasing the amount of PO to 20 wt%, (PO/VGO) the increment of LCO reaction index (ΔY_{LCO}) becomes more negative, achieving a value of -4.1 wt% at 440ºC.

To sum up, the complementary analysis of yields, conversion and selectivity points out that although this catalyst is very good for naphtha production, it is

mandatory to optimize the operation conditions and, if it would be necessary, the catalyst properties, to reduce the gas fraction and increase the selectivity to fuels.

4.2.2 Gas composition

The gas obtained in the hydrocracking reactions (Figure 4.11) is composed by: methane (CH_4), ethane (C_2H_6), propane (C_3H_8), i-butane (C_4H_{10}) and n-butane (C_4H_{10}) (butane, C_4).

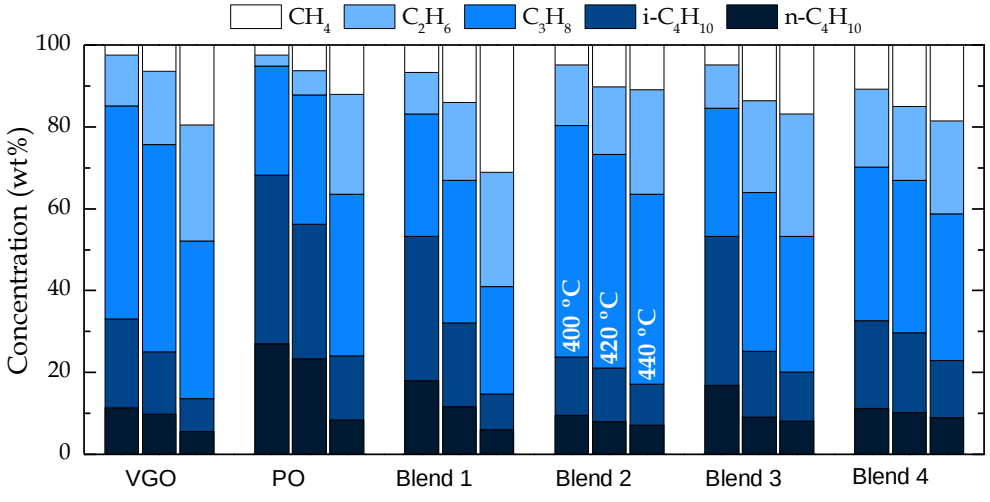

Figure 4.11 Effect of temperature on gas composition for different feedstocks. Reaction conditions: PtPd/HY catalyst; 80 bar; C/F ratio, 0.1; reaction time, 120 min. Key: Blend 1, PO/VGO; Blend 2, HDPE/VGO; Blend 3, PO/HDPE/VGO; Blend 4, PP/VGO. The data of the hydrocracking of neat VGO and HDPE/VGO (Blend 2) have been obtained from section 3.3.

When VGO is hydrocracked at 400 ºC, the gas is fundamentally formed by C_3H_8 (52 wt%) and C_4 (33.2 wt%). It is noticeable that the amount of i-C_4 is larger than n-C_4, indicating that the reactions are being conducted by hydrocracking on acid sites through carbenium ion mechanism [380]. This pattern is also shown by neat PO hydrocracking. For this feed, C_4 are the main compounds (> 65 wt%), where i-C_4 is the main one, and the lowest amount of dry gas (CH_4 and C_2H_6) is obtained at 400ºC (5.1 wt%).

On the other hand, the blends that contain PO (PO/VGO, Blend 1; PO/HDPE/VGO, Blend 3), likewise as PO, describe a similar behavior, with high production of C_4 compounds being 53.4 and 53.3 wt% for Blend 1 and Blend 3 respectively and with higher concentration of i-C_4 than n-C_4. On the other side, for HDPE/VGO (Blend 2) C_3H_8 is the main product (56.6 wt%), the highest at 400 ºC. Thus, the sum of C_3H_8 and C_4 is 80.5 wt%. The main product in PP/VGO (Blend 4)

hydrocracking is C_3H_8 (37.5 wt%) and this blend fosters C_4 (32.8 wt%) longer than Blend 2. Furthermore, it has to be pointed that the gas yield from PP/VGO hydrocracking has the highest amount of dry gas (CH_4 and C_2H_6) (29.7 wt%) at 400 ºC, due to its lower degradation temperature (section 2.1).

When temperature is increased, thermal reaction gains relevance. The raising of temperature from 400 to 420 ºC fosters the concentration of dry gas (CH_4 and C_2H_6) versus C_3H_8 and C_4. For VGO hydrocracking, the concentration of the formers increases until 24.2 wt% in detriment of C_4 (25.1 wt%) whereas C_3H_8 is still the main compound (50.5 wt%). However, the PO hydrocracking does not display the same behavior. Although dry gas (CH_4 and C_2H_6) increase up until 12.2 wt%, the concentration of C_3H_8 also shows an increase of 5 wt%, being 31.5 wt% while C_4 fraction decreases to 56.2 wt%; nevertheless, even now they are the major compounds.

On the other hand, in the case of HDPE/VGO (Blend 2) and PP/VGO (Blend 4) hydrocracking, progressive changes are observed, and similar to those experimented in the VGO hydrocracking, when temperature rises. For each blend, the combination of dry gas compounds increases (26.7 and 33 wt%, respectively at 420 ºC) while the reduction of C_3H_8 and C_4 occurs (72.1 and 66.9 wt%, respectively). In both cases, and as was the case with VGO hydrocracking, C_3H_8 is the main compound at 420 ºC, with 52.2 and 37.2 wt%, respectively. This temperature increase has a higher impact on PO/VGO (Blend 1) and PO/HDPE/VGO (Blend 3) gas composition. For the former, dry gas concentration is twice higher at 420 than at 400 ºC for both feeds, being ~33 wt% at 420 ºC. As was the case for PO hydrocracking, C_3H_8 concentration slightly increases with temperature, obtaining 34.8 wt% at 420 ºC, and C_4 concentration decrease seriously, being 32.1 wt%.

In the case of ternary mixture (PO/HDPE/VGO, Blend 3) hydrocracking, as it happened with previous feeds containing PO, the CH_4, C_2H_6 and C_3H_8 concentrations increase with temperature, while C_4 decreases, being 13.5, 22.5, 38.7 and 25.3 wt% respectively, at 420 ºC, and becoming C_3H_8 the main compound.

At the highest temperature (440 ºC), huge changes are observed in terms of composition, as it happened with the gas yield in Figure 4.9. This fact is due to the higher the temperature is, the stronger the thermal hydrocracking by radical mechanism, which promotes the production of low molecular weight compounds [114,382]. For VGO hydrocracking, dry gas concentration suffers an increment of more than 20 wt%, obtaining a value of 47.8 wt% at 440 ºC. Conversely, C_3H_8 concentration is the one that decreases the most (until 38.4 wt% at 440 ºC) and C_4 concentration decreases as well (13.7 wt%). For PO hydrocracking, CH_4, C_2H_6 and C_3H_8 concentrations increase, with a concentration of 36.4 wt% for dry gas whereas

the propane becomes the main compound (39.4 wt%). So, C_4 compounds are reduced to a greater extent (24.2 wt%).

According to the blends hydrocracking, gas obtained for PO/VGO shows the highest dry gas concentration (59 wt%). C_3H_8 concentration decreases until 26.2 wt% and C_4 concentration is only 14.7 wt%. PO/HDPE/VGO hydrocracking also produces an important amount of dry gas (CH_4 and C_2H_6) (46.8 wt%). Therefore, the addition of PO, which contains lighter compounds in the boiling point of naphtha fraction, not only produces more gas but also produces more dry gases (CH_4 and C_2H_6) at 440 ºC, since its easier thermal hydrocracking. The C_3H_8 concentration has been reduced until 33.2 wt% and C_4 concentration is only 17 wt%.

For PP/VGO hydrocracking, the concentration of dry gas is lower than that obtained with other blends at 440 ºC (41 wt%). Moreover, it produces the largest C_4 concentration in the gas stream (23 wt%) and the C_3H_8 concentration is reduced until 35.9 wt%. For these reasons, the presence of PP in the feedstock looks like reduces thermal hydrocracking compared to PO containing feeds.

Finally, for the HDPE/VGO blend, dry gas concentration increases (36.3 wt%) but C_3H_8 remains as the main compound (46.5 wt%). Furthermore, C_4 concentration continues the decreasing trend till values of 17.1 wt%. Rodriguez et al. [125] also reported that the concentration of C_3 is higher than C_4 for the catalytic co-cracking of HDPE and VGO. Furthermore, both n-C_4 and i-C_4 compounds follow a decreasing trend when temperature increases (being i-C_4 higher than n-C_4).

As a conclusion, the general trend shows some similarities with results in Section 4.1.2 for the NiW/HY catalyst. Generally speaking, at lower temperature, C_3H_8 and C_4 are the main compounds (more than 70 wt%) but when temperature is raised, dry gas (CH_4 and C_2H_6) increases. Furthermore, i-C_4H_{10} is produced in larger amount than n-C_4H_{10}. But when temperature rises, C_4 and C_3 are the compounds that suffer a greater reduction.

4.2.3 Naphtha composition and RON

The naphtha is one of the main products that this catalyst produces, so it is important to analyze its composition and the effect of temperature on this lump. The results are shown in Figure 4.12. The composition it has been grouped in PIONA compounds.

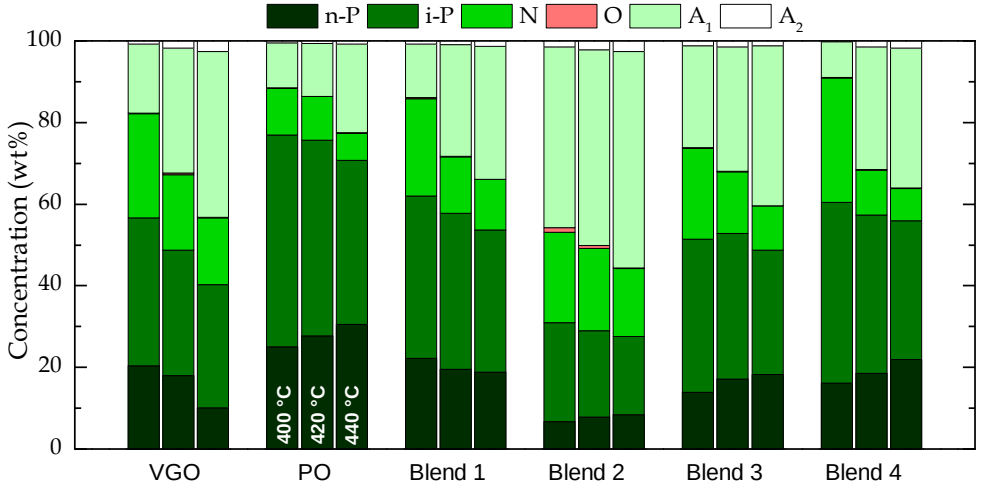

Figure 4.12 Effect of temperature on naphtha composition for different feedstocks. Reaction conditions: PtPd/HY catalyst; 80 bar; C/F ratio, 0.1; reaction time, 120 min. Key: Blend 1, PO/VGO; Blend 2, HDPE/VGO; Blend 3, PO/HDPE/VGO; Blend 4, PP/VGO. The data of the neat VGO and HDPE/VGO hydrocracking (Blend 2) have been obtained from section 3.3.

The composition of the naphtha clearly depends on feedstock load and the formation of some compounds is favored against others. As expected, temperature also affects the naphtha composition promoting or depressing certain compounds as a result of the thermodynamics influence through hydrocracking route [109]. Generally speaking, temperature favors the aromatic concentration. Naphtha from neat VGO hydrocracking has more naphthenic and aromatic compounds, while naphtha from PO hydrocracking is more paraffinic, attending to the different composition of the feedstocks.

However, when temperature rises, generally naphthenic compounds are reduced due to dehydrogenation reactions are favored, thus, increasing aromatic compounds, specially A_1 [383]. In this way, for neat VGO hydrocracking, the A_1 concentration in naphtha increases from 16.9 wt% at 400 ^{o}C up to 40.7 wt% at 440 ^{o}C. By contrast, A_2 concentration is negligible but it also increases with temperature achieving a maximum concentration of 2.5 wt% at 440 ^{o}C.

Conversely to that, naphtha from PO hydrocracking is less aromatic for all the temperature range, showing A_1 concentration smaller differences between 400 and 440 ^{o}C (11 and 21.7 wt%, respectively) with marginal A_2 concentration (<1 wt%).

The concentration of naphthenic compounds is also higher for naphtha from VGO than PO (25.5 wt% and 11.4 wt% at 400 ºC, respectively) and diminishing when increasing the temperature (ought to the reduction of hydrogenation activity) achieving a 16.3 and 6.7 wt% at 440 ºC. Paraffins are the main compounds for both feedstocks at 400 ºC, with values of 56.6 and 76.9 wt%, respectively and reducing till 40.3 and 50.8 wt% at 440ºC, respectively. Although total paraffin concentration decreases with temperature for both neat feeds, the evolution of n-paraffins displays an opposite behavior for PO. The concentration of n-paraffins increases in detriment of i-paraffins as the skeletal rearrange decreases with temperature as Weitkamp et al. obtained [114,384]. In this way, a maximum concentration of i-paraffins is obtained at 400 ºC (51.9 wt%), which are desired compounds from a quality point of view. Notwithstanding, temperature reduces i-paraffins concentration, but at 440 ºC its concentration is still quite important (40.2 wt%). Besides, no olefins have been detected due to the great hydrogenation capacity of noble metals [21].

The addition of PO to VGO (PO/VGO, Blend 1) improves the naphtha composition, diminishing the concentration of aromatics and increasing the concentration of paraffins. At 400 ºC, the main compounds are paraffins, which they account the 62 wt% and they diminish to 53.7 wt% at 440 ºC. Regarding to aromatics, A_1 are the main aromatic compounds at 400ºC (13.1 wt%) which rapidly increase up to 32.6 wt% at 440 ºC, whereas A_2 concentration is negligible for all temperature range (1.2 wt% at the highest temperature). On the other side, naphthenic compounds concentration is significant at 400ºC, conforming 23.9 wt%, but they are rapidly reduced to 13.9 wt% at 420 ºC with a subsequent slight decrease at 440 ºC (12.3 wt%).

On the other side, naphtha from Blend 2 (HDPE/VGO) shows a higher aromatic concentration and less paraffin concentration than the naphtha from other blends. The paraffin concentration smoothly decreases with temperature. The concentration of A_1 increases with temperature, rising up to 53.1 wt% at 440 ºC. The A_2 concentration in naphtha is comparable to that obtained from VGO hydrocracking. It has to be pointed that olefins appear in small amount only at 400 and 420 º C. Naphthenic concentration suffers a small reduction when temperature increases.

For PO/HDPE/VGO (Blend 3), aromatics concentration in naphtha is comparable to that obtained from VGO hydrocracking. At 400 ºC, aromatics account the 26 wt% and they increase up to 40.2 wt% at 440 ºC, though A_2 concentration is similar for all the temperature range (~1.1 wt%). Naphthenic and paraffins decrease with temperature from 22.3 to 10.8 wt% and from 51.4 to 48.8 wt%, respectively.

Finally, naphtha from PP/VGO (Blend 4) is the less aromatic one, with a concentration of 8.7 wt% for A_1 at 400ºC and the highest naphthenic concentration at that temperature (30.5 wt%). However, the concentration of these groups changes drastically to values of 30.1 and 10 wt%, respectively, when temperature rises to 420 ºC. A subsequent increase of temperature (440 ºC) hardly affects the concentration of these compounds as before, being 36 and 7.9 wt%, respectively. The paraffin concentration stood at similar levels to that of Blend 1, decreasing with temperature from 60.4 to 55.9 wt% at 400 and 440 ºC, respectively. The behavior shown at 400 ºC with Blend 4 is due to (i) the nature of PP (that has branches in its structure) which boosts the formation of secondary alkylcarbenium ions easing the β-scission and (ii) the low dehydrogenation reactions rate at this temperature. Consequently, the naphtha coming from this blend attains a high paraffin concentration, especially i-paraffins. Furthermore, although when temperature raises i-paraffins concentration diminishes, its concentration is higher than that obtained from HDPE/VGO hydrocracking at whatever temperature, producing also lower aromatic concentration.

The evolution of naphtha RON with temperature for each feed is collected in Figure 4.13. This way, the quality of naphtha obtained from different feedstocks can be compared and the effect of temperature can be also studied. The results show that at 400 and 420 ºC, naphtha from VGO hydrocracking has the lowest RON (78.6 and 79, respectively). However, for this feed a substantial RON increase (up to 84.1) is achieved when operating at 440 ºC. This trend of increasing RON with temperature is the same as in VGO catalytic cracking under the conditions of a FCC unit [125]. The trend of RON for naphtha from neat PO hydrocracking is similar to that shown in the case of VGO hydrocracking but with less slope, changing from 81.3 to 82.7 between 400 and 440 ºC. Those values are very similar to those obtained by Joo and Guin [376], who hydrotreated plastic pyrolysis oil from a mixture of plastics at 435 ºC obtaining a RON of 84.7 for their naphtha, but lower than those obtained by Vasile et al. [367],who obtained a naphtha with 87.9 RON hydrotreating plastic pyrolysis oil at lower temperature (350 ºC).

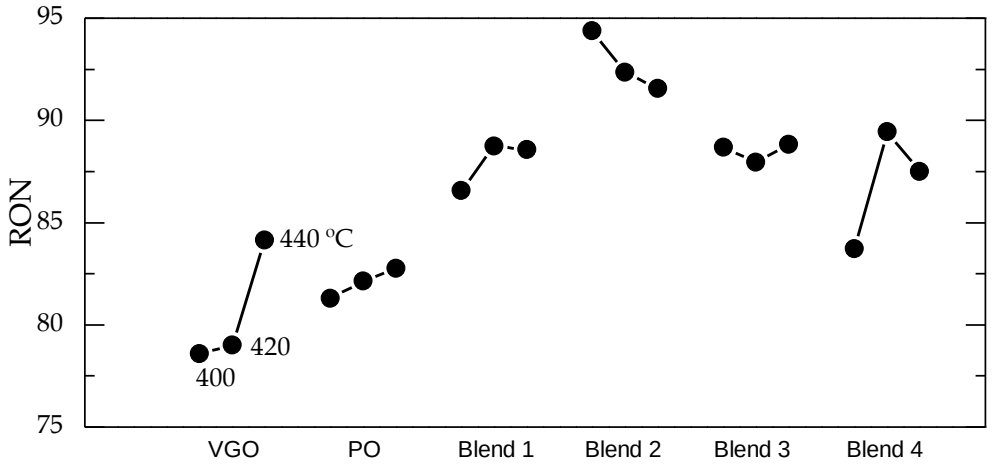

Figure 4.13 Effect of temperature on RON of naphtha for different feedstocks. Reaction conditions: PtPd/HY catalyst; 80 bar; C/F ratio, 0.1; reaction time, 120 min. Key: Blend 1, PO/VGO; Blend 2, HDPE/VGO; Blend 3, PO/HDPE/VGO; Blend 4, PP/VGO. The data of the hydrocracking of neat VGO and HDPE/VGO (Blend 2) have been obtained from section 3.3.

Regarding the blends hydrocracking, addition of PO to VGO (Blend 1) depicts a synergy that increases RON values for all temperatures, with a value of 86.6 at 400 ºC and 88.7 as the maximum value at 420 ºC. The highest RON values are achieved with HDPE/VGO (Blend 2), although depicted a drawdown, being 94.4 and 91.6 at 400 and 440 ºC. This fact is in line with that observed by Rodriguez et al. [125] who obtained lower RON values for HDPE/VGO catalytic cracking. On the other hand, a low effect of temperature is observed for the ternary mixture (PO/HDPE/VGO) hydrocracking, but RON values are lower than that obtained for HDPE/VGO and more similar to that of the PO/VGO, being c.a. 88.7 at all temperatures. This trend may be due to the fact that ternary mixture carries PO and HDPE which display opposite trends. The addition of PP to VGO also has a positive effect in naphtha RON, with values of 83.7 at 400 ºC and 89.5 at 420 ºC, respectively. However, pushing the temperature to 440 ºC produces changes in the composition that harm the RON value a little bit (87.5).

As a conclusion, the large amount of naphtha produced from hydrocracking of waste plastics has, in most cases, a composition similar to that obtained from neat VGO hydrocracking but with a higher quality (greater RON). As a consequence, it is proven that the addition of different polyolefinic wastes means an improvement to the process, since naphtha from their hydrocracking is suitable to be added to naphtha pool which after its adaptation will be marketed.

4.2.4 LCO composition and cetane index

Although a small amount of LCO is produced by this catalyst, its composition (Figure 4.14) and cetane index (Figure 4.15) are analyzed. LCO composition seems to be related to the corresponding naphtha composition. Therefore, each feedstock promotes the formation of some preferred compounds over others and then temperature plays its role. For all the feeds, raising the temperature leads to: (i) an increase of the total aromatic content (mainly A_2 and A_{3+}) (as the condensation of the olefins is promoted) and; (ii) a decrease of the i-paraffins concentration whereas n-paraffins increase. It is noteworthy that alternative feeds (PO, Blend 1, Blend 2, Blend 3 and Blend 4) denote a minor A_{3+} content in the LCO lump. Besides, no olefins are detected.

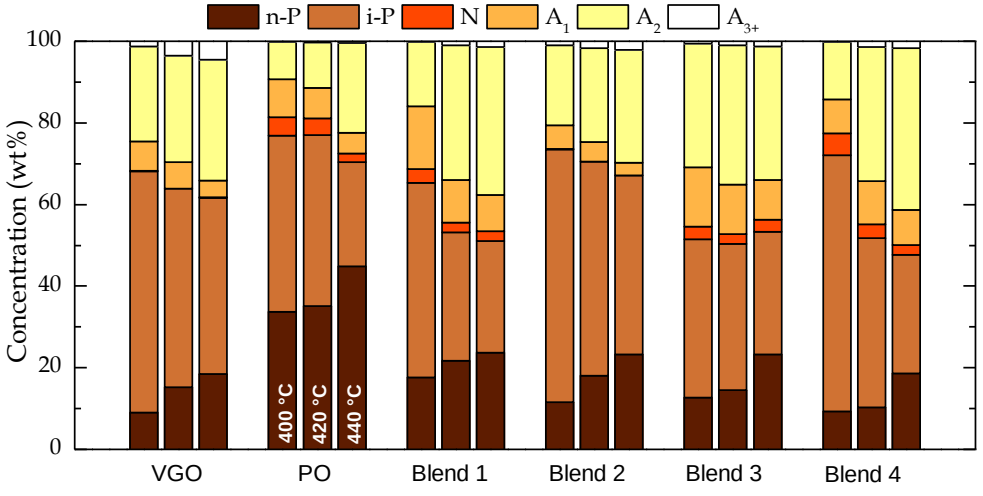

Figure 4.14 Effect of temperature on LCO composition for different feedstocks. Reaction conditions: PtPd/HY catalyst; 80 bar; C/F ratio, 0.1; reaction time, 120 min. Key: Blend 1, PO/VGO; Blend 2, HDPE/VGO; Blend 3, PO/HDPE/VGO; Blend 4, PP/VGO. The data of the hydrocracking of neat VGO and HDPE/VGO (Blend 2) have been obtained from section 3.3.

Attending to the results of Figure 4.14, the composition of LCO from VGO hydrocracking is mainly paraffinic (68 wt% at 400 ^{o}C), although paraffin concentration diminishes a little when temperature rises (61.6 wt% at 440 ^{o}C). Nevertheless, the evolution of the concentrations of n-paraffins and i-paraffins has opposite trend inside paraffin lump. When temperature goes up, n-paraffins concentration increases whereas i-paraffins concentration is lessens due to unfavorable skeletal rearrangement with temperature [385]. Meanwhile, the n-paraffins concentration is growing from 8.9 to 18.5 wt%, at 400 and 440 ^{o}C, respectively. On the other side, aromatics are the second largest group. In the case of A_2 they are the more abundant aromatics, which increase with temperature from 23.3 to 29.7 wt% at 400 and 440 ^{o}C, as well as poly-aromatics (A_{3+}) comes from 1.2 to 4.5 wt% whereas A_1 decrease from 7.3 to 4.1 wt%, due to the boosting of

condensation reactions with temperature. It has to be considered that together with reduction in isomerization rate, the reduction of the hydrogenation when increase the temperature is a fact due to reaction thermodynamics [109]. On the other hand, LCO from neat PO hydrocracking depicted a more paraffinic nature. The total paraffin concentration goes from 76.8 wt% at 400 ºC till 70.2 wt% at 440 ºC. For this feed, naphthenic compounds appear which are less than 5 wt% at 400 ºC and this concentration decreases with temperature. The lowest aromatic concentration is observed for this feed. This way, A_1 and A_2 are observed in the same amount ~9.2 wt% at 400 ºC, but temperature pushes upwards A_2 concentration (21.9 wt%) and decreases A_1 concentration (5.1 wt%) due to condensation reactions. Moreover, the concentration of A3 is negligible.

According to the blends, the LCO from HDPE/VGO (Blend 2) hydrocracking is the one which share more similarities with the LCO obtained from VGO. However, this LCO was slightly less aromatic and more paraffinic due to the addition of HDPE. On the other hand, LCOs from PO/VGO and PP/VGO (Blend 1 and 4, respectively) hydrocracking display similar composition. The maximum paraffin concentration is observed at 400 ºC (65.2 and 72 wt%, for the blends 1 and 4, respectively) and diminish up to 440 ºC (51.1 and 47.5 wt%, respectively) with an abrupt drop at 420 ºC. Nevertheless, naphthenic compounds concentration does not change with temperature (~3.5 wt%). Finally, the ternary mixture (PO/HDPE/VGO, Blend 3) shows a particular behavior. Total paraffins concentration increases smoothly with temperature at expense of aromatics, which decreases from 45.2 to 43.7 wt%. However, A_1 concentration is reduced from 14.4 to 9.7 wt% whereas A_2 cocentration increases from 30.3 to 32.7 wt% at 400 ºC and 440 ºC, respectively. One more time, naphthenic compounds concentration does not change noticeably with temperature (~2.7 wt%).

Cetane index of the LCOs has been calculated and results are depicted in Figure 4.15. The results unveil that in the case of neat VGO and PO hydrocracking, the maximum value of cetane index is achieved at the lowest temperature (400 ºC), being 62.9 and 69.9, respectively. The latter is close to the cetane index obtained by Bezergianni et al. [386] (71.5) in the pyrolysis oil hydroprocessing using a fixed bed reactor, at 375 ºC and 100 H_2 bar. However, when temperature rises, cetane index decreases reaching values of 48.6 and 51.7 at 440 ºC for neat feedstocks.

On the other hand, a negative synergy (opposite in comparison with the observed for the RON of the naphtha) is observed for LCO when PO/VGO (Blend 1) is hydrocracked, as the cetane index decreases from 43.1 at 400 ºC to 35.2 at 440 ºC. This decreasing trend is also seen for PP/VGO (Blend 4) hydrocracking. Nonetheless, for this feedstock a higher cetane index is obtained at 400 ºC (53.5), though at higher temperatures it decreases significantly (35.8 at 440 ºC). For the

HDPE/VGO (Blend 2) hydrocracking, cetane index of LCO improves with temperature with a maximum value of 55.7 at 440 ºC. On the other side, for PO/VGO/HDPE (Blend 3) hydrocracking, the cetane index shows a minimum at 420 ºC (35) and a maximum at 440 ºC (42.2). This behavior is consequence of the different trend shown by the binary mixtures of PO/VGO and HDPE/VGO.

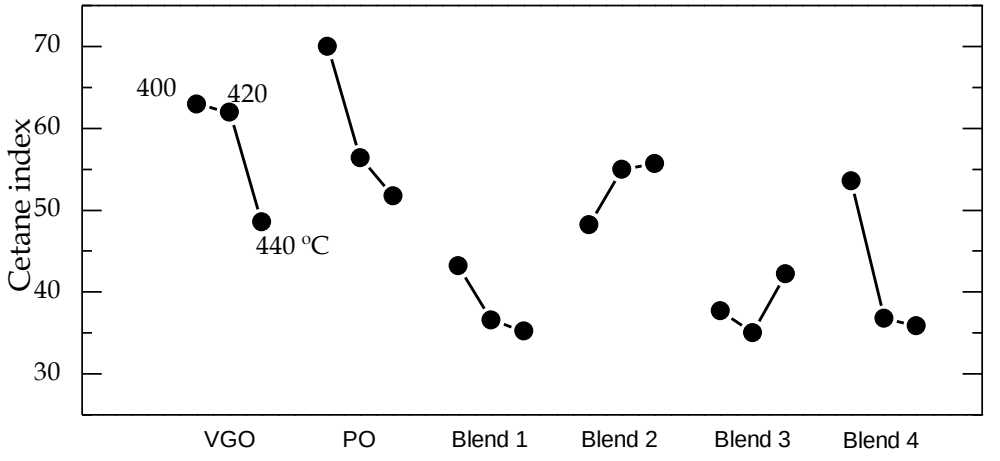

Figure 4.15 Effect of temperature on the cetane index of LCO for different feedstocks. Reaction conditions: PtPd/HY catalyst; 80 bar; C/F ratio, 0.1; reaction time, 120 min. Key: Blend 1, PO/VGO; Blend 2, HDPE/VGO; Blend 3, PO/HDPE/VGO; Blend 4, PP/VGO. The data of the hydrocracking of neat VGO and HDPE/VGO (Blend 2) have been obtained from section 3.3.

To conclude, although a low yield to LCO is achieved with this catalyst, the quality of LCO is enough good (proper composition and cetane index). On one hand, the composition depicted low concentration of polycyclic aromatics and on the other hand the cetane index values are closed or greater than those established by regulations (46 in EN-590). As a result, it is suitable to be added at diesel pool in refineries to be commercialized.

4.3 PtPd/HY CATALYST MODIFICATION BY ALKALINE TREATMENT OF THE ZEOLITE

The PtPd/HY catalyst has shown generally a good performance in hydrocracking of alternative feedstocks (Section 4.2). However, when a high temperature is used and at long reaction times, it has been observed an important limitation in the selectivity to LCO and naphtha fractions, as a consequence of their undesired hydrocracking to gas. In this section we have studied the modification of the properties of the HY support zeolite to minimize this problem. The strategy used has been the desilication by means of a controlled alkali treatment. It is well established that this treatment results in the attenuation of acidity and the generation of mesopores in zeolites. In this way, the extent of undesirable reactions are limited, such as overcracking of desired products and the coke formation. These undesired reactions are hydrogen transfer and aromatics condensation, catalyzed by strong acid sites and favored by the density of acid sites [387–389]. In addition, the ability of the mesopores to retain the coke formed reduces the blocking of the pore of the zeolites [211,388,390–393]. The procedure and the results are presented along this section, the alkaline treatment of the catalysts in section 4.3.1, its effect on the properties of the catalyst in section 4.3.2 and its behavior in HDPE/VGO hydrocracking in section 4.3.3.

4.3.1 Desilication procedure

It is a fact that the generation of mesoporosity through desilication produces very heterogeneous results. This is due to the fact that many changes can be made in the desilication process to innovate in the results obtained, thus creating an infinite number of possible results. Figure 4.16 is a scheme that sums up the variables that affect the desilication and hence the modification of catalyst properties and how these ones together with other factors have an effect over reaction products. The desilication variables are: (i) the zeolite chosen; (ii) the alkaline metal hydroxide or the organic hydroxide chosen; (iii) the different desilication conditions to generate mesoporosity; and (iv) in the case of alkaline metal hydroxide, the addition or not of an organic hydroxide as a pore directing reagents to control pore growth, such as tetramethylammonium hydroxide (TMAOH), tetrapropylammonium hydroxide (TPAOH), tetrapropylammonium bromide (TPABr), tetrabutylammonium hydroxide (TBAOH), among others [394–401]. These variables act over (i) chemical composition, (ii) textural and (iii) acidic properties which conforms the catalyst properties.

The reaction products can depend on (i) catalyst properties, (ii) reaction system, (iii) feedstock chosen and (iv) the operating conditions. Nevertheless, in the

present study, the operating conditions, the feed used and the reaction system have been kept constant, thus making it possible to assess the changes in the catalyst properties throughout the desilication process.

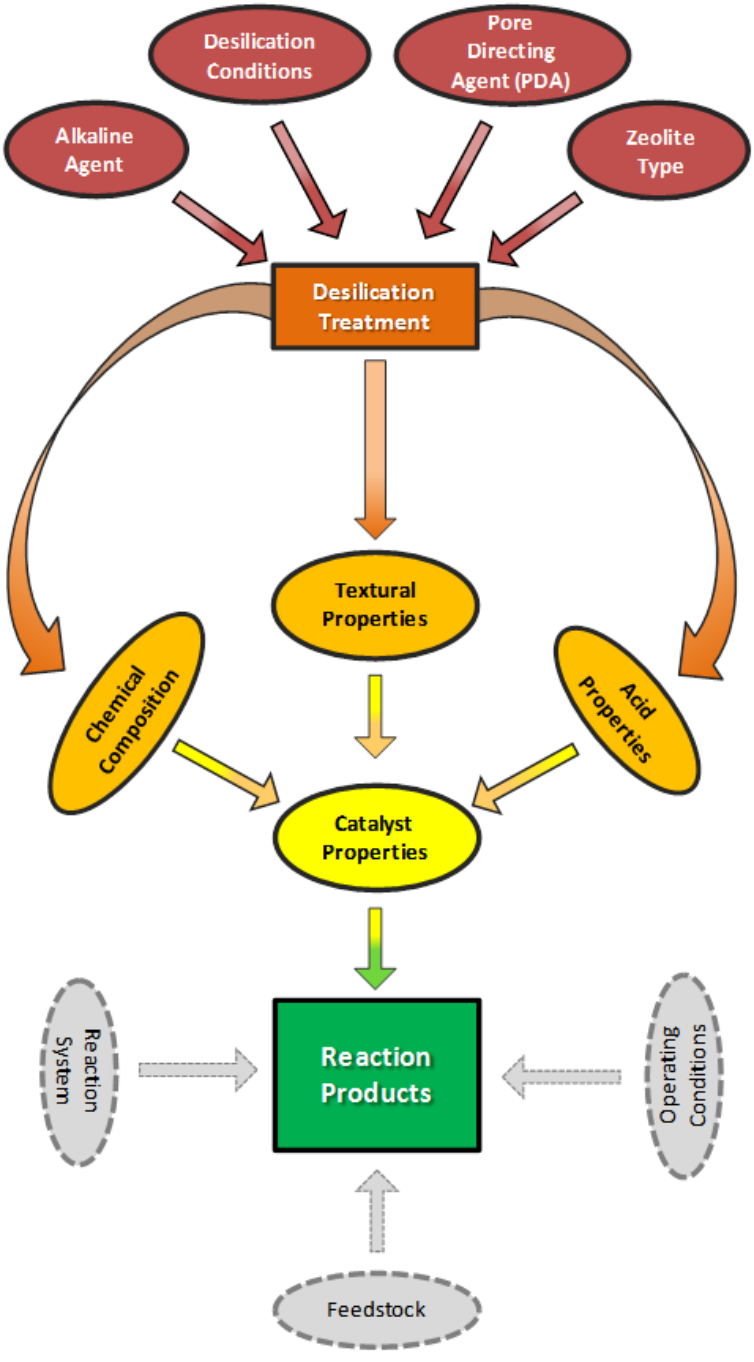

Figure 4.16 Effect of desilication over catalyst properties and reaction products.

As it has been mentioned in section 1.4.4.2, some authors [206–208] carried out experiments in a fixed-bed reactor, working continuously by several hours. Their feedstocks did not contain complex aromatic compounds. However, it has

been proven that if feedstock is changed from simple or model compounds, like methanol, 1-hexene or n-C_{16}, to complex mixtures like bio-oil, pyrolysis oil or LCO among others, even in a continuous fixed-bed reactor coke is produced in similar or slightly higher yields than parent catalysts. Tarach et al. [402] studied the catalytic conversion of LCO in a fixed-bed reactor using two alkaline agents to carry out the catalyst desilication. For the same conversion, they obtained a similar or higher coke yield than with the parent catalyst when used NaOH as alkaline agent and lower coke yield when added tetra-butylammonium hydroxide (TBAOH) to the desilication treatment as a pore growth moderator. Nevertheless, they also achieved greater gas yield than with parent catalyst. In the same line, Kim et al. [388] hydrocracked pyrolysis fuel oil to BTX compounds in a fixed-bed reactor using Ni_2PB/β-zeolite and its desilicated version using NaOH and tetrapropylammonium bromide (TPABr) as a pore directing agent which moderate pore growth. They reported that higher conversions were obtained for longer time with the desilicated catalyst. Furthermore, the coke yield for the same reaction length it is much lower. According to stirred batch reactor runs, Munir et al. [373] developed an in-house prepared zeolite beta based on a desilication technique through alkaline treatment with NaOH. They studied the performance of those catalysts in comparison with parent zeolite beta and reported that the desilicated zeolite reduced the gas yield in the waste plastic hydrocracking. Nevertheless, the conversion was also reduced.

Given the scarcity of papers that study the effect of desilication on the HDPE/VGO hydrocracking in a stirred batch reactor, it has been decided to approach the subject taking NaOH as the alkaline metal hydroxide reagent to carry out the desilication treatment over the PtPd/HY catalyst. In addition, the detailed analysis of the products will provide information on their quality (RON and cetane index), pushing the knowledge beyond the yields and the conversion achieved. In addition, the nature and location of the coke deposited on the desilicated catalyst will be studied, comparing them with the coke deposited on the parent catalyst.

The alkaline treatment method of HY zeolite has been established following the description in literature [211,373,395,396,402,403], with the next steps:

- 10 g of a commercial zeolite Y (Zeolyst CBV 712) were suspended in 300 mL of 0.1 M aqueous NaOH solution (Sigma-Aldrich) and kept under stirring for 15 min at room temperature.
- The suspension was neutralized with an equivalent amount of 1.0 M HCl solution (Sigma-Aldrich) to stop the desilication process. This is because using NaOH, most of the mesoporosity is developed in the first 15 min of the treatment [394,404].
- The desilicated zeolites were filtered and washed with deionized water.
- The zeolites were subjected to two ion exchanges with aqueous solutions of NH_4Cl (Sigma-Aldrich, 99.5%) 0.50 M for 24 h at room temperature with a zeolite/solution ratio of 1 g/5 mL, in order to remove the Na introduced during the leaching stage.
- The samples were filtered, washed with deionized water, dried in an oven at 110 °C for 16 h and calcined in a muffle with a ramp of 12 °C min^{-1} up to 550 ^{o}C and kept at that temperature for 4 h.

After this process, the desilicated zeolite support is impregnated with 1 wt% of Pt and 0.5 wt% of Pd following the procedures described in section 2.3 and then the catalyst obtained is called Cat-B.

Furthermore, the above desilicated procedure was carried out completely two times before loading the noble metals in the same amounts, resulting on a catalyst that it was named Cat-C.

4.3.2 Catalysts properties

The modified catalysts were characterized by several techniques previously used for the characterization of the parent catalyst and described in section 2.3 ((i) N_2 adsorption-desorption isotherms, (ii) ICP-AES, (iii) TPD of t-BA, (iv) FTIR of pyridine, (v) XRF, (vi) XRD and (vii) TEM).

4.3.2.1 N_2 absorption-desorption isotherm

The N_2 adsorption-desorption isotherms of parent (Cat-A) and modified catalysts (Cat-B and Cat-C) are displayed in Figure 4.17. The three catalysts show hybrid isotherms type I-a and type IV according to microporous and mesoporous materials, respectively, as IUPAC nomenclature establishes [315]. Furthermore, all the catalysts also exhibit a hysteresis loop that, in concordance with IUPAC, they are the results of controlled cavitation of N_2 evaporation when it is desorbed in pores whose neck diameter is smaller than a critical size (estimated in 5-6 nm). These phenomena can be found in the multi-layer of micro-mesoporous silica, zeolites and some active carbons. On the other hand, the morphology of these hysteresis loop resembles with H4 type and is related with slit-like pores [389,405]. Nevertheless, some differences can be found between N_2 adsorption-desorption isotherms as result of the desilication treatment. It can be seen a reduction of adsorbed volume in where plateau appears, which is correlated with a reduction of microporous surface [396]. Therefore, micropore area is reduced from Cat-A to Cat-B and Cat-C stepwise due to the destruction of zeolite crystal, which is studied using XRD in Figure 4.21. Moreover, a change in the hysteresis loop can be appreciated where the difference between adsorbed and desorbed volume becomes greater when the severity of the alkali-treatment increases.

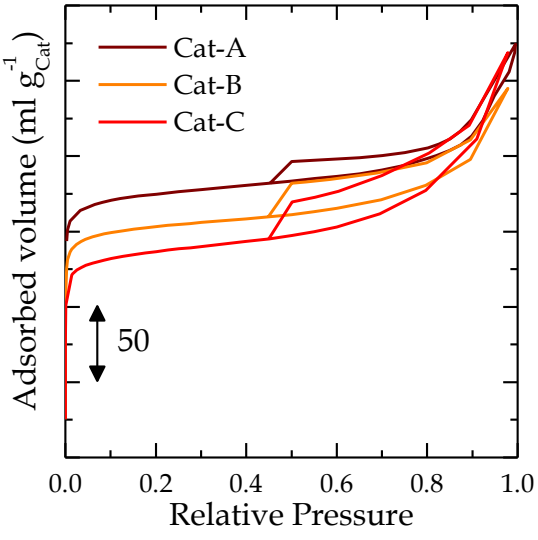

Figure 4.17 N_2 adsorption-desorption isotherms of parent and desilicated catalysts.

4.3.2.2 Transmission electron microscopy (TEM)

Figure 4.18 depicts the images from high resolution transmission electron microscopy of parent and desilicated catalysts. The parent catalyst (Figure 4.18a and Figure 4.18b) shows a smooth surface with an excellent dispersion of PtPd particles (small dark dots). However, since the first desilication treatment the TEM image of Cat-B (Figure 4.18c) displays a clear degradation of the surface due to the alkali-treatment with NaOH, emerging '*craters*'. Nevertheless, the Figure 4.18d shows that the metal dispersion keeps being very good. The mesoporous formation was also observed in the SEM and TEM photographs reported by Sree et al. [406] who also carried out a HZSM-5 zeolite desilication and they reported that the mesopores emerge with different diameters appreciated through high angle annular dark field (HAADF) in STEM image. Moreover, Tarach et al. [402] used different alkali-agents and discovered that with NaOH the mesoporosity is located in the more external surface of the particle while the inner part almost remains unmodified. Figure 4.18e shows the results after two desilication cycles (Cat-C). As reported in the literature Su et al. [206], the more severe the desilication conditions, the greater the degradation of the catalyst. In this case, it can be seen that although the degradation is harder with bigger *craters (*Figure 4.18e), the dispersion of the metal remains being successful (Figure 4.18f).

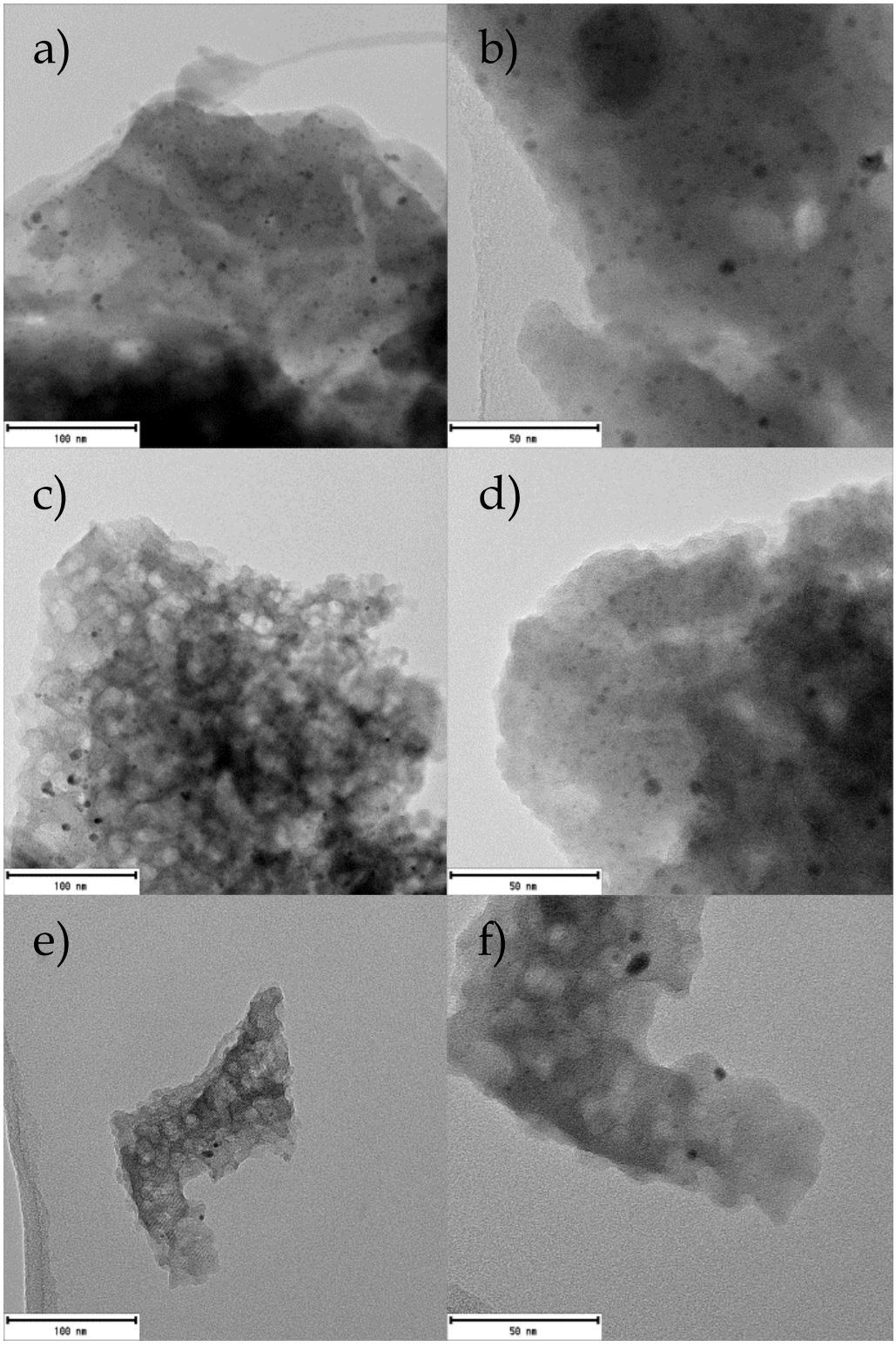

Figure 4.18 Transmission electron microscopy (TEM) of Cat-A (a and b), Cat-B (c and d) and Cat-C (e and f).

4.3.2.3 Temperature programmed desorption (TPD) of tert-butylamine

The analysis of total acidity by TPD of tert-butylamine (t-BA) has higher sensitivity than that NH_3 TPD [303] and is used to quantify the acidity of the catalysts. In Figure 4.19 it can be seen the profile of released butane for parent (Cat-A) and desilicated catalysts (Cat-B and Cat-C). Comparing temperatures at which butane is released, there are small differences between Cat-A, Cat-B and Cat-C, and the peaks are at 283, 286 and 285 °C respectively. Therefore, there is a slight increase in acidic strength of the catalysts which also can be related to the number of Brønsted sites with respect to Lewis (section 4.3.2.4). Gayubo et al. [407] obtained a reduction of acidic strength of desilicated HZSM-5 zeolites when using TPD-NH_3, but the conditions of the desilication treatment (temperature, time and NaOH concentration) and the zeolite type lead to obtain very varied results with different properties and behaviors [394–396]. Furthermore, Figure 4.19 shows that TPD signals are attenuated from Cat-A to Cat-B and Cat-C. The reduction on TPD signal is lower for Cat-B than for Cat-C, depicting that two desilication steps on Cat-C harm in larger extent the acidity of the catalyst. These results are in line with those obtained by Li et al., [396], who compared the acidic properties of parent HZSM-5 and alkali-treated with NaOH. Using TPD of NH_3, they observed that the temperature maximum of TPD profiles did not change but they show an attenuation of the signal.

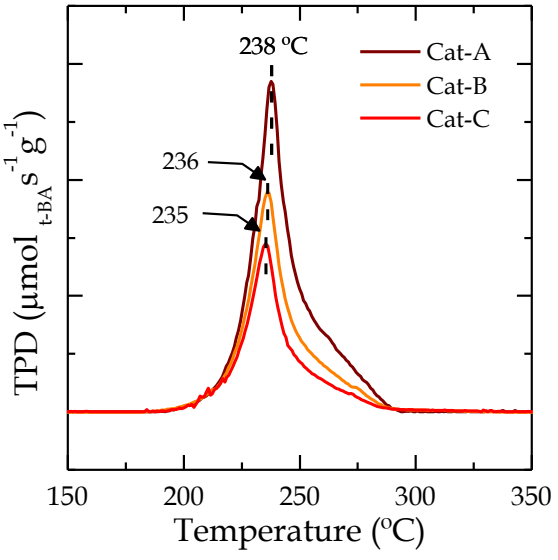

Figure 4.19 TPD-tBA analysis of parent catalyst (Cat-A), those undergoing to one desilication stage (Cat-B) and two stages (Cat-C).

4.3.2.4 Fourier-transform infrared spectroscopy (FTIR) of adsorbed pyridine

The FTIR of pyridine profiles have been used to identify the nature of the acidic sites. The FTIR analysis of pyridine profiles in Figure 4.20 shows that the peak related with Lewis sites is taller than Brønsted ones for Cat-A. Nevertheless, the deconvolution of these peaks in Table 4.3 shows the concentration of the Brønsted sites, which is represented in µmol of adsorbed pyridine per g of catalyst, is greater than the area of Lewis sites, and the calculated B/L ratio is 1.53. However, after the first desilication step (Cat-B), Lewis sites are more affected than Brønsted sites. This is clearly identifiable through the results from Table 4.3 and the change between the slope of line A and the slope of line B in Figure 4.20. These results are in line with those reported by Gil et al. [391] in the desilication of HZSM-5, who obtain a higher reduction in Lewis sites. Finally, the two desilication steps in Cat-C describe a further reduction in both Brønsted and Lewis sites. Nonetheless, the latter are reduced again in a greater extent. Furthermore, the slope of line C even changes (Table 4.3).

Table 4.3 Pyridine adsorbed on acidic sites from FTIR.

Catalyst	Brønsted (µmol/g)	Lewis (µmol/g)	B/L
Cat. A	726	476	1.525
Cat. B	643	332	1.937
Cat. C	137	57	2.404

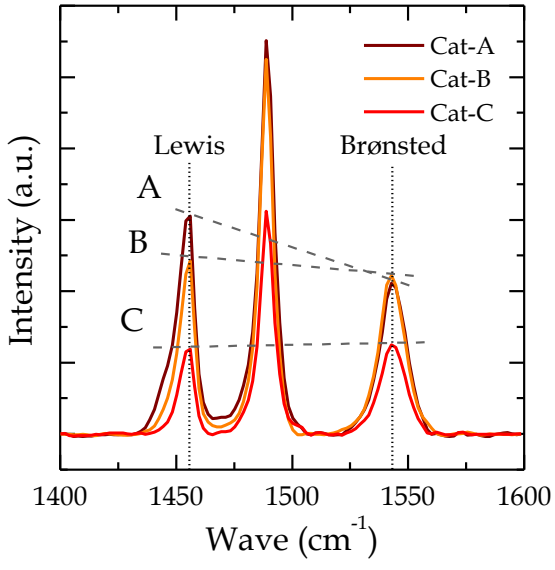

Figure 4.20 FTIR-pyridine profiles of parent (Cat-A) and desilicated catalysts (Cat-B and Cat-C).

4.3.2.5 X-ray fluorescence (XRF)

Table 4.4 shows the chemical composition of the three catalysts obtained from X-ray fluorescence technique. Regarding to metal content, results obtained are quite different to those obtained with ICP/AES (Table 4.6) and quite far from nominal values (specially for Cat-A). As is mentioned, this technique only can provide a semi-quantitative analysis of these metals.

As it can be seen, Al_2O_3 content shows a slight decreasing trend with desilication treatment, increasing the total Si/Al ratio, but contrary to expectations, no clear decreasing trend is observed for SiO_2 content. However, as Qin et al. [408] mention, XRF measures not only the amount of SiO_2 and Al_2O_3 in the zeolite framework, but also in the amorphous phase; so, it is necessary to use other techniques to identify the Si and Al in the crystalline phase, like X-ray diffraction (XRD) [408,409] or nuclear magnetic resonance (NMR) [391].

Table 4.4 XRF results of parent (Cat-A) and modified catalysts (Cat-B and Cat-C).

Catalyst	Cat-A	Cat-B	Cat-C
SiO_2 (wt%)	87.15	87.35	86.91
Al_2O_3 (wt%)	12.06	11.13	10.90
Pt (wt%)	0.48	1.08	1.45
Pd (wt%)	0.31	0.45	0.74
Si/Al	6.38	6.93	7.05

4.3.2.6 X-ray diffraction (XRD)

Analyzing the XRD patterns in Figure 4.21, the alkaline attack reduces the crystallinity diminishing the intensity of peaks in XRD pattern and increases the amorphous phase raising the background from 20 to 30 2θ degrees. The loss in the crystallinity is associated to the extraction of Si from the framework [409]. However, the increase in the amorphous phase means a rearrangement of Si, thus, changes in total content of Si are almost negligible as XRF report. This behavior is also reported by Qin et al. [408] in TEM images or by Gackowski et al. [409] in XRD spectra.

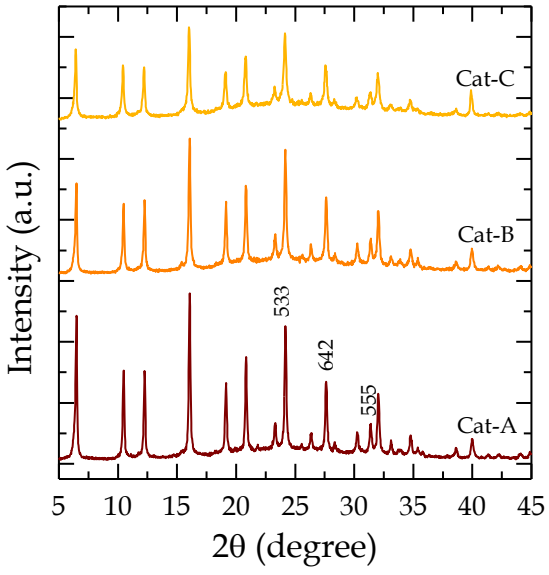

Figure 4.21 XRD pattern of parent (Cat-A) and modified catalysts (Cat-B and Cat-C).

When Si is removed from the framework, the crystalline structure changes due to greater bond length of Al-O compared to Si-O bond, modifying the unit cell size of zeolite [410]. Based on this principle the Si/Al ratio can be estimated using the Breck-Flanigen correlation, according to Ferdov et al. [411]:

$$Si/Al = \left[\left(2\frac{192}{(\overline{UCS} - 24{,}191)}\right) - 1\right] \tag{4.1}$$

where $\overline{UCS}$ is the average of UCS for each plane.

The unit cell size (UCS) (Å) of the zeolitic materials can be determined from XRD following the procedure described in the ASTM-D 3942 standard, by applying Bragg's Law, according to:

$$UCS = [(d_{hkl})^2(h^2 + k^2 + l^2)]^{1/2} \tag{4.2}$$

where h, k, and l are Miller indexes of catalysts (Table 4.5), which are correlated with reflection planes detected at different 2θ for each catalyst, and d_{hkl} (Å) is the distance between the crystalline planes obtained as follows:

$$d_{hkl} = \frac{\lambda}{2\ sen\,\theta} \tag{4.3}$$

where λ (Å) is the wavelength of the X-ray source (1.5418 Å for the CuKα radiation source used in this work), and θ (°) the half angle of reflection where a certain peak is observed.

Table 4.5 Planes and reflections degree (2θ) in XRD of the catalysts used to calculate the unit cell size.

Planes (h,k,l)	Cat-A	Cat-B	Cat-C
533 (5,3,3)	24.18	24.15	24.13
642 (6,4,2)	27.62	27.62	27.54
555 (5,5,5)	31.40	31.40	31.34

4.3.2.7 Properties Comparison

Table 4.6 shows the main physicochemical properties of the parent catalyst (Cat-A), and after one desilication cycle (Cat-B) and after two desilication cycles of the zeolite support (Cat-C).

Table 4.6 Physicochemical properties of alkali-treated catalysts and the parent catalyst.

Physical Properties	PtPd/ZY-A	PtPd/ZY-B	PtPd/ZY-C
S_{BET} ($m^2\ g^{-1}$)	620	535	478
S_{micro} ($m^2\ g^{-1}$)	543	448	377
S_{meso} ($m^2\ g^{-1}$)	77	87	101
V_{micro}($cm^3\ g^{-1}$)	0.24	0.20	0.17
d_P (nm)	8.44	9.56	10.24
Composition			
Pt (wt%)[a]	1.19	1.13	1.11
Pd (wt%)[a]	0.53	0.49	0.47
Si/Al ratio[b]	11.44	10.83	8.01
Acidic Properties			
Total Acidity ($mmol_{tba}\ g^{-1}$)	1.69	1.18	0.96
A_S ($KJ\ mol_{tba}^{-1}$)[c]	135	147	150
Brønsted/Lewis ratio	1.53	1.93	2.40

[a]ICP/AES
[b]calculated from XRD
[c]average value from calorimetric analysis

The comparison of surface area values reflects a reduction of S_{BET} and S_{micro} when alkaline treatment is applied. The parent catalyst is mainly microporous (543 of 620 $m^2\ g^{-1}$) but the catalysts after the NaOH treatments show less microporous

area (377 of 478 m^2 g^{-1} on Cat-C), increasing the mesoporous area. This leads to a reduction in the micropore volume (V_{micro}) of the catalysts, going from 0.24 to 0.17 cm^3 g^{-1} for Cat-A and Cat-C, respectively. Furthermore, since the mesopore area increases, the mean pore diameter (d_p) also does so, increasing from 8.4 to 10.2 nm for Cat-A and Cat-C, respectively. These changes in physical properties are in line with reported by other authors for other zeolites [211,389,409].

Regarding chemical composition, the results in Table 4.6 show that metallic content of the catalysts is close to the nominal one (1 and 0.5 wt%, respectively) which reveals that impregnation has been carried out successfully. About Si/Al, this ratio decreases stepwise from Cat-A to Cat-C, 11.4 to 8, respectively. The Si/Al ratio has been estimated from XRD spectra using the Breck-Flanigen correlation [411] due to XRF technique cannot distinguish between the Si on the crystalline structure of the zeolite and in the amorphous phase, showing negligible changes in Si and Al composition for the different catalysts (Table 4.4).

The results of the acidity collected in Table 4.6 display a reduction in the total acidity after desilication treatments from 1.7 to 0.9 $mmol_{tba}$ g^{-1} in Cat-A (parent) and Cat-C, respectively. Furthermore, the acidic strength slightly increases for desilicated catalysts in comparison with parent one. But this is not due to an increase in Brønsted sites (Table 4.3), but to a greater loss of Lewis sites than Brønsted [391].

4.3.3 Effect of the alkaline treatment on hydrocracking performance

The modified catalysts have shown interesting changes in their physicochemical properties as a reduction of micropore area, total acidity, increase in B/L ratio and loss of crystallinity of the zeolite support. Therefore, in this section, the catalysts will be tested in the hardest operating conditions in which gas and coke yields are highly favored. In this way, it can be studied how these catalyst modifications contribute to improve its behavior. The reaction conditions have been:

- Feedstock: HDPE/VGO (20 wt%)
- Temperature: 440 ºC
- Pressure: 80 bar H_2
- Catalyst to Feed ratio: 0.1 (in mass)
- Stirrer speed: 1300 rpm
- Reaction time: 120 min

Thus, an extensive analysis of reaction indicators (product yield, conversion, product composition and fuel quality) has been accomplished to assess the behavior of the catalysts. Besides, these analysis help to understand the catalyst performance regarding to the catalyst properties.

4.3.3.1 Hydrocracking yields and conversion

The effect of catalyst modifications on catalyst performance in terms of product yields and conversion are collected in Figure 4.22. As it has been done in previous sections, products are divided into 6 lumps (with their corresponding yields) and it has been taken into account the conversion of both HCO and HDPE separately (X_{HCO} and X_{HDPE}, respectively).

Although Cat-A achieves the greater X_{HCO} (91.1 wt%) with interesting naphtha and LCO yields (31.3 and 9.3 wt%, respectively), gas yield overcomes them (49.6 wt%). Besides, there are no waxy compounds in the product. Consequently, there is a complete HDPE conversion. The coke yield for this catalyst is 3.1 wt%, being the highest yield for all the catalysts, what can be attributed to the fact that it is the most acidic one, with higher number of Brønsted sites (Table 4.3 and Table 4.6).

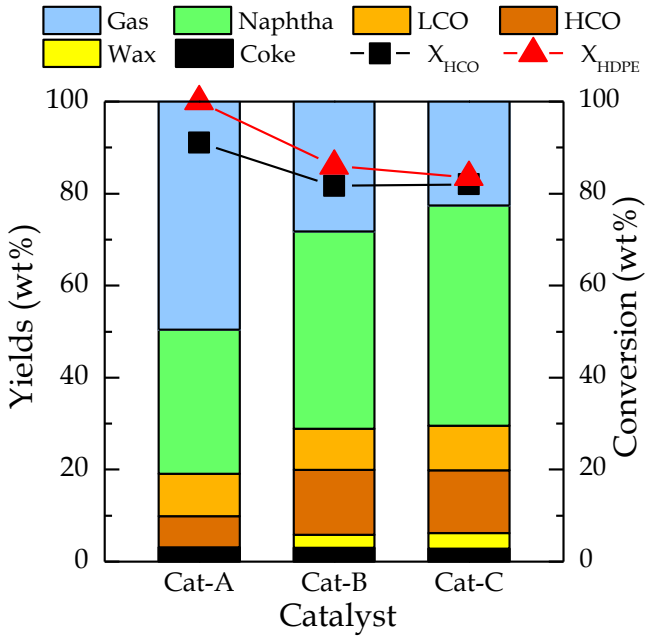

Figure 4.22 Effect of catalyst desilication on yields and conversions. Reaction conditions: 440 °C; 80 bar of H_2; C/F, 0.1; 120 min.

When Cat-B is tested under the same operating conditions, the HCO lump is higher than Cat-A (14.1 wt%) with the consequent reduction in X_{HCO} (81.5 wt%). Nevertheless, naphtha yield rises and LCO yield is almost the same, 42.9 and 8.9 wt%, respectively. This increase means a reduction of gas yield to 28.2 wt%, which is a good improvement. However, the X_{HDPE} is not complete as before, although it is still high (86 wt%). In the same line, Munir et al. [373] report that there is no significant change in LCO yield using desilicated catalysts (with beta zeolite) and also report the reduction in the plastic conversion. On the other side, the coke yield diminishes up to 3 wt%, being slightly lower than that of Cat-A due to the reduction in the acidic properties of desilicated catalyst (Table 4.3 and Table 4.6). Similar results were reported by other authors working with a wide variety of feedstocks: hydrocracking of n-C_{16} [412]; catalytic pyrolisis of biomass [413]; cracking of 1-Butene [389]; co-pyrolysis of oil sludge with HDPE [414].

On the other hand, the Cat-C achieves a slight reduction in HCO lump (13.7 wt%) and comparing with Cat-B it improves the conversion (82.1 wt%) while producing greater naphtha yield and slightly higher LCO yield (47.9 and 9.6 wt%, respectively) in detriment of gas yield, which decreases (22.5 wt%). However, the Cat-C also obtains larger wax yield than Cat-B (3.3 vs. 2.8 wt% respectively) which means of slight reduction in X_{HDPE} (83.5 wt%). Besides, as was expected, a harder alkali-treatment also has an effect over coke yield. In this case, the coke yield decreases up to 2.9 wt%, being the lowest obtained. This result is due to Cat-C has the lowest acidity (Table 4.6), and hence, a significant reduction of both Brønsted

and Lewis acidic sites (Table 4.3). This effect also was reported by other authors who increased the severity of the treatment increasing the concentration of the alkaline metal hydroxide, thus, reducing the coke yield [389,412–414].

Generally speaking, the desilicated catalysts (Cat-B and Cat-C) are less active due to their lower acidity (Table 4.3, Table 4.6 and Figure 4.19) which implies a reduction in both conversions (X_{HCO} and X_{HDPE}). However, the overcracking of naphtha is reduced, with the subsequent gas yield reduction. However, the changes in the acidity and textural properties do not have a significant effect over LCO yield. This behavior is reflected in the S_F of parent and modified catalysts depicted in Figure 4.23. It can be seen that desilications have a positive effect on the S_F, which is 0.7 for parent catalyst, which means that the higher conversion produces more undesired sub-products as gas and coke at the same time that minimize the yield of desired products (naphtha and LCO). However, after the first and second desilications (Cat-B and Cat-C, respectively) the S_F increases stepwise to 1.1 and 1.4, respectively, maximizing the production of naphtha and LCO. It has to be mentioned that as yields shows, the enhancement of S_F is because of naphtha yield increase.

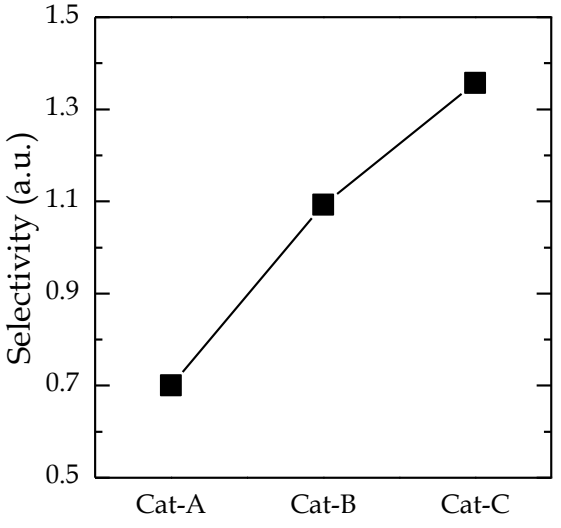

Figure 4.23 Effect of catalyst desilication on selectivity to fuel index (S_F). Reaction conditions: 440 ^oC; 80 bar of H_2; C/F, 0.1; 120 min.

4.3.3.2 Gas composition

The gas composition is shown in Figure 4.24 for each catalyst, where the identified compounds are CH_4, C_2H_6, C_3H_8, i-C_4H_{10} and n-C_4H_{10}.

For Cat-A the main components are C_3 and C_4 (LPG), with concentrations of 46.5 and 17.2 wt%, respectively. Regarding C_4 compounds, the percentage of i-C_4 is slightly higher than that of n-C_4, 9.9 and 7.2 wt%, respectively. The concentration of dry gas, i.e., CH_4 and C_2H_6 (minority fraction) is 36.3 wt%, where the main compound is C_2H_6 (25.5 wt%).

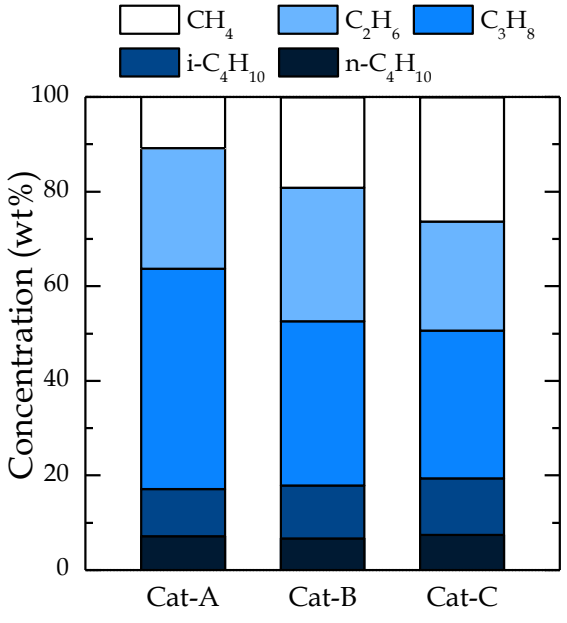

Figure 4.24 Effect of catalyst desilication on gas composition. Reaction conditions: 440 ºC; 80 bar of H_2; C/F, 0.1; 120 min.

For Cat-B, the concentration of the components in dry gas increases to 19.1 and 28.2 wt% for CH_4 and C_2H_6, respectively. The desilication also provokes the diminishing of LPG compounds, but they still account for more than half of the composition (52.6 wt%). Within LPG fraction, the C_3H_8 and n-C_4H_{10} concentration diminishes whereas the i-C_4H_{10} slightly increases (34.7, 6.6 and 11.2 wt%, respectively). Therefore, desilication treatment not only causes a reduction of gas yield but also changes the composition of gas fraction, increasing the amount of dry gas in detriment of LPG fraction. This result can be explain because since the reduction of cracking activity of the catalyst, thermal cracking (radicalary mechanism) is favored with preferential formation of dry gas to the detriment of LPG [114,374,415].

Finally, the gas obtained with catalyst subjected to two desilication cycles (Cat-C) displays small changes in composition comparing with Cat-B. Continuing

with previously observed trend, the LPG concentration slightly diminishes, representing almost half of the gas (50.6 wt%). Within LPG fraction, C_4 grow stepwise (both i-C_4H_{10} and n-C_4H_{10} are slightly higher than those obtained with Cat-B) meanwhile C_3H_8 decreases, being these concentrations 19.3 and 31.3 wt%, respectively.

4.3.3.3 Naphtha composition and RON

The effect of catalyst modification trough desilication on the composition of naphtha is depicted in Figure 4.25, where compounds from naphtha fraction have been grouped in six lumps: paraffins (n-P and i-P), naphthenes (N), olefins (O) and aromatics (one ring A_1, and two rings A_2).

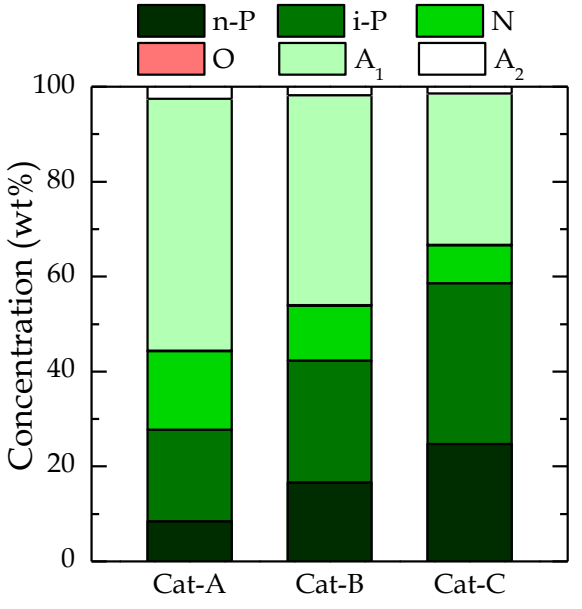

Figure 4.25 Effect of catalyst desilication on naphtha composition. Reaction conditions: 440 ^oC; 80 bar of H_2; C/F, 0.1; 120 min.

Desilication affects to naphtha composition. While the olefin content is almost negligible, always below 0.1 wt%, as desilication increases, both paraffin concentration (n-P and i-P) increases, going from 27.6 wt% for Cat-A to 58.5 wt% for Cat-C, and the naphthene concentration decreases, going from 16.6 wt% for Cat-A to 8 wt% for Cat-C. Besides, the increase in paraffins is in detriment of aromatics (both 1-ring and 2-ring). Thus, aromatics go from 55.5 wt% with Cat-A to 33.3 wt% with Cat-C. In line with these results, Garcia et al. [211] report an increase in the aliphatic compounds whilst aromatics are reduced in naphtha lump when desilicated catalysts are used in the catalytic cracking of bio-oils.

In this case, we can see that the reduction of acidity (Table 4.6 and Figure 4.19) and the modification of the acidic sites type by desilication (Table 4.3 and

Figure 4.20) have a stepwise reduction of aromatics and naphthenic whereas paraffins increase. This change in the catalysts performance can be due to an alteration of the reaction mechanism pathway as a consequence of the decrease in acidity. It seems that the hydrodearomatization reaction (HDA) of polyaromatics to A_1 occurs to a lesser extent, reducing A_1 concentration. Moreover, the reduction of catalyst activity and the overcracking suppression of naphtha lump revert mainly over paraffins lumps, since they can go faster through β-scission (producing gas) than aromatics or naphthenic compounds which firstly need to be saturated and pass through ring opening and skeletal rearrangement before the β-scission takes place [114,416].

Small variations are observed in RON values for each catalyst (Figure 4.26), although there is a slight decreasing trend whilst desilication cycles are increased in Cat-B and Cat-C. In that way, the RON value achieved by Cat-A is the highest one and then decreases for Cat-B and Cat-C stepwise in such a way that RON is 91.6, 89.6 and 88.5, respectively. Both the reduction of aromatics and the increase of n-P concentration play in detriment of RON.

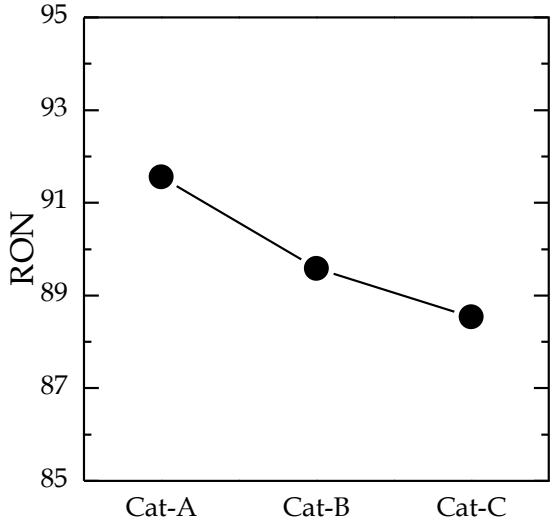

Figure 4.26 Effect of catalyst desilication on RON. Reaction conditions: 440 ºC; 80 bar of H_2; C/F, 0.1; 120 min.

4.3.3.4 LCO composition and cetane index

Figure 4.27 shows the composition of the LCO fraction obtained with different catalysts. The compounds have been grouped into six lumps according to its nature (PIONA).

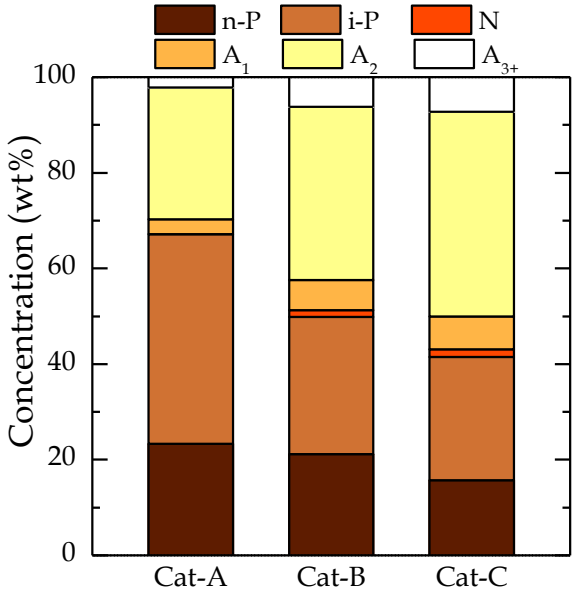

Figure 4.27 Effect of catalyst desilication on LCO composition. Reaction conditions: 440 °C; 80 bar of H2; C/F, 0.1; 120 min.

Desilication of the catalysts provokes the aromatization of the LCO fraction while the concentration of saturate compounds diminishes. The concentration of paraffins (n-P and i-P) decreas, going from 67.1 wt% for Cat-A (43.8 wt% of i-P) to 41.5 wt% (25.5 wt% of i-P) for Cat-C. The concentration of naphthenes increases, going from less than 0.1% for Cat-A to 1.6 wt% for Cat-C. The concentration of aromatics increases (all of them), going from 32.9 wt% for Cat-A to 56.9 wt% for Cat-C. In line with the obtained results, Tarach et al. [402] reported that LCO composition turns to greater aromatic and less saturated compounds for catalyst treated with NaOH in comparison with parent catalyst when VGO is hydrocracked.

This increase in aromatic compounds is also related to the reduction of the HDA activity, which is closely related to the cracking activity of the catalysts and therefore the attenuation of the hydrogenation equilibrium displacement. All this leads to the no hydrocracking of aromatics present in the VGO. Furthermore, these results reinforce the arguments given before about the reduction of aromatics in naphtha yield when desilicated catalysts are used. Naphtha and LCO yields are interrelated and thus, aromatic compounds in naphtha come from LCO yield according HDA reaction pathways explained by Karakhanov et al. [416] and summed up in Figure 5.7.

Figure 4.28 collects the cetane index of LCO fraction obtained with the parent catalyst (Cat-A) and with both modified catalysts (Cat-B and Cat-C). The proper analysis depicts a decreasing trend where the maximum cetane index is achieved by Cat-A and then drops stepwise for Cat-B and Cat-C, being 55.7, 43.1 and 37.9, respectively. The cetane index is inversely correlated with the aromatic compounds and branched hydrocarbons [186,417]. However, the values of CI obtained for all the catalysts are higher than those obtained by Gutierrez et al. [142] in the LCO hydrocracking with PtPd/HY in a fixed-bed reactor, who report values of cetane index lower than 30. Nevertheless, Escola et al. [417], obtained higher cetane index (above 70) in neat plastic hydrocracking since their LCO lump had a low aromatic concentration which enhance the cetane index.

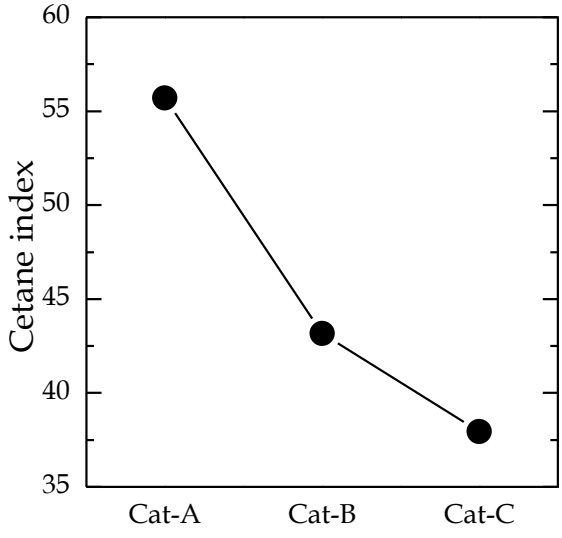

Figure 4.28 Effect of catalyst desilication on cetane index. Reaction conditions: 440 ºC; 80 bar of H2; C/F, 0.1; 120 min.

4.3.3.5 Coke deposition

The modification of the catalyst through basic desilication of the support has displayed to have an impact on the acidity of the catalyst (sections 4.3.2.3 and 4.3.2.4) and on the textural properties (section 4.3.2.1). These properties have shown to be highly relevant in the coke nature and location [387,418]. This effect has been studied in the literature by TPO analysis of the spent catalysts [418–422].

The TPO results for the spent parent and modified catalysts are plotted on Figure 4.29. Moreover, results from deconvolution (T_{Max} and percentage of each coke type) and coke content per 100 g of catalyst are shown on Table 4.7.

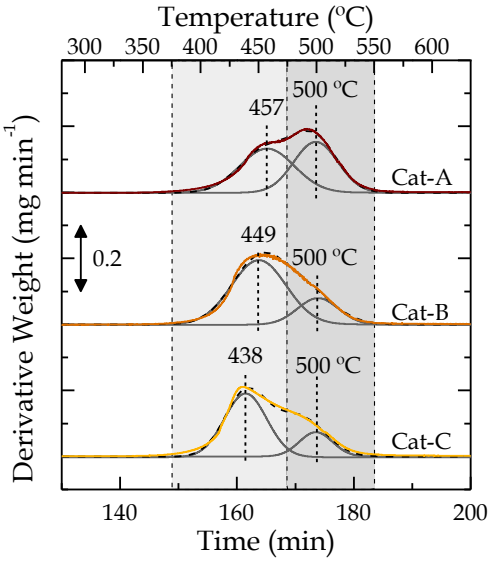

Figure 4.29 TPO profiles of parent catalyst (Cat-A) and modify by one (Cat-B) and two desilication treatments (Cat-C). Reaction conditions: 440 °C; 80 bar H_2; C/F, 0.1; 120 min.

Table 4.7 Deconvolution results of TPO profiles from parent and modify catalysts.

Catalyst	Cat-A	Cat-B	Cat-C
Coke content (wt%)	28.7	27.2	24.7
Peak 1			
Temperature (°C)	457	449	438
Fraction (wt%)	48.27	74.78	77.39
Peak 2			
Temperature (°C)	500	500	500
Fraction (wt%)	51.7	25.2	22.6

For the three catalysts, the signal from TPO can be deconvoluted into two peaks, peak 1, at lower temperatures and peak 2, at higher temperatures. For Cat-A, although both peaks have similar height, the peak 2 is slightly higher. Peak 1 appears at T_{Max} of 457 °C and it can be associated with medium developed coke, burned in the meso and macropores due to its facility to be burned without diffusional limitations. Furthermore, its proximity to metallic sites can catalyze its combustion. Nevertheless, its nature is non-filamentous or amorphous coke, presumably composed of macromolecular chains of HDPE located on the outside of the catalyst particles, which facilitates their combustion at low temperatures. For those reasons, peak 1 is classified as coke-type I [423]. On the other side, peak 2 has the T_{Max} at higher temperature, 500 °C. Its combustion temperature can be correlated with well-developed coke, with low H/C ratio and mainly made from the condensation of aromatic structures [421]. It is located in the micropores of the

zeolite, away from metallic sites, hence, it requires greater temperatures to be burned [108]. Consequently, this coke is correlated with coke-type II. In addition, the high amplitude of both peaks reveals the heterogeneity in the composition of both external and internal coke [108].

On the other hand, the deconvolution of derivative weight signal for Cat-B, that has only one desilication cycle, has a different peak distribution. The first peak (peak 1), which appears in the first range of temperature at 449 ^{o}C, is the most relevant one. Hence, the major coke produced during the reaction is less developed coke. This coke typically grows in the external surface of the zeolite. It can be encapsulated coke with amorphous structure (mainly macromolecular chains of HDPE) and close to metallic sites which promotes its combustion [418,424]. Therefore, according to its nature and location it can be associated with coke-type I. The peak 2 is placed at 500 ^{o}C located is in the inner of zeolite crystal (micropores), close to acidic sites which have hydrogen-transfer capacity and promoting its growth [108]. The nature of this coke is highly aromatic with low H/C ratio. This description of coke fits with coke-type II proposed by Bauer and Kargue [423].

Finally, Cat-C, which has two desilication cycles, displays a similar derivative weight signal than Cat-B. The first peak, which is the major one, has its T_{Max} at 438 ^{o}C. The nature of this coke is non-developed with amorphous structure, developed in the proximity of external active sites where metallic sites catalyze its combustion. The second peak appears at 500 ^{o}C (peak 2) and is even smaller than the analogous peak of Cat-B. Nonetheless, it has a complex polyaromatic nature, where the H/C ratio is low, forming filamentous/condensed coke. It is associated with part of the coke placed in the zeolite channels where there may be diffusional mass/heat limitations [418,425,426].

It is observed that as desilication degree increases, the first peak grows while the second decreases. Furthermore, the temperatures corresponding to the first peak decrease with desilication which reveals that desilication, and so, higher mesoporosity and lower acidity, favors the formation of less developed coke in macro and mesopores. These results are in line with the data obtained by Garcia et al. [211] in the catalytic cracking of bio-oil. They report that when mesoporosity is increased, lower condensation level is achieved by coke. The reduction of the second peak is linked with the micropores reduction in Cat-B and Cat-C (Table 4.6).

The coke content on the catalysts is shown in Table 4.7 and goes from 28.7 to 27.2 wt% for Cat-A and Cat-B, respectively, and continues diminishing to 24.7 wt% for Cat-C. The decrease in coke content when desilication is done (Cat-B and Cat-C) can be attributed to (i) the increase of mesoporosity that enhance the diffusional limitations of the zeolite and the accessibility of large molecules to active sites promoting its hydrocracking [388], which facilitates the access of polyaromatics

from VGO and other coke precursors to active sites, and (ii) the decrease in the acidity of the catalyst diminishing both Lewis and Brønsted sites, which the latter are the acidic sites responsible for the formation of coke [388,427–430].

On the other hand, Cat-A has the more developed coke compared with desilicated catalysts, as it can be deduced from the higher T_{Max} of peak 1. Furthermore, peak 2 (more developed coke) is the main type of coke, 51.7 wt%, compared with 48.3 wt% of peak 1. So, for this catalyst, the main type of coke is coke-type II which cause more severe deactivation and also requires higher temperatures to its combustion [108,421]. However, desilication treatment not only achieves a reduction in T_{Max} for peak 1 but also changes the coke distribution becoming peak 1 the main type of coke and coke-type I is the predominant coke nature in desilicated catalyst. Therefore, peak 1 is 74.8 and 77.4 wt% for Cat-B and Cat-C, respectively. Thus, the more developed and internal coke is reduced in comparison with parent catalyst (Cat-A).

CHAPTER 5

EFFECT OF OPERATING CONDITIONS ON HYDROCRACKING OF HDPE/VGO OVER PtPd/HY CATALYST

5 EFFECT OF OPERATING CONDITIONS ON HDPE/VGO HYDROCRACKING OVER PtPd/HY CATALYST

The HDPE/VGO hydrocracking has been chosen as model feed to study the effect of operating variables. This section collects the main results from an extensive parametric study (yields, conversion, naphtha and LCO composition, RON, cetane index, and coke analysis) with the PtPd/HY catalyst under the following operating conditions:

- Feedstock: HDPE/VGO (20 wt%)
- Temperature: 400 - 440 ^{o}C
- Pressure: 20 - 110 bar H_2
- Catalyst to Feed (C/F) ratio: 0.05 – 0.1 (in mass)
- Stirrer speed: 1300 rpm
- Reaction time: 15 - 120 min

5.1 EFFECT OF THE REACTION TIME

5.1.1 Hydrocracking yields and conversion

Figure 5.1 depicts the evolution of component distribution (yields) and both HCO and HDPE conversion (X_{HCO} and X_{HDPE}, respectively) with time.

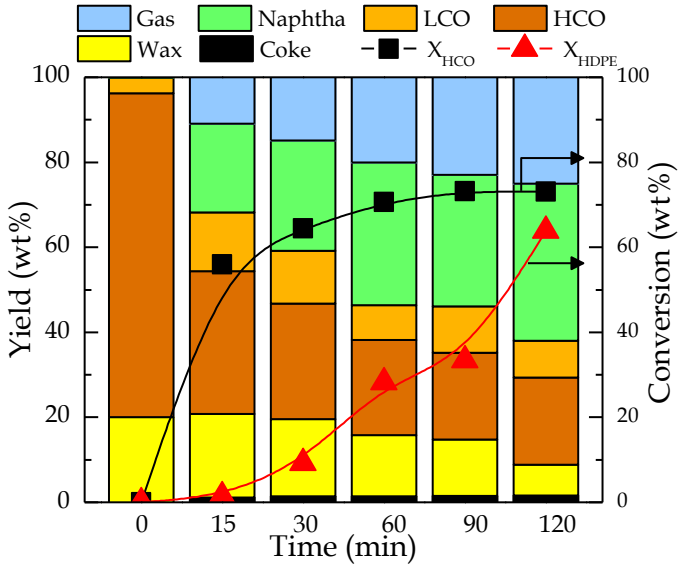

Figure 5.1 Effect of time on yields and conversions. Reaction conditions: 420 °C; 80 bar H_2; C/F, 0.075.

Attending to the results in Figure 5.1, VGO reacts very quickly. Within 15 min of reaction length the HCO yield decreases until 33.6 w%t (X_{HCO} of 55.9 wt%) and continues decreasing gradually up to 90 min (20.4 wt%) when it reaches a pseudo-steady value. So, at 90 min and 120 min the same X_{HCO} value of 73.2 wt% is obtained. Naphtha yield displays a continuous progress with reaction time, from 20.9 to 36.9 wt% at 15 and 120 min, respectively while LCO yield slightly decreases from 13.7 wt% at 15 min to 8.7 wt% at 120 min. In the case of gas, its yield increases continually as the reaction time growths, from 10.9 to 25 wt% at 15 min and 120 min, respectively. A similar behavior was reported by Pan et al. [431] for HDPE hydrocracking at 400 °C, 1 MPa H_2, and with a Ni/Al_2O_3 catalyst. Finally, coke yield increases with reaction time, from 1.1 to 1.6 wt% at 15 min and 120 min, respectively.

On the other side, the initial rate of HDPE hydrocracking is low. X_{HDPE} is almost negligible at 15 min but slightly raises at 30 min (X_{HDPE} 9.2 wt%). After that, the X_{HDPE} increases drastically to 28.2 wt% at 60 min and it continues rising up to 120 min (63.9 wt%). These results agree with those obtained by Ali et al. [312] who reported an increase in the conversion from 30.9 to 86.9 wt%, in the 30-60 min range for the hydrocracking of LDPE/petroleum resid at 430 °C and 1200 psi H_2 using

NiMo/γ-Al as catalyst. Joo and Curtis [432] also obtained a qualitatively similar evolution of the conversion of plastic when hydrocracking a ternary blend of LDPE/coal/petroleum resid at 430 ºC, 8.3 MPa of H_2 and a NiMo/Al_2O_3 catalyst, for 360 min.

It has to be mentioned that the reason why the HCO conversion is settled at 120 min is a result of abrupt increase in HDPE conversion. This is because, as reported by Pan et al. [431] and Artetxe et al. [433], the decomposition of HDPE takes place in compounds C_{13+}, so it would increase the concentration of LCO and HCO. Therefore, this increase in HCO lump leads to a decrease in its apparent conversion.

The different hydrocracking rates of HDPE and VGO can be due to a combination of two events: (i) there is preferential adsorption of the VGO compounds in the active sites and (ii) the limitations to the catalytic cracking of HDPE by the previous stage of thermal cracking of the HDPE macromolecules to others with suitable size for their diffusion in the porous structure of the catalyst.

Figure 5.2 displays the evolution with time of the selectivity to fuel (S_F) for different C/F ratios. The results show that S_F grows stepwise for 0.05 and 0.075 C/F ratios with reaction time. In the first case, S_F grows from 0.46 at 15 min until 0.67 at 120 min, and in the second case from 0.53 until 0.84 in this time range. However, for 0.1 C/F ratio the S_F goes through a maximum at 30 min (S_F = 1), decreasing up until 0.5 at 120 min. Considering these results, for the range of studied operating conditions, with the perspective of maximizing this index, working with a reaction time of less than 90 min, a C/F ratio of 0.1 is adequate, while with a reaction time of 120 min, the highest fuel selectivity corresponds to an intermediate ratio (C/F = 0.075).

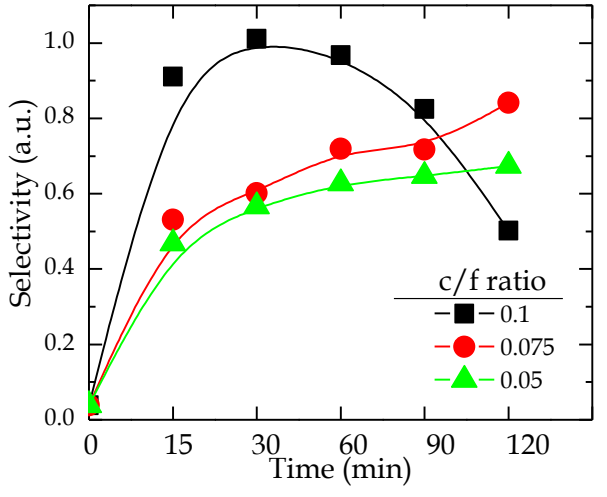

Figure 5.2 Effect of time on selectivity to fuel index (S_F) for different C/F ratios. Reaction conditions: 420 ºC; 80 bar H_2.

5.1.2 Gas composition

The evolution with time of gas composition is collected in Figure 5.3. The results depict a clear predominance of C_3 and C_4 compounds for all reaction times. Hence, the mechanism with carbenium ion as intermediate is the predominant [114].

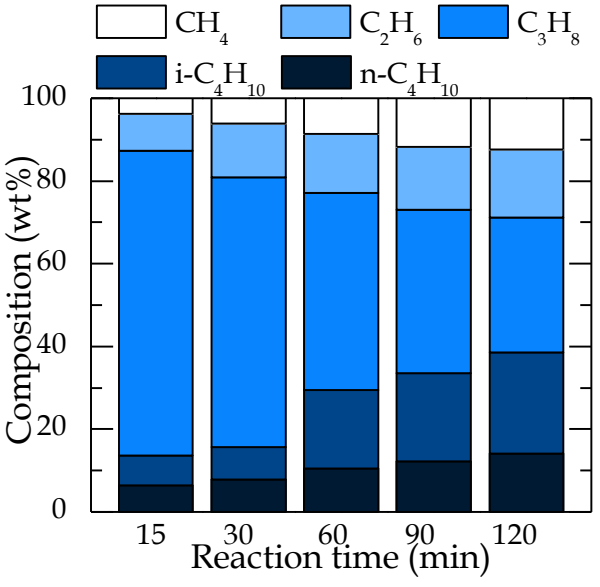

Figure 5.3 Effect of time on gas composition. Reaction conditions: 420 ^{o}C; 80 bar H_2; C/F, 0.075.

At 15 min, gases are mainly formed by C_3H_8 (73.6 wt%), dry gas (CH_4, 3.7 wt% and C_2H_6, 9 wt%) and small amounts of C_4 paraffins (13.7 wt%). Both dry gas and C_4 compounds show an increasing trend but C_3H_8 decreases when time rises. So, at 120 min, dry gas increases but is the minor fraction (28.7 wt%) and i-C_4H_{10} concentration is higher than that of n-C_4H_{10} (24.4 and 14.2 wt%, respectively). The C_3H_8 concentration (32.6 wt%) is still the highest one.

It is noticeable that at 60 min and henceforth the i-C_4H_{10} concentration increases noticeable, as a consequence of the remarkable HDPE conversion (see Figure 5.1). So, the free radicals formed by thermal cracking of dissolved HDPE macromolecules suffer not only β-scission but also isomerization in the acidic sites of the catalyst.

5.1.3 Naphtha composition and RON

Figure 5.4 shows the effect of reaction time on the composition of naphtha fraction (according to its PIONA nature).

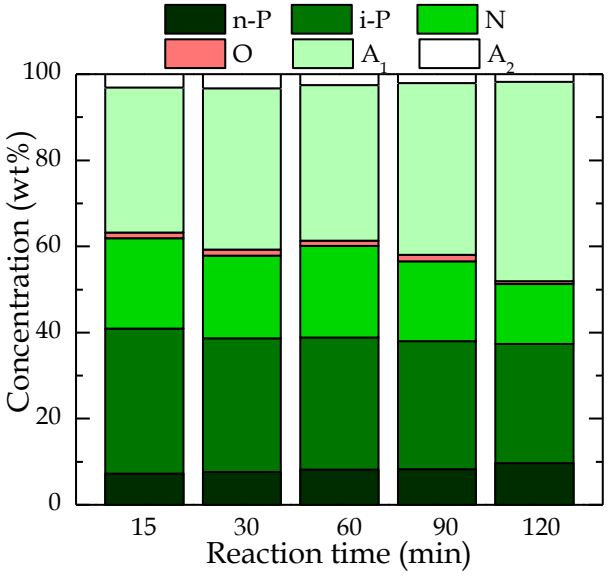

Figure 5.4 Effect of time on naphtha composition. Reaction conditions: 420 ºC; 80 bar H_2; C/F, 0.075.

At 15 min, the paraffin concentration is slightly higher than the other components (with a i-P concentration of 33.7 wt% and n-P of 7.2 wt%), followed by aromatics (concentrations of A_1 and A_2 are 33.7 and 3.1 wt%, respectively) and with a remarkable naphthenic concentration (20.9 wt%) and a negligible olefin concentration (1.3 wt%), due to the high hydrogenation performance of the catalyst.

As reaction extent increases, the changes in composition follow a shallow decreasing trend in paraffin, naphthenics and olefins concentration meanwhile aromatic fraction rises (A_2 is reduced meanwhile A_1 is increased), with a concentration of paraffins, naphthenic and olefin compounds of 37.3, 13.9 and 0.6 wt%, respectively at 120 min. At this reaction time, aromatics are the major lump with a corresponding 48.1 wt% of the naphtha (1.8 wt% of A_2 and 46.3 wt% of A_1). Nonetheless, although the paraffins concentration diminish, n-P concentration increases slightly (from 7.2 wt% at 15 min to 9.7 wt% at 120 min) whereas i-P concentration decreases (from 33.7 wt% to 27.6 wt%). The same tendencies were observed by Pan et al. [431] in liquid-product composition in neat HDPE hydrocracking at 400 ºC, 1 MPa using Ni/Al_2O_3 catalyst.

The increase with time in A_1 fraction concentration and the reduction of A_2 in naphtha can be attributed to the hydrodearomatization (HDA) of A_2 compounds of naphtha and, specially, polyaromatic compounds of LCO, since the main products

from HDA reactions are A_1 compounds (Benzene, Toluene and Xylenes) [416]. In the mechanism of these HDA reactions, the Brønsted acid sites of the catalyst play an important role, whose polarity favors the strong adsorption of the highly polar A_2 and A_{3+} compounds [171]. Another possibility is that these aromatics are formed by cyclization of olefins from the degradation of HDPE. These reactions are favored by temperature and time [417].

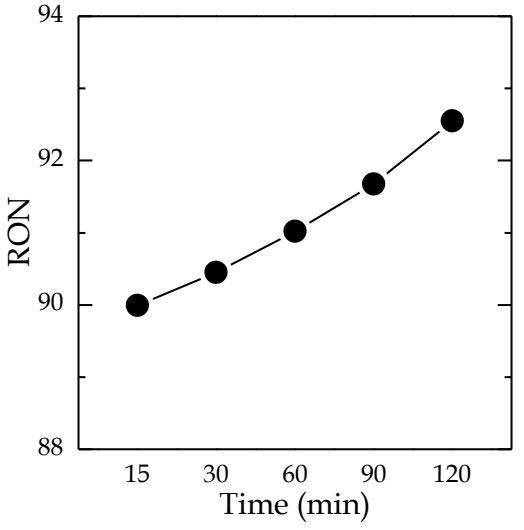

Figure 5.5 Effect of time on RON of naphtha fraction. Reaction conditions: 420 °C; 80 bar H_2; C/F, 0.075.

The evolution of RON of naphtha fraction with time is collected in Figure 5.5. The results show a good value of RON even at lower hydroprocessing time, 89.9 at 15 min, which increases until 92.5 at 120 min. This tendency is mainly due to the increase of aromatics in the naphtha fraction (Figure 5.4), which has a positive impact over RON. Besides, as reaction time goes by, the chain length diminishes and branching number increases, encouraging both the RON number [434]. Vasile et al. [367] obtained 90.9 as his greatest value of RON in the hydrocracking of oil from pyrolysis of plastic electronic devices, at 350 °C, 6.5 MPa and 120 min reaction length with a DHC-8 commercial catalyst. Their lower values maybe are due to a significant difference in feed composition. In their case, the i-P concentration in naphtha is almost negligible in comparison with n-P, which plays in detriment of the RON.

According to the RON and composition, the naphtha obtained has quality enough to be added to gasoline pool in refineries. This naphtha, blended with other naphthas from different refinery units can be treated and adequate to fulfill the European policies before its commercialization as gasoline.

5.1.4 LCO composition and cetane index

The evolution of LCO composition with reaction time is collected in Figure 5.6. It is noticeable that inverse tendency is observed between naphtha (Figure 5.4) and LCO (Figure 5.6) composition when time rises. Similar composition of LCO at 15 and 30 min is obtained. This LCO is mainly aromatic, where A_2 is the main fraction (43.4 wt%) followed by A_1 and A_3 (8 and 6.9 wt%, respectively). Paraffins account around 40 wt% of the LCO. In this case, i-P are predominant versus n-P (33.8 and 7.9 wt%). Naphthenic compounds were not detected.

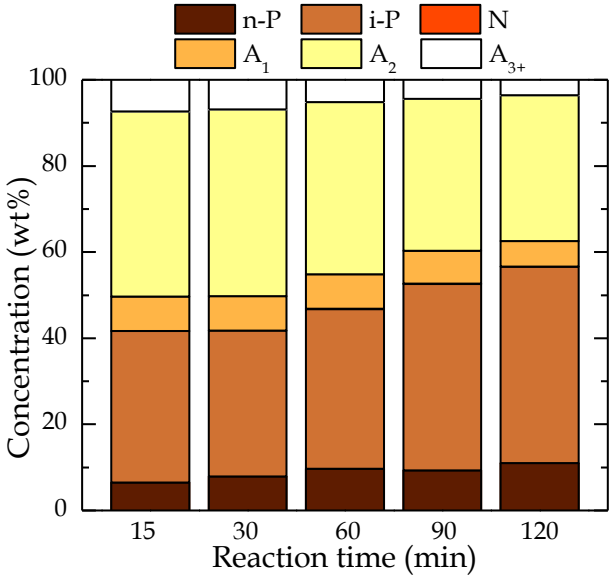

Figure 5.6 Effect of time on LCO composition. Reaction conditions: 420 ºC; 80 bar H_2; C/F, 0.075.

According to the effect of reaction time on yields (Figure 5.1), the X_{HDPE} undergoes a drastic change at 60 min. In Figure 5.6 is observed that for this time LCO composition (with a paraffin concentration of 46.74 wt% and aromatic concentration of 53.18 wt%) begins to change, becoming more paraffinic and less aromatic (although aromatics continue being the main products). At 120 min, the LCO is mainly paraffinic (paraffin concentration is 56.6 wt% while aromatic concentration is 43.1 wt%). Contribute to these results: (i) the activity of the catalyst by the LCO hydrodearomatization [106,145,186,416], and (ii) the conversion of HDPE chains to lighter compounds which are long lineal paraffins that are in LCO boiling point range [21,435,436]. In addition, under the same operating conditions, when the extent of hydrocracking pathway is higher, the long n-P formed from depolymerization are isomerized through skeletal rearrangement and then hydrocracked in Brønsted acid sites [114] following the steps mentioned in Figure 4.2 and described in section 4.1.1.

The HDA pathway is shown in Figure 5.7, taking methylnaphthalene as a model compound representing A_2 aromatics (the main aromatic fraction in LCO) [416]. HDA mechanism implies a complex reaction system that can be simplified in: (i) hydrogenation reactions (reversible), also called saturation reactions; (ii) isomerization reactions (reversible), also called skeletal rearrangement; (iii) hydrocracking reactions, which are the C-C bond break reactions for the formation of new C-H bonds (opening of naphthenic rings reactions are also considered); and (iv) dealkylation reactions, which are the C-C bond break reactions between benzene ring and alkyl chain result in removal of the alkyl substituent.

Thus, the aromatics from the LCO fraction of the feed (like methylnaphthalene, benzodicycloparaffin, acenaphthylene and pyrenes, among others) are degraded to simpler aromatics (like alkylbenzene and benzocycloparaffin, among others) which some of them are in the naphtha boiling point range. Then, these aromatics can undergo deeper conversion through the previously mentioned reactions to simple non-aromatic compounds (naphthenic, olefins, paraffins and gas) [106,145,186]. Besides, the monoaromatics and non-aromatic compounds also can interact with polyaromatics to produce well-structured coke [437].

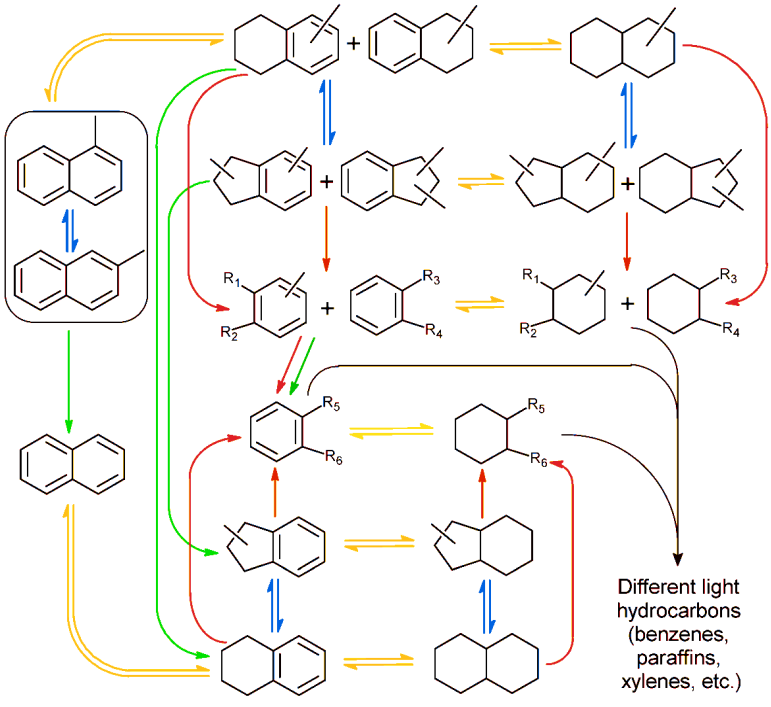

Figure 5.7 Hydrodearomatization (HDA) pathway of methylnaphthalene (complex aromatic). Yellow arrows, hydrogenation reactions; red arrows, hydrocracking reactions; blue arrows, isomerization reactions; green arrows, dealkylation reactions. Adapted from Karakhanov et al. [416].

On the other hand, to explain the conversion of HDPE, melted plastic undergoes depolymerization reactions towards long chain hydrocarbons. Some authors [435,436] who studied the polyethylene (HDPE and LDPE) degradation, reported that depolymerization of polyethylene chains by random scissions produces long alkenes (olefins) in LCO range. In the presence of high H_2 pressure the olefins are converted to paraffins through the carbocationic mechanism [114]. So, attending to the mechanisms of the HDA of the VGO and wax depolymerization and subsequent hydrogenation reaction, the longer reaction time has as a consequence on LCO fraction being more paraffinic and less aromatic.

The results of the cetane index of the LCO fraction versus reaction time are collected in Figure 5.8. In a way, results are related to LCO composition, since cetane index is inversely proportional to aromatics concentration [139]. Hence, the cetane index shows a clear trend to increase from 33.3 at 15 min to 43.7 at 120 min, exhibiting an abrupt change at 60 min reaction length as a result of remarkable increase in X_{HDPE} (Figure 5.1). Nevertheless, the cetane index growing trend is smoothed between 90 and 120 min (43 and 43.7, respectively) as a result of aromatic decrease in that time range. Therefore, after 90 min reaction, the LCO composition and quality is appropriated to be added to the diesel pool in refineries.

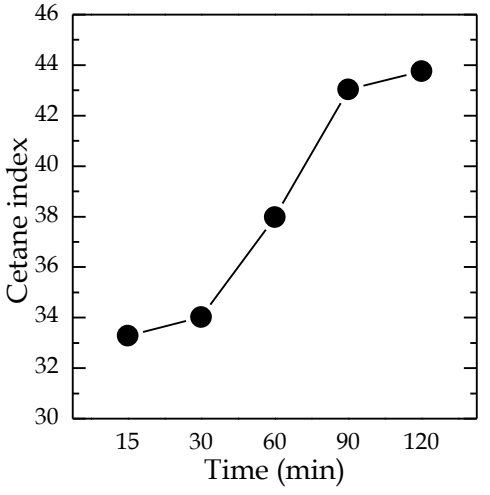

Figure 5.8 Effect of time on cetane index of LCO fraction. Reaction conditions: 420 ^{o}C; 80 bar H_2; C/F, 0.075.

5.1.5 Coke deposition

The study of the coke deposited on the catalyst has been carried out by means of temperature programmed oxidation (TPO) analysis, whose methodology has been explained in detail in section 2.5.4. The relation of combustion temperature with coke nature and its location is based on the literature about hydrocracking of LCO with HY zeolite catalysts [108], polyolefins cracking using HZSM-5 catalysts

[418,433], conversion of crude bio-oil to hydrocarbons on HZSM-5 catalyst [422], pyrenes hydrocracking on NiW/Al catalyst [437] and steam reforming of bio-oil on Ni/La2O3-αAl$_2$O$_3$, [421,424]. Those authors complement TPO analysis with other techniques such as FTIR-TPO, TPO-MS and Raman spectroscopy to a more accurate identification of coke compounds.

Figure 5.9 shows TPO profiles of the catalysts used in the HDPE/VGO hydrocracking at 420 ºC for reaction times of 15, 60 and 120 min. The profiles has been deconvoluted (total deconvolution, black dot line) in two Gaussian peaks (gray line) corresponding to coke burning at low temperature range (375-440 ºC) and coke burning at higher temperatures (440-475 ºC). The results are summarized in Table 5.1: (i) total coke content per 100 g of catalyst, (ii) the burning maximum temperature (T_{Max}) for deconvoluted peaks and (iii) percentage of each coke type.

The evolution of total coke content with reaction time (Table 5.1) depicts that almost all of the coke is formed in the first 30 min of the reaction, increasing notably from 15.9 wt% at 15 min to 19.3 wt% at 30 min. Then, it continues growing at a slower pace from 30 to 120 min.

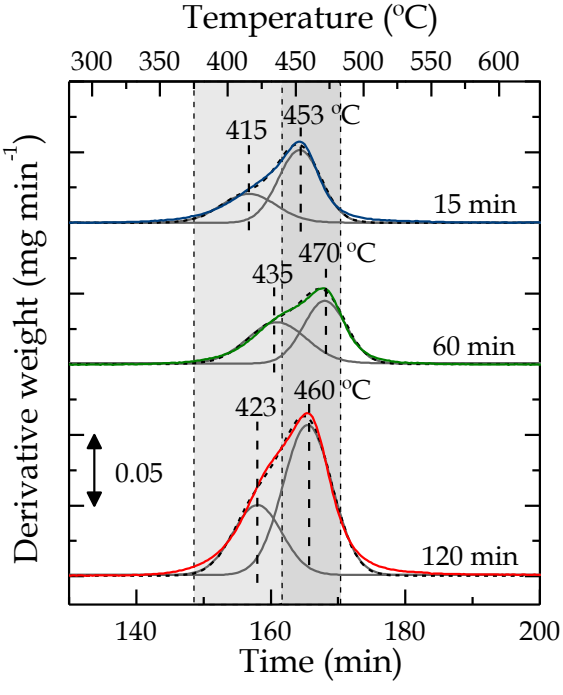

Figure 5.9 TPO profiles of coke for different reaction times. Reaction conditions: 420 ºC; 80 bar H_2; C/F, 0.075.

Table 5.1 Deconvolution results of Gaussian peaks from TPO profiles of spent catalysts for different reaction times.

Reaction time (min)	15	30	60	90	120
Coke content (wt%)	14.86	19.30	18.83	19.43	21.20
Peak 1					
T_{Max} (°C)	415	407	435	430	423
Fraction (wt%)	33.90	26.53	47.32	40.30	31.79
Peak 2					
T_{Max} (°C)	453	446	470	464	460
Fraction (wt%)	66.10	73.47	52.68	59.70	68.21

The results on Figure 5.9 depict that coke deposited at 15 min have the first peak of combustion at 415 °C (peak 1) and the second one at 453 °C (peak 2). The peak 1 can be attributed to the combustion of bulky molecules with higher H/C ratio and low aromaticity nature retained on the surface of the catalyst particles [421]. This coke is made up presumably by the depolymerization of HDPE chains and with the possible contribution of very heavy components in the VGO adsorbed on the catalyst surface. In addition, peak 1 is lower than peak 2, so the amount of this type of coke is lower. The higher temperatures of peak 2 are associated with the combustion of coke with lower H/C ratio and is highly probable to be placed inside of the porous structure of the catalyst [108]. Moreover, its T_{Max} (< 480 °C) is also moderate, which indicates that also is amorphous coke [438]. Also noteworthy is the amplitude of the two peaks, which is associated with the heterogeneity of its composition and its location regarding to the metallic sites [108].

On the other side, Bauer and Karge [423] grouped the coke in two types: (i) the hydrogen-rich species with amorphous structure (called in advance coke-type I) and (ii) the highly condensed coke formed by polyaromatic and therefore lower H/C ratio (called in advance coke-type II). Hence, according to the properties above mentioned of both peaks, they can be correlated with coke-type I according to that classification. The absence of coke-type II can be attributed to the hydrogenation of the intermediates coke precursors, which will limit their condensation towards polyaromatic structures [387].

In the TPO profile for the spent catalyst at 60 min, peak 1 is higher than that obtained for 15 min and both peaks are shifted towards higher temperatures; peak 1 burns at 435 °C and peak 2 at 470 °C, which can be related with the more condensed coke and with its greater presence in the catalyst micropores [418–422,437]. For this reaction time, coke under peak 2 continues being the main one. Equally to coke deposited at 15 min, both peaks of coke denote coke-type I behavior [423].

At 120 min, the total content of coke is higher than for the shorter reaction times. However, comparing its TPO profile with the corresponding to 60 min, the increasing reaction time reduces the T_{Max} for both peaks: peak 1 has its T_{Max} at 423 ºC and peak 2 at 460 ºC. Therefore, from 60 min on coke is not more and more condensed and instead of that, coke precursors are hydrogenated. This fact can be due to HDPE hydrogen donor character [155] that can reduce the aromaticity of coke and increase its H/C ratio. Although these peaks are sharper which indicate that the coke is more homogeneous. Peak 2 is probably located partially in the micropores of the zeolite where there are some diffusional mass and/or heat limitations [421,439]. The reduction of T_{Max} and the properties that entail make that coke-type of both peaks still being correlated with coke-type I [423].

To explain the commented effect of the reaction time on the content and characteristics of the coke, the change in the composition of the reaction medium must be taken into account. According to yields and conversion evolution with time (Figure 5.1), the coke formed until 30 min comes from VGO hydrocracking since the X_{HDPE} is very low. Due to the aromatic nature of the VGO (Table 2.1) its hydrocracking produces more developed coke [437] reported as the shifting of the peaks to greater temperatures at 60 min. For higher reaction times, when HDPE conversion is significant, the composition of coke starts to change reducing its combustion temperature (Table 5.1). This behavior also was reported by Guisnet and Magnoux [387], increasing the H/C ratio in the coke. Moreover, according to the results of Table 5.1 when X_{HDPE} is low (up to 60 min) the fraction of coke corresponding to peak 1 increases with higher time meanwhile the fraction of peak 2 decreases, being almost equal both fractions at 60 min (47.3 and 52.7 wt%, respectively). However, from 60 to 120 min, the trend is reverse and the percentage of peak 2 increases. Nevertheless, their aromaticity is reduced since lower T_{Max}.

5.2 EFFECT OF THE TEMPERATURE

The effect of temperature, which is one of the most influential operating variable in hydrocracking reactions, has been already studied along the present work in sections 3.3, 4.1 and 4.2 for different feeds and catalysts. Thus, in this section the effect of temperature will be studied under the standard conditions in which the parametric study is being carried out.

5.2.1 Hydrocracking yields and conversion

The product yields and conversions (X_{HCO} and X_{HDPE}) at 120 min are collected and shown in Figure 5.10.

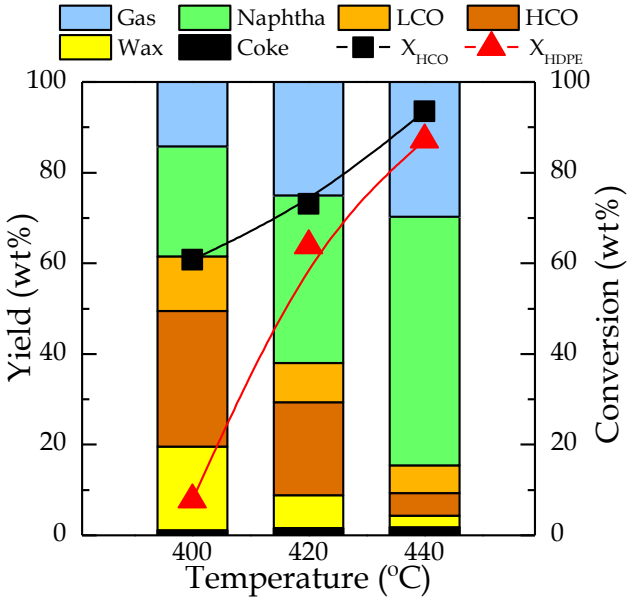

Figure 5.10 Effect of temperature on product yields and conversions. Reaction conditions: 80 bar H_2; C/F, 0.075; 120 min.

The temperature greatly affects the yields and conversions, so, with an increment of 20 ºC, both parameters suffer from a remarkable increase. At the lowest temperature (400 ºC) the conversion of HCO is noticeable (X_{HCO} of 60.7 wt%). Naphtha is the main product (yield of 24.3 wt%) followed by gas and LCO (14.1 and 11.9 wt%, respectively). At this temperature the X_{HDPE} is very low (7.8 wt%), as indicates the high wax yield. This HDPE conversion is lower than that obtained by Palos et al. [156] who obtained a X_{HDPE} of 30 wt% in a HDPE/LCO hydrocracking in a batch autoclave reactor at 400 ºC and using even lower C/F ratio (0.05). They achieved greater results due to: (i) their reaction time was longer (180 min) and (ii) they conducted the experiment with lower HDPE/LCO ratio (0.1). The differences on HDPE/Oil ratio are crucial as Siddiqui and Redhwi [154]

reported that the lower plastic content the higher X_{HDPE} achieves in LDPE/Petroleum Resid hydrocracking.

When temperature rises to 420 ºC, the HCO apparent yield is reduced to 20.5 wt% increasing the X_{HCO} up to 73.1 wt%. Naphtha yield increases up to 36.9 wt%, being the main product followed by gas (yield of 25 wt%). However, LCO yield decreases to 8.7 wt%. X_{HDPE} increases significantly from 400 to 420 ºC (until 63.9 wt%) with its corresponding wax yield decrease. Likewise, Ali et al. [312] obtained similar behavior for LDPE/petroleum resid hydrocracking at 8.3 MPa of hydrogen. They had an improvement in the conversion from 17.6 to 86.9 wt% at 400 and 430 ºC, respectively, and gas yield increased as well as liquid products yields.

At the highest temperature studied (440 ºC), the HCO apparent yield is the lowest one and hence, the highest X_{HCO} (93.5 wt%) is achieved. Naphtha yield increases drastically up to 54.8 wt%, while gas yield increases up to 29.7 wt% and LCO diminishes up to 6.2 wt%. At this temperature, however, a small amount of unconverted HDPE (wax yield) is obtained, with a corresponding X_{HDPE} of 87.2 wt%. As it has been observed by other authors [153,440] when hydrocracking PE/VGO, coke yield increases with temperature from 1.1 to 1.8 wt% at 400 and 440 ºC, respectively, but the catalyst has not shown signs of deactivation.

Figure 5.11 displays the effect of temperature on the values of selectivity to fuel for 120 min of reaction time with different C/F ratios.

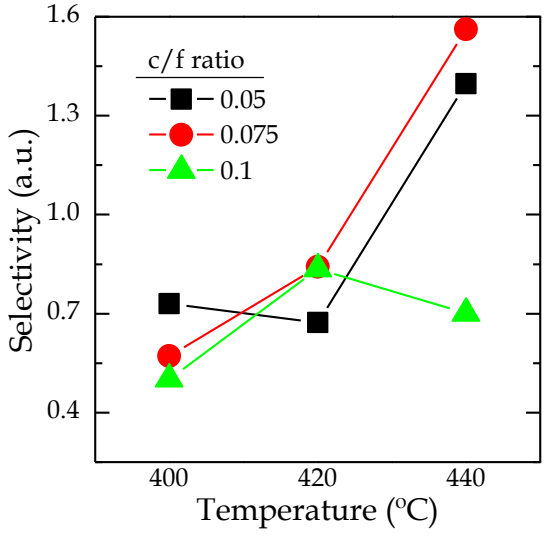

Figure 5.11 Effect of temperature on selectivity to fuel (S_F) for different C/F ratios. Reaction conditions: 80 bar H_2; C/F, 0.05, 0.075 and 0.1; 120 min.

The effect of temperature on S_F is not the same for all the C/F ratios. For 0.05 C/F ratio, increasing the temperature from 400 to 420 ºC reduces the S_F from 0.72 to 0.67 due to the high gas yield obtained at 420 ºC. However, when increasing the

temperature to 440 ºC the S_F improves vastly (until 1.39) due to the high X_{HCO} and X_{HDPE} conversions and low gas yield. When increasing the C/F ratio to 0.075, a better performance on S_F is achieved when temperature rises and the highest value of S_F, 1.56, is obtained at 440 ºC. For even higher C/F ratio, 0.1, the lowest values of S_F are obtained at 400 ºC. Nevertheless, arousing the temperature from 400 to 420 ºC, S_F increases from 0.5 to 0.83, but the increase in temperature up to 440 ºC reduces the S_F to 0.7, obtaining the lowest value at this temperature. So, 0.075 C/F ratio seems to be the optimal due to greater S_F values are obtained, achieving the biggest value (1.56) at 440ºC under the experimental conditions used.

In conclusion, the low X_{HDPE} at 400 ºC denote that it is not an appropriate temperature to conduct the HDPE/VGO hydrocracking, with also poor S_F. Working at higher temperature is a key factor to achieve interesting HCO and HDPE conversion. However, although desired products increase at 420 ºC, this temperature is not good enough to overcome the S_F = 1. At the end, 440 ºC has become the more interesting temperature using 0.075 in mass C/F ratio to maximize the desired products yield.

5.2.2 Gas composition

The effect of temperature on the composition of gas fraction is shown in Figure 5.12.

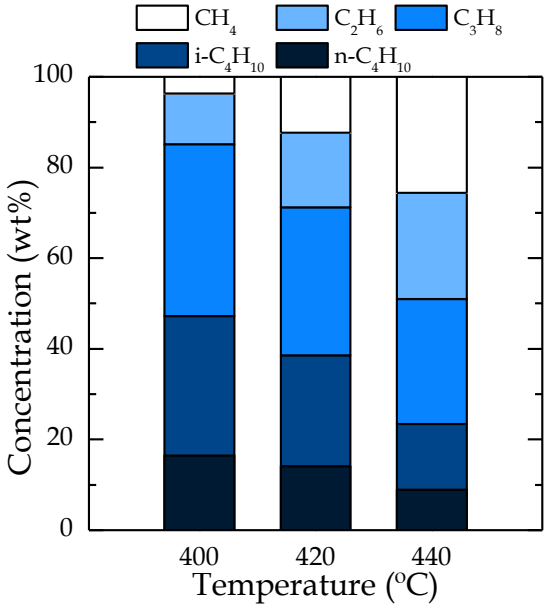

Figure 5.12 Effect of temperature on gas composition. Reaction conditions: 80 bar H_2; C/F, 0.075; 120 min.

At 400 ºC, dry gas (CH_4 and C_2H_6) is the minor lump (14.9 wt%) indicating a minimal activity of the radical mechanism at this temperature [140]. On the other side, C_3H_8 is the main compound followed by i-C_4H_{10} and n-C_4H_{10} (37.8, 30.8 and 16.4 wt%, respectively). This results are in agreement with the results from Metecan et al. [375], who reported that the main compound in the gas stream was C_3H_8 hydrocracking HDPE in a shaking type batch reactor at 400 ºC, 5.0 MPa of H_2 and 60 min reaction time.

Temperature favors the radical mechanism and also cracking reactions, increasing the yield of light gas products (dry gas fraction) in detriment of propane and C_4 compounds [375]. So, when temperature rises to 420 ºC, the dry gas fraction (CH_4 and C_2H_6) increases up to 28.9 wt% while the yield of C_3H_8, i-C_4H_{10} and n-C_4H_{10} are reduced to 32.6, 24.4 wt% and 14.1 wt%, respectively. At even higher temperature (440 ºC), the dry gas fraction accounts for almost the half of gas lump (49 wt%), as a result of naphtha overcracking by means of cracking with a radical mechanism. C_3H_8 continues being the main compound (27.6 wt%) while the concentration of C_4 compounds, i-C_4H_{10} and n-C_4H_{10}, diminish (to 14.6 wt% and 8.9 wt%, respectively).

5.2.3 Naphtha composition and RON

The temperature has a clear effect on the composition of naphtha fraction as it is shown in Figure 5.13.

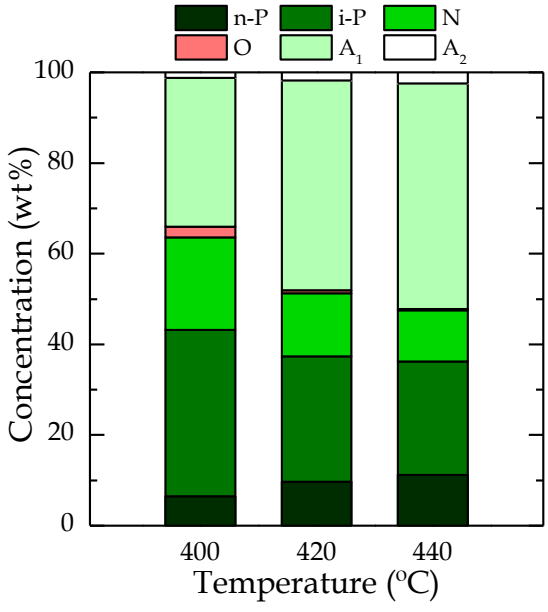

Figure 5.13 Effect of temperature on the composition of naphtha fraction. Reaction conditions: 80 bar H_2; C/F, 0.075; 120 min.

At 400 ºC, the main compounds are paraffins (6.5 wt% n-P and 36.7 wt% i-P) and aromatic concentration are slightly lower (32.8 and 1.2 wt% for A_1 and A_2, respectively). The naphthenic compounds account for the concentration of 20.5 wt% and small olefin concentration is detected, being only the 2.4 wt%.

Raising the temperature, paraffins, naphthenics and olefins decrease meanwhile aromatics became the most abundant fraction. Nonetheless, n-P fraction increases with temperature, not following the trend shown by i-P due to the inhibition of hydrogen transfer reactions. As a result, at 440 ºC, n-P concentration increases up to 11.2 wt% and i-P fraction diminishes until 25 wt%. In the same way, naphthenic compounds decrease until 11.3 wt% and olefinic compounds are almost negligible (0.3 wt%). On the other hand, arousing the temperature promotes condensation reactions, due to thermodynamic limitations of the hydrocracking [109], favoring the formation of aromatics and especially A_1 aromatics [368]. The aromatics concentration of the naphtha fraction at 440 ºC accounts for more than 50 wt%, being 49.8 wt% A_1 fraction and 2.4 wt% A_2 fraction.

These changes in the composition affect the RON as it is shown in Figure 5.14. RON at 400 ºC has a value of 93 and it diminishes up to 90 at 440 ºC, due to the reduction of i–P and the increase of n-P. The RON values obtained for all temperature range are, however, high enough to add the naphtha obtained to the gasoline pool in refinery.

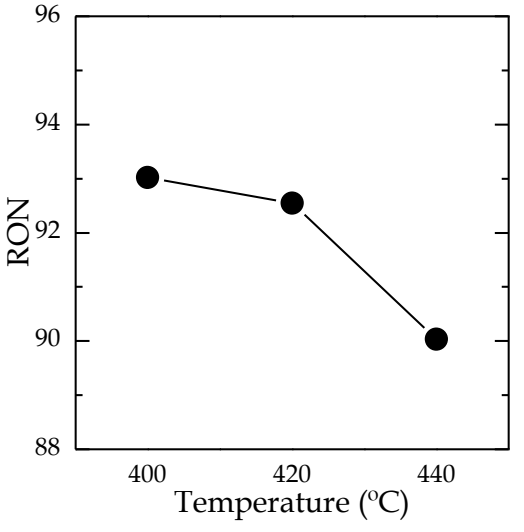

Figure 5.14 Effect of temperature on RON values of naphtha fraction. Reaction conditions: 80 bar H_2; C/F, 0.075; 120 min.

5.2.4 LCO composition and cetane index

Figure 5.15 displays the changes on the composition of LCO fraction when temperature rises.

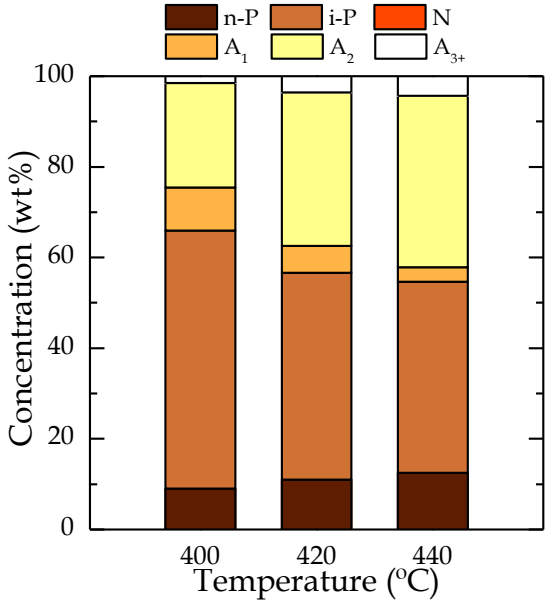

Figure 5.15 Effect of temperature on the composition of LCO fraction. Reaction conditions: 80 bar H_2; C/F, 0.075; 120 min.

At 400 °C, the LCO is mainly paraffinic and the less aromatic one, being i-P the main compounds with the lowest content of n-P (56.9 and 9 wt%, respectively). Regarding the aromatics, A_2 are the most abundant ones followed by A_1 and A_3 (23, 9.6 and 1.5 wt%, respectively). The increase of temperature favors the aromatic formation in detriment of alkanes [431]. Specifically from 400 to 440 °C, i-P concentration is reduced to 42.2 wt% and conversely n-P fraction slightly increases up to 12.5 wt%. On the other hand, A_2 and A_{3+} compounds increase (37.8 and 4.4 wt%, respectively) while A_1 fraction is reduced (3.2 wt%).

Furthermore, temperature has a positive effect on LCO cetane index, as it can be seen in Figure 5.16. Increasing the temperature from 400 to 440 °C, the cetane index goes from 38.4 to 61.4, overcoming the minimum value required for diesel to be commercialized in Europe (46). Commercial diesel has a minimum cetane index of 52 and contains aromatics in more than 50 wt% [378], so the LCO obtained at 440 °C is suitable to be added to the diesel pool in refineries.

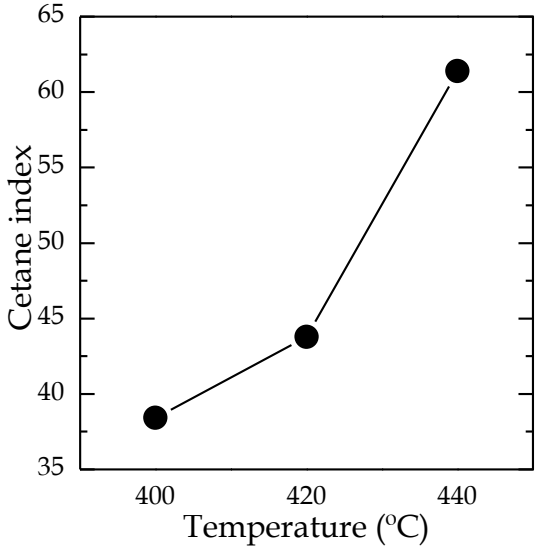

Figure 5.16 Effect of temperature on cetane index of LCO fraction. Reaction conditions: 80 bar H_2; C/F, 0.075; 120 min.

5.2.5 Coke deposition

The results of the TPO analysis are depicted in Figure 5.17. The T_{max} (maximum combustion temperature of different peaks), the total coke content and the percentage of each coke type are collected in Table 5.2, for three hydrocracking temperatures (400, 420 and 440 °C).

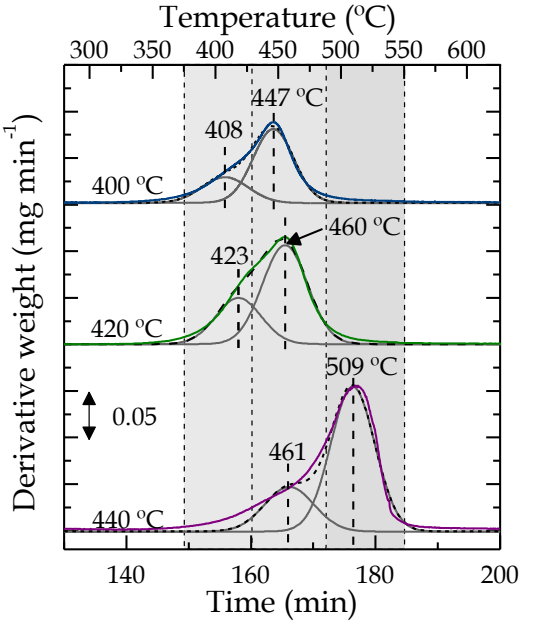

Figure 5.17 Effect of temperature on TPO profiles of coke. Reaction conditions: 80 bar H_2; C/F, 0.075; 120 min.

Table 5.2 Deconvolution results of Gaussian peaks from TPO profiles of spent catalyst for different reaction temperatures.

Reaction Temperature (ºC)	400	420	440
Coke content (wt%)	15.34	21.20	23.97
Peak 1			
Temperature (ºC)	408	423	-
Fraction (wt%)	28.81	31.79	-
Peak 2			
Temperature (ºC)	447	460	461
Fraction (wt%)	71.19	68.21	25.67
Peak 3			
Temperature (ºC)	-	-	509
Fraction (wt%)	-	-	74.33

At 400 ºC the coke combustion describes two peaks. The first peak, peak 1, has the T_{Max} at 408 ºC. The coke associated to peak 1 is less developed coke (with high H/C ratio), probably placed on external sites of zeolite and constituted by macromolecular chains of HDPE located on the outside of the catalyst particles, which ease their combustion at low temperatures. The second peak, peak 2, corresponds to another fraction of the coke that burns with a maximum velocity at 447 ºC. This coke is probably placed in the inner of catalyst particle. The high amplitude of both peaks reveals the heterogeneity in the composition of both the external and internal coke. The external one suffer a faster combustion and at a lower temperature since presumably this coke is deposited close to metallic sites, which catalyze the combustion. The slower and prolonged combustion at higher temperatures in the TPO analysis will correspond to the coke inside the crystalline channels of the HY zeolite, which is a condensed coke (with a reduced H/C ratio) and whose formation (by condensation of aromatic structure) is catalyzed by the strong acid sites in the zeolite [108,438]. As a result of their low combustion temperatures, peak 1 and 2 are related with coke-type I or unstructured coke [423].

Reaction temperature highly affects to coke nature and sometimes to its location [387,441] since the increasing the hydrocracking temperature, reduces the hydrogenation reactions and the cracking and condensation reactions are more favored. When the hydrocracking temperature is raised to 420 ºC, TPO profile can be also deconvoluted into two peaks (peak 2 is bigger than peak 1) which are in the same range of temperatures than before but with the maximum shifted towards higher temperatures: 423 and 460 ºC for peaks 1 and 2, respectively, which must be attributed to a higher condensation degree of carbonaceous structures. Therefore,

according to their T_{Max}, both peaks (peak 1 and 2) also are categorized as coke-type I.

At the highest hydrocracking temperature, 440 ºC, the TPO profile also has two peaks, but increasing to higher range of temperature: T_{Max} 461 ºC for peak 2 and 509 ºC for peak 3. Thus, the complexity of the coke has increased. As has been mentioned, the peak 2 is associated with external coke derived from HDPE, with low H/C ratio attending to the speed of maximum combustion temperature. The peak 3 (the greatest peak) can be related with condensed and well-structured coke, with the lowest H/C ratio, and placed in the micropores and inside the HY zeolite crystals where it can suffer from diffusional limitations that hinder its combustion, requiring higher temperatures [424,442]. Therefore, according to the combustion temperatures, peak 3 can be correlated with coke-type II whereas the peak 2 is correlated with coke-type I [423].

Total coke content in the catalyst (Table 5.2) changes from 15.3 wt% up to 23.9 wt% from 400 to 440 ºC. So, coke content grows with increasing the temperature, favoring the condensation reactions of aromatics [441]. On the other hand, the effect of the reaction temperature on the distribution of coke fractions is relevant. At 400 ºC, the coke distribution is 28.8 wt% for peak 1 and 71.2 wt% for peak 2. For 420 ºC, the percentage of peak 1 grows up to 31.8 wt% while peak 2 diminishes to 68.2 wt%. At the highest hydrocracking temperature (440 ºC), the content of peak 2 diminish (25.7 wt%), whereas peak 3, associated with more developed coke, accounting the 74.3 wt%, which corresponds to the greatest fraction of the coke. Therefore, the second peak (peak 3) not only reflects more well-structured coke but also in a greater extent.

5.3 EFFECT OF THE CATALYST/FEED RATIO

5.3.1 Hydrocracking yields and conversion

In Figure 5.18 the conversions of VGO and HDPE in the blend and yields are depicted for different C/F ratios.

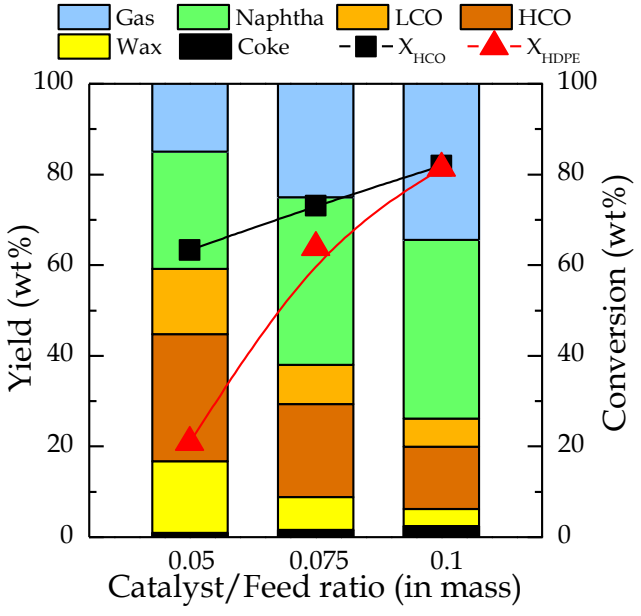

Figure 5.18 Effect of C/F ratio on conversions and yields. Reaction conditions: 420 °C; 80 bar H_2; 120 min.

Attending to Figure 5.18, with 0.05 C/F ratio, the HCO yield is reduced from 76.3 wt% (feed content) to 27.9 wt%, which corresponds to X_{HCO} of 63.3 wt%. Therefore, naphtha became the major product with a yield of 25.9 wt% followed by gas and LCO with a yield of 15 and 14.4 wt%, respectively. On the other hand, the X_{HDPE} has a reduced value (20.9 wt%). The gas yield is similar to that obtained by Munir and Usman [443] when hydrocracking a plastic mixture at 425 °C, 20 bar H_2, 0.05 C/F ratio and 60 min. They report that gas yield was around 17 wt% and the liquid yield achieved 60 wt%. Furthermore, also for these authors, the main fraction in the liquid phase is the naphtha followed far by LCO (C_{13}-C_{18}) and C_{19+} (HCO), with yields of 65, 22 and 13 wt%, respectively. Their higher conversion can be due to they use neat plastic mixture which does not have some refractive compounds of VGO.

Increasing the C/F ratio has a positive effect [154,432], as a consequence of the greater availability of active sites. Hence, a greater conversion is achieved at the same reaction time [431,435]. As a result, the increase of C/F ratio to 0.075 produces a decrease in HCO apparent yield, rising up X_{HCO} to 73.1 wt%. The naphtha yield is 36.9 wt%, being the greater yield. This is followed by an increase of gas yield up to

25 wt%. However, opposite to that, the LCO yield diminishes (8.7 wt%). Nevertheless, the most remarkable change is the sharply increase in X_{HDPE} up to 63.8 wt%.

At the highest C/F ratio (0.1) the HCO yield diminishes up to 13.8 wt%, pushing the X_{HCO} to 81.9 wt%. Naphtha yield continues growing (39.4 wt%) and still being the greatest one, but closely followed by gas yield (34.6 wt%). Furthermore, as before, LCO yield drops to 6.2 wt%. On the other side, the increase in C/F ratio also improves X_{HDPE} which is 81.3 wt% (almost equal to X_{HCO}). Those results are in agreement with similar results obtained by Uçar et al. [440] hydrocracking PE/VGO at 425 and 450 ºC, 6.5 MPa of hydrogen and 120 min reaction time. Regarding to coke, the larger the C/F ratio, the bigger the coke yield is. Thus, the coke yield is 0.9 and 2.5 wt% for 0.05 and 0.1 C/F ratios, respectively.

In Figure 5.19 the effect of C/F ratio on fuel selectivity is analyzed at different reaction temperatures. Increasing C/F ratio causes different trends, depending on the temperature. At low temperature (400 ºC), the lesser C/F ratio, the higher S_F is reached. Thus, S_F is 0.7 for 0.05 C/F ratio, that is reduced to 0.5 for 0.1 C/F ratio. This behavior is due to (i) the conversions, especially of HDPE, are low-moderate for all C/F ratios at this temperature, and (ii) gas yield increases when C/F ratio rises [417].

At 420 ºC, different behavior is observed. At 0.05 C/F ratio is obtained the lowest S_F (0.67) and when C/F ratio is increased S_F rises up to 0.8 and it remains constant for 0.1 C/F ratio, revealing that the sum of naphtha and LCO yields are almost the same and also the divisor in ec. (2.6) (section 2.5.5) despite of HCO and wax yields decrease in favor of gas yield.

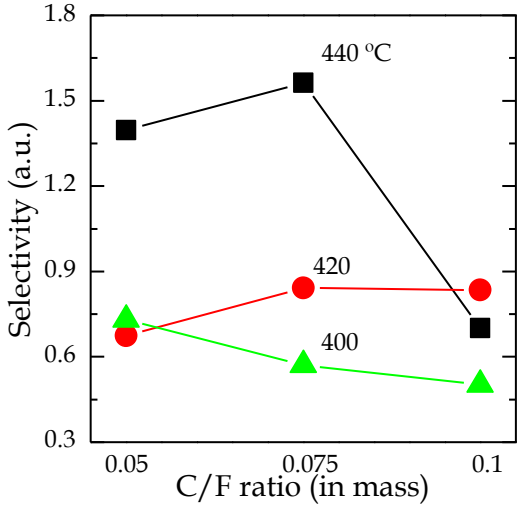

Figure 5.19 Effect of C/F ratio on selectivity to fuel (S_F) for different reaction temperatures. Reaction conditions: 80 bar H_2; 120 min.

At 440 ºC, a maximum value of S_F is observed for 0.075 C/F ratio. There is an increase in S_F from 1.4 to 1.6 when C/F ratio rises from 0.05 to 0.075, due to the extent of cracking reactions are favored, that becomes more relevant at higher temperatures. Consequently, X_{HCO} and X_{HDPE} improve producing lighter products. However, for 0.1 C/F ratio, S_F significantly diminishes reaching a value of 0.7 (lower that that obtained at 420 ºC). The reason is the overcracking of naphtha and LCO to gas. In that way, 0.075 C/F ratio seems to be the best one when temperatures higher than 400 ºC are used, achieving the greatest S_F (1.56) at 440 ºC.

5.3.2 Gas composition

Figure 5.20 displays the change in the composition of gas yield with C/F ratio, which provides useful information about not only the product distribution but also the reaction mechanism.

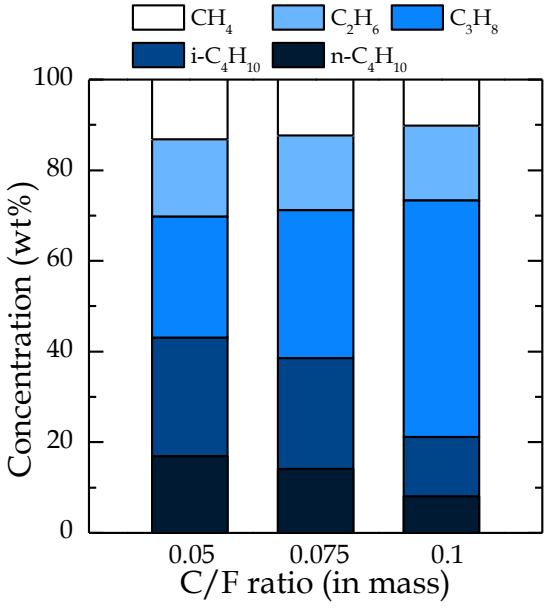

Figure 5.20 Effect of C/F ratio on gas composition. Reaction conditions: 420 ºC; 80 bar H_2; 120 min.

When C/F ratio of 0.05 is used, the concentration of dry gas (CH_4 and C_2H_6) is 30.2 wt% and C_3H_8, i-C_4H_{10} and n-C_4H_{10} are 26.7, 26.2 and 16.9 wt%, respectively. Similar results are reported by Metecan et al. [375] hydrocracking a blend of polyolefin plastics (HDPE, LDPE and PP) in the range of 400 - 450 ºC, 5.0 bar of H_2, and 60 min reaction time in a shaking batch reactor. They report that dry gas was 37.2 wt%, 37.6 wt% of C_3H_8 and 16.1 wt% of C_4 paraffins. Their lower C_4 concentration can be due to the different feedstock used and the different properties of the catalyst.

When C/F ratio is increased, the C_3H_8 concentration rises while the i-C_4H_{10} and n-C_4H_{10} concentrations are reduced. Furthermore, the CH_4 concentration slightly diminishes whereas the C_2H_6 concentration remains almost constant. Thus, for 0.1 C/F ratio, the gas composition is: 26.8 wt% of dry gas (CH_4 and C_2H_6), 52.2 wt% of C_3H_8 and 13.1 and 8.1 wt% of i-C_4H_{10} and n-C_4H_{10}, respectively. The trend shown by the composition can be due to (i) the increase in C/F ratio promotes the overcracking of light products releasing C_3H_8 [444] (ii) the carbocationic mechanism is favored by higher C/F ratios regarding to thermal cracking, which reduces the formation of the dry gas fraction.

5.3.3 Naphtha composition and RON

The composition of naphtha fraction in the liquid product at three C/F ratios is depicted in Figure 5.21.

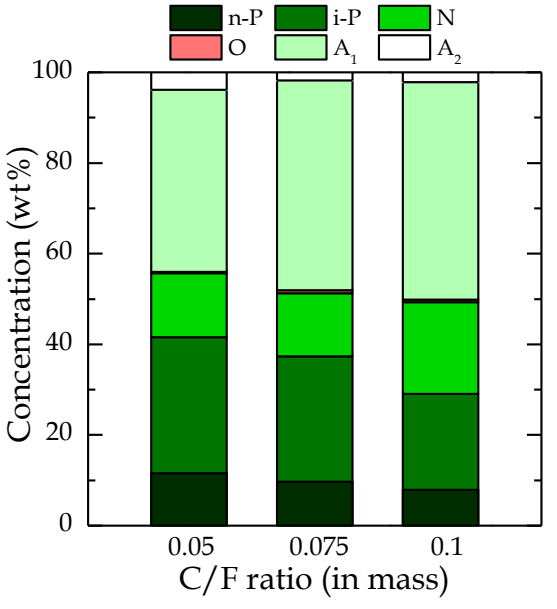

Figure 5.21 Effect of C/F ratio on the composition of naphtha fraction. Reaction conditions: 420 °C; 80 bar H_2; 120 min.

For 0.05 C/F ratio, more than 50 wt% of the naphtha is composed by aliphatic hydrocarbons: paraffins (41.5 wt%) and cycloparaffins (14.1 wt%). Regarding to paraffins, i-P prevail over n-P (30 and 11.5 wt%, respectively). The aromatics concentration is 43.9 wt%, mostly A_1 (40.1 wt%) versus A_2 (3.8 wt%). According to literature [417,436], the larger the C/F ratio, is expected greater aromatic concentration and lower of alkanes. So, the increase in C/F ratio provokes the decrease of paraffins concentration (i-P and n-P), and an increase in concentration of naphthenic and aromatic compounds (although A_2 fraction decreases). At the highest C/F ratio (0.1), the naphtha composition is 21.2 wt% of i-P, 7.9 wt% of n-P,

20.2 wt% of naphthenic compounds and 47.9 and 2.1 wt% of A_1 and A_2, respectively. This behavior of increasing A_1 and decreasing A_2 was already seen in section 5.1.3 and it was attributed to hydrodearomatization (HDA) of the LCO fraction. Hence, it is likely that the main reason of A_1 increases in naphtha fraction comes from polyaromatics decomposition in LCO through HDA, releasing alkylbenzenes compounds as byproduct [416] (Figure 5.7).

Moreover, cyclization of olefins and hydrogen transfer reactions of naphthenes to aromatics take place in the micropores of zeolite [435,436,445]. These reaction and the HDA reactions before mentioned are likely to form benzene, toluene and especially xylenes (BTX) among other alkylbenzenes compounds [436]. These assumptions are supported by studing the main compounds in naphtha. Thus, for 0.05 C/F ratio, the BTX concentration in naphtha is 20.6 wt% (Xylenes, 13.2; Toluene, 4.9, and; Benzene, 2.5 wt%). The BTX concentration in naphtha increases sharply to 27.6 wt% when C/F ratio rises to 0.075. For 0.1 C/F ratio, the highest concentration of BTX is obtained (29.2 wt%), being 16.2, 8.3 and 4.7 wt% for Xylenes, Toluene and Benzene, respectively.

The effect of C/F ratio on RON is depicted in Figure 5.22. At the lowest C/F ratio (0.05) RON is 94. When C/F ratio is increased to 0.075, RON shows a decreasing value (92.5). This is associated with the change in the composition, since i-P are reduced in a greater extent than n-P, which provokes a decrease of the RON value [417]. At the highest C/F ratio (0.1), the RON hardly changes (92.3). In spite of this, all the naphthas are suitable to be added to the naphtha pool in refinery

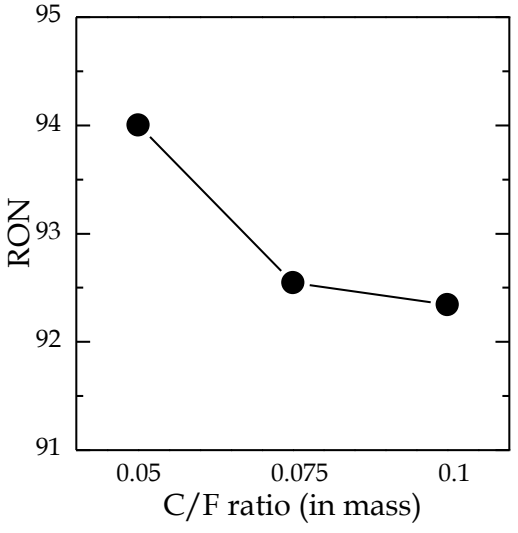

Figure 5.22 Effect of C/F ratio on RON of naphtha fraction. Reaction conditions: 420 ^{o}C; 80 bar H_2; 120 min.

5.3.4 LCO composition and cetane index

In this section, the effect of C/F ratio on LCO composition is studied under the standardized conditions and results are depicted in Figure 5.23.

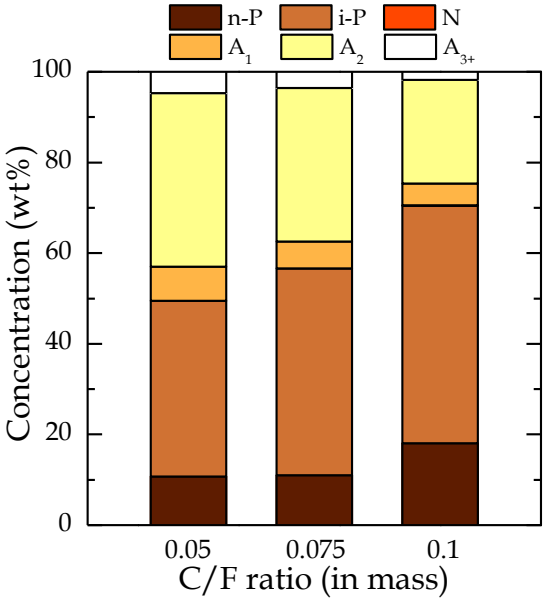

Figure 5.23 Effect of C/F ratio on LCO composition. Reaction conditions: 420 ^{o}C; 80 bar H_2; 120 min.

Attending to Figure 5.23, the lowest C/F ratio (0.05) produces a balanced composition between paraffins and aromatics (50 wt% of each one). In paraffins, i-P are in much higher concentration than n-P (38.7 and 10.7 wt%, respectively). Likewise, A_2 are the main compounds in aromatics followed far behind by A_1 and A_{3+} (38.3, 7.5 and 4.7 wt%, respectively). When C/F ratio increases, in general, paraffin concentration increases whereas the corresponding to aromatic diminishes. Therefore, for 0.1 C/F ratio, the paraffins are more than 70 wt% where i-P predominate over n-P (52.4 and 18.1 wt%, respectively) and aromatics decrease up to 22.9, 4.8 and 1.7 wt% for A_2, A_1 and A_{3+}, respectively. For all C/F ratios the concentration of naphthenic compounds is negligible (< 1 wt%). This effect of increasing C/F ratio is due to: (i) the increase of acidic sites, in particular those present on the outside of zeolite crystals, which are essential for primary degradation of HDPE to hydrocarbons in LCO range [435], and (ii) the increase of HDA capability of LCO fraction (section 5.1.4), reducing the aromatics in LCO fraction.

Cetane index was calculated following the procedure described in Section 2.5.2 and the values are displayed in

Figure 5.24. The composition is closely related to cetane index, so, the lower aromatics concentration in liquid product favors higher cetane index [417]. Besides,

there is a direct correlation between cetane index and C/F ratio [383]. Thus, for 0.05 C/F ratio, the lowest cetane index is achieved (40.5) since the more aromatic LCO is obtained. Increasing the C/F ratio, and therefore reducing the aromatic concentration, cetane index also increases and for C/F = 0.1 cetane index enhances up to 54.9.

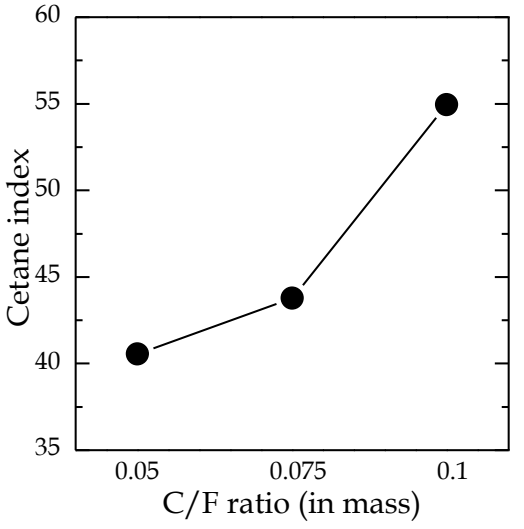

Figure 5.24 Effect of C/F ratio on cetane index in LCO fraction. Reaction conditions: 420 ºC; 80 bar H_2; 120 min.

5.3.5 Coke deposition

In Figure 5.25 the TPO profiles corresponding to spent catalysts at different C/F ratios are compared. The results of the deconvolution such as T_{Max}, the percentage of each type of coke and total coke content are collected in Table 5.3.

The TPO profile can be deconvoluted into three peaks in the following temperature ranges: (i) 375–435 ºC; (ii) 435–490 ºC; and (iii) 490–538 ºC. For 0.05 C/F ratio, two peaks are detected: (i) the smallest one with T_{Max} at 404 ºC and (ii) the biggest one with T_{Max} at 444 ºC. The coke that burns at the lowest temperature (peak 1) can be associated with amorphous coke with higher H/C ratio [387] presumably deposited on the outside of the catalyst particles, and constituted by HDPE (which undergoes a primary cracking process on the surface of the particles) [424]. On the other hand, the second peak (peak 2) corresponds to a more developed coke (lower H/C ratio) placed mainly in the mesopores and also micropores of the zeolite. The presence in the micropores, and the partial block of the pores, can delay the combustion of coke as a result of diffusional limitations [108,446]. Nevertheless, the temperature to burn the coke under both peaks can be correlated with coke-type I according the classification proposed by Bauer and Karge [423].

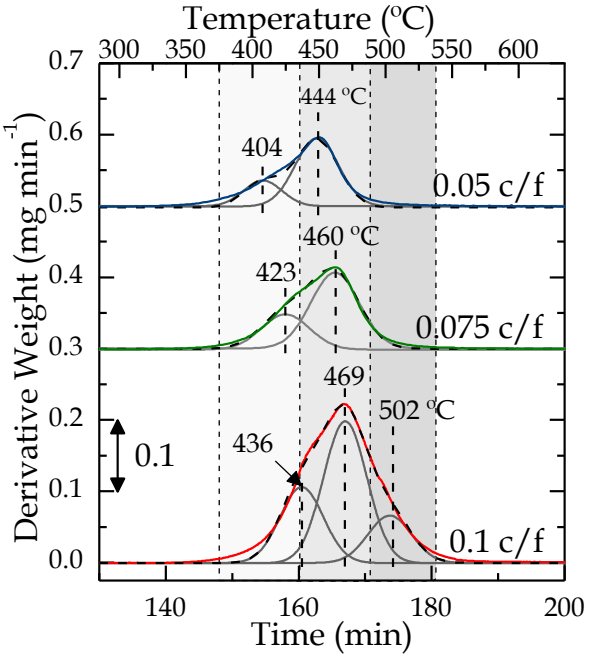

Figure 5.25 Effect of C/F ratio on el TPO profile of coke. Reaction conditions: 420 °C; 80 bar H_2; 120 min.

Table 5.3 Deconvolution results of Gaussian peaks from TPO profiles of used catalyst at different C/F ratios.

C/F ratio (in mass)	0.05	0.075	0.1
Coke content (wt%)	18.58	21.20	26.73
Peak 1			
T_{Max} (°C)	404	423	436
Fraction (wt%)	24.98	31.79	28.61
Peak 2			
T_{Max} (°C)	444	460	469
Fraction (wt%)	75.02	68.21	53.53
Peak 3			
T_{Max} (°C)	-	-	502
Fraction (wt%)	-	-	17.86

When C/F ratio increases to 0.075, the deconvolution of weight derivative shows the same distribution than before but the signal is shifted toward higher temperatures: the T_{Max} of peak 1 is at 423 °C and of peak 2 at 460 °C. This displacement of the peaks toward higher temperatures is associated to a greater condensation of the components of the two types of coke. However, both peaks are associated with coke-type I [423].

At the largest C/F ratio (0.1), the TPO profile has deconvoluted into three Gaussian peaks. The first peak is correlated with more external coke, which burns at 436 ºC and it can be classified as coke-type I. The second peak (peak 2) has the T_{Max} at 469 ºC and can be related with more developed coke, located in meso- and mainly micropore. Nevertheless, although peak 2 has higher T_{Max}, this temperature also represents coke-type I with amorphous structure [108,446,447]. The peak 3 (T_{Max} 502 ºC) fits to condensed coke, with higher content in aromatics and hence with low H/C ratio. The location of this coke is on the crystalline channels of the zeolite where polyaromatics and other molecules condense to structured coke promoted by hydrogen-transfer ability of acid sites [108,446,448]. It can be associated with coke-type II according to the classification of Bauer and Kargue [423].

On the other hand, summarizing the deconvolution results like total amount of deposited coke. At 0.05 C/F ratio, the amount of coke is the lowest one (18.6 wt%) and this content increases stepwise when the C/F ratio raises, attaining 26.7 wt% at 0.1 C/F ratio. Regarding to coke distribution, increasing C/F ratio, the portion of coke regarding peak 1 grows while peak 2 decreases. In this way, for 0.05 C/F ratio, the percentage of peaks 1 and 2 is 24.9 and 75 wt%, respectively, but for 0.075 C/F ratio is 31.8 and 68.2 wt%, respectively. Nonetheless, as has before been analyzed, the T_{Max} of each peak rises, increasing the complexity of the coke. However, for 0.1 C/F ratio the distribution changes from two to three peaks. The percentage of coke under each peak is as follows: 28.6, 53.5 and 17.9 wt% for peaks 1, 2 and 3, respectively. Hence, the 82.1 wt% is associated with amorphous coke (cokes 1 and 2) whereas 17.9 wt% is well-developed and condensed coke (coke 3).

Attending to these results, coke content and its development (well-developed coke with low H/C ratio) increase when C/F ratio is raised. The greater amount of catalyst implies that the catalytic reactions are enhanced compared to the thermal ones and also the reactions which produce coke-precursors are favored as well as their condensation to generate catalytic coke (or internal coke). Wang et al. [437] studied the coke precursors formation by thermal and deep hydroprocessing of vacuum residue. They reported that thermal reactions produce less coke with also lower condensation level (higher H/C ratio) compared to catalytic reactions. This fact is because if polyaromatics within the feed (i.e. VGO) are less or not hydrocracked, they will conform a bulky agglomeration with slight condensation level in the external surface of the catalyst. However, when those polyaromatics are hydrocracked and produce lighter aromatics and other aliphatic compounds, the simple compounds condense together with polyaromatics in the feed, achieving complex polyaromatics hydrocarbons (PAH). Therefore, the resulting coke requires higher temperatures to be burned as a result of its greater condensation level.

5.4 EFFECT OF PRESSURE

The hydrogen partial pressure is a relevant parameter in hydrocracking reactions of heavy feedstocks in order to promote some reactions like polyaromatics hydrogenation, heteroatoms removal, incorporation of H_2 when a C-C bond is broken, and reducing/retarding coke formation. So, the effect of H_2 pressure over the yields, conversion and products composition for HDPE/VGO hydrocracking has been studied in this section. The total pressure has been varied from 20 to 110 bar, using hydrogen to pressurize.

5.4.1 Hydrocracking yields and conversion

The effect of pressure on yields and conversion is depicted in Figure 5.26.

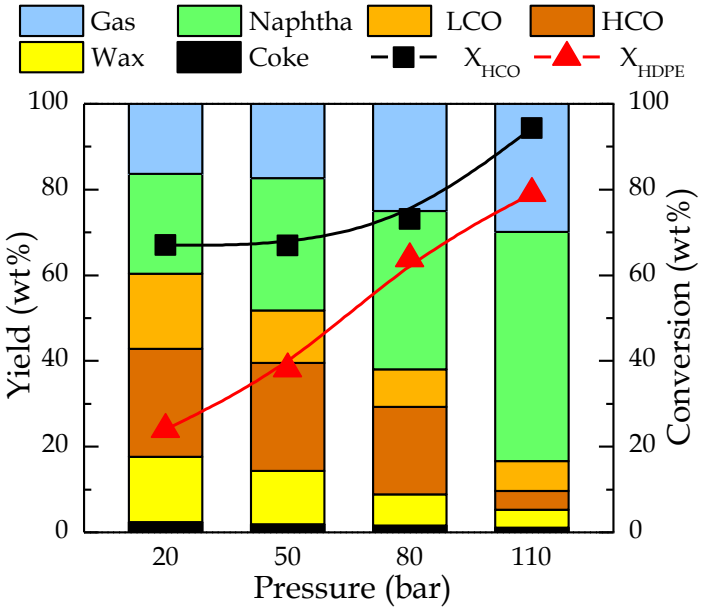

Figure 5.26 Effect of pressure on yields and conversions. Reaction conditions: 420 ºC; C/F, 0.075; 120 min.

Attending to the results in Figure 5.26, at 20 bar of H_2 pressure, the yield of HCO is 25.2 wt%, which is a considerable reduction from HCO in the feedstock, involving a 67 wt% of X_{HCO}. Regarding to lighter lumps, the naphtha yield is the highest one with 23.3 wt% followed by LCO and gas (17.6 and 16.3 wt%, respectively). In accordance to plastic conversion, the yield of wax is 15.2 wt%, involving a 24 wt% of X_{HDPE}. Finally, the coke yield is 2.4 wt%.

The yields of light products (naphtha and gas) increase with pressure, as well as hydrocracking and plastic conversion, while coke yield decreases [21,154,444,449]. So, when the pressure increases up to 50 bar, although similar X_{HCO} is obtained (67 wt%), different products distribution is obtained, rising naphtha and gas yields in detriment of LCO yield (30.9, 17.3 and 12.3 wt%,

respectively). Besides, X_{HDPE} increases to 38.1 wt% and a reduction of coke yield (1.9 wt%) is observed. At 80 bar, still under mild-hydrocracking conditions, HCO yield decreases pushing upward the X_{HCO} to 73.1 wt%. Naphtha and gas yields continue growing, whereas LCO yield diminishes (36.9, 25 and 8.7 wt%, respectively). X_{HDPE} continues its vigorous increase with a value of 63.9 wt% at this pressure. Coke yield also gets lower (1.6 wt% yield). Finally, the highest working pressure (110 bar) corresponds to real hydrocracking conditions. The HCO yield reaches its minimum, achieving the greatest X_{HCO} (94.4 wt%), mainly producing naphtha (53.4 wt% yield) while gas yield slightly rises (29.9 wt%).

Selectivity to fuel has been calculated in order to quantify the quality of the achieved conversion and results are depicted in Figure 5.27.

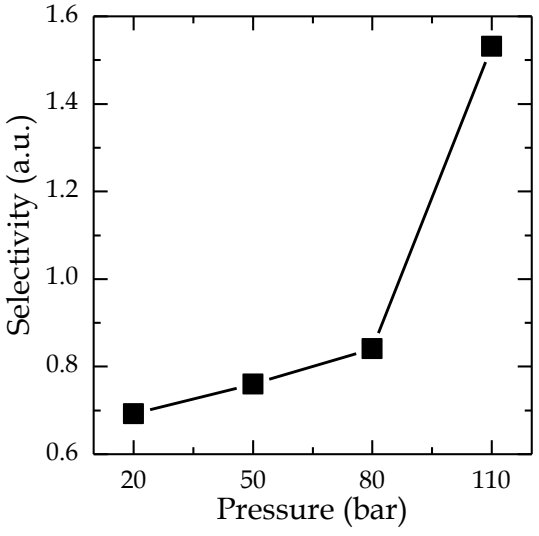

Figure 5.27 Effect of pressure on selectivity to fuel index (S_F). Reaction conditions: 420 ^oC; C/F, 0.075; 120 min.

The evolution of selectivity to fuel index (S_F) (Figure 5.27) shows that when pressure is increased from 20 to 80 bar the S_F rises stepwise from 0.7 to 0.8 since although LCO yield decreases, the naphtha yield raises progressively meanwhile HCO and wax yields are reduced. The sharp change in yields from 80 to 110 bar (naphtha lump increases while gas yield remains almost constant and HCO and wax yields reduce drastically) pushes upward S_F, achieving the biggest value for this index (1.5). Thus, it is clear that increase the pressure has a positive effect on S_F. Moreover, the most interesting operating conditions are over 80 bar in the severe hydrocracking conditions.

5.4.2 Gas composition

The effect of the pressure on gas composition is shown in Figure 5.28. The gas fraction is composed of hydrocarbons between one and four carbon atoms (CH_4, C_2H_4, C_2H_6, C_3H_6, C_3H_8, i-C_4H_{10}, C_4H_8 and n-C_4H_{10}). C_1–C_2 compounds are considered as dry gas (DG) and C_3-C_4 as LPG.

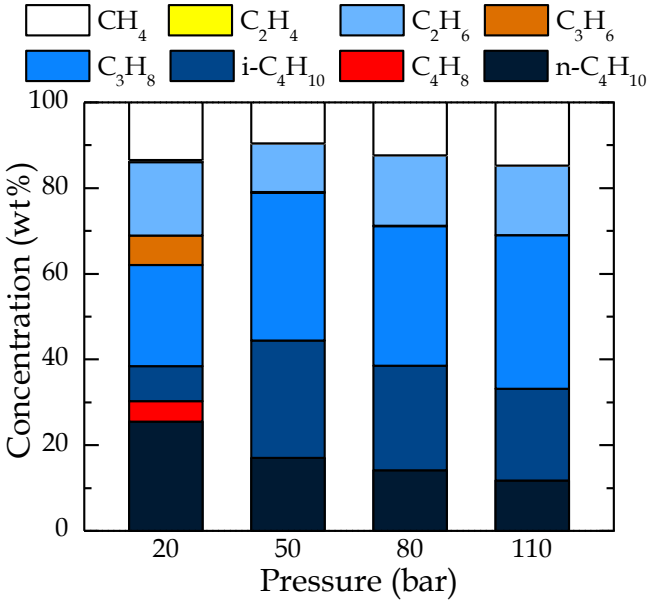

Figure 5.28 Effect of pressure on gas composition. Reaction conditions: 420 ºC; C/F, 0.075; 120 min.

The results in Figure 5.28 depict that at the lowest pressure (20 bar), although being under a hydrogen atmosphere, it is not high enough to saturate all the gaseous compounds in the reaction media. Thus, there are olefins in low concentration in both dry gas and LPG. On the one hand, dry gas is the lowest fraction (DG 31.1 wt% and LPG 68.9 wt). The CH_4 and C_2H_6 compounds are the major ones in dry gas, being C_2H_4 negligible (13.5, 17.1 and 0.4 wt%, respectively). On the other hand, LPG is composed mainly by n-C_4H_{10} and C_3H_8 (25.5 and 23.6 wt%, respectively). At this pressure, i-C_4H_{10} is in low concentration followed by the olefins C_3H_6 and C_4H_8 (8.2, 6.9 and 4.7 wt%, respectively).

It is noticeable that at 50 bar, there is a noticeable difference in gas composition: olefins almost disappear and isomerization gains relevance. Besides, increasing the pressure produces a reduction in DG fraction while C_4 and C_3 become the main products [450]. So, at 50 bar a lower DG fraction is obtained (20.8 wt%). Regarding, LPG, the concentration of C_3H_8 increases, being the main compound closely followed by the concentration of i-C_4H_{10} which also increases while that of n-C_4H_{10} diminishes, obtaining concentrations of 34.5, 27.3 and 16.9 wt% for each of them.

When pressure is raised up to 80 bar, DG concentration increases moderately in detriment of C_4 compounds; nevertheless, C_3H_8 grows slightly, still being the main compound. Furthermore, no olefins are detected at this pressure. At the highest pressure (110 bar), DG concentration grows up to 30.9 wt% (C_2H_6 and CH_4, are 16.2 and 14.7 wt%, respectively). On the other side, C_3H_8 has the largest concentration of LPG followed by i-C_4H_{10} and then n-C_4H_{10}, 35.9, 21.4 and 11.8 wt%, respectively.

5.4.3 Naphtha composition and RON

The composition of naphtha lump for the pressure range studied is shown in Figure 5.29.

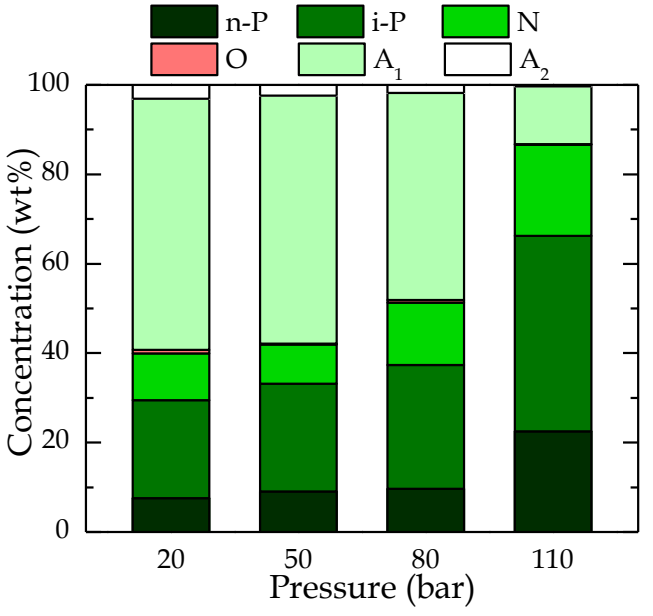

Figure 5.29 Effect of pressure on the composition of naphtha fraction. Reaction conditions: 420 ^oC; C/F, 0.075; 120 min.

According to Figure 5.29, at 20 bar of H_2 pressure paraffins account for almost 30 wt% of naphtha, being i-P the main component (21.9 wt%). Naphthenic compounds are in low amount (10.5 wt%) and despite working at the lowest pressure, the olefin concentration is very low, with a concentration of 0.7 wt%. Therefore, aromatics are the predominant compounds 59.3 wt%: Alkylbenzenes (A_1) are the most abundant compounds followed by 2-ring aromatics (56.2 and 3.1 wt%, respectively).

When pressure is increased, aromatics are reduced in detriment of saturate compounds since hydrogenation reactions are favored [417]. Therefore, when the pressure is increased up to 80 bar, stepwise changes are observed in the

composition: i-P, n-P and naphthenes increase (27.6, 9.7 and 13.9 wt%, respectively) to the detriment of aromatics (46.3 and 1.8 wt% for A_1 and A_2, respectively) and olefins disappear. The effect of pressure increase is much more noticeable at 110 bar. Hence, paraffins become the predominant compounds in naphtha, having a concentration of 43.7 wt% of i-P and a 22.5 wt% of n-P. Naphthenic compounds are boosted up to 20.4 wt% whereas aromatics are reduced to just alkylbenzene compounds (A_1, 12.9 wt%). Olefins concentration is negligible (< 0.5 wt%). The observed non-lineal trend is also reported by other authors [141,450].

A positive effect of pressure has been reported by some authors in the hydrocracking of oil-derived streams regarding to RON of naphtha when work at pressure lower than 75 bar [141], which has been also observed in the hydrocracking of HDPE/VGO (Figure 5.30) but at 80 bar. At 20 bar, RON is 89.9 but it does not change significantly up to 50 bar (90.2). However, at 80 bar there is a noticeable enhancement of RON, being 92.5. This performance can be due to the increase in i-P and the aromatics concentration, which also improves RON. Finally, at the highest pressure (110 bar), due to the low aromatics concentration and increase in n-P concentration, RON slightly decreases to 91.5.

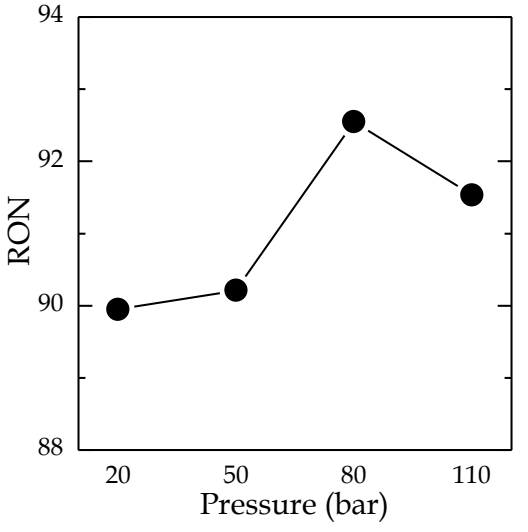

Figure 5.30 Effect of pressure on RON of the naphtha fraction. Reaction conditions: 420 ºC; C/F, 0.075; 120 min.

5.4.4 LCO composition and cetane index

The effect on the composition of LCO fraction for the different H_2 pressures studied is displayed in Figure 5.31. Compounds are grouped according to its nature: n-P, i-P, N, A_1, A_2 and A_{3+}.

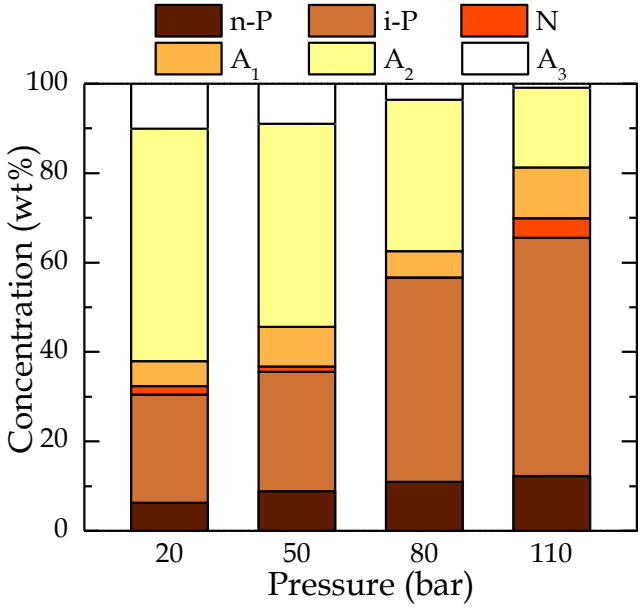

Figure 5.31 The effect of pressure on LCO fraction composition. Reaction conditions: 420 °C; C/F, 0.075; 120 min.

At 20 bar of H_2 pressure a low concentration of paraffins is obtained (30.4 wt%). Its composition clearly shows that i-P are in greater amount than n-P, 24.2 and 6.2 wt%, respectively. Naphthenic concentration is 1.9 wt%. Therefore, aromatics are the predominant group with a concentration close to 70 wt%, being A_2 the main compounds, representing the 51.9 wt% of the LCO, followed far behind by A_{3+} and A_1, 10.1 and 5.6 wt%, respectively.

When the pressure is increased, the composition shows a clear trend where an increase of paraffins concentration and the reduction of aromatics are observed, as it has been previously observed for naphtha composition (Figure 5.29). In paraffins, the increase is mainly in i-P concentration whereas n-P concentration rises stepwise with pressure. Furthermore, naphthenic compounds depict a reduction but increase significantly at 110 bar. Regarding aromatic compounds, A_2 and A_{3+} show a reduction whereas A_1 depicts an increase. Pan et al. [431], for HDPE hydrocracking between 1 to 4 MPa , reported an increase in alkanes whereas there was a reduction in cycloalkanes (naphthenic compounds) and aromatics which almost disappeared. This fact confirms that the increase in pressure discourages the formation of aromatics and naphthenic compounds and enhances the paraffin content. Nevertheless, at 110 bar naphthenic compounds appears again. In the same line,

Gutierrez et al. [141] studied the effect of pressure on hydrotreating LCO and show that it not only discourages aromatic formation but also promotes HDA of aromatics within the feedstock to paraffinic compounds.

According to the described trend, at 110 bar, i-P concentration corresponds to more than half of LCO (53.3 wt%) whereas n-P concentration increases up to 12.3 wt%. At this pressure, the naphthenic compounds achieve its highest concentration (4.4 wt%). In terms of aromatics, the concentration of A_2 and A_{3+} become 17.8 and 0.9 wt%, respectively, whereas the A_1 is 11.4 wt%.

The accurate study of the composition enable to calculate the cetane index of the LCO fraction when pressure is increased and results are depicted in Figure 5.32. There is a clear effect on cetane index when the pressure is varying due to there is a correlation with the composition. As noted, at the lowest pressure (20 bar of H_2 pressure), the LCO fraction has the poorest cetane index (31.6). However, when pressure rises, the cetane index also increases, achieving its maximum of 53.1 at 110 bar. This result can be correlated with the content of aromatics and paraffin, thus, the greater the paraffin concentration, the higher the cetane index. However, at 50 and 80 bar, the composition and quality (cetane index) of LCO are high enough to add the LCO to the diesel pool in refinery.

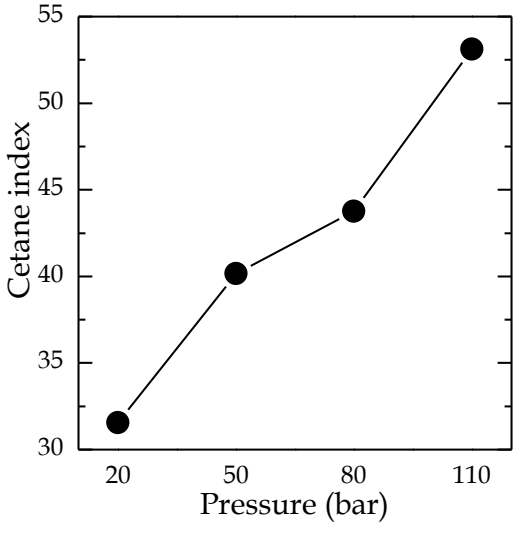

Figure 5.32 The effect of pressure on cetane index of LCO fraction. Reaction conditions: 420 ^{o}C; C/F, 0.075; 120 min.

5.4.5 Coke deposition

The effect of pressure on coke deposition on the catalyst is studied by TPO analysis and results are depicted in Figure 5.33. The results of the deconvolution such as T_{Max}, the percentage of each type of coke and total coke content are collected in Table 5.4.

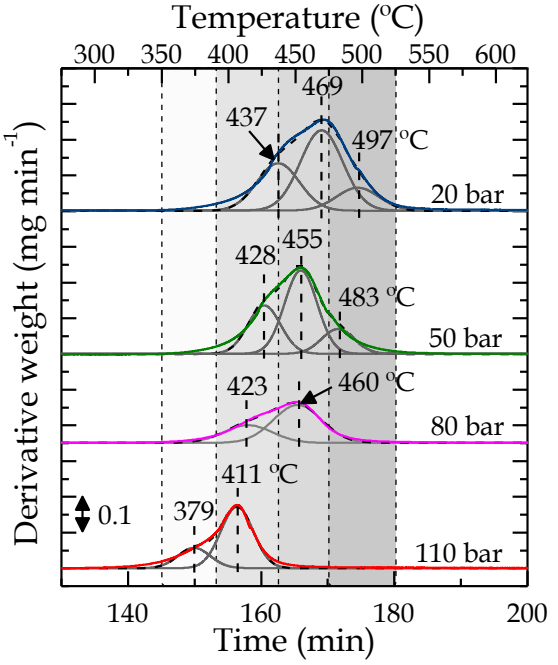

Figure 5.33 Effect of pressure on the TPO profile of coke. Reaction conditions: 420 °C; C/F, 0.075; 120 min.

Table 5.4 Deconvolution results of Gaussian peaks from TPO profiles of spent catalyst at different pressure.

Pressure (bar)	20	50	80	110
Coke content (wt%)	32.06	25.59	21.20	15.04
Peak 1				
Temperature (°C)	437	428	423	379
Fraction (wt%)	31.52	30.86	31.79	24.77
Peak 2				
Temperature (°C)	469	455	460	411
Fraction (wt%)	53.28	53.28	68.21	75.23
Peak 3				
Temperature (°C)	497	483		
Fraction (wt%)	15.20	15.86		

The deconvolution can be found in four ranges of temperature: (i) 350-390 ºC; (ii) 390–437 ºC; (iii) 437–475 ºC; and (iv) 475-525 ºC. At 20 bar, there are three Gaussian peaks, with T_{Max} at 437, 469 and 497 ºC, corresponding, from lower to higher combustion temperature, to the coke fractions deposited outside the catalyst particles, in the mesopores and in the micropores of the zeolite, as previously considered and in accordance with the criteria established in the literature to assess the TPOs of deactivated catalysts [108,421,424]. According to the classification of Bauer and Kargue [423], the first two peaks correspond to coke-type I, while the temperature of peak 3 fits to coke-type II.

At 50 bar of H_2, there are also three peaks in the TPO profile with slight reduction in T_{Max} of each peak (428, 455 and 483 ºC) regarding to peaks at 20 bar. Therefore, the peaks 1 and 2 are correlated with coke-type I and the peak 3 is a coke-type II [423].

At 80 bar the deposition of coke has been attenuated, which can be related to a greater extent of the hydrocracking reactions of the components in HDPE/VGO blend. Likewise, at this high H_2 pressure, the hydrocracking reactions of the coke precursors are favored and the condensation reactions towards coke structures are greatly attenuated. Thus, the formation of coke inside the micropores of the zeolite is negligible (peak 3 observed at lower pressure). Presumably, the catalyst will maintain a high residual activity under these reaction conditions. However, the hydrocracking of the precursors of cokes under peak 1 and 2 explains that those cokes have a lower degree of condensation than at lower pressure and therefore their combustion takes place at lower temperatures. Consequently, both fractions of the coke resemble with coke-type I as a result of their T_{Max} and nature [423].

At the highest pressure (110 bar), the trend of decreasing deposition and condensation of coke is more pronounced. At this pressure, a clear decrease in T_{Max} can be seen for both peaks (379 and 411 ºC). According to their T_{Max} and nature, both peaks 1 and 2 can be classified as coke-type I.

The results of the deconvolution such as T_{Max}, the percentage of each type of coke and total coke content are collected in Table 5.4.

Table 5.4 shows that the highest total coke content is at 20 bar (32.1 wt%) and when pressure is increased the coke content decreases stepwise until reaching a minimum value of 15 wt% at 110 bar. Comparing the amount of different coke fractions, it can be appreciated that at 20 and 50 bar the distribution is almost the same (~31, 53 and 15 wt% for peaks 1, 2 and 3, respectively). From 50 to 80 bar, the most developed coke, internal coke placed in the micropores of the zeolite and corresponding to peak 3, disappears. Therefore, 80 bar is the threshold pressure to inhibit the well-structured internal coke, which is presumably primarily responsible

for the deactivation of the catalyst. At this pressure, peak 1 is 31.8 wt% whereas peak 2 is 68.2 wt%. Hence, comparing with previous pressures, the percentage of coke under peak 1 does not change too much, being the second peak the one that only increases. Finally, at the highest pressure (110 bar), the T_{Max} of both peaks highly decreases and coke under peak 1 is reduced, 24.8 wt%, whereas coke under peak 2 increases to 75.2 wt%. The lower content of coke under peak 1 can be attributed to the increase in HDPE conversion, decreasing the presence of its adsorbed chains on the catalyst surface, which are the precursors of this fraction of coke.

Attending to the aforementioned results it can be seen that the greater the pressure, the lower temperatures are required to burn the coke on the spent PtPd/HY catalyst, preventing its development and consequently attenuating the catalyst deactivation. Obviously, this situation delays the need for the regeneration step.

CHAPTER 6

KINETIC MODELING

6 KINETIC MODELING

6.1 REACTION SCHEME FOR HDPE/VGO HYDROCRACKING

Based on all the previously mentioned studies (section 1.5), a kinetic model of 6 lumps and 19 reactions, shown in Figure 6.1, is proposed to illustrate the reaction mechanism of HDPE /VGO hydrocracking.

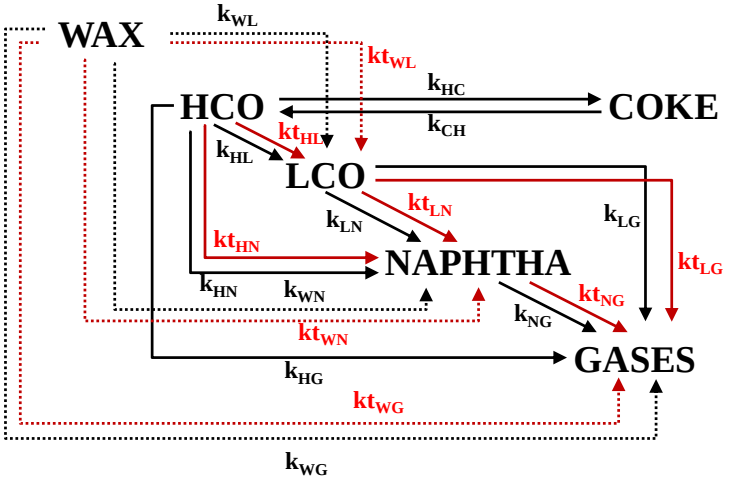

Figure 6.1 Proposed reaction scheme for HDPE/VGO hydrocracking based on literature review, where black arrows are catalytic reactions and red arrows are thermal reactions.

In this reaction scheme, the 6 lumps are named as follows: wax, heavy diesel (HCO, > 350 °C), light cycle oil (LCO, 216–350 °C), naphtha (35–216 °C), gases and coke. It should be noted that the lump of HDPE is called wax, since in this way the coherence with the reaction mechanism previously explained is maintained. Thus, it is a series-parallel reaction scheme where all the lumps are cascading cracked: the wax cracks to LCO, naphtha and gases; HCO cracks into LCO, naphtha, and gases; LCO cracks into naphtha and gases; and naphtha cracks into gases. Furthermore, the probability of coke formation from light products (LCO, naphtha and gases) is considered to be negligible according to the literature [242,283,284]. It is also stated that the formation of coke from HCO can be reversible.

6.2 METHODOLOGY

The runs in chapter 5, conducted to study the effect of the operating conditions, will be taken as the basis for developing a lumps based kinetic model following the reaction scheme shown in Figure 6.1.

The conservation equations for each lump can be classified as a system of ordinary differential equations (ODEs). The ODEs have been integrated using an implicit Runge-Kutta method based on numerical differentiation formulas of orders 1–5 (Matlab® command ode15s) following the flow chart displayed in Figure 6.2.

The procedure for estimating and optimizing the kinetic parameters through Matlab® consists essentially of three iteratively repeated steps: (i) an initial set of kinetic parameters is supplied to solve the differential equations that define the reaction rates; (ii) the sum of the square of the difference between the theoretical results and the experimental data is calculated; and (iii) this difference is minimized to obtain optimal values of kinetic constants.

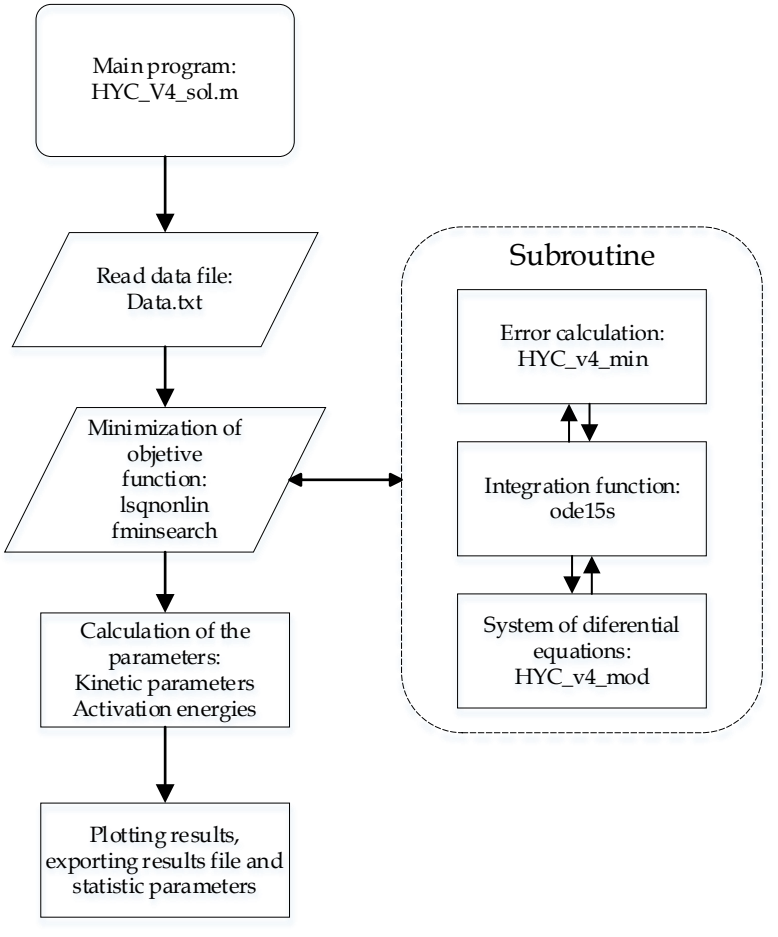

Figure 6.2 Flow chart for the computation of the kinetic parameters in the lumps based kinetic modeling.

As with any ODE, integration requires that boundary conditions have been established which allow finding the characteristic solution. In the case of study, the boundary conditions (eq. (6.1)) are those corresponding to the initial composition (t = 0) of 40 g of feed (HDPE 20 wt%; VGO 80 wt%, VGO composition: naphtha 0.1 wt%, LCO 4.5 wt% and HCO 95.4 wt%).

$$\mathrm{m_i^0} = \left[\mathrm{m_W^0},\ \mathrm{m_H^0},\ \mathrm{m_L^0},\ \mathrm{m_N^0},\ \mathrm{m_G^0}, \mathrm{m_C^0}\right] \tag{6.1}$$

The fit of the conservation equations to the experimental data has been carried out by minimizing the sum of errors (objective function), defined as follows:

$$\mathrm{SSE} = \sum_{\mathrm{j=1}}^{\mathrm{n_t}} \sum_{\mathrm{i=1}}^{\mathrm{n_l}} w_i \left(\mathrm{m_i^{exp}} - \mathrm{m_i^{calc}}\right)^2 \tag{6.2}$$

where n_t is the total number of reaction times for all operating conditions, n_l is the number of lumps used in model, w_i is the weighting factor for each lump, m_i^{exp} is the experimental yield of lump i in mass and m_i^{calc} is the model computed yield of lump i in mass.

To find the kinetic parameters that minimize the objective function and therefore fit the experimental values in the best way, two Matlab® commands have been used. These are, on the one hand, the *lsqnonlin* command, capable of solving nonlinear regression problems [244] and, on the other hand, the *fminsearch* command, which uses the Levenberg-Marquardt algorithm. This algorithm is the result of the combination of the descending gradient and Gauss-Newton methods for finding the extremes of functions, frequently used to solve problems of nonlinear least-squares minimization [451].

It should be noted that the optimization algorithms require initial values of the variables to be optimized. If these initial estimates of the variables, which in this case are the kinetic parameters, are very far from an optimal result, it is possible that the resolution will converge towards a local minimum that does not necessarily result in a satisfactory fitting. Furthermore, estimates cannot be obtained from an external source since no model for HDPE/VGO hydrocracking has been proposed in the literature.

Therefore, the optimization has been carried out in steps, solving the adjustment for 9 simplified models of the original model that have progressively acquired complexity. The intermediate models are shown in Figure 6.3. Thus, these have been successively resolved where the optimal parameters of each model have been used as initial estimates for the next model, until ending up in the model originally described in Figure 6.1. For model 1 (2L-M1), the initial parameters were estimated in the range of the typical kinetic constants for VGO hydrocracking

reactions, assuming a similar behavior of the wax. This resolution technique has been widely described by Ancheyta and Sotelo-Boyás [452].

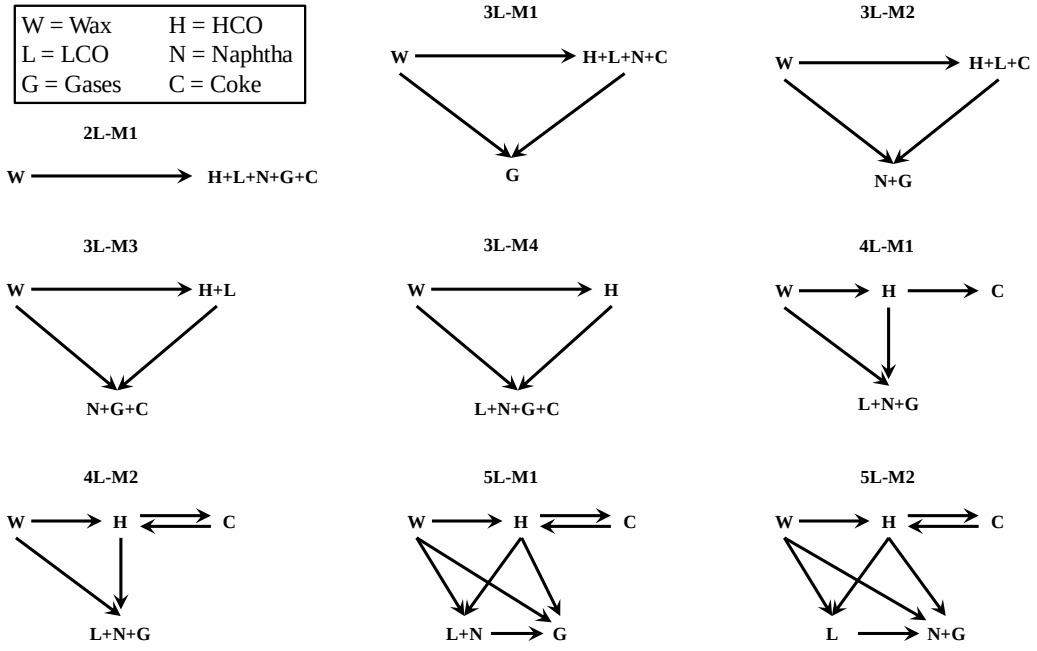

Figure 6.3 Simplify schemes from original reaction scheme (Figure 6.1).

6.3 KINETIC EQUATIONS

The conservation equations for each pseudo-component in the proposed 6-lump reaction scheme (Figure 6.1) are shown below:

$$\frac{dm_{WAX}}{dt} = -\varphi\,(\eta_{WL}\,k_{WL} + \eta_{WN}\,k_{WN} + \eta_{WG}\,k_{WG})\,m_{WAX}\,W\,F - (kt_{WL} + kt_{WN} + kt_{WG}) * m_{WAX} \tag{6.3}$$

$$\frac{dm_{HCO}}{dt} = \varphi\,[\eta_{CH}\,k_{CH}\,m_{COKE} - (\eta_{HC}\,k_{HC} + \eta_{HL}\,k_{HL} + \eta_{HN}\,k_{HN} + \eta_{HG}\,k_{HG})\,m_{HCO}^2]\,W\,F - (kt_{HL} + kt_{HN}) * m_{HCO}^2 \tag{6.4}$$

$$\frac{dm_{LCO}}{dt} = \varphi\,[\eta_{WL}\,k_{WL}\,m_{WAX} + \eta_{HL}\,k_{HL}\,m_{HCO}^2 - (\eta_{LN}\,k_{LN} + \eta_{LG}\,k_{LG})\,m_{LCO}]\,W\,F + kt_{WL}m_{WAX} + kt_{HL}m_{HCO}^2 - (kt_{LN} + kt_{LG})m_{LCO} \tag{6.5}$$

$$\frac{dm_{NAPHTHA}}{dt} = \varphi\,(\eta_{WN}\,k_{WN}\,m_{WAX} + \eta_{HN}\,k_{HN}\,m_{HCO}^2 + \eta_{LN}\,k_{LN}\,m_{LCO} - \eta_{NG}\,k_{NG}\,m_{NAPHTHA})\,W\,F + kt_{WN}m_W + kt_{HN}m_{HCO}^2 + kt_{LN}m_{LCO} - kt_{NG}m_{NAPHTHA} \tag{6.6}$$

$$\frac{dm_{GAS}}{dt} = \varphi\,(\eta_{WG}\,k_{WG}\,m_{WAX} + \eta_{HG}\,k_{HG}\,m_{HCO}^2 + \eta_{LG}\,k_{LG}\,m_{LCO} + \eta_{LG}\,k_{NG}\,m_{NAPHTHA})\,W\,F + kt_{WG}m_W + kt_{LG}m_L + kt_{NG}m_N \tag{6.7}$$

$$\frac{dm_{COKE}}{dt} = \varphi\,(\eta_{HC}\,k_{HC}\,m_{HCO}^2 - \eta_{CH}\,k_{CH}\,m_{COKE})\,W\,F \tag{6.8}$$

As can be seen, those equations correspond to a semi-continuous reactor, and are formulated considering the yields of each lump (m_i) in mass, the catalyst/feed ratio W, the total feedstock F, the kinetic constants for each reaction stage (k_{ij}), the efficiency factor (η_{ij}) and catalytic activity (φ).

The kinetic constants are temperature dependent, as stated by the Arrhenius equation in its modify form [242,283]:

$$k_{ij} = k_{ij,0}\exp\left[-\frac{E_{ij}}{R}\left(\frac{1}{T} - \frac{1}{T_m}\right)\right] \tag{6.9}$$

where k_{ij} is the kinetic constant of the formation of j from i to the temperature T, $k_{ij,0}$ is the kinetic constant of the formation of j from i to the reference temperature T_m, E_{ij} is the apparent activation energy of the formation of j starting from i, R is the universal gas constant and T_m is the central reference temperature located in the middle range of the reaction temperatures used.

The efficiency factor of the reaction of formation of j from i, η_{ij}, is evaluated by means of its corresponding Thiele modulus, Φ_{ij}. Since the Thiele modulus

represents the relationship between the kinetics of side reaction and the diffusion rate of reactants, the equation of the efficiency as a function of the Thiele modulus depends on the reaction order. Thus, an expression is obtained for the disappearance of the second order HCO and another for the rest of the first order stages, taking the catalyst particles as if they were completely spheres [453]:

$$\eta_{ij} = \frac{1}{\sqrt{1 + \Phi_{ij}^2}} \tag{6.10}$$

$$\eta_{ij} = \frac{3\,\Phi_{ij}\coth\left(3\Phi_{ij}\right) - 1}{3\,\Phi_{ij}^2} \tag{6.11}$$

Similarly, the expression of Thiele's modulus is different if it is a second order reaction or if it is a first order reaction. Thus, and assuming that the catalyst is completely spherical, it has been defined as follows [453]:

$$\Phi_{ij} = \frac{r}{3}\sqrt{\frac{3}{2}\frac{k_{ij}\,W\,m_i}{D_i}} \tag{6.12}$$

$$\Phi_{ij} = \frac{r}{3}\sqrt{\frac{k_{ij}\,W}{D_i}} \tag{6.13}$$

where r is the average catalyst particle radius, W is the mass of catalyst, m_i is the yield of reactant i in mass and D_i is the diffusivity of reactant i. It should be noted that equations (6.10) and (6.12) correspond to second-order reactions, while equations (6.11) and (6.13) correspond to first-order ones.

Given the complexity of determining the diffusivity of each lump, it was decided to include it together with the kinetic constants and activation energies among the variables to be optimized. Thus, the dependence of diffusivity with the temperature is given by the Erying equation [454]:

$$D_i = D_{i,0}\exp\left[-\frac{E_{d,i}}{R}\left(\frac{1}{T} - \frac{1}{T_m}\right)\right] \tag{6.14}$$

where $D_{i,0}$ is the diffusivity of i at the reference temperature T_m and $E_{d,i}$ is the activation energy of the diffusivity of i.

Regarding the catalyst activity, in the review of hydrocracking models, two main types of deactivation functions have been identified. On the one hand, functions of exponential decrease in activity are commonly used to model units on an industrial scale [265,283]. On the other hand, for laboratory-scale research, hydrocracking models usually characterize the fall in activity over time through the following hyperbolic function [269,270]:

$$\varphi = \frac{1}{(1 + k_d t)^m} \tag{6.15}$$

where k_d is the deactivation constant and m the deactivation order. Likewise, the deactivation constant also follows the Arrhenius equation.The deactivation constant is defined as a function of temperature as follows [145]:

$$k_d = k_{d_0} \exp\left[-\frac{E_{kd}}{R}\left(\frac{1}{T} - \frac{1}{T_m}\right)\right] \tag{6.16}$$

where k_{d0} is the kinetic constant at the reference temperature T_m and E_{kd} is the activation energy.

The proposed model assumes that all reactions are of the first order except the disappearance of HCO due to the excess of H_2 present in the reactor. In this way, in the conservation equations (eqs.(6.3)-(6.8)) all concentrations (except that of HCO) are raised to 1 and are independent of both partial pressure of H_2 and its stoichiometry [244–246,276,281,282].

Regarding the reaction order of the heaviest fraction (HCO), several authors used order 1 [241,243,253,263,268,271,455]. For example, Sánchez et al. [268] reported that for the hydrocracking of a Maya vacuum residue at 70 bar and 380-420 ^{o}C, there was no significant improvement in the prediction of the results when establishing a higher reaction order. However, later, these same authors analyzed the effect of pressure on hydrocracking by carrying out the same runs at different pressures (69-98 bar) and they determined that a second order for the rate of disappearance of the feeding fitted better the experimental data at pressures higher than 70 bar [271]. Specifically, they reported that a second order accurately represented the different reactivity of the great variety of compounds present in the residue fraction. In fact, this second order reflected that the more reactive compounds disappear first and quickly, leaving the more refractory compounds in the residue. Other subsequent studies of hydrocracking of heavy fractions have also followed this criterion regarding a second order of reaction [269,270].

So the second order is considered to be more representative for the case study, following the analogy with the vacuum residue. In fact, Al-Attas et al. [242], Al-Rashidy et al. [283] and Bdwi et al. [284], which are the ones that most closely resemble the reaction scheme proposed in this study, reported second order for their feed (VGO) in their models. Other authors, such as Sadighi et al. [265], also used the second order model of 6-lumps and 5 reactions to model an industrial hydrocracker of VGO (LSHV 0.53 h^{-1}, 410-425 ^{o}C, trilobular Ni-W and high pressure). Consequently, the second reaction order is more accurate due to (i) it has worked at high pressure and (ii) it has used a hydrotreated VGO (remove the sulfur compounds increase the reactivity of the VGO).

6.4 RESULTS

The kinetic equations have been solved stepwise following the simplified schemes (Figure 6.3) until reaches the scheme in Figure 6.1, increasing the number of parameters and hence the difficulty. The kinetic constants are summarized in Table 6.1. It should be noted that this fitting provides an SSE of 259 following the definition of equation (6.2), which is equivalent to an SSE of 0.16 if the model was defined in mass fractions. Thus, it can be considered that the model fits satisfactory with the experimental data.

Table 6.1 Kinetic parameters for the proposed hydrocracking model.

Parameter	Reaction	Value	Conf. L.	Value	Conf. L.
k_{WL}	Wax → LCO	1.55E-01	± 4.63E-02	48.58	± 7.29
k_{WN}	Wax → Naphtha	7.02E-02	± 1.56E-02	46.13	± 12.11
k_{WG}	Wax → Gas	1.13E-05	± 2.78E-06	37.48	± 10.61
k_{HC}	HCO → Coke	1.62E-03	± 3.91E-04	27.45	± 3.13
k_{HL}	HCO → LCO	2.20E-02	± 4.77E-03	20.09	± 2.39
k_{HN}	HCO → Naphtha	2.37E-02	± 4.03E-03	33.36	± 4.82
k_{HG}	HCO → Gas	9.34E-03	± 2.19E-03	29.07	± 7.54
k_{LN}	LCO → Naphtha	9.75E-01	± 2.28E-01	13.78	± 1.41
k_{LG}	LCO → Gas	1.08E-05	± 2.82E-06	9.27	± 2.47
k_{NG}	Naphtha → Gas	3.33E-01	± 5.06E-02	1.24	± 0.15
k_{CH}	Coke → HCO	1.01E-04	± 2.88E-05	0.00	± 0.00
kt_{WL}	Wax → LCO	3.54E-02	± 5.64E-03	50.89	± 8.14
kt_{WN}	Wax → Naphtha	9.72E-03	± 1.28E-03	69.83	± 16.93
kt_{WG}	Wax → Gas	1.51E-04	± 2.09E-05	68.57	± 11.34
kt_{HL}	HCO → LCO	1.33E-05	± 1.03E-06	49.56	± 6.08
kt_{HN}	HCO → Naphtha	4.02E-03	± 6.49E-04	64.62	± 13.26
kt_{LN}	LCO → Naphtha	4.18E-03	± 8.36E-04	26.24	± 2.90
kt_{LG}	LCO → Gas	1.11E-05	± 1.48E-06	30.99	± 7.85
kt_{NG}	Naphtha → Gas	1.01E-04	± 2.18E-05	38.96	± 9.77
D_W		4.04E-07	± 7.49E-08	32.54	± 9.04
D_H		1.32E-06	± 2.90E-07	11.12	± 1.34
D_L		1.47E-05	± 3.24E-06	6.55	± 0.66
D_N		7.49E-04	± 8.40E-05	4.51	± 0.75
D_C		4.25E-08	± 1.24E-08	12.11	± 1.30
K_{d0}		8.51	± 2.29	8.48	± 2.53
m		0.60	± 0.12		

As it was observed by Pham et al. [277], higher kinetic constants are achieved for the catalytic reactions than for thermal ones. According to the values obtained, it is evident that the most important reactions for each lump are those that represent the serial conversion with contiguous lumps (for example, $k_{HN} < k_{LN}$). This reinforces the idea, broadly reported in literature, that conversion of heavy fractions occurs through a cascade mechanism and mainly through series reactions [268,271]. In that way, wax is mainly converted to LCO (k_{WL}), LCO to naphtha (k_{LN}) and naphtha to gas (k_{NG}). Nevertheless, the HCO lump is converted to naphtha and LCO at similar ratio (k_{HN} and k_{HL}, respectively).

Despite this, the importance of serial conversion reactions from the heaviest fractions such as wax and HCO to LCO is less than the formation of naphtha from LCO and the formation of gases from naphtha (k_{HL} or k_{WL} are lower than k_{LN} or k_{NG}). This fact is contrary to the observations reported in the literature where in series reaction the importance of reaction decrease from the heavier to the lighter ($k_{HL} > k_{LN} > k_{NG}$) [270,273]. This is due to the low yields obtained by LCO compared to the yields of naphtha and gases. Thus, the LCO formed from both wax and HCO tends to produce mainly naphtha, which is also the most important reaction that occurs among those shown in Table 6.1. These results are due to the high hydrocracking activity depicted by the catalyst, which is highly selective towards naphtha and gas and differs from the literature, given that no case above mentioned has a catalyst with similar properties to this PtPd/HY catalyst.

Furthermore, the deactivation order (m = 0.60) is greater than that obtained by Martinez and Ancheyta [270] which means that a higher deactivation is obtained maybe due to the catalyst used (pure Y zeolite). Nevertheless, the deactivation rate constant is slightly lower, so it takes place at lower pace.

Regarding the behavior of wax lump, it should be noted that, as expected, HDPE degrades mainly to LCO, through both catalytic and thermal routes, which subsequently continues its conversion. Likewise, the formation of naphtha from plastic is a reaction to taken into account but the production of gases from plastic is practically negligible. In somehow, these results support that in HDPE hydrocracking the most important reactions are those that generate middle distillates and light distillates and to a lesser extent the production of gases [21,288]. In the same line, the kinetics of thermal degradation corroborates the data reported by the literature on the thermal decomposition of this plastic to $>C_{16+}$ (kt_{WL} and kt_{WN}) [431,435,456].

HCO is converted to a greater extent to naphtha and LCO and to a lesser extent to gases, according to the values of the kinetic constants obtained in Table 6.1. These results are in line with the reported by Martinez and Ancheyta [268] where they mentioned that the priority conversion of heavy oil fractions (both

vacuum residue and VGO) are toward naphtha and LCO. However, the thermal reactions not fulfill this decomposition trend for HCO because $k_{HG} > k_{LG}$. This fact is maybe due to the thermal reactions follow a different reaction mechanism pathway in comparison with catalytic ones. Nevertheless, there are some authors who support the trend describes by thermal reactions, pointing to HCO as the main source of gases [243].

As it has been shown along the chapter 5, LCO yield was much lower than naphtha or gas yields, decreasing when reaction time increase. With the kinetic model, it can be seen how the consumption reaction for LCO (k_{LN}, and k_{LG}) is higher than its formation (k_{WL}, k_{HL}, kt_{WL} and kt_{HL}). Therefore, it is an intermediate product, which explains why its dynamics is characterized by a maximum. This behavior has been contrasted in the literature for other intermediate products such as heavy oil yield for Ramdoss and Tarrer [288] and gas oil for De Almeida and Guirardello [287]. Moreover, thermal parameter (kt_{LN}, kt_{LG}, kt_{WL} and kt_{HL}) also encourages this behavior since thermally LCO is consumed faster (kt_{LN} and kt_{LG},) than it is produced (kt_{WL} and kt_{HL}), reinforcing the trend of the maximum observed. This performance was also reported by Pham et al. [277] on maltene lump, which is an intermediate lump in the thermal hydroconversion of asphaltenes.

Taking into account the values of the kinetic constants in Table 6.1 comes mainly from LCO hydrocracking. This route is highly favored as has been explained above. However, it is a component whose formation is also conditioned by the conversion of wax and HCO. Specifically, the formation of naphtha from HCO is slightly more favored than LCO production by either thermal or catalytic pathway. Thus, this fact is consistent with the experimental results obtained, indicating that the low yields of LCO are due to both its cracking and the fact that the heavier fractions are more likely to form naphtha.

According to where the gases come from, there is no unanimity. There are works that obtain most of the gas from the heaviest products (i.e. $k_{VG} > k_{NG}$) [243,270,284] and others from the lightest fractions ($k_{NG} > k_{VG}$) [278,288,457]. This disparity in results can be due to multiple factors such as the feedstock and, of course, the activity of the catalyst among others. In the present case, the kinetic results in Table 6.1 reveal that gas is more prone to be formed from naphtha hydrocracking than from HCO and LCO hydrocracking, especially at higher catalyst/feed ratio. These results are associated with the characteristics of the bifunctional catalyst used, which is very different compared with any other study done before. However, for the thermal reaction pathway, the kinetic constants show a contrary performance. In that case, most of the gas comes from LCO and HCO than from naphtha. This behavior also was reported in some thermal kinetic studies [277,285].

The rate constant values of coke formation from HCO (k_{HC}) are one order of magnitude higher that the value obtained for the reverse reaction of disappearance of coke towards HCO (k_{CH}). This fact resembles with considerations made by Purón at al. [244], who take into account the existence of a reverse reaction from coke to HCO, attributed to the reactivity of the coke. Thus, they explain that part of the coke is related with *soft coke*, which can be hydrogenated again to give polyaromatic hydrocarbons (PAHs), thus, decreasing the coke deposits. Despite this, the increase in coke yield with reaction time is due to both the adsorption of polymerized PAHs on the acid sites of the catalyst and the reduction of the H/C ratio that form the called *hard coke*, which is very stable. This effect also was observed and analyzed on section 5.2.5.

Regarding the activation energies, it can be seen that the production of LCO from wax has the highest one while the lowest one is for the production of HCO from coke, being therefore the latter less affected by temperature. Furthermore, reactions that implies the hydrocracking of LCO or naphtha to lighter products have lower activation energies than the production of LCO because are secondary hydrocracking reactions [244,458]. The activation energies of HCO to produce LCO, naphtha and gas are very similar to those reported by Martinez and Ancheyta [270] and Sanchez and Ancheyta [271], requiring the LCO production (HCO → LCO) lower activation energy than naphtha and gas, which have similar activation energies. However, these authors did not study the formation of coke in their reaction scheme. Nevertheless, Al-Attas et al. [242] contemplated formation of coke from VGO, reporting an activation energy of 35.9 kcal/mol for this pathway, being very similar to the value of the present work. On the other hand, the activation energies for reactions from middle distillates (LCO) to naphtha and gas (LCO → Naphtha; LCO → Gas) are lower than from the VGO to LCO and naphtha, which is also supported by other authors [270,271,278]. As mentioned above, few authors consider the formation of gas from naphtha. Of those who consider this reaction pathway [278,281,457], the values reported by Hassanzad and Abedi [457] are the most closely results in comparison with this study (1.24 kcal/mol), reporting an activation energy of 6.6 kcal/mol. In general, it is observed that the lighter the products from hydrocracking each lump, the lower the activation energy. This behavior is observed when light reaction products are obtained and the reactions have been carried out at high temperatures (> 380 °C) [458].

There are few studies about thermal kinetic modeling of [277,285–287] and only De Almeida and Guirardello [287] take into account thermal and catalytic reactions simultaneously. In the same line of the results obtained in the present work, Pham et al. [277] have reported an increase in activation energies for thermal reactions compared to catalytic ones separately. On the other hand, De Almeida and Guirardello [287], who jointly evaluated the thermal and catalytic reactions,

have chosen to give the same values of activation energies for catalytic reactions and their thermal homology. The scarcity of studies of this type highlights the need to continue developing the model here presented.

On the one hand, with regard to the estimated values of the diffusivities, the low diffusivity value of coke stands out (one order of magnitude lower) regarding the remaining lumps. This observation is consistent with the fact that the diffusivity of solids is usually significantly lower than that of liquids.

The good fitting of the model can be proved from the comparison of experimental yields vs. the calculated yields (parity diagram) displayed in Figure 6.4, and, as well as through Figure 6.5, Figure 6.6 and Figure 6.7 where are plotted the experimental yields (dots) and the calculated yields by the kinetic model (lines) for three C/F ratio (0.05, 0.075 and 0.1).

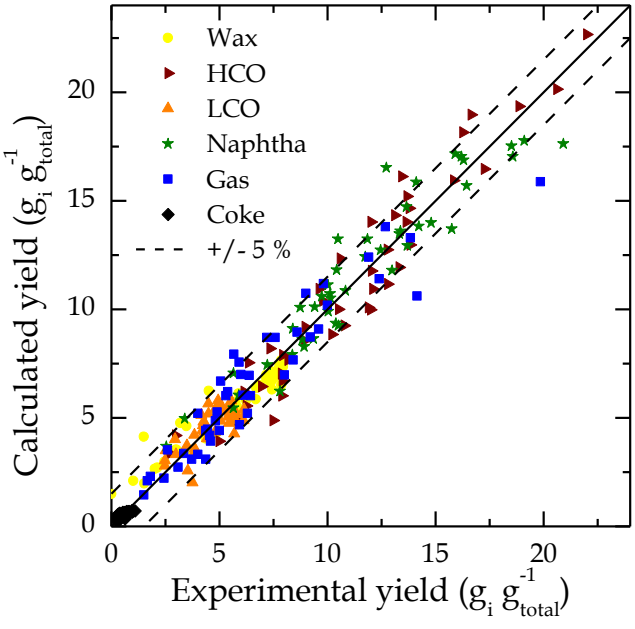

Figure 6.4 Parity diagram for the proposed hydrocracking kinetic model.

Therefore, this kinetic modeling is presented as a first approach to tackle the complex reaction mechanism behind HDPE/VGO hydrocracking with satisfactory results. Nevertheless, it is aware that it is necessary a further work to continue its development and improvement.

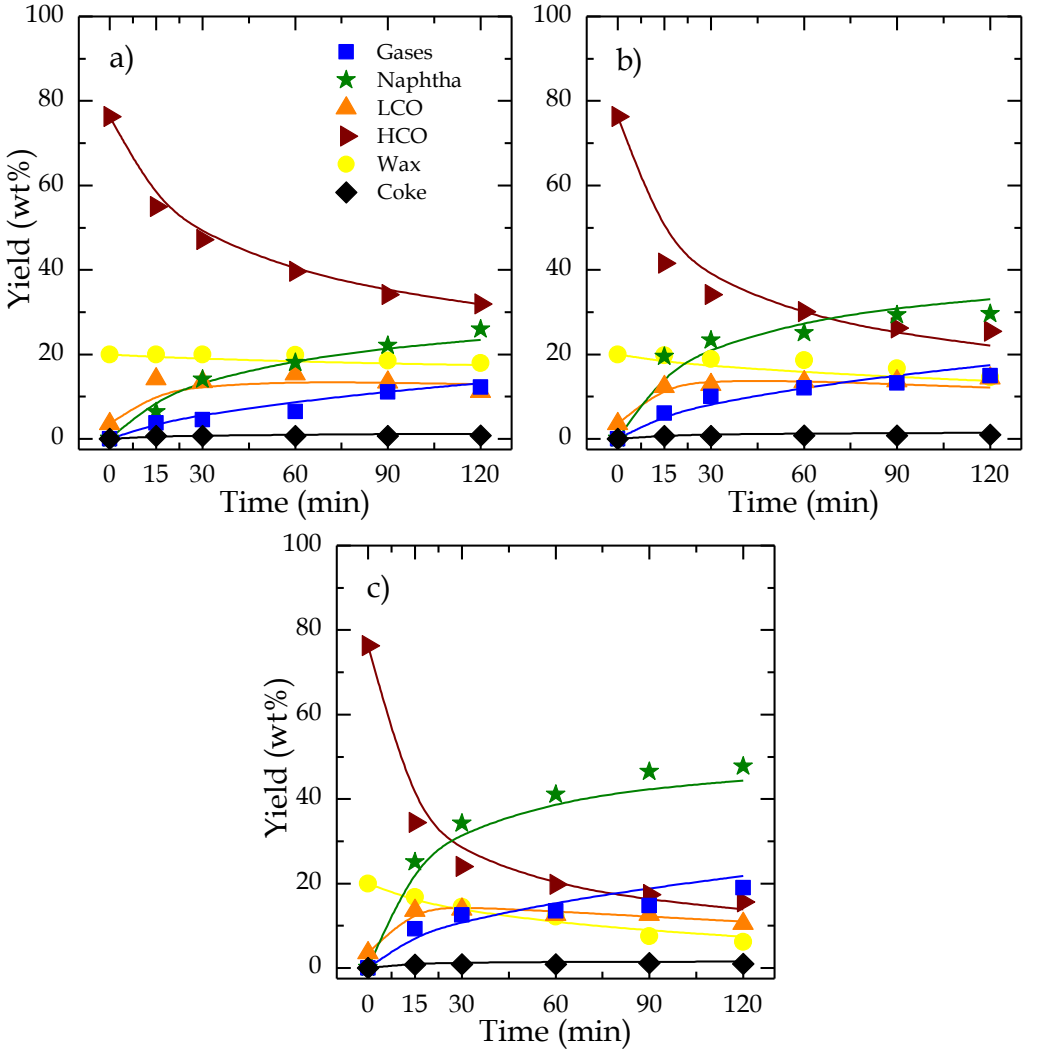

Figure 6.5 Experimental yield versus calculated yields at (a) 400 °C; (b) 420 °C; (c) 440 °C. Reaction conditions: 80 bar H_2 and 0.05 C/F ratio.

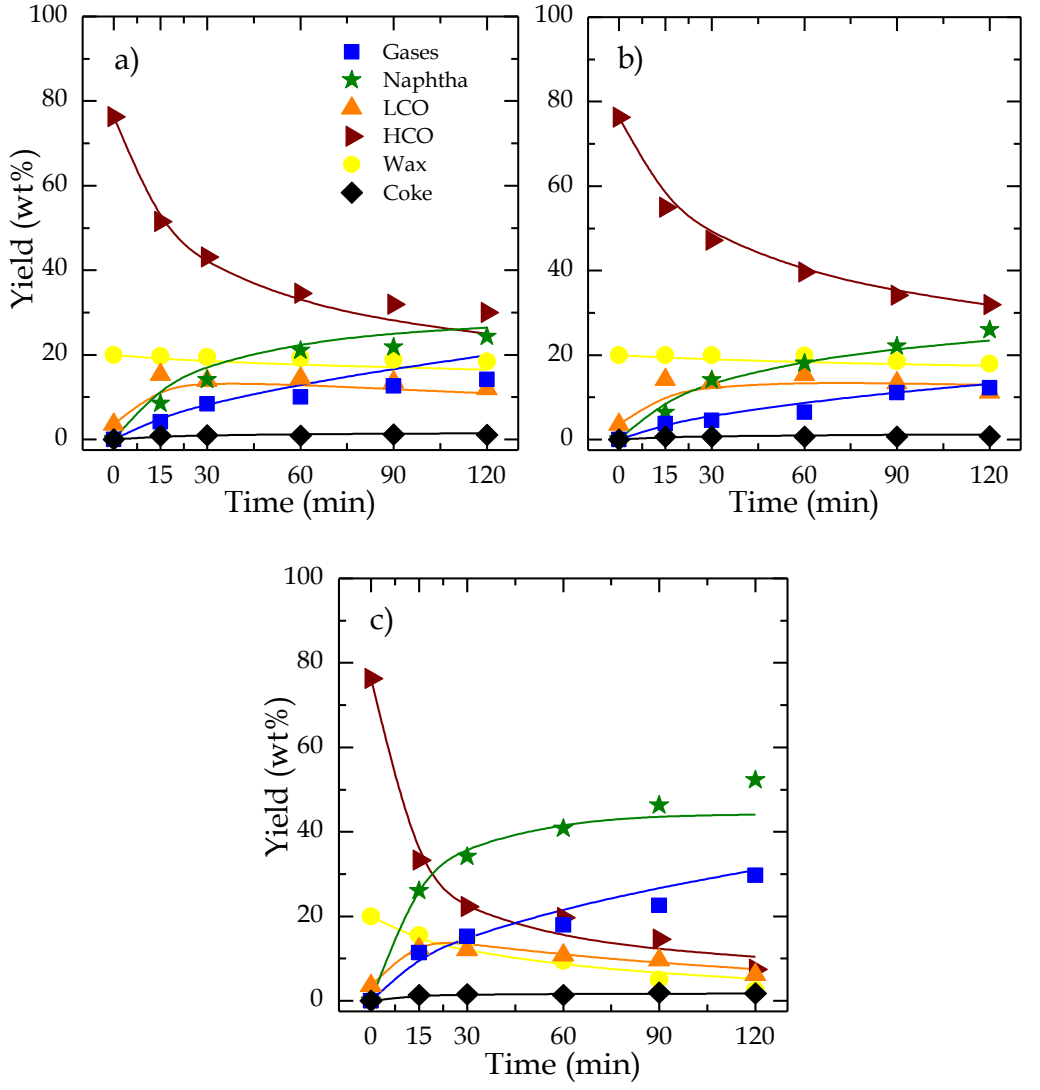

Figure 6.6 Experimental yield versus calculated yields at (a) 400 °C; (b) 420 °C; (c) 440 °C. Reaction conditions: 80 bar H2 and 0.075 C/F ratio.

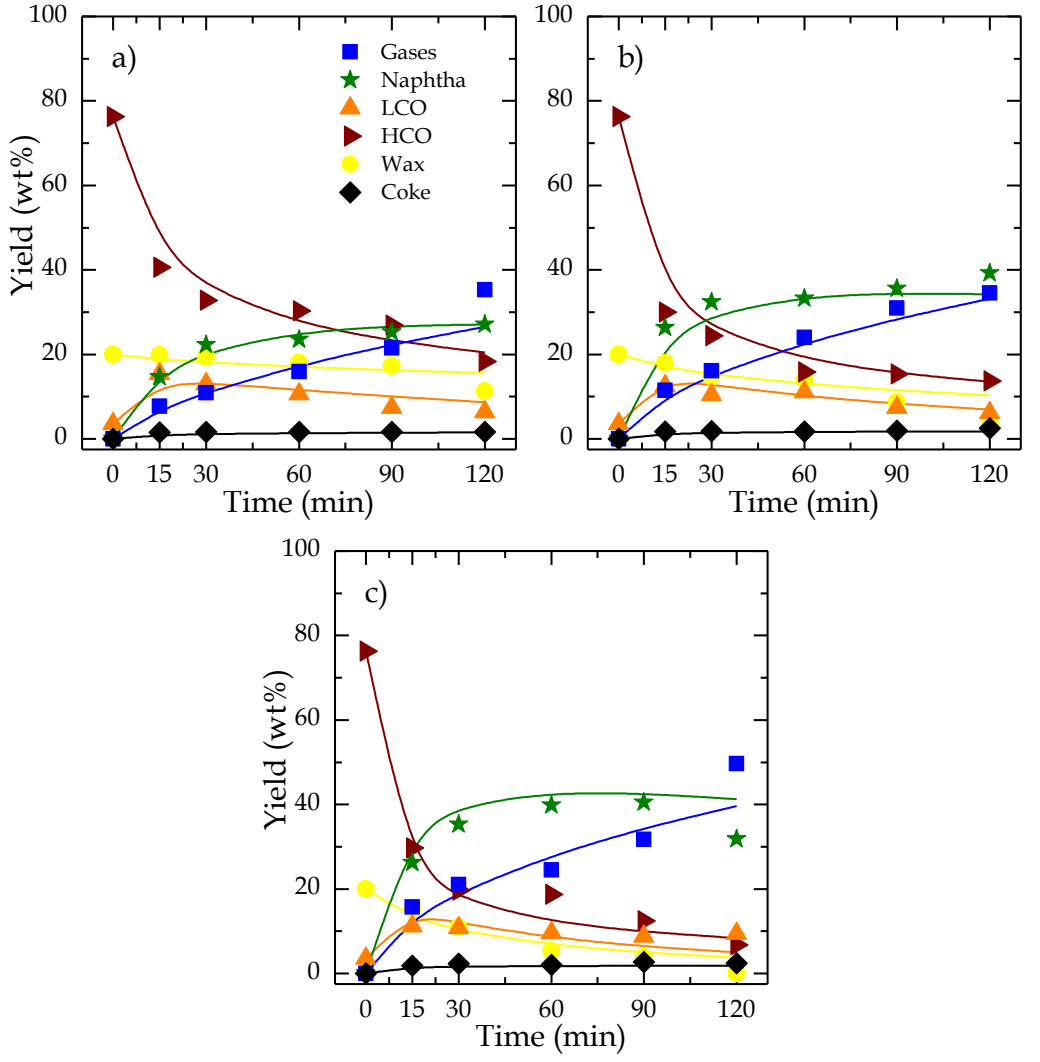

Figure 6.7 Experimental yield versus calculated yields at (a) 400 °C; (b) 420 °C; (c) 440 °C. Reaction conditions: 80 bar H2 and 0.1 C/F ratio.

6.5 SIMULATION AND OPTIMAL OPERATING CONDITIONS

Using the lumps based model proposed in this chapter and the corresponding computed kinetic parameters, a simulation of conversion and the selectivity to fuel has been carried out with temperature (400 - 440 °C) and reaction time (0 - 120 min) for three C/F ratios (0.05 - 0.1). Results are depicted from Figure 6.8 to Figure 6.10. The different values of conversions and selectivity to fuel are displayed as a color gradient, from the lowest value (blue) to the highest one (yellow).

6.5.1 Conversion of HCO and HDPE

Figure 6.8 shows that for the three C/F ratios simulated there is an enhancing effect of both temperature and reaction time, as both favor the X_{HCO} to lighter products. When C/F ratio is increased, higher conversion is achieved for the same operating conditions. In that way, the X_{HCO} reaches values greater than 80 wt% for temperatures higher than 435 °C and 120 min reaction length or 440 °C and 95 min with 0.05 C/F ratio (Figure 6.8a). Nevertheless, increasing the C/F ratio, the area in which this conversion values are achieved increases progressively (Figure 6.8b and Figure 6.8c). Thus, this mean that less severe operating conditions are required to reach conversion values higher than 80 wt%.

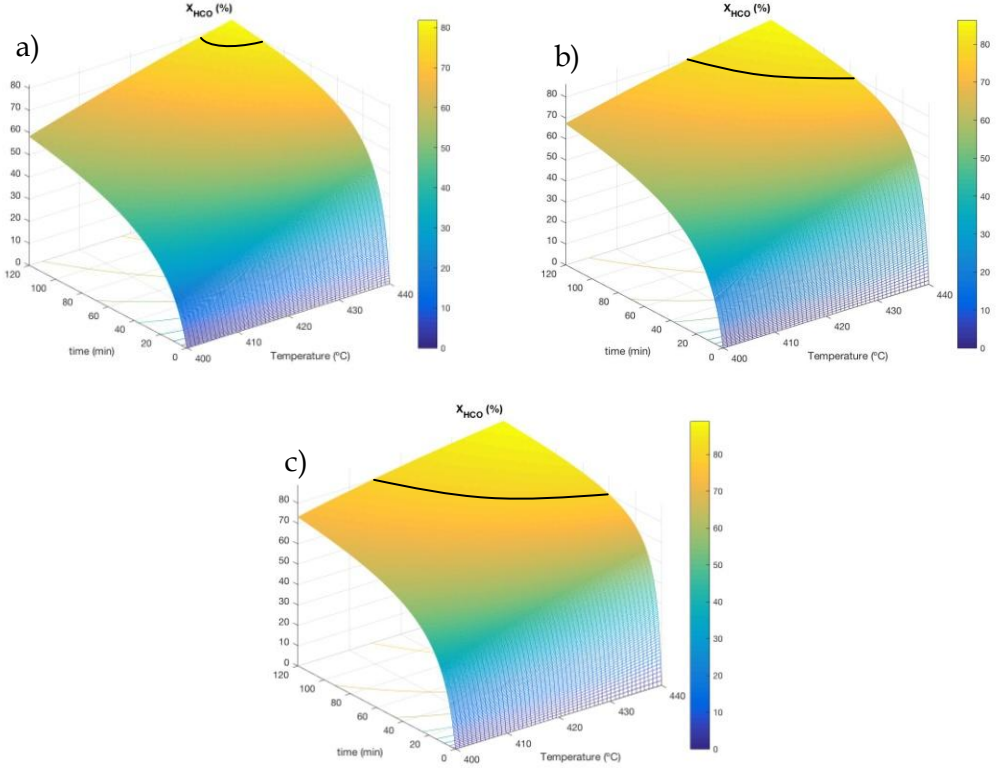

Figure 6.8 Conversion of HCO vs. time and temperature for different C/F ratios: a) 0.05, b) 0.075 and c) 0.1.

As it happens with HCO conversion, the HDPE conversion is also favored for greater values of both temperature and reaction time, as it is shown in Figure 6.9. Furthermore, it can be seen the relevance of the C/F ratio, achieving higher X_{HDPE} with higher C/F ratios for the same operating conditions. When 0.05 C/F ratio is used (Figure 6.9a), few operating conditions reach X_{HDPE} higher than 60 wt%, being 61.2 wt% the maximum conversion value achieved at 440 ºC and 120 min. Nevertheless, an increase in the C/F ratio to 0.075 (Figure 6.9b) enhances the performance of the reaction, reducing the requirements in the operating conditions to achieve 60 wt% of X_{HDPE} and the maximum X_{HDPE} achieved is 73 wt% at 440 ºC and 120 min. Finally, with 0.1 C/F ratio (Figure 6.9c) a HDPE conversion of 60% or higher is achieved with soft temperature (lower than 430 ºC) and shorter reaction length (lower than 30 min).

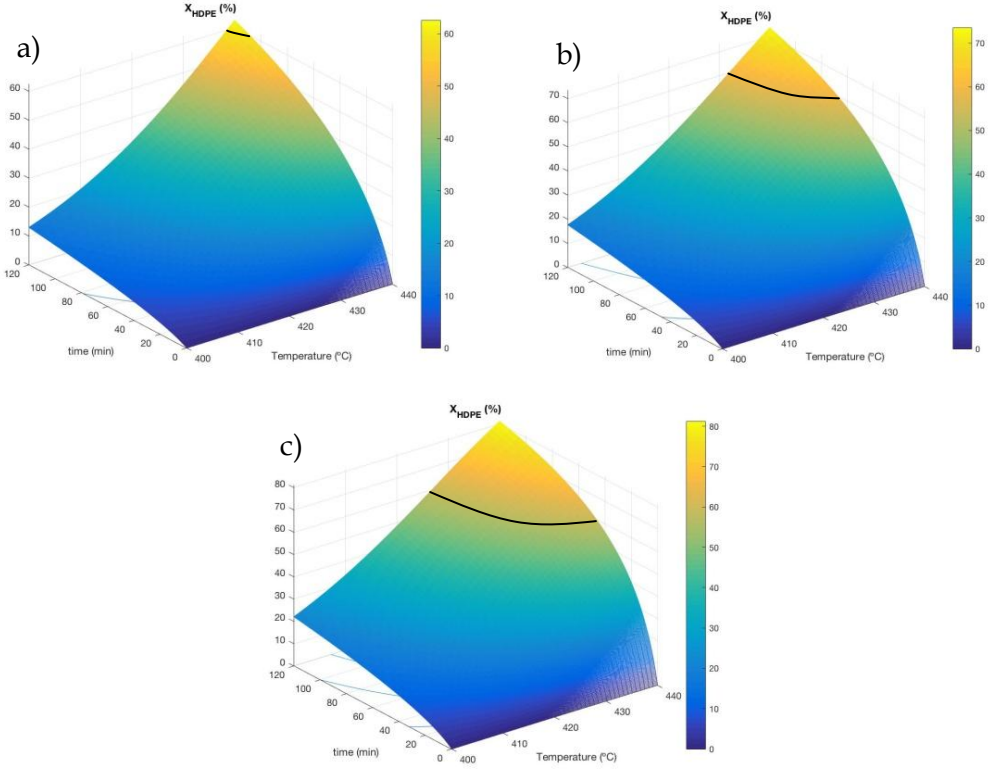

Figure 6.9 Conversion of HDPE vs. time and temperature for different C/F ratios: a) 0.05, b) 0.075 and c) 0.1**.**

6.5.2 Selectivity to fuel (S_F)

The selectivity to fuel depicts different behaviors with temperature and reaction time when C/F ratio changes (Figure 6.10). For 0.05 C/F ratio (Figure 6.10a), selectivity to fuel increases with both temperature and reaction time.

However, the selectivity to fuel increases with temperature but not always with time when 0.075 and 0.1 C/F ratios are used (Figure 6.10b and c, respectively). The highest selectivity value (1.24) is achieved with 0.05 C/F ratio (Figure 6.10a), at 440 ºC and 120 min. However, for 0.075 C/F ratio (Figure 6.10b), the maximum selectivity diminishes up to 1.13 and it is achieved at 67 min and at 440 ºC. Finally, with the highest C/F ratio (0.1) (Figure 6.10a), the maximum S_F reached is 1.09 (at 440 ºC and at 41 min). Furthermore, the area corresponding to S_F values higher than 1 is also depicted in Figure 6.10. It can be seen that when the C/F ratio is increased, the area, like it happens with the S_F maximum value, also shifts toward lower time values.

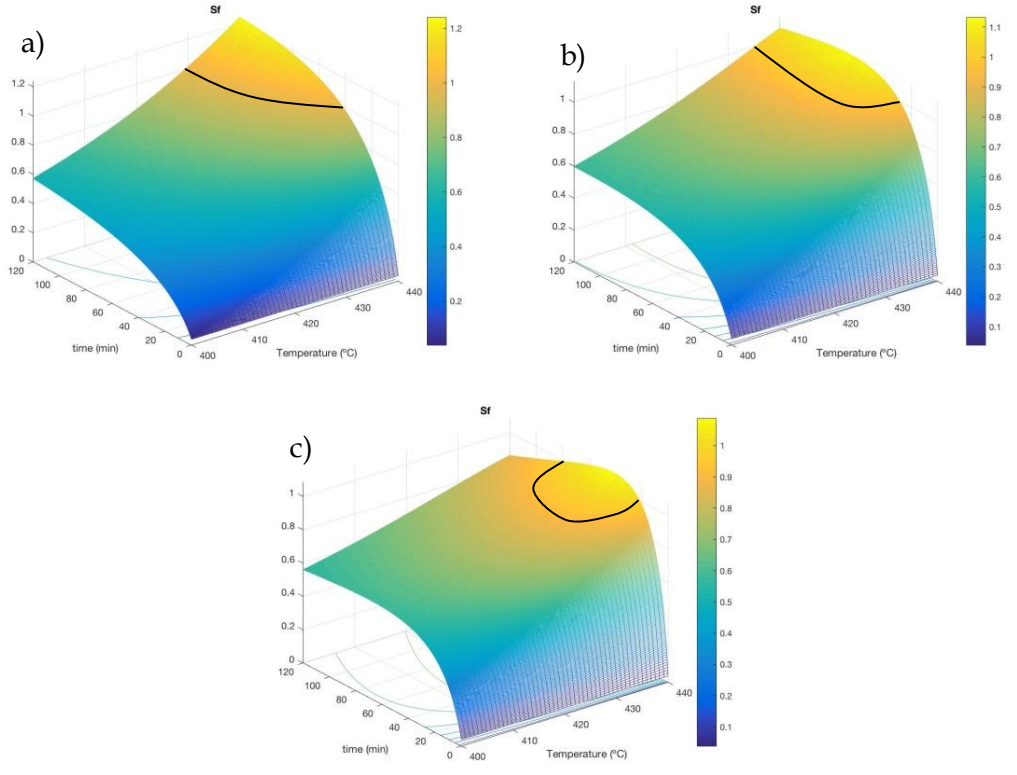

Figure 6.10 Selectivity to fuel vs. time and temperature for a) 0.05, b) 0.075 and c) 0.1 C/F ratio.

Based on these expected results according to the kinetic model, it can be concluded that the optimal operating conditions for hydrocracking of HDPE/VGO within the range of conditions studied in this Thesis are: 0.075 C/F ratio, temperatures between 433-440 °C and reaction times of 67-120 min. These operating conditions achieve a commitment between X_{HCO}, X_{HDPE} and S_F, obtaining a X_{HCO} higher than 80 wt%, with good X_{HDPE} (greater than 60 wt%) and a S_F greater than 1.

CHAPTER 7

SUMMARY

7 SUMMARY

This thesis is focused in hydrotreating and hydrocracking secondary refinery streams that have been previously hydrotreated (drastically reducing their heteroatom content) for their valorization both, alone and co-processed with alternative feeds from consumer waste such as HDPE and PP (since polyolefins represent the majority fraction of plastics in municipal solid waste, MSW) or plastic pyrolysis oil (PO) (in this case from HDPE waste). The challenge of the study has been to progress towards the Waste Refinery, obtaining high quality fuels (naphtha and diesel) as a product with the appropriate composition for their incorporation into the fuel pools in refinery, thus contributing to intensify the recovery of oil and the recycling of a fraction of municipal solid waste.

The reaction equipment used has been designed for the hydroprocessing of heavy feeds. The hydroprocessing of VGO, PO and the mixtures of PO/VGO, HDPE/VGO, PO/HDPE/VGO and PP/VGO, has been carried out in a totally automatized stirred tank batch reactor with a volume of 100 mL in a semi-continuous regime. The analysis of the liquid products has been carried out with different chromatographic techniques, highlighting that of two-dimensional gas chromatography to measure the concentration of the fractions (n-paraffins and i-paraffins, naphthenes and aromatics of 1, 2 and 3 rings). The bifunctional catalysts used (commercial and prepared in the laboratory) are made up of transition metals (Co, Ni, Mo and W) and noble metal (Pt and Pd) with different acid supports (Al_2O_3, SiO_2-Al_2O_3, HY zeolite and MCM-41). The properties of the catalysts have been analyzed with different techniques (adsorption-desorption of N_2, X-ray diffraction, differential adsorption and desorption at programmed temperature of tert-butylamine, adsorption and infrared spectroscopy of pyridine, reduction at programmed temperature, photoelectric spectroscopy of X-rays, sulfur desorption at programmed temperature and transmission electron microscopy), to determine the physical properties (specific surface, pore volume distribution), metallic properties, acid properties (total acidity, nature of acid sites), and chemical and structural properties.

The reaction conditions in the hydroprocessing of the different feeds have been the following: (i) in the screening of catalysts: temperature, 420 °C; pressure, 80 bar; C/F ratio, 0.1; stirring speed, 1300 rpm; and reaction time, 120 min; (ii) in the hydrocracking of alternative feedstocks: temperature, 400-440 °C; pressure, 80 bar; C/F ratio, 0.1; stirring speed, 1300 rpm; and reaction time, 120 min; (iii) for the parametric study: temperature, 400-440 °C; pressure, 20-110 bar; C/F ratio, 0.05-0.1; stirring speed, 1300 rpm; and reaction time, 15 min - 120 min. The study of the enhancement of the PtPd/HY catalyst through desilication was carried out at: temperature, 440 °C; pressure, 80 bar; C/F ratio, 0.1; stirring speed, 1300 rpm; and

reaction time, 120 min. Attention has been paid to the main reactions in hydroprocessing: hydrodearomatization (HDA) and hydrocracking (HC), by studying the effect of the properties of the catalysts and the reaction conditions on the distribution of products and their nature.

The results of the parametric study with the selected catalyst have allowed proposing, in the first place, a reaction scheme based on lumps for HDPE/VGO hydrocracking. Subsequently, the kinetic model based on ordinary differential equations (ODEs) for each lump has been solved through a data analysis program of Matlab® to optimize the kinetic parameters and quantify the HYC reactions extent. Furthermore, this kinetic model has been used in the simulation of the reactor to obtain the optimal reaction conditions, maximizing the conversions (both HCO and HDPE) and the selectivity to fuels (naphtha and diesel desired products).

The results show the capability of hydroprocessing unit (either in new units or adapting the currently existing ones) to treat a refinery stream (in this case VGO) together with waste plastic and their pyrolysis oils (PO), obtaining fuels with composition and quality enough to be added into the fuel pools in refineries. In addition, with this initiative refineries are effectively incorporated into the large-scale recycling of materials that are derived from petroleum. At the same time, this co-feeding, also helps to the decarbonization of refinery's activity, reducing the costly payments of CO_2 emission rights.

CHAPTER 8

CONCLUSIONS

8 CONCLUSIONS

This section contains the main conclusions drawn from the results of this Thesis, which have been selected based on their contribution to the hydrocracking knowledge, their interest for the forthcoming work, and fundamentally their applied interest to progress towards the industrial implementation of polyolefin waste plastic hydrocracking together with refinery streams.

On the catalysts screening for VGO and HDPE/VGO hydrocracking

- This first stage of catalyst discrimination based on VGO hydrocracking has proven to be fundamental to find the most promising catalysts among those proposed. As already anticipated when analyzing their physicochemical properties, the NiW/MCM41 and NiW/SiAl catalysts had a poor HDT performance, reporting VGO conversions of 27 and 32 wt% respectively, similar to the conversion values of thermal hydrocracking (28 wt%). The CoMo/Al and NiMo/SiAl catalysts showed better performance, with conversions close to ~50 wt%. However, they showed much lower conversion results than those reported by NiW/HY and PtPd/HY catalysts, which showed conversions of 69 and 91 wt% respectively. Furthermore, it is noteworthy that the NiW/HY catalyst showed a balanced performance of both naphtha and LCO yield. In contrast, the PtPd/HY catalyst showed a preferential production of naphtha lump with low LCO yield and the highest gas yield. These results of PtPd/HY catalyst are mainly attributable to its acidic and textural properties.

- It has been observed a linear relationship of both BET surface and total acidity with conversion for almost all the catalysts, in such a way the higher the property value, the higher conversion is achieved. The selectivity to fuel, which reflects the naphtha and LCO yields regarding the non-desired products yields, showed the highest values for NiW/HY and PtPd/HY catalysts (S_F = 1.2 and 2.1 respectively), and, being greater than 1 implies that desired products are in a greater extent than the rest of the lumps. Furthermore, those catalysts achieved a naphtha with RON of 86 for NiW/HY and 91 for PtPd/HY. The composition of those naphthas depicted that they have the lowest n-P concentration, a high concentration of i-P and the lowest A_2 content. For all these reasons, NiW/HY and PtPd/HY were the catalysts chosen to carry out the HDPE/VGO hydrocracking.

- The incorporation of HDPE to the reaction medium has a positive effect on the apparent HCO conversion for the NiW/HY catalyst in the temperature range studied. Furthermore, this catalyst achieves a good HDPE conversion

from the lowest temperature used in this work (60 wt% at 400 ºC). This result can be attributed to the activity of the strongly acidic (Brønsted) sites of this catalyst that activate the carbocationic cracking mechanism of the dissolved HDPE chains, which is the first stage of the hydrocracking mechanism of polyolefins. Then, the increase of temperature enhances both conversions: HDE conversion and VGO conversion. According to the product yields, naphtha and LCO lumps are produced in a greater extent when HDPE is added to the reaction medium but the gas yield also increases. Moreover, the quality of these fuels measured by naphtha RON and LCO cetane index exhibits equal or better results when HDPE/VGO is hydrocracked.

- For the HDPE/VGO hydrocracking with the PtPd/HY catalyst, the conversion of HCO is lower than that obtained without HDPE in the feed at 400 and 420 ºC, but higher at 440 ºC. This result can be attributed to the micropore area of this catalyst (S_{micro}), that is the highest one, difficulting the access of large molecules of VGO to the active sites. However, when temperature rises, the radical mechanism is boost which reduces the size of the large molecules enhancing the access to the active sites, reporting the best results above 420 ºC with a HCO conversion of 93 wt% and a HDPE conversion of 100 wt%. This catalyst displays an excessive over-cracking when the blend is fed, which leads to a high yield of gases and to a subsequent reduction of the yields of naphtha and LCO; however, although the naphtha yield is diminished, it is still high. Despite these results, it is a very promising catalyst whose results can be greatly improved in the optimal operating conditions. So, it is necessary to carry out the corresponding parametric study.

On the analysis of alternative strategies for waste plastic and VGO valorization

For NiW/HY catalyst:

- When a decentralized strategy is used in the management of waste plastic, the plastic pyrolysis oil (PO) produced in the pyrolysis units can be (i) individually hydrocracked or (ii) co-fed with VGO since they have similar density and PO is less viscous. The hydrocracking of neat PO has reported better HCO conversions than neat VGO at all temperatures studied with also higher naphtha yields. Nevertheless, the gas yield is higher since PO is composed by molecules with a wide range of boiling point (including

molecules in naphtha and LCO range) and the operating conditions cause their overcracking. However, when PO is co-fed (PO/VGO), the aforementioned problem is solved. Comparing with VGO hydrocracking, it maintains both higher HCO conversion and higher naphtha yield and the formation of gases is reduced, so, this co-feeding is therefore presented as a viable alternative to waste plastic valorization. Furthermore, the fuels produced have acceptable quality to be incorporated into commercial fuel pools at refineries.

- The strategy of centralized management of waste plastic in the refinery (direct plastic feed (HDPE, PP) to the conversion units dissolved in VGO) for HDPE/VGO hydrocracking has resulted in satisfactory conversions of both HCO and HDPE (> 70 wt% from 420 ºC). The obtained fuels show to be valuable, especially naphtha, due to its high RON (90). On the other hand, the PP/VGO hydrocracking shows low conversion of both HCO and PP at temperatures lower than or equal to 420 ºC. However, when the reaction temperature arouses to 440 °C, the conversion of PP increases to 95.9 %. This fact is due to lower PP reactivity, but when working at temperatures close to its cracking temperature, good results are obtained. Furthermore, the fuels produced at all temperatures showed a proper composition and enough quality to be incorporated into the naphtha and diesel pools in refineries.

- The option of combining both strategies of management is represented by PO/HDPE/VGO hydrocracking and it has been dismissed due to the poor results obtained with this catalyst. For this feed, there are low HCO and HDPE conversions for temperatures lower than or equal to 420 ºC (< 40 and < 10 wt%, respectively) and for the maximum temperature (440 ºC) the HCO conversion improves but the HDPE conversion does not. Therefore, for the ternary mixture there is a competition for acidic sites adsorption which blocks the adsorption of larger alkanes from HDPE, discouraging its conversion.

<u>For PtPd/HY catalyst:</u>

- Hydrocracking of neat PO with this catalyst is not a viable alternative either, since: (i) lower HCO conversions than those obtained for VGO hydrocracking have been achieved and (ii) excessively high gas yield has been obtained at all temperatures studied. The high overcracking of the PO with the PtPd/HY catalyst is due to its higher total acidity. On the other hand, the hydrocracking of PO/VGO seems to be a viable alternative in the range of temperatures worked. It has shown HCO conversions similar or

higher to those of the VGO hydrocracking, also reducing the gas yield. With this feed, naphtha yields achieved 67 wt% at 420 ºC.

- The hydrocracking of HDPE dissolved in VGO reaches HCO and HDPE conversion values of ~80 wt% for temperatures higher than 420 ºC. At 440 ºC, this catalyst achieves HCO conversion of 90 wt% and total HDPE conversion. Nonetheless, the gas yield is remarkable, surpassing that reported by the neat VGO hydrocracking. On the other hand, the PP/VGO hydrocracking has shown good values of conversion, reporting both HCO and PP conversions similar to those reported for HDPE/VGO hydrocracking with this catalyst for all temperatures. From 420 °C onwards HCO and PP conversions are slightly less than 80 wt%. It is noteworthy that for this blend the complete conversion of PP is also achieved at 440 ºC and the gas yields were similar or lower than those reported by neat VGO hydrocracking at all temperatures.

- A mixture of both strategies (PO/HDPE/VGO) seems to be again a failed alternative even for this catalyst. When the temperature is equal or lower than 420 ºC, although the HCO conversion is greater than 80 wt%, the HDPE conversion barely reaches 50 wt%, discouraging further studies with this ternary mixture. Therefore, no synergy is observed for the ternary mixture at low temperatures (lower than 420 ºC). Nevertheless, at 440 °C, PtPd/HY catalyst has reported HCO and HDPE conversions of 91 and 100 wt%, respectively, but with a huge gas yield.

- With this catalyst, the fuels (naphtha and LCO) obtained in the hydrocracking of the different blends of plastics and/or plastics pyrolysis waxes with VGO, fulfill the composition and quality (RON or cetane index) requirements needed to be included in the corresponding fuel pool in refineries.

- This catalyst has shown a great versatility to hydrocracking a wide variety of alternative feeds achieving acceptable conversions for all the feedstocks. This catalyst has a significant drawback which is the high gas yields, but this inconvenience can be solved by: (i) reducing the acidity of the catalyst and increasing the mesoporous area through a catalyst desilication process or (ii) conducting a parametric study to find out the more suitable reaction conditions that minimize gas formation while maintaining high conversions and naphtha and LCO yields.

On the tuning PtPd/HY catalyst properties through desilication for HDPE/VGO hydrocracking

- The desilication treatment to the PtPd/HY catalyst has proven to be very useful, obtaining very promising results. When the treatment has been carried out once (Cat-B), the effect on gas yield has been remarkable, with a reduction of 43 wt%. In turn, this reduction has led to an increase in naphtha yield of 34 wt%. As expected, by reducing the activity of the catalyst, the conversions achieved with Cat-B has been reduced. However, these conversions continue being satisfactorily high, being 82 and 86 wt% for the conversion of HCO and HDPE respectively. Therefore, in general, satisfactory results are obtained after one desilication treatment.

- After performing 2 consecutive desilication cycles (Cat-C) this catalyst report excellent results. The overcracking has been further reduced with a minimum impact on conversion, being almost the same that for Cat-B. In that way, the gas yield reduction has been approximately 54 wt% for Cat-C, notably increasing the naphtha yield (the desired product of this catalyst) from 31.8 to 47.9 wt%, which is a growth of 51 wt%. In addition, these outstanding results have been obtained keeping both conversions (HDPE and HCO) at values higher than 80 wt%.

- However, it should be mentioned that it has not been possible to increase the LCO yield, remaining practically unchanged for both Cat-B and Cat-C. It is remarkable that both catalysts have shown a reduction of coke yield, especially Cat-C. This is due to both (i) the improved mass transfer within the catalyst particle by increasing the mesoporous surface and (ii) the acidity decreasing. This is an interesting result since the severity of the deactivation by coke is reduced, thus presumably lengthening the life of the catalyst. In addition, the coke combustion analysis show that not only lower temperatures are required (in Cat-B and especially Cat-C) to eliminate most of the coke but also the hard coke deposited in the crystalline structure of the zeolite is lower.

On the parametric study of HDPE/VGO hydrocracking on PtPd/HY catalyst

- The study of the operating variables has shown to be of great interest, providing valuable knowledge about the effect of each operating variable on the HDPE/VGO hydrocracking. In general, severe reaction conditions (time,

temperature, C/F ratio and pressure) increase the conversions (HCO and HDPE) and the yields of gases and naphtha. Coke yield also increases when the operating variables become more severe, except for the pressure which has an inversely proportional relationship. On the other hand, reaction conditions also influence in the composition of the product lumps and therefore in its quality. However, among the reaction conditions studied, it has not been found those that significantly increase the LCO yield, due to the inherent physicochemical properties of the catalyst which promote its hydrocracking toward lighter compounds.

- The effect of time has been shown to be important for both conversions but especially for the HDPE one, which depicts an exponential increase with reaction time. The HDPE conversion is quite low for reaction times lower than 60 min, with 0.075 C/F ratio, 420 ºC and 80 bar, and after that time, it progressively increases with reaction time. In addition, the effect of time has a positive impact on the quality of the fuels obtained, thus increasing both the naphtha RON and the LCO cetane index.

- Regarding the temperature, it can be concluded that working at temperatures below 420 ºC is not advisable since although the HCO conversion is at least 60 wt%, the HDPE conversion is almost non-existent (ca. 10 wt %). This variable has also a noticeable effect on product yields and, in general, it increases the selectivity to fuels. The gas composition analysis revealed that an increase in temperature leads to an increase in thermal reactions, increasing the concentration of dry gas (DG). Working at higher temperatures also reflects a change in the nature and location of coke, becoming more aromatic and being located mostly in the micropores of the catalyst.

- As mentioned, the results report that in the first instance, an increase in the amount of catalyst favors the conversions and yield to naphtha. However, a more detailed analysis of selectivity to fuels reveals that this statement is not always true and the effect of C/F ratio depends on the temperature. It has been observed that at 400 ºC the increase of C/F ratio leads to lower selectivity to fuels and, reversely, at 420 ºC the increase in C/F ratio enhances that selectivity reaching its maximum value (1.56) for 0.075 C/F ratio, 80 bar, 120 min and at 440 ºC. On the other hand, increasing the C/F ratio leads to a higher catalytic coke yield, more aromatic and developed in the micropores of the catalyst.

- The results obtained regarding pressure advice to work at the highest possible hydrogen pressure since it has a positive effect on all the variables studied: increasing pressure both HCO and HDPE conversions and naphtha yield increase, which reduces both the quantity and the complexity of the coke formed. In addition, fuels of better quality are obtained. The best results were obtained at 110 bar 420 ^{o}C, 0.075 C/F ratio and 120 min.

On the kinetic modeling of HDPE/VGO hydrocracking on PtPd/HY catalyst

- A discrete lumps kinetic model has been established for HDPE/VGO hydrocracking for an in-house prepared PtPd/HY catalyst selected due to its versatility and the high selectivity to fuels obtained; considering the hydrocracking reactions take place both between contiguous and non-contiguous lumps,

- For the kinetic modeling, the different hydrocarbon species have been grouped into the following lumps, based on their chemical nature and boiling point range: Gas, Naphtha, LCO, HCO, Wax and Coke. In this way, the proposed reaction scheme is a cascade scheme, formed by a reduced number of reaction stages. The proposed reaction mechanism is based on kinetic equations referred to the concentrations of the different lumps. It has been achieved a good fitting of the model to the experimental results (satisfactory parity plot). Nevertheless, there is a slight deviation between experimental and model prediced yield values for naphtha and gas lumps at high reaction times, high C/F ratio and at the highest temperature (440 ^{o}C). These deviations are attributed to the fact that they are specific events under specific conditions and they are not the general trend since the model prioritizes the general trend of the data and not a specific event.

- In general, higher kinetic constants have been obtained for the catalytic reactions than for thermal ones. According to the values of the kinetic constants obtained, it is evident that the most important reactions are those that represent the serial conversion of each lump with its contiguous lumps. Furthermore, the more important reaction is the formation of naphtha from LCO followed by the formation of gas from naphtha. This is why the LCO yields are low compared to the yields of naphtha and gases as a result of the high hydrocracking activity depicted by the catalyst.

- On the other side, this model also considers thermal reactions which unveil lower kinetic constants in comparison with the catalytic ones. Besides, the activation energies of thermal reactions are also higher than those of catalytic ones in general. The scarcity of studies that consider both thermal and catalytic reactions highlights the need to continue developing the model presented here.

- Using the lumps based model proposed and the corresponding computed kinetic parameters, simulations have been carried out under the studied operating conditions in order to predict values of conversions and selectivity to fuels. It can be concluded that the optimal operating conditions for the hydrocracking of HDPE/VGO within the range of conditions studied in this Thesis are 0.075 C/F ratio, temperature between 433-440 °C and reaction time of 67-120 min.

- The development of a new kinetic scheme has led to a methodological contribution, including the wax in the scheme and taking into account that both catalytic and thermal reactions co-exist. In addition, the acquired information on the reaction mechanisms and in particular the proposed kinetic model to predict the product distribution, have a great interest in order to progress in the design of large-scale reactors for the industrial hydrocracking of these new feedstocks, in the context of the current challenges of refineries of waste plastic valorization.

On the capacity of hydrocracking units for the recovery of wastes polyolefin derivatives

- Based on the above conclusions, it can be established that the hydrocracking units can incorporate alternative feedstocks such as plastics (polyolefins) or their pyrolysis oil together with intermediate refinery stream (VGO) without significant problems or disadvantages in the conversions and yields whenever the optimal operating conditions for the PtPd/HY catalyst are chosen.

- Results obtained with NiW/HY (commercial) and with PtPd/HY (in-house prepared) have allowed to reach an overview of the role of catalyst properties in their behavior in the hydrocracking reactions of these plastic waste-derived feeds, which will serve as the basis for future studies to improve their properties, especially in order to optimize them for their use on a large scale or with other reactors.

- Furthermore, co-feeding can even improve some results compared to neat VGO hydrocracking, through the important selection of both the catalyst and the appropriate operating conditions to achieve the desired hydrocracking performance toward desired products. However, in a practical conception and oriented to the large-scale implantation of the co-feeding, the waste plastic or PO quantities that would be introduced in the refinery units would be smaller than those studied in this Thesis (20 wt%).

CHAPTER 9

NOMENCLATURE

9 NOMENCLATURE

a_0, a_1	Kinetic parameters
A_S	Acidic strength
A_T	Total acidity
c(k,t)	Concentration of the component with reactivity k
C_d	Cross section area of the pill
Cj $H^{\oplus}_{2j+1}$	Alkylcarbenium ion
D(k)	Distribution function
d_{hkl}	Distance between the crystalline planes
D_i	Diffusivity of reactant *i*
$D_{i,0}$	Diffusivity of *i* at the reference temperature T_m
d_P	Diameter of the particle
$E_{d,i}$	Activation energy of the diffusivity of *i*
E_{ij}	Apparent activation energy of the formation of *j* starting from *i*
E_{kd}	Activation energy
F	Total feedstock
k	Kinetic constant
K	Constant of the viscometer
k_d	Deactivation constant
k_{d0}	Deactivation kinetic constant at the reference temperature
k_{ij}	Catalytic kinetic constant from lump i to lump j
k_{max}	Reactivity of the species with the highest TBP
kt_{ij}	Thermal kinetic constant from lump i to lump j
$\bar{L}$	Slab length
m	Deactivation order
$(m_{HCO})_{final}$	Amount of HCO in the liquid product
$(m_{HCO})_{initial}$	Amount of HCO in the feed
$(m_{Plastic})_{final}$	Amount of unconverted plastic (wax)
$(m_{Plastic})_{initial}$	Amount of plastic fed

m_i	Mass of lump *i*
m_i^{calc}	Model computed yield of lump *i* in mass
m_i^{exp}	Experimental yield of lump *i* in mass
$m_{Plastic}$	Mass of plastic
m_{PO}	Mass of PO
m_{VGO}	Mass of VGO
$\bar{N}$	Stacking degree
n_B	Total number of micromoles of pyridine per gram of sample adsorbed at Brønsted sites
n_L	Total number of micromoles of pyridine per gram of sample adsorbed at Lewis sites
n_l	Number of lumps used in model
n_t	Total number of reaction times for all operating conditions
p(k,K)	Yield distribution function that determines the amount of formation of species of reactivity k
R	Universal gas constant
r	Mean catalyst particle radius
R1	Temperature ramp 1
R2	Temperature ramp 2
R3	Temperature ramp 3
S_0	
S_{BET}	BET surface area
S_F	Selectivity to fuel
S_{meso}	Mesoporous surface
S_{micro}	Microporous surface
t	Time
T	Temperature
T_{10}	Temperature at wich boils the the 10 wt% of the sample
T_{50}	Temperature at wich boils the the 50 wt% of the sample
T_{95}	Temperature at wich boils the the 95 wt% of the sample

T_m	Central reference temperature located in the middle range of the reaction temperatures used
T_{Max}	Temperature maxima
v	Corrector factor of viscosity
V_{micro}	Volume de micropore
V_{pore}	Pore volume
W	C/F ratio in the model lump
X_{HCO}	Conversion of HCO
X_{HDPE}	Conversion of HDPE
$X_{plastic}$	Conversion of plastic
X_{PP}	Conversion of PP
Y_{Coke}	Coke yield
Y_{Gas}	Gas yield
Y_{HCO}	HCO yield
Y_i	Yield of each lump
Y_{LCO}	LCO yield
$Y_{Naphtha}$	Naphtha yield
Y_{Wax}	Wax yield

Greek letters	**Columna1**
2θ	Angle between incident rays and disparity planes
α	Model parameter
C(θ,t)	Concentration distribution function corresponding to a normalized TBP
δ	Model parameter
ΔY_t	Extent of formation of each lump
θ	Normalized TBP
ε	Molar absorption coefficient
η_{ij}	Efficiency factor
λ	Wavelength of the X-ray source

v	Viscosity
ρ	Density
φ	Catalytic activity
Φ_{ij}	Thiele modulus

Abbreviations and acronyms

A	Aromatics
A_1	mono-Aromatics
A_2	di-Aromatics
A_{3+}	Polyaromatics
AR	Atmospheric Residue
ASA	Amorphous silica-alumina
ASTM	American Society for Testing and Materials
B/L	Brønsted-Lewis ratio
BET	Brunauer–Emmett–Teller
BJH	Barrett-Joyner-Halenda
BP	British Petroleum
bpd	Barrels per day
BTX	Benzene-Toluene-Xylene compounds
C/F	Catalyst to feed ratio
C/O	Carbon to oxygen ratio
CIS	Commonwealth International States
CSi	Carborundum or silicon carbide
CSTR	Continuous Stirred Tank Reactor
CW	Cold water
DG	Dry gas
DSC	Differentia scanning calorimetry
DTG	Weight Loss derivative
EOL	End of life
EU	European union

FAME	Free Fatty Acids Methyl Esters
FBP	Final boiling point
FCC	Fluid catalytic cracking
FFA	Free Fatty Acid
FID	Flame ionized detector
FTIR	Fourier-transform infrared spectroscopy
GC	Gas chromatographer
GHG	Greenhouse gases
H/C	Hydrogen to carbon ratio
HAADF	High angle annular dark field
HC	Hydrocarbons
HCO	Heavy cycle oil
HCV	Higher calorific value
HDA	Hydrodearomatization
HDM	Hydrodemetallization
HDN	Hydrodenitrogenation
HDO	Hydrodeoxigenation
HDPE	High density polyethilen
HDS	Hydrodesulfuration
HDT	Hydrotreating
HGO	Heavy Gas oil
HTL	Hydro-liquefaction
HT-STPO	Hydrotreated STPO
HW	Hot water
HYC	Hydrocracking
IBP	Initial boiling point
ICP-AES	Inductively coupled plasma atomic emission spectroscopy
IEA	International Energy Agency
i-P	iso-Paraffins
IR	Infrared
IUPAC	International union of pure and applied chemistry

LCO	Light cycle oil
LDPE	Low density polyethylene
LGO	Light Gas Oil
LHSV	Liquid Hourly Space Velocity
LLDPE	Linear low density polyethylene
LPG	Liquefied petroleum gases
MAT	Fixed bed microactivity type reactor
MD	Middle Distillate
MHYC	Mild Hydrocracking
MP	Micro-plastics
MS	Mass spectrometer
MSW	Municipal solid waste
MTPP	Metal-tetraphenylporphyrin
N	Naphthenes
NMR	Nuclear magnetic resonance
NP	Nano-plastics
n-P	normal-Paraffins
O	Olephins
ODE	Ordinary differential equations
PAHs	Polyaromatic hydrocarbons
PE	Polyethylene
PET	Polyethylene terephthalate
PIONA	n-paraffins, i-paraffins, olefins, naphthene and aromatics
PM	Solid particle
PNA	Paraffins/naphthenes/aromatics
PO	Pyrolysis Oil
PP	Polypropylene
ppm	Part per million
PPO	Plastic Pyrolysis Oil
PS	Polystyrene
PS-BD	Polyethylene-Butadiene

PVC	Polyvinyl chloride
RON	Research Octane Number
rpm	Revolutions per minute
SEM	Scanning electron microscope
Si/Al	Silica-Alumina ratio
SMSI	Strong metal-support interactions
SSE	Sum of squared of error
STEM	Scanning transmission electron microscopy
STP	Standard conditions of temperature and pressure
STPO	Scrap tire pyrolysis oil
TBP	True boiling point
TCD	Thermal conductivity detector
TEM	Transmission electron microscopy
TGA	Thermo gravimetric Analysis
Th	Thermal reaction
THF	Tetrahydrofurane
TOS	Time on stream
TPD	Temperature-programmed-desorption
TPO	Temperature programmed oxidation
TPO	Temperature programmed oxidation
TPR	Temperature programmed reduction
TWh	Terawatt-hours
UCS	Unit Cell size
$\overline{UCS}$	Average unit Cell size
ULSD	Ultra low sulfur diesel
US	United states
UV	Ultraviolet
VGO	Vacuum gasoil
VR	Vacuum residue

CHAPTER 10

REFERENCES

10 REFERENCES

[1] A. Gutierrez, Valorisation of aromatic streams by hydrocracking in a sustainable bio-refinery. Ph.D. dissertation., University of Basque Country, Bilbao, Spain, 2010.

[2] I. Hita, Valorization of Scrap Tires Pyrolysis Oil (STPO) through a 2-stage hydrotreating-hydrocraking strategy. Process variables and kinetic modeling, Tesis Doctoral, Universidad del País Vasco, Bilbao, 2015.

[3] R. Palos, Valorisation of secondary streams, tyres and plastics in the Waste-Refinery. Ph.D. Dissertations, (2018) 292.

[4] PEMRG Plastics Europe's Market Research and Statistics Group, Plastics - the Facts 2019. An Analysis of European Plastics Production, Demand and Waste Data, Brussels, 2019.

[5] G. Lopez, M. Artetxe, M. Amutio, J. Alvarez, J. Bilbao, M. Olazar, Recent advances in the gasification of waste plastics. A critical overview, Renew. Sustain. Energy Rev. 82 (2018) 576–596.

[6] R. Palos, A. Gutiérrez, F.J. Vela, M. Olazar, J.M. Arandes, J. Bilbao, Waste Refinery: The Valorization of Waste Plastics and End-of-Life Tires in Refinery Units. A Review, Energy and Fuels. 35 (2021) 3529–3557.

[7] P.-A. Enkvist, P. Klevnäs, The Circular Economy - A powerful force for climate mitigtaion, Material Economics, Sweden, 2018.

[8] A.L. Patrício Silva, J.C. Prata, T.R. Walker, A.C. Duarte, W. Ouyang, D. Barcelò, T. Rocha-Santos, Increased plastic pollution due to COVID-19 pandemic: Challenges and recommendations, Chem. Eng. J. 405 (2021) 126683.

[9] S. Perdan, Introduction to Sustainable Development, in: A. Azapagic, S. Perdan (Eds.), Sustain. Dev. Pract. Case Stud. Eng. Sci., 2nd ed., Wiley-Blackwell, Hoboken, NJ, USA, 2011: pp. 3–25.

[10] A.K. Panda, R.K. Singh, D.K. Mishra, Thermolysis of waste plastics to liquid fuel. A suitable method for plastic waste management and manufacture of value added products-A world prospective, Renew. Sustain. Energy Rev. 14 (2010) 233–248.

[11] R. Geyer, J.R. Jambeck, K.L. Law, Production, use, and fate of all plastics ever made, Sci. Adv. 3 (2017) 25–29.

[12] L. Hou, D. Kumar, C.G. Yoo, I. Gitsov, E.L.W. Majumder, Conversion and removal strategies for microplastics in wastewater treatment plants and landfills, Chem. Eng. J. 406 (2021) 126715.

[13] I.B. Jâms, F.M. Windsor, T. Poudevigne-Durance, S.J. Ormerod, I. Durance, Estimating the size distribution of plastics ingested by animals, Nat. Commun. 11 (2020) 1594.

[14] J.C. Prata, J.P. da Costa, I. Lopes, A.C. Duarte, T. Rocha-Santos, Environmental exposure to microplastics: An overview on possible human health effects, Sci. Total Environ. 702 (2020) 134455.

[15] Y. Zhou, J. Wang, M. Zou, Z. Jia, S. Zhou, Y. Li, Microplastics in soils: A review of methods, occurrence, fate, transport, ecological and environmental risks, Sci. Total Environ. 748 (2020) 141368.

[16] Y. Zhang, S. Pu, X. Lv, Y. Gao, L. Ge, Global trends and prospects in microplastics research: A bibliometric analysis, J. Hazard. Mater. 400 (2020) 123110.

[17] P. Oblak, J. Gonzalez-Gutierrez, B. Zupančič, A. Aulova, I. Emri, Processability and mechanical properties of extensively recycled high density polyethylene, Polym. Degrad. Stab. 114 (2015) 133–145.

[18] R.U. Cook, C. R.; Halden, Ecological and Health Issues of Plastic WasteEcological and Health Issues of Plastic Waste, in: Plast. Waste Recycl., Elsevier, 2020: pp. 513–527.

[19] M. Tsakona, I. Rucevska, Plastic Waste partnership working group, Plastic Waste Background Report, Sychelles, 2020.

[20] G. Lopez, M. Artetxe, M. Amutio, J. Bilbao, M. Olazar, Thermochemical routes for the valorization of waste polyole fi nic plastics to produce fuels and chemicals . A review, Renew. Sustain. Energy Rev. 73 (2017) 346–368.

[21] D. Munir, M.F. Irfan, M.R. Usman, Hydrocracking of virgin and waste plastics: A detailed review, Renew. Sustain. Energy Rev. 90 (2018) 490–515.

[22] R.G. Santos, W. Loh, A.C. Bannwart, O. V. Trevisan, An overview of heavy oil properties and its recovery and transportation methods, Brazilian J. Chem. Eng. 31 (2014) 571–590.

[23] J.G. Speight, The Refinery of the Future, Elsevier Inc., 2011.

[24] J.H. Gary, J.H. Handwerk, M.J. Kaiser, D. Geddes, Petroleum Refining:

Technology and Economics, Fifth Edition, CRC Press. (2007).

[25] M.A. Fahim, T.A. Alsahhaf, A. Elkilani, Refinery Feedstocks and Products. Fundamentals of Petroleum Refining, Elsevier, Amsterdam, 2010.

[26] J. Ancheyta, G. Betancourt, G. Marroquín, G. Centeno, L.C. Castañeda, F. Alonso, J.A. Muñoz, M.T. Gómez, P. Rayo, Hydroprocessing of Maya heavy crude oil in two reaction stages, Appl. Catal. A. 233 (2002) 159–170.

[27] E. Lazzaroni, M. Elsholkami, E. Martelli, A. Elkamel, Design and simulation of a petcoke gasification polygeneration plant integrated with a bitumen extraction and upgrading facility and net energy analysis, Energy. 141 (2017) 880–891.

[28] International Energy Agency, World oil supply and demand, 1971-2018, Int. Energy Agency. (2020). https://www.iea.org/data-and-statistics/charts/world-oil-supply-and-demand-1971-2019 (accessed July 22, 2021).

[29] Our world in data, Oil consumption- Report 2020, Univ. Oxford. (2020). https://ourworldindata.org/grapher/oil-consumption-by-country?country=OWID_WRL~CHN (accessed July 22, 2021).

[30] BP, BP statistical review of world energy, London, 2020. www.bp.com/statisticalreview. (accessed August 31, 2021).

[31] BP, Statistical Review of World Energy 2021 – Full report, London. (2021).

[32] International Energy Agency, Oil 2021 - Analysis and forecast to 2026, 2021. www.iea.org/t&c/ (accessed July 22, 2021).

[33] J.W. Day, C.A. Hall, A. Yáñez-Arancibia, D. Pimentel, C.I. Martí, W.J. Mitsch, Ecology in times of scarcity, Bioscience. 59 (2009) 321–331.

[34] A. Stratas, Seven countries move up in top 100 ranking on Diesel sulfur limits | Stratas Advisors, 2021. https://stratasadvisors.com/insights/2019/022819-top-100-diesel-sulfur-ranking.

[35] N. Hooftman, M. Messagie, J. Van Mierlo, T. Coosemans, A review of the European passenger car regulations – Real driving emissions vs local air quality, Renew. Sustain. Energy Rev. 86 (2018) 1–21.

[36] S. Venkata Mohan, Reorienting Waste Remediation Towards

Harnessing Bioenergy: A Paradigm Shift, in: Ind. Wastewater Treat. Recycl. Reuse, Butterworth-Heinemann, 2014: pp. 235–281.

[37] S. Venkata Mohan, Sustainable waste remediation: A paradigm shift towards environmental biorefinery, Chem. Eng. World. 49 (2014) 32–40.

[38] K. Saidi, A. Omri, Reducing CO2 emissions in OECD countries: Do renewable and nuclear energy matter?, Prog. Nucl. Energy. 126 (2020) 103425.

[39] Q. ul A. Ali, U. Khayyam, U. Nazar, Energy production and CO2 emissions: The case of coal fired power plants under China Pakistan economic corridor, J. Clean. Prod. 281 (2021) 124974.

[40] T. Kandaramath Hari, Z. Yaakob, N.N. Binitha, Aviation biofuel from renewable resources: Routes, opportunities and challenges, Renew. Sustain. Energy Rev. 42 (2015) 1234–1244.

[41] K.R. Choi, S. Jiao, S.Y. Lee, Metabolic engineering strategies toward production of biofuels, Curr. Opin. Chem. Biol. 59 (2020) 1–14.

[42] A.S. Silitonga, H.H. Masjuki, H.C. Ong, A.H. Sebayang, S. Dharma, F. Kusumo, J. Siswantoro, J. Milano, K. Daud, T.M.I. Mahlia, W.H. Chen, B. Sugiyanto, Evaluation of the engine performance and exhaust emissions of biodiesel-bioethanol-diesel blends using kernel-based extreme learning machine, Energy. 159 (2018) 1075–1087.

[43] B.H. Diya'Uddeen, A.R. Abdul Aziz, W.M.A.W. Daud, M.H. Chakrabarti, Performance evaluation of biodiesel from used domestic waste oils: A review, Process Saf. Environ. Prot. 90 (2012) 164–179.

[44] P.K. Swain, L.M. Das, S.N. Naik, Biomass to liquid: A prospective challenge to research and development in 21st century, Renew. Sustain. Energy Rev. 15 (2011) 4917–4933.

[45] D. Sági, P. Baladincz, Z. Varga, J. Hancsók, Co-processing of FCC light cycle oil and waste animal fats with straight run gas oil fraction, J. Clean. Prod. 111 (2016) 34–41.

[46] J. Milano, H.C. Ong, H.H. Masjuki, A.S. Silitonga, W.H. Chen, F. Kusumo, S. Dharma, A.H. Sebayang, Optimization of biodiesel production by microwave irradiation-assisted transesterification for waste cooking oil-Calophyllum inophyllum oil via response surface methodology, Energy Convers. Manag. 158 (2018) 400–415.

[47] H. Mazaheri, H.C. Ong, H.H. Masjuki, Z. Amini, M.D. Harrison, C.T.

Wang, F. Kusumo, A. Alwi, Rice bran oil based biodiesel production using calcium oxide catalyst derived from Chicoreus brunneus shell, Energy. 144 (2018) 10–19.

[48] R.A. Lee, J.-M. Lavoie, From first- to third-generation biofuels: Challenges of producing a commodity from a biomass of increasing complexity, Anim. Front. 3 (2013) 6–11.

[49] B. Kamm, Introduction of Biomass and Biorefineries, Hoboken, 2012. https://onlinelibrary.wiley.com/doi/full/10.1002/9781118449400.ch1 (accessed August 31, 2021).

[50] J. Littlejohns, L. Rehmann, R. Murdy, A. Oo, S. Neill, Current state and future prospects for liquid biofuels in Canada, Biofuel Res. J. 5 (2018) 759–779.

[51] A.V. V. Bridgwater, Renewable fuels and chemicals by thermal processing of biomass, Chem. Eng. J. 91 (2003) 87–102.

[52] Q. Fu, H. Xie, D.S. Argyropoulos, Pyrolysis Oils from Biomass and Their Upgrading, Hoboken, 2012. https://onlinelibrary.wiley.com/doi/full/10.1002/9781118449400.ch8 (accessed August 31, 2021).

[53] M. Amutio, G. Lopez, M. Artetxe, G. Elordi, M. Olazar, J. Bilbao, Influence of temperature on biomass pyrolysis in a conical spouted bed reactor, Resour. Conserv. Recycl. 59 (2012) 23–31.

[54] J. Makibar, A.R. Fernandez-Akarregi, M. Amutio, G. Lopez, M. Olazar, Performance of a conical spouted bed pilot plant for bio-oil production by poplar flash pyrolysis, Fuel Process. Technol. 137 (2015) 283–289.

[55] A.V. V. Bridgwater, G. Grassi, Review of fast pyrolysis of biomass and product upgrading, Biomass and Bioenergy. 38 (2012) 68–94.

[56] Y. Makarfi Isa, E.T. Ganda, Bio-oil as a potential source of petroleum range fuels, Renew. Sustain. Energy Rev. 81 (2018) 69–75.

[57] K.D. Maher, D.C. Bressler, Pyrolysis of triglyceride materials for the production of renewable fuels and chemicals, Bioresour. Technol. 98 (2007) 2351–2368.

[58] A.E. Pütün, Ö.M. Koçkar, S. Yorgun, H.F. Gerçel, J. Andresen, C.E. Snape, E. Pütün, Fixed-bed pyrolysis and hydropyrolysis of sunflower bagasse: Product yields and compositions, Fuel Process. Technol. 46 (1996) 49–62.

[59] S. Bezergianni, A. Dimitriadis, O. Kikhtyanin, D. Kubička, Refinery co-processing of renewable feeds, Prog. Energy Combust. Sci. 68 (2018) 29–64.

[60] S. van Dyk, J. Su, J.D. Mcmillan, J. (John) Saddler, Potential synergies of drop-in biofuel production with further co-processing at oil refineries, Biofuels, Bioprod. Biorefining. 13 (2019) 760–775.

[61] I. Hita, J.M. Arandes, J. Bilbao, Upgrading of bio-oil via fluid catalytic cracking, in: Chem. Catal. Biomass Upgrad., John Wiley & Sons, Ltd, 2019: pp. 61–96.

[62] Á. Ibarra, E. Rodríguez, U. Sedran, J.M. Arandes, J. Bilbao, Synergy in the Cracking of a Blend of Bio-oil and Vacuum Gasoil under Fluid Catalytic Cracking Conditions, 55 (2016) 1872–1880. https://pubs.acs.org/doi/abs/10.1021/acs.iecr.5b04502 (accessed August 31, 2021).

[63] Á. Ibarra, I. Hita, M.J. Azkoiti, J.M. Arandes, J. Bilbao, Catalytic cracking of raw bio-oil under FCC unit conditions over different zeolite-based catalysts, J. Ind. Eng. Chem. 78 (2019) 372–382.

[64] Á. Ibarra, I. Hita, J.M. Arandes, J. Bilbao, Influence of the Composition of Raw Bio-Oils on Their Valorization in Fluid Catalytic Cracking Conditions, Energy & Fuels. 33 (2019) 7458–7465.

[65] Á. Ibarra, R. Palos, J.M. Arandes, M. Olazar, J. Bilbao, H. de Lasa, Synergy in the Cocracking under FCC Conditions of a Phenolic Compound in the Bio-oil and a Model Compound for Vacuum Gasoil, Ind. Eng. Chem. Res. 59 (2020) 8145–8154.

[66] Á. Ibarra, I. Hita, J.M. Arandes, J. Bilbao, A Hybrid FCC/HZSM-5 Catalyst for the Catalytic Cracking of a VGO/Bio-Oil Blend in FCC Conditions, Catal. 2020, Vol. 10, Page 1157. 10 (2020) 1157.

[67] F.A.A. Twaiq, A.R. Mohamad, S. Bhatia, Performance of composite catalysts in palm oil cracking for the production of liquid fuels and chemicals, Fuel Process. Technol. 85 (2004) 1283–1300.

[68] L.T.H. Nam, T.Q. Vinh, N.T.T. Loan, V.D.S. Tho, X.Y. Yang, B.L. Su, Preparation of bio-fuels by catalytic cracking reaction of vegetable oil sludge, Fuel. 90 (2011) 1069–1075.

[69] C.M.R. Prado, N.R. Antoniosi Filho, Production and characterization of the biofuels obtained by thermal cracking and thermal catalytic cracking of vegetable oils, J. Anal. Appl. Pyrolysis. 86 (2009) 338–347.

[70] J. Xu, J. Jiang, J. Chen, Y. Sun, Biofuel production from catalytic cracking of woody oils, Bioresour. Technol. 101 (2010) 5586–5591.

[71] C. Kordulis, K. Bourikas, M. Gousi, E. Kordouli, A. Lycourghiotis, Development of nickel based catalysts for the transformation of natural triglycerides and related compounds into green diesel: a critical review, Appl. Catal. B Environ. 181 (2016) 156–196.

[72] C.S. Freeman Jones AB Padmaperuma M Santosa C Valkenburg J Shinn, Initial Assessment of U.S. Refineries for Purposes of Potential Bio-Based Oil Insertions, (2013). http://www.ntis.gov/ordering.htm (accessed August 31, 2021).

[73] A. Corma, L. Sauvanaud, FCC testing at bench scale: New units, new processes, new feeds, Catal. Today. 218–219 (2013) 107–114.

[74] M.S. Talmadge, R.M. Baldwin, M.J. Biddy, R.L. McCormick, G.T. Beckham, G.A. Ferguson, S. Czernik, K.A. Magrini-Bair, T.D. Foust, P.D. Metelski, C. Hetrick, M.R. Nimlos, A perspective on oxygenated species in the refinery integration of pyrolysis oil, Green Chem. 16 (2014) 407–453.

[75] M. Bertero, U. Sedran, Upgrading of bio-oils over equilibrium FCC catalysts. Contribution from alcohols, phenols and aromatic ethers, Catal. Today. 212 (2013) 10–15.

[76] D.V.D.V. Naik, V. Kumar, B. Prasad, B. Behera, N. Atheya, K.K. Singh, D.K. Adhikari, M.O. Garg, Catalytic cracking of pyrolysis oil oxygenates (aliphatic and aromatic) with vacuum gas oil and their characterization, Chem. Eng. Res. Des. 92 (2014) 1579–1590.

[77] Á. Ibarra, A. Veloso, J. Bilbao, J.M. Arandes, P. Castaño, Dual coke deactivation pathways during the catalytic cracking of raw bio-oil and vacuum gasoil in FCC conditions, Appl. Catal. B Environ. 182 (2016) 336–346.

[78] D.S.J. Jones, P.P. Pujadó, Handbook of Petroleum Processing, Springer Netherlands, Dordrecht, Netherland, 2006.

[79] R.G. Egeberg, N.H. Michaelsen, L. Skyum, Novel hydrotreating technology for production of green diesel, Haldor Topsoe. (2010) 1–21. http://www.topsoe.com/business_areas/refining/~/media/PDF files/Refining/novel_hydrotreating_technology_for_production_of_green_diesel.ashx (accessed August 31, 2021).

[80] G.E.L. and E.K. Egeberg R., Knudsen K., Nyström S., Industrial-scale production of renewable diesel, Pet Technol Q. 16 (2011) 59–65.

[81] M. Al-Sabawi, J. Chen, S. Ng, Fluid Catalytic Cracking of Biomass-Derived Oils and Their Blends with Petroleum Feedstocks: A Review, Energy and Fuels. 26 (2012) 5355–5372.

[82] F. Obeid, T. Chu Van, R. Brown, T. Rainey, Nitrogen and sulphur in algal biocrude: A review of the HTL process, upgrading, engine performance and emissions, Energy Convers. Manag. 181 (2019) 105–119.

[83] G. Ramya, T. Sivakumar, M. Arif, Z. Ahmed, Application of Microporous Catalysts in the Production of Biofuels from Non Edible Vegetable Oils and Used Restaurant Oil, Energy Sources, Part A Recover. Util. Environ. Eff. 37 (2015) 878–885.

[84] R.O. Idem, S.P.R. Katikaneni, N.N. Bakhshi, Catalytic conversion of canola oil to fuels and chemicals: roles of catalyst acidity, basicity and shape selectivity on product distribution, Fuel Process. Technol. 51 (1997) 101–125.

[85] X. Zhao, L. Wei, S. Cheng, Y. Huang, Y. Yu, J. Julson, Catalytic cracking of camelina oil for hydrocarbon biofuel over ZSM-5-Zn catalyst, Fuel Process. Technol. 139 (2015) 117–126.

[86] S. Cheng, L. Wei, X. Zhao, J. Julson, Application, Deactivation, and Regeneration of Heterogeneous Catalysts in Bio-Oil Upgrading, 6 (2016). https://www.mdpi.com/2073-4344/6/12/195/htm (accessed August 31, 2021).

[87] J. Chen, H. Farooqi, C. Fairbridge, Experimental Study on Co-hydroprocessing Canola Oil and Heavy Vacuum Gas Oil Blends, Energy and Fuels. 27 (2013) 3306–3315.

[88] I. Kubičková, D. Kubička, Utilization of Triglycerides and Related Feedstocks for Production of Clean Hydrocarbon Fuels and Petrochemicals: A Review, Waste Biomass Valorization 2010 13. 1 (2010) 293–308.

[89] C. Tóth, P. Baladincz, J. Hancsók, Production of bio gas oil containing diesel fuel with upgraded cold flow properties by co-processing, in: Chem. Eng. Trans., 2012: pp. 613–618.

[90] T.M. Sankaranarayanan, M. Banu, A. Pandurangan, S. Sivasanker, Hydroprocessing of sunflower oil–gas oil blends over sulfided Ni–Mo–Al–zeolite beta composites, Bioresour. Technol. 102 (2011) 10717–10723.

[91] Z. Eller, A. Holló, J. Hancsók, Production of Low Reduced Aromatic

Jet Fuel from Sunflower Oil - Kerosene Mixture, Eur. Biomass Conf. Exhib. Proc. (2012) 1786–1791.

[92] D. Sági, A. Holló, G. Varga, J. Hancsók, Co-hydrogenation of fatty acid by-products and different gas oil fractions, J. Clean. Prod. 161 (2017) 1352–1359.

[93] S. Bezergianni, A. Dimitriadis, Temperature effect on co-hydroprocessing of heavy gas oil–waste cooking oil mixtures for hybrid diesel production, Fuel. 103 (2013) 579–584.

[94] A. Dimitriadis, S. Bezergianni, Co-hydroprocessing gas-oil with residual lipids: effect of residence time and H2/Oil ratio, J. Clean. Prod. 131 (2016) 321–326.

[95] P. Baladincz, J. Hancsók, Fuel from waste animal fats, Chem. Eng. J. 282 (2015) 152–160.

[96] K. Fan, J. Liu, X. Yang, L. Rong, Hydrocracking of Jatropha oil over Ni-H3PW12O40/nano-hydroxyapatite catalyst, Int. J. Hydrogen Energy. 39 (2014) 3690–3697.

[97] E.D. Bruce, R. Frety, C.M. Teixeira, C.B.M. Barbosa, J.G.A. Pacheco, Thermocatalytic cracking kinetics of myristic acid adsorbed on catalysts with different acidity, Catal. Today. 289 (2017) 280–288.

[98] T. Li, J. Cheng, R. Huang, J. Zhou, K. Cen, Conversion pathways of palm oil into jet biofuel catalyzed by mesoporous zeolites, RSC Adv. 6 (2016) 103965–103972.

[99] T. Ahmad, D. Zhang, A critical review of comparative global historical energy consumption and future demand: The story told so far, Energy Reports. 6 (2020) 1973–1991.

[100] G. Jiménez-García, R. Aguilar-López, R. Maya-Yescas, The fluidized-bed catalytic cracking unit building its future environment, Fuel. 90 (2011) 3531–3541.

[101] I.S. Tiscornia, G. de la Puente, U. Sedran, Recycling of Low-Value Hydrocarbon Cuts by Means of Multiple Injections to FCC Units, Ind. Eng. Chem. Res. 41 (2002) 5976–5982.

[102] A. Corma, F. Melo, L. Sauvanaud, F. Ortega, Different process schemes for converting light straight run and fluid catalytic cracking naphthas in a FCC unit for maximum propylene production, Appl. Catal. A-General - APPL CATAL A-GEN. 265 (2004) 195–206.

[103] R. Palos, A. Gutiérrez, M.L. Fernández, D. Trueba, J. Bilbao, J.M. Arandes, Upgrading of heavy coker naphtha by means of catalytic cracking in refinery FCC unit, Fuel Process. Technol. 205 (2020) 106454.

[104] R. Palos, A. Gutiérrez, M.L. Fernández, M.J. Azkoiti, J. Bilbao, J.M. Arandes, Taking advantage of the excess of thermal naphthas to enhance the quality of FCC unit products, J. Anal. Appl. Pyrolysis. 152 (2020).

[105] R. Palos, A. Gutiérrez, M.L. Fernández, M.J. Azkoiti, J. Bilbao, J.M. Arandes, Converting the Surplus of Low-Quality Naphtha into More Valuable Products by Feeding It to a Fluid Catalytic Cracking Unit, Ind. Eng. Chem. Res. 59 (2020) 16868–16875.

[106] A. Gutiérrez, P. Castaño, M.J.M.J. Azkoiti, J. Bilbao, J.M.J.M. Arandes, Modelling product distribution of pyrolysis gasoline hydroprocessing on a Pt-Pd/HZSM-5 catalyst, Chem. Eng. J. 176–177 (2011) 302–311.

[107] A. Gutiérrez, J.M.J.M. Arandes, P. Castaño, A.T.A.T. Aguayo, J. Bilbao, Role of acidity in the deactivation and steady hydroconversion of light cycle oil on noble metal supported catalysts, Energy and Fuels. 25 (2011) 3389–3399.

[108] P. Castaño, A. Gutiérrez, I. Hita, J.M. Arandes, A.T. Aguayo, J. Bilbao, Deactivating species deposited on Pt-Pd catalysts in the hydrocracking of light-cycle oil, Energy and Fuels. 26 (2012) 1509–1519.

[109] R. Palos, A. Gutiérrez, I. Hita, P. Castaño, J.W. Thybaut, J.M. Arandes, J. Bilbao, Kinetic Modeling of Hydrotreating for Enhanced Upgrading of Light Cycle Oil, Ind. Eng. Chem. Res. 58 (2019) 13064–13075.

[110] G.C. Laredo, P. Pérez-Romo, J. Escobar, J.L. Garcia-Gutierrez, P.M. Vega-Merino, Light Cycle Oil Upgrading to Benzene, Toluene, and Xylenes by Hydrocracking: Studies Using Model Mixtures, 56 (2017) 10939–10948. https://pubs.acs.org/doi/abs/10.1021/acs.iecr.7b02827 (accessed July 25, 2021).

[111] R. Aguado, M. Olazar, San José María J., B. Gaisán, J. Bilbao, Wax Formation in the Pyrolysis of Polyolefins in a Conical Spouted Bed Reactor, Energy & Fuels. 16 (2002) 1429–1437.

[112] G. Lopez, J. Alvarez, M. Amutio, N.M. Mkhize, B. Danon, P. van der Gryp, J.F. Görgens, J. Bilbao, M. Olazar, Waste truck-tyre processing by flash pyrolysis in a conical spouted bed reactor, Energy Convers. Manag. 142 (2017) 523–532.

[113] Eurostat, Energy Production and Imports, Brussels. (2020).

https://ec.europa.eu/eurostat/statistics-explained/index.php?title=Energy_production_and_imports#Production_of_primary_energy_decreased_between_2009_and_2019 (accessed September 6, 2021).

[114] J. Weitkamp, Catalytic Hydrocracking-Mechanisms and Versatility of the Process, ChemCatChem. 4 (2012) 292–306.

[115] A. Gala, D. Catalán-Martínez, M. Guerrero, J.M. Serra, Simulation-assisted design of a catalytic hydrogenation reactor for plastic pyrolysis fuels, Fuel. 287 (2021) 119400.

[116] C. Marcilly, Evolution of Refining and Petrochemicals: What Is the Place of Zeolites, Oil {&} Gas Sci. Technol. 56 (2001) 499–514.

[117] S.H. Ng, Conversion of Polyethylene Blended with VGO to Transportation Fuels by Catalytic Cracking, Energy and Fuels. 9 (1995) 216–224.

[118] J.M. Arandes, I. Abajo, D. López-Valerio, I. Fernández, M.J. Azkoiti, M. Olazar, J. Bilbao, Transformation of Several Plastic Wastes into Fuels by Catalytic Cracking, Ind. Eng. Chem. Res. 36 (1997) 4523–4529.

[119] F.J. Passamonti, U. Sedran, Recycling of waste plastics into fuels. LDPE conversion in FCC, Appl. Catal. B Environ. 125 (2012) 499–506.

[120] J.M. Arandes, J. Ereña, J. Bilbao, D. López-Valerio, G. De la Puente, Valorization of the blends polystyrene/light cycle oil and polystyrene-butadiene/light cycle oil over HZSM-5 zeolites, Ind. Eng. Chem. Res. 42 (2003) 3700–3710.

[121] J.M. Arandes, J. Ereñea, M. Olazar, J. Bilbao, G. De la Puente, Valorization of the blends polystyrene/light cycle oil and polystyrene-butadiene/light cycle oil over different HY zeolites under FCC unit conditions, Energy and Fuels. 18 (2004) 218–227.

[122] A. Marcilla, M. del R. Hernández, Á.N. García, Degradation of LDPE/VGO mixtures to fuels using a FCC equilibrium catalyst in a sand fluidized bed reactor, Appl. Catal. A Gen. 341 (2008) 181–191.

[123] A.O. Odjo, A.N. García, A. Marcilla, Conversion of low density polyethylene into fuel through co-processing with vacuum gas oil in a fluid catalytic cracking riser reactor, Fuel Process. Technol. 113 (2013) 130–140.

[124] A.O. Odjo, A.N. García, A. Marcilla, Refinery nonconventional feedstocks: Influence of the coprocessing of vacuum gas oil and low

density polyethylene in fluid catalytic cracking unit on full range gasoline composition, Energy and Fuels. 28 (2014) 1579–1593.

[125] E. Rodríguez, A. Gutiérrez, R. Palos, F.J. Vela, M.J. Azkoiti, J.M. Arandes, J. Bilbao, Co-cracking of high-density polyethylene (HDPE) and vacuum gasoil (VGO) under refinery conditions, Chem. Eng. J. 382 (2020) 122602.

[126] D. Iribarren, J. Dufour, D.P. Serrano, Preliminary assessment of plastic waste valorization via sequential pyrolysis and catalytic reforming, J. Mater. Cycles Waste Manag. 14 (2012) 301–307.

[127] E. Rodríguez, A. Gutiérrez, R. Palos, F.J. Vela, J.M. Arandes, J. Bilbao, Fuel production by cracking of polyolefins pyrolysis waxes under fluid catalytic cracking (FCC) operating conditions, 93 (2019) 162–172.

[128] E. Rodríguez, R. Palos, A. Gutiérrez, F.J. Vela, J.M.J.M. Arandes, J. Bilbao, E. Rodr, R. Palos, A. Gutie, E. Rodríguez, R. Palos, A. Gutiérrez, F.J. Vela, J.M.J.M. Arandes, J. Bilbao, E ff ect of the FCC Equilibrium Catalyst Properties and of the Cracking Temperature on the Production of Fuel from HDPE Pyrolysis Waxes, Energy & Fuels. 33 (2019) 5191–5199.

[129] P. Lovás, P. Hudec, B. Jambor, E. Hájeková, M. Horňáček, Catalytic cracking of heavy fractions from the pyrolysis of waste HDPE and PP, Fuel. 203 (2017) 244–252.

[130] E. Rodríguez, R. Palos, A. Gutiérrez, D. Trueba, J.M. Arandes, J. Bilbao, Towards waste refinery: Co-feeding HDPE pyrolysis waxes with VGO into the catalytic cracking unit, Energy Convers. Manag. 207 (2020) 112554.

[131] E. Rodríguez, A. Gutiérrez, R. Palos, M.J. Azkoiti, J.M. Arandes, J. Bilbao, Cracking of Scrap Tires Pyrolysis Oil in a Fluidized Bed Reactor under Catalytic Cracking Unit Conditions. Effects of Operating Conditions, Energy and Fuels. 33 (2019) 3133–3143.

[132] E. Rodríguez, R. Palos, A. Gutiérrez, J.M. Arandes, J. Bilbao, Production of Non-Conventional Fuels by Catalytic Cracking of Scrap Tires Pyrolysis Oil, Ind. Eng. Chem. Res. 58 (2019) 5158–5167.

[133] E. Rodríguez, R. Palos, A. Gutiérrez, J.M. Arandes, J. Bilbao, Scrap tires pyrolysis oil as a co-feeding stream on the catalytic cracking of vacuum gasoil under fluid catalytic cracking conditions, Waste Manag. 105 (2020) 18–26.

[134] E. Rodríguez, S. Izaddoust, J. Valecillos, J. Bilbao, J.M. Arandes, P.

Castaño, E. Epelde, G. Elordi, Lessening coke formation and boosting gasoline yield by incorporating scrap tire pyrolysis oil in the cracking conditions of an FCC unit, Energy Convers. Manag. 224 (2020) 113327.

[135] R. Sahu, B.J. Song, J.S. Im, Y.-P.P. Jeon, C.W. Lee, A review of recent advances in catalytic hydrocracking of heavy residues, J. Ind. Eng. Chem. 27 (2015) 12–24.

[136] S. Suganuma, N. Katada, Innovation of catalytic technology for upgrading of crude oil in petroleum refinery, Fuel Process. Technol. 208 (2020) 106518.

[137] A. Gruia, Recent Advances in Hydrocracking, Pract. Adv. Pet. Process. (2006) 219–255.

[138] B. Viswanathan, Petroleum, Energy Sources. (2017) 29–57.

[139] A. Gutiérrez, J.M. Arandes, P. Castaño, M. Olazar, J. Bilbao, Preliminary studies on fuel production through LCO hydrocracking on noble-metal supported catalysts, Fuel. 94 (2012) 504–515.

[140] A. Gutiérrez, J.M. Arandes, P. Castaño, M. Olazar, A. Barona, J. Bilbao, Effect of Temperature in Hydrocracking of Light Cycle Oil on a Noble Metal-Supported Catalyst for Fuel Production, Chem. Eng. Technol. 35 (2012) 653–660.

[141] A. Gutiérrez, J.M. Arandes, P. Castaño, M. Olazar, J. Bilbao, Effect of pressure on the hydrocracking of light cycle oil with a Pt-Pd/HY catalyst, Energy and Fuels. 26 (2012) 5897–5904.

[142] A. Gutiérrez, J.M. Arandes, P. Castaño, M. Olazar, A. Barona, J. Bilbao, Effect of space velocity on the hydrocracking of Light Cycle Oil over a Pt-Pd/HY zeolite catalyst, Fuel Process. Technol. 95 (2012) 8–15.

[143] A. Gutiérrez, J.M. Arandes, P. Castaño, A.T. Aguayo, J. Bilbao, Influence of the support on the deactivation of bifunctional catalysts (Pt-Pd/support) in the hydrocracking of LCO, in: Chem. Eng. Trans., Italian Association of Chemical Engineering - AIDIC, 2011: pp. 97–102.

[144] I. Hita, A. Gutiérrez, M. Olazar, J. Bilbao, J.M. Arandes, P. Castaño, Upgrading model compounds and Scrap Tires Pyrolysis Oil (STPO) on hydrotreating NiMo catalysts with tailored supports, Fuel. 145 (2015) 158–169.

[145] I. Hita, A.T. Aguayo, M. Olazar, M.J. Azkoiti, J. Bilbao, J.M. Arandes, P. Castaño, Kinetic Modeling of the Hydrotreating and Hydrocracking Stages for Upgrading Scrap Tires Pyrolysis Oil (STPO) toward High-

Quality Fuels, Energy and Fuels. 29 (2015) 7542–7553.

[146] R. Palos, T. Kekäläinen, F. Duodu, A. Gutiérrez, J.M. Arandes, J. Jänis, P. Castaño, Screening hydrotreating catalysts for the valorization of a light cycle oil/scrap tires oil blend based on a detailed product analysis, Appl. Catal. B Environ. 256 (2019) 117863.

[147] I. Hita, T. Cordero-Lanzac, G. Bonura, C. Cannilla, J.M. Arandes, F. Frusteri, J. Bilbao, Hydrodeoxygenation of raw bio-oil towards platform chemicals over FeMoP/zeolite catalysts, J. Ind. Eng. Chem. 80 (2019) 392–400.

[148] I. Hita, T. Cordero-Lanzac, F.J. García-Mateos, M.J. Azkoiti, J. Rodríguez-Mirasol, T. Cordero, J. Bilbao, Enhanced production of phenolics and aromatics from raw bio-oil using HZSM-5 zeolite additives for PtPd/C and NiW/C catalysts, Appl. Catal. B Environ. 259 (2019).

[149] R. Palos, A. Gutiérrez, J.M. Arandes, J. Bilbao, Catalyst used in fluid catalytic cracking (FCC) unit as a support of NiMoP catalyst for light cycle oil hydroprocessing, Fuel. 216 (2018) 142–152.

[150] I. Hita, E. Rodríguez, M. Olazar, J. Bilbao, J.M. Arandes, P. Castaño, Prospects for Obtaining High Quality Fuels from the Hydrocracking of a Hydrotreated Scrap Tires Pyrolysis Oil, Energy & Fuels. 29 (2015) 5458–5466.

[151] H.K. Joo, C.W. Curtis, Catalytic coprocessing of plastics with coal and petroleum resid using NiMo/Al2O3, Energy and Fuels. 10 (1996) 603–611.

[152] S. Karagöz, J. Yanik, S. Uçar, C. Song, Catalytic coprocessing of low-density polyethylene with VGO using metal supported on activated carbon, Energy and Fuels. 16 (2002) 1301–1304.

[153] S. Karagöz, J. Yanik, S. Uçar, M. Saglam, C. Song, Catalytic and thermal degradation of high-density polyethylene in vacuum gas oil over non-acidic and acidic catalysts, Appl. Catal. A Gen. 242 (2003) 51–62.

[154] M.N. Siddiqui, H.H. Redhwi, Catalytic coprocessing of waste plastics and petroleum residue into liquid fuel oils, J. Anal. Appl. Pyrolysis. 86 (2009) 141–147.

[155] K. Kohli, R. Prajapati, S.K. Maity, B.K. Sharma, Hydrocracking of heavy crude/residues with waste plastic, J. Anal. Appl. Pyrolysis. 140 (2019) 179–187.

[156] R. Palos, A. Gutiérrez, J.M.J.M. Arandes, J. Bilbao, Upgrading of high-density polyethylene and light cycle oil mixtures to fuels via hydroprocessing, Catal. Today. 305 (2018) 212–219.

[157] A. Gruia, Distillate hydrocracking, in: Handb. Pet. Process., 2006: pp. 287–320.

[158] F.S. Mederos, J. Ancheyta, I. Elizalde, Dynamic modeling and simulation of hydrotreating of gas oil obtained from heavy crude oil, Appl. Catal. A Gen. 425–426 (2012) 13–27.

[159] P.R. Robinson, G.E. Dolbear, Hydrotreating and Hydrocracking: Fundamentals, in: Pract. Adv. Pet. Process., Springer New York, 2007: pp. 177–218.

[160] J.G. Speight, Upgrading Heavy Oil, in: Enhanc. Recover. Methods Heavy Oil Tar Sands, Elsevier, 2009: pp. 261–294.

[161] J. Uchytil, E. Jakubíčková, M. Kraus, Hydrogenation of alkenes over a cobalt-molybdenum-alumina catalyst, J. Catal. 64 (1980) 143–149.

[162] D. Valencia, L. Peña, I. García-Cruz, Reaction mechanism of hydrogenation and direct desulfurization routes of dibenzothiophene-like compounds: A density functional theory study, Int. J. Quantum Chem. 112 (2012) 3599–3605.

[163] T.E. Klimova, D. Valencia, J.A. Mendoza-Nieto, P. Hernández-Hipólito, Behavior of NiMo/SBA-15 catalysts prepared with citric acid in simultaneous hydrodesulfurization of dibenzothiophene and 4,6-dimethyldibenzothiophene, J. Catal. 304 (2013) 29–46.

[164] D.A. Solís-Casados, A.L. Agudo, J. Ramírez, T. Klimova, Hydrodesulfurization of hindered dibenzothiophenes on bifunctional NiMo catalysts supported on zeolite–alumina composites, Catal. Today. 116 (2006) 469–477.

[165] D. Valencia, T. Klimova, Kinetic study of NiMo/SBA-15 catalysts prepared with citric acid in hydrodesulfurization of dibenzothiophene, Catal. Commun. 21 (2012) 77–81.

[166] L. Peña, D. Valencia, T. Klimova, CoMo/SBA-15 catalysts prepared with EDTA and citric acid and their performance in hydrodesulfurization of dibenzothiophene, Appl. Catal. B Environ. 147 (2014) 879–887.

[167] M.E.E. Abashar, Investigation of coupling dehydrogenation and hydrogenation reactions in a fixed bed catalytic reactor with well-

mixed catalyst pattern, J. Saudi Chem. Soc. 17 (2013) 181–189.

[168] E. Furimsky, F.E. Massoth, Hydrodenitrogenation of Petroleum, Catal. Rev. 47 (2005) 297–489.

[169] S. Hu, G. Luo, T. Shima, Y. Luo, Z. Hou, Hydrodenitrogenation of pyridines and quinolines at a multinuclear titanium hydride framework, Nat. Commun. 8 (2017) 1866.

[170] Z.X. Giustra, J.S.A. Ishibashi, S.-Y. Liu, Homogeneous metal catalysis for conversion between aromatic and saturated compounds, Coord. Chem. Rev. 314 (2016) 134–181.

[171] C.M. Halmenschlager, M. Brar, I.T. Apan, A. de Klerk, Hydrocracking vacuum gas oil with wax, Catal. Today. 353 (2020) 187–196.

[172] J. Ancheyta, A. Alvarez-Majmutov, C. Leyva, Hydrotreating of oil fractions, in: Z.I. Önsan, A.K. Avci (Eds.), Multiph. Catal. React., 1st ed., John Wiley {&} Sons, Inc., Hoboken, NJ, USA, 2016: pp. 295–329.

[173] A.J. García-López, R. Cuevas, J. Ramírez, J. Ancheyta, A.A. Vargas-Tah, R. Nares, A. Gutiérrez-Alejandre, Hydrodemetallation (HDM) kinetics of Ni-TPP over Mo/Al2O3-TiO2 catalyst, Catal. Today. 107–108 (2005) 545–550.

[174] T. Liu, J. Lu, X. Zhao, Y. Zhou, Q. Wei, C. Xu, Y. Zhang, S. Ding, T. Zhang, X. Tao, L. Ju, Q. Shi, Distribution of Vanadium Compounds in Petroleum Vacuum Residuum and Their Transformations in Hydrodemetallization, Energy & Fuels. 29 (2015) 2089–2096.

[175] L. Ju, T. Liu, J. Lu, Y. Zhou, Q. Wei, S. Li, S. Ding, Y. Zhang, Q. Shi, Transformation of Nickel Octaethylporphine in Hydrodemetallization Reactions, Energy & Fuels. 30 (2016) 6933–6941.

[176] M.S. Rana, J. Ancheyta, P. Rayo, S.K. Maity, Heavy oil hydroprocessing over supported NiMo sulfided catalyst: An inhibition effect by added H2S, Fuel. 86 (2007) 1263–1269.

[177] S.J. Ardakani, K.J. Smith, A comparative study of ring opening of naphthalene, tetralin and decalin over Mo2C/HY and Pd/HY catalysts, Appl. Catal. A Gen. 403 (2011) 36–47.

[178] M. Ibáñez, B. Valle, J. Bilbao, A.G. Gayubo, P. Castaño, Effect of operating conditions on the coke nature and HZSM-5 catalysts deactivation in the transformation of crude bio-oil into hydrocarbons, Catal. Today. 195 (2012) 106–113.

[179] J.R. González Velasco, Cinética química aplicada, Editoriál Síntesis, Madrid, 1999.

[180] M. Marafi, A. Stanislaus, E. Furimsky, Handbook of spent hydroprocessing catalysts, Elsevier, Amsterdam, 2017.

[181] P. Castaño, B. Pawelec, J.L.G.G. Fierro, J.M. Arandes, J. Bilbao, Aromatics reduction of pyrolysis gasoline (PyGas) over HY-supported transition metal catalysts, Appl. Catal. A Gen. 315 (2006) 101–113.

[182] P. Castaño, A.G. Gayubo, B. Pawelec, J.L.G. Fierro, J.M. Arandes, Kinetic modelling of methylcyclohexane ring-opening over a HZSM-5 zeolite catalyst, Chem. Eng. J. 140 (2008) 287–295.

[183] P. Castaño, A. Gutiérrez, I. Villanueva, B. Pawelec, J. Bilbao, J.M.J.M. Arandes, Effect of the support acidity on the aromatic ring-opening of pyrolysis gasoline over Pt/HZSM-5 catalysts, Catal. Today. 143 (2009) 115–119.

[184] E. Furimsky, Catalysts for upgrading heavy petroleum feeds, Elsevier, Amsterdam, 2007.

[185] H. Topsøe, B.S. Clausen, F E Massoth, Hydrotreating catalysis. Science and Technology, Springer, 1996.

[186] A. Gutiérrez, J.M. Arandes, P. Castaño, M. Olazar, J. Bilbao, Enhancement of aromatic hydro-upgrading on a Pt catalyst by promotion with Pd and shape-selective supports, Fuel Process. Technol. 101 (2012) 64–72.

[187] J. Ancheyta, M.S. Rana, E. Furimsky, Hydroprocessing of heavy petroleum feeds: Tutorial, Catal. Today. 109 (2005) 3–15.

[188] * S. K. Maity, and J. Ancheyta, M.S. Rana, Support Effects on Hydroprocessing of Maya Heavy Crude, Energy and Fuels. 19 (2005) 343–347.

[189] S.K. Maity, J. Ancheyta, F. Alonso, M.S. Rana, Preparation, characterization and evaluation of Maya crude hydroprocessing catalysts, Catal. Today. 98 (2004) 193–199.

[190] P. Rayo, J. Ancheyta, J. Ramírez, A. Gutiérrez-Alejandre, Hydrotreating of diluted Maya crude with NiMo/Al2O3-TiO2 catalysts: effect of diluent composition, Catal. Today. 98 (2004) 171–179.

[191] J. Ramírez, P. Rayo, A. Gutiérrez-Alejandre, J. Ancheyta, M.S. Rana,

Analysis of the hydrotreatment of Maya heavy crude with NiMo catalysts supported on TiO2-Al2O3 binary oxides: Effect of the incorporation method of Ti, Catal. Today. 109 (2005) 54–60.

[192] M.S. Rana, M.L. Huidobro, J. Ancheyta, M.T. Gómez, Effect of support composition on hydrogenolysis of thiophene and Maya crude, Catal. Today. 107–108 (2005) 346–354.

[193] B. Caloch, M.S. Rana, J. Ancheyta, Improved hydrogenolysis (C–S, C–M) function with basic supported hydrodesulfurization catalysts, Catal. Today. 98 (2004) 91–98.

[194] P. Castaño, J. María Arandes, B. Pawelec, M. Olazar, J. Bilbao, J.M. Arandes, B. Pawelec, M. Olazar, B. Javier, Kinetic Modeling for Assessing the Product Distribution in Toluene Hydrocracking on a Pt/HZSM-5 Catalyst, Ind. {&} Eng. Chem. Res. 47 (2008) 1043–1050.

[195] P. Castaño, B. Pawelec, A.T. Aguayo, A.G. Gayubo, J.M. Arandes, The Role of Zeolite Acidity in Coupled Toluene Hydrogenation and Ring Opening in One and Two Steps, Ind. {&} Eng. Chem. Res. 47 (2008) 665–671.

[196] R. Henry, M. Tayakout-Fayolle, P. Afanasiev, C. Lorentz, G. Lapisardi, G. Pirngruber, Vacuum gas oil hydrocracking performance of bifunctional Mo/Y zeolite catalysts in a semi-batch reactor, Catal. Today. 220–222 (2014) 159–167.

[197] F.A. Khowatimy, Y. Priastomo, E. Febriyanti, H. Riyantoko, W. Trisunaryanti, Study of Waste Lubricant Hydrocracking into Fuel Fraction over the Combination of Y-Zeolite and ZnO Catalyst, Procedia Environ. Sci. 20 (2014) 225–234.

[198] J.L. Agudelo, B. Mezari, E.J.M. Hensen, S.A. Giraldo, L.J. Hoyos, On the effect of EDTA treatment on the acidic properties of USY zeolite and its performance in vacuum gas oil hydrocracking, Appl. Catal. A Gen. 488 (2014) 219–230.

[199] K. Inamura, A. Iino, Development of zeolite hydrocracking catalyst and system for resid hydrodesulfurization unit, Catal. Today. 164 (2011) 204–208.

[200] S. Chen, Y. Yang, K. Zhang, J. Wang, BETA zeolite made from mesoporous material and its hydrocracking performance, Catal. Today. 116 (2006) 2–5.

[201] J.F.M. Denayer, B. Jonckheere, M. Hloch, G.B. Marin, G. Vanbutsele, J.A. Martens, G. Baron, Molecular Competition of C7 and C9n-Alkanes

in Vapor- and Liquid-Phase Hydroconversion over Bifunctional Pt–USY Zeolite Catalysts, J. Catal. 210 (2002) 445–452.

[202] A. Corma, State of the art and future challenges of zeolites as catalysts, J. Catal. 216 (2003) 298–312.

[203] J. Francis, E. Guillon, N. Bats, C. Pichon, A. Corma, L.J. Simon, Design of improved hydrocracking catalysts by increasing the proximity between acid and metallic sites, Appl. Catal. A Gen. 409–410 (2011) 140–147.

[204] P.P. Dik, I.S. Golubev, M.O. Kazakov, V.Y. Pereyma, M.Y. Smirnova, I.P. Prosvirin, E.Y. Gerasimov, D.O. Kondrashev, V.A. Golovachev, A. V. Kleimenov, O.S. Vedernikov, O. V. Klimov, A.S. Noskov, Influence of zeolite content in NiW/Y-ASA-Al2O3 catalyst for second stage hydrocracking, Catal. Today. 377 (2021) 50–58.

[205] M.O. Kazakov, K.A. Nadeina, I.G. Danilova, P.P. Dik, O. V. Klimov, V.Y. Pereyma, E.A. Paukshtis, I.S. Golubev, I.P. Prosvirin, E.Y. Gerasimov, I. V. Dobryakova, E.E. Knyazeva, I.I. Ivanova, A.S. Noskov, Influence of USY zeolite recrystallization on physicochemical properties and catalytic performance of NiMo/USY-Al 2 O 3 hydrocracking catalysts, Catal. Today. 329 (2019) 108–115.

[206] L. Su, L. Liu, J. Zhuang, H. Wang, Y. Li, W. Shen, Y. Xu, X. Bao, Creating mesopores in ZSM-5 zeolite by alkali treatment: A new way to enhance the catalytic performance of methane dehydroaromatization on Mo/HZSM-5 catalysts, Catal. Letters. 91 (2003) 155–167.

[207] F.L. Bleken, K. Barbera, F. Bonino, U. Olsbye, K.P. Lillerud, S. Bordiga, P. Beato, T.V.W. Janssens, S. Svelle, Catalyst deactivation by coke formation in microporous and desilicated zeolite H-ZSM-5 during the conversion of methanol to hydrocarbons, J. Catal. 307 (2013) 62–73.

[208] P. Lanzafame, S. Perathoner, G. Centi, E. Heracleous, E.F. Iliopoulou, K.S. Triantafyllidis, A.A. Lappas, Effect of the Structure and Mesoporosity in Ni/Zeolite Catalysts for n-Hexadecane Hydroisomerisation and Hydrocracking, ChemCatChem. 9 (2017) 1632–1640.

[209] K. Na, M. Choi, R. Ryoo, Recent advances in the synthesis of hierarchically nanoporous zeolites, Microporous Mesoporous Mater. 166 (2013) 3–19.

[210] M. Choi, K. Na, J. Kim, Y. Sakamoto, O. Terasaki, R. Ryoo, Stable

single-unit-cell nanosheets of zeolite MFI as active and long-lived catalysts, Nature. 461 (2009) 246–249.

[211] J.R. García, M. Bertero, M. Falco, U. Sedran, Catalytic cracking of bio-oils improved by the formation of mesopores by means of y zeolite desilication, Appl. Catal. A Gen. 503 (2015) 1–8.

[212] A. Taguchi, F. Schüth, Ordered mesoporous materials in catalysis, Microporous Mesoporous Mater. 77 (2005) 1–45.

[213] W.J.J. Stevens, K. Lebeau, M. Mertens, G. Van Tendeloo, P. Cool, E.F. Vansant, Investigation of the Morphology of the Mesoporous SBA-16 and SBA-15 Materials, J. Phys. Chem. B. 110 (2006) 9183–9187.

[214] F. Zhang, Y. Yan, H. Yang, Y. Meng, C. Yu, B. Tu, D. Zhao, Understanding effect of wall structure on the hydrothermal stability of mesostructured silica SBA-15, J. Phys. Chem. B. 109 (2005) 8723–8732.

[215] R. Silva-Rodrigo, F. Hernández-López, K. Martinez-Juarez, A. Castillo-Mares, J.A. Melo Banda, A. Olivas-Sarabia, J. Ancheyta, M.S. Rana, Synthesis, characterization and catalytic properties of NiMo/Al2O3–MCM-41 catalyst for dibenzothiophene hydrodesulfurization, Catal. Today. 130 (2008) 309–319.

[216] R. Silva-Rodrigo, H. Castillo Jimenez, A. Guevara-Lara, J.A.A. Melo-Banda, A. Olivas Sarabia, A.I. Reyes de la Torre, F. Morteo Flores, A. Castillo Mares, Synthesis , characterization and catalytic properties of NiMoP/MCM41-gAl2O3 catalysts for DBT hydrodesulfurization, Catal. Today. 250 (2015) 2–11.

[217] M. Hussain, S.K. Song, S.K. Ihm, Synthesis of hydrothermally stable MCM-41 by the seed crystallization and its application as a catalyst support for hydrodesulfurization, Fuel. 106 (2013) 787–792.

[218] G.M. Esquivel, J. Ramírez, A. Gutiérrez-Alejandre, HDS of 4,6-DMDBT over NiW/Al-SBA15 catalysts, Catal. Today. 148 (2009) 36–41.

[219] A. Soriano, P. Roquero, T. Klimova, Behavior of NiMo(W)/Zr-SBA-15 deep hydrodesulfurization catalysts in presence of aromatic and nitrogen-containing compounds, Stud. Surf. Sci. Catal. 175 (2010) 525–528.

[220] O.Y. Gutiérrez, G.A. Fuentes, C. Salcedo, T. Klimova, SBA-15 supports modified by Ti and Zr grafting for NiMo hydrodesulfurization catalysts, Catal. Today. 116 (2006) 485–497.

[221] R. Huirache-Acuña, B. Pawelec, E. Rivera-Muñoz, R. Nava, J. Espino,

J.L.G.L.G. Fierro, Comparison of the morphology and HDS activity of ternary Co-Mo-W catalysts supported on P-modified SBA-15 and SBA-16 substrates, Appl. Catal. B Environ. 92 (2009) 168–184.

[222] K.K. Soni, P.E. Boahene, N. Rambabu, A.K. Dalai, J. Adjaye, Hydrotreating of coker light gas oil on SBA-15 supported nickel phosphide catalysts, Catal. Today. 207 (2013) 119–126.

[223] V. Sundaramurthy, I. Eswaramoorthi, A.K. Dalai, J. Adjaye, Hydrotreating of gas oil on SBA-15 supported NiMo catalysts, Microporous Mesoporous Mater. 111 (2008) 560–568.

[224] P.E. Boahene, K.K. Soni, A.K. Dalai, J. Adjaye, Application of different pore diameter SBA-15 supports for heavy gas oil hydrotreatment using FeW catalyst, Appl. Catal. A Gen. 402 (2011) 31–40.

[225] P.E. Boahene, K.K. Soni, A.K. Dalai, J. Adjaye, Hydroprocessing of heavy gas oils using FeW/SBA-15 catalysts: Experimentals, optimization of metals loading, and kinetics study, Catal. Today. 207 (2013) 101–111.

[226] U.T. Turaga, C. Song, MCM-41-supported Co-Mo catalysts for deep hydrodesulfurization of light cycle oil, Catal. Today. 86 (2003) 129–140.

[227] H. Fukuyama, S. Terai, M. Uchida, J.L. Cano, J. Ancheyta, Active carbon catalyst for heavy oil upgrading, Catal. Today. 98 (2004) 207–215.

[228] E. Gonzalez-Serrano, T. Cordero, J. Rodriguez-Mirasol, L. Cotoruelo, J.J. Rodriguez, Removal of water pollutants with activated carbons prepared from H3PO4 activation of lignin from kraft black liquors, Water Res. 38 (2004) 3043–3050.

[229] J.M. Rosas, R. Ruiz-Rosas, J. Rodríguez-Mirasol, T. Cordero, Kinetic study of the oxidation resistance of phosphorus-containing activated carbons, Carbon N. Y. 50 (2012) 1523–1537.

[230] J. Jaramillo, P.M. Álvarez, V. Gómez-Serrano, Oxidation of activated carbon by dry and wet methods: Surface chemistry and textural modifications, Fuel Process. Technol. 91 (2010) 1768–1775.

[231] Y. Gokce, Z. Aktas, Nitric acid modification of activated carbon produced from waste tea and adsorption of methylene blue and phenol, Appl. Surf. Sci. 313 (2014) 352–359.

[232] H. ShamsiJazeyi, T. Kaghazchi, Investigation of nitric acid treatment of activated carbon for enhanced aqueous mercury removal, J. Ind. Eng.

Chem. 16 (2010) 852–858.

[233] J.X. Guo, J. Liang, Y.H. Chu, M.C. Sun, H.Q. Yin, J.J. Li, Desulfurization activity of nickel supported on acid-treated activated carbons, Appl. Catal. A Gen. 421–422 (2012) 142–147.

[234] E. Auer, A. Freund, J. Pietsch, T. Tacke, Carbons as supports for industrial precious metal catalysts, Appl. Catal. A Gen. 173 (1998) 259–271.

[235] R. Zarchin, M. Rabaev, R. Vidruk-Nehemya, M. V. Landau, M. Herskowitz, Hydroprocessing of soybean oil on nickel-phosphide supported catalysts, Fuel. 139 (2015) 684–691.

[236] T.T. Viet, J.H. Lee, F. Ma, G.R. Kim, I.S. Ahn, C.H. Lee, Hydrocracking of petroleum vacuum residue with activated carbon and metal additives in a supercritical m-xylene solvent, Fuel. 103 (2013) 553–561.

[237] N. Prabhu, A.K. Dalai, J. Adjaye, Hydrodesulphurization and hydrodenitrogenation of light gas oil using NiMo catalyst supported on functionalized mesoporous carbon, Appl. Catal. A Gen. 401 (2011) 1–11.

[238] H. Purón, J.L.L. Pinilla, I. Suelves, M. Millan, Acid treated carbon nanofibers as catalytic support for heavy oil hydroprocessing, Catal. Today. 249 (2015) 79–85.

[239] J.L.L. Pinilla, H. Purón, D. Torres, S. De Llobet, R. Moliner, I. Suelves, M. Millan, Carbon nanofibres coated with Ni decorated MoS2 nanosheets as catalyst for vacuum residue hydroprocessing, Appl. Catal. B Environ. 148–149 (2014) 357–365.

[240] S.K. Maity, J. Ancheyta, Carbon modified Y zeolite used as support material for hydroprocessing catalysts, Catal. Today. 150 (2010) 231–236.

[241] Z. Till, T. Varga, L. Szabó, T. Chován, Identification and Observability of Lumped Kinetic Models for Vacuum Gas Oil Hydrocracking, Energy and Fuels. 31 (2017) 12654–12664.

[242] T.A. Al-Attas, M.H. Zahir, S.A. Ali, S.A. Al-Bogami, Z. Malaibari, S.A. Razzak, M.M. Hossain, Kinetics of the synergy effects in heavy oil upgrading using novel Ni-p-tert-butylcalix[4]arene as a dispersed catalyst with a supported catalyst, Fuel Process. Technol. 185 (2019) 158–168.

[243] D. Faraji, S. Sadighi, H. Mazaheri, Modeling and Evaluating Zeolite

and Amorphous Based Catalysts in Vacuum Gas Oil Hydrocracking Process, Int. J. Chem. React. Eng. 16 (2018) 1–14.

[244] H. Purón, P. Arcelus-Arrillaga, K.K. Chin, J.L. Pinilla, B. Fidalgo, M. Millan, H. Puron, P. Arcelus-Arrillaga, K.K. Chin, J.L. Pinilla, B. Fidalgo, M. Millan, Kinetic analysis of vacuum residue hydrocracking in early reaction stages, Fuel. 117 (2014) 408–414.

[245] A. Quitian, J. Ancheyta, Experimental Methods for Developing Kinetic Models for Hydrocracking Reactions with Slurry-Phase Catalyst Using Batch Reactors, Energy and Fuels. 30 (2016) 4419–4437.

[246] S.D.S. Asaee, L. Vafajoo, F. Khorasheh, A new approach to estimate parameters of a lumped kinetic model for hydroconversion of heavy residue, Fuel. 134 (2014) 343–353.

[247] S.A. Qader, G.R. Hill, Hydrocracking of Gas Oil, Ind. Eng. Chem. Process Des. Dev. 8 (2002) 98–105.

[248] M.A. Callejas, M.T. Martínez, Hydrocracking of a Maya Residue. Kinetics and Product Yield Distributions, Ind. Eng. Chem. Res. 38 (1999) 3285–3289.

[249] S.M. Yui, E.C. Sanford, Mild hydrocracking of bitumen-derived coker and hydrocracker heavy gas oils: kinetics, product yields, and product properties, Ind. Eng. Chem. Res. 28 (1989) 1278–1284.

[250] A.K. Aboul-Gheit, Hydrocracking of vacuum gas oil (VGO) for fuels production - (2) reaction kinetics, Erdoel Erdgas Kohle/EKEP. 105 (1989) 319–320.

[251] D.I. Orochko, Applied over-all kinetics of hydrocracking of heavy petroleum distillates, Khimiya I Tekhnologiya Topl. i Masel. 8 (1970) 2–6.

[252] C. Botchwey, A.K. Dalai, J. Adjaye, Kinetics of bitumen-derived gas oil upgrading using a commercial NiMo/Al2O3 catalyst, Can. J. Chem. Eng. 82 (2004) 478–487.

[253] L. Han, X. Fang, C. Peng, T. Zhao, Application of discrete lumped kinetic modeling on vacuum gas oil hydrocracking, China Pet. Process. Petrochemical Technol. 15 (2013) 67–73.

[254] A.T. Lapinas, M.T. Klein, B.C. Gates, A. Macris, J.E. Lyons, Catalytic hydrogenation and hydrocracking of fluorene: reaction pathways, kinetics, and mechanisms, Ind. Eng. Chem. Res. 30 (1991) 42–50.

[255] C.L. Russell, M.T. Klein, R.J. Quann, J. Trewella, Catalytic Hydrocracking Reaction Pathways, Kinetics, and Mechanisms of n-Alkylbenzenes, Energy and Fuels. 8 (1994) 1394–1400.

[256] E.N. Sudakov, Method of calculation of product yields in hydrocracking middle distillates, Chem. Technol. Fuels Oils. 32 (1996) 85–90.

[257] A.M. Benito, M.A. Callejas, M.T. Martínez, Kinetics of asphaltene hydroconversion: 2. Catalytic hydrocracking of a coal residue, Fuel. 76 (1997) 907–911.

[258] A.R. Ayasse, H. Nagaishi, E.W. Chan, M.R. Gray, Lumped kinetics of hydrocracking of bitumen, Fuel. 76 (1997) 1025–1033.

[259] S.C.K. and, M.T. Klein*, R.J. Quann, Hydrocracking of Polynuclear Aromatic Hydrocarbons. Development of Rate Laws through Inhibition Studies, Ind. Eng. Chem. Res. 36 (1997) 2041–2050.

[260] V. Calemma, S. Peratello, F. Stroppa, R. Giardino, C. Perego, Hydrocracking and Hydroisomerization of Long-Chain n-Paraffins. Reactivity and Reaction Pathway for Base Oil Formation, Ind. Eng. Chem. Res. 43 (2004) 934–940.

[261] Z. Cao, X. Xu, Y. Qi, S. Lu, B. Qi, Hydrocracking of Tetralin over Mo–Ni/Usy Dual Functional Catalysts, Http://Dx.Doi.Org/10.1081/LFT-120034204. 22 (2003) 617–629.

[262] L. Pellegrini, S. Locatelli, S. Rasella, S. Bonomi, V. Calemma, Modeling of Fischer–Tropsch products hydrocracking, Chem. Eng. Sci. 59 (2004) 4781–4787.

[263] G. Valavarasu, M. Bhaskar, B. Sairam, K.S.S. Balaraman, K. Balu, A four lump kinetic model for the simulation of the hydrocracking process, Pet. Sci. Technol. 23 (2005) 1323–1332.

[264] R.C. Patil, P. Patra, A. Gupta, A. Das, Effect of reactor configuration on performance of vacuum gas oil (VGO) hydrotreater: Modelling studies, Comput. Chem. Eng. 104 (2017) 89–106.

[265] S. Sadighi, A. Ahmad, S.K.K. Masoudian, Effect of lump partitioning on the accuracy of a commercial vacuum gas oil hydrocracking model, Int. J. Chem. React. Eng. 10 (2012) 1–22.

[266] C. Botchwey, A.K. Dalai, J. Adjaye, C. Botchwey, A.K. Dalai, J. Adjaye, Product Selectivity during Hydrotreating and Mild Hydrocracking of Bitumen-Derived Gas Oil, Energy and Fuels. 17 (2003) 1372–1381.

[267] J.F.F. Mosby, R.D.D. Buttke, J.A.A. Cox, C. Nikolaides, Process characterization of expanded-bed reactors in series, Chem. Eng. Sci. 41 (1986) 989–995.

[268] S. Sánchez, M.A. Rodríguez, J. Ancheyta, Kinetic model for moderate hydrocracking of heavy oils, Ind. Eng. Chem. Res. 44 (2005) 9409–9413.

[269] M.F.F. Abid, S.M.M. Ahmed, H.H.H. Hassan, S.M.M. Ali, Modeling and Kinetic Study of an Ebullated Bed Reactor in the H-Oil process, Arab. J. Sci. Eng. 43 (2018) 5733–5743.

[270] J. Martínez, J. Ancheyta, Kinetic model for hydrocracking of heavy oil in a CSTR involving short term catalyst deactivation, Fuel. 100 (2012) 193–199.

[271] S. Sánchez, J. Ancheyta, Effect of pressure on the kinetics of moderate hydrocracking of Maya crude oil, Energy and Fuels. 21 (2007) 653–661.

[272] S. Ramírez, J. Martínez, J. Ancheyta, Kinetics of thermal hydrocracking of heavy oils under moderate hydroprocessing reaction conditions, Fuel. 110 (2013) 83–88.

[273] T. Huang, B. Liu, Z. Wang, X. Guo, Kinetic model for hydrocracking of Iranian heavy crude with dispersed catalysts in slurry-phase, Pet. Sci. Technol. 35 (2017) 1846–1851.

[274] H. Loria, G. Trujillo-Ferrer, C. Sosa-Stull, P. Pereira-Almao, Kinetic modeling of bitumen hydroprocessing at in-reservoir conditions employing ultradispersed catalysts, Energy and Fuels. 25 (2011) 1364–1372.

[275] P. Álvarez, B. Browning, T. Jansen, M. Lacroix, C. Geantet, I. Pitault, M. Tayakout-Fayolle, Modeling of atmospheric and vacuum petroleum residue hydroconversion in a slurry semi-batch reactor: Study of hydrogen consumption, Fuel Process. Technol. 185 (2019) 68–78.

[276] F.J.J. Ortega Garcia, J.A.A. Muñoz Arroyo, P. Flores Sánchez, E. Mar Juárez, J.M.M. Dominguez Esquivel, Hydrocracking Kinetics of a Heavy Crude Oil on a Liquid Catalyst, Energy and Fuels. 31 (2017) 6794–6799.

[277] H.H. Pham, N. Thuy Nguyen, K.S. Go, S. Park, N. Sun Nho, G.T. Kim, C. Wee Lee, G. Felix, Kinetic study of thermal and catalytic hydrocracking of asphaltene, Catal. Today. 353 (2020) 112–118.

[278] H.H. Pham, K.H. Kim, K.S. Go, N.S. Nho, W. Kim, E.H. Kwon, R.H.

Jung, Y. il Lim, S.H. Lim, D.A. Pham, Hydrocracking and hydrotreating reaction kinetics of heavy oil in CSTR using a dispersed catalyst, J. Pet. Sci. Eng. 197 (2021) 107997.

[279] B. Umana, N. Zhang, R. Smith, Development of Vacuum Residue Hydrodesulphurization–Hydrocracking Models and Their Integration with Refinery Hydrogen Networks, Ind. Eng. Chem. Res. 55 (2016) 2391–2406.

[280] C. Mang, Y. Ying, Z. Jiamin, A lumped kinetic model for low- and medium- temperature coal tar hydrocracking process, China Pet. Process. Petrochemical Technol. 22 (2020) 98–103.

[281] G. Félix, J. Ancheyta, Using Separate Kinetic Models to Predict Liquid, Gas, and Coke Yields in Heavy Oil Hydrocracking, Ind. Eng. Chem. Res. 58 (2019) 7973–7979.

[282] E. Manek, J. Haydary, Hydrocracking of vacuum residue with solid and dispersed phase catalyst: Modeling of sediment formation and hydrodesulfurization, Fuel Process. Technol. 159 (2017) 320–327.

[283] A.H. Al-Rashidy, T.A. Al-Attas, S.A. Ali, S.A. Al-Bogami, S.A. Razzak, M.M. Hossain, Hydrocracking of LVGO Using Dispersed Catalysts Derived from Soluble Precursors: Performance Evaluation and Kinetics, Ind. Eng. Chem. Res. 58 (2019) 14709–14718.

[284] E.A.S. Bdwi, S.A. Ali, M.R. Quddus, S.A. Al-Bogami, S.A. Razzak, M.M. Hossain, Kinetics of Promotional Effects of Oil-Soluble Dispersed Metal (Mo, Co, and Fe) Catalysts on Slurry Phase Hydrocracking of Vacuum Gas Oil, Energy and Fuels. 31 (2017) 3132–3142.

[285] T. Kaminski, M.M. Husein, Kinetic modelling of thermal cracking of Arabian atmospheric and vacuum residue, Fuel Process. Technol. 189 (2019) 89–97.

[286] Y. Zhao, Y. Yu, Kinetics of asphaltene thermal cracking and catalytic hydrocracking, Fuel Process. Technol. 92 (2011) 977–982.

[287] R.M. De Almeida, R. Guirardello, Hydroconversion kinetics of Marlim vacuum residue, Catal. Today. 109 (2005) 104–111.

[288] P.K.K. Ramdoss, A.R.R. Tarrer, High-temperature liquefaction of waste plastics, Fuel. 77 (1998) 293–299.

[289] M. Adam, V. Calemma, F. Galimberti, C. Gambaro, J. Heiszwolf, R. Ocone, Continuum lumping kinetics of complex reactive systems,

Chem. Eng. Sci. 76 (2012) 154–164.

[290] C.S. Laxminarasimhan, R.P. Verma, P.A. Ramachandran, Continuous Lumping Model for Simulation of Hydrocracking, AIChE J. 42 (1996) 2645–2653.

[291] M.Y. Chou, T.C. Ho, Continuum theory for lumping nonlinear reactions, AIChE J. 34 (1988) 1519–1527.

[292] H.M.S. Lababidi, F.S. AlHumaidan, Modeling the Hydrocracking Kinetics of Atmospheric Residue in Hydrotreating Processes by the Continuous Lumping Approach, Energy and Fuels. 25 (2011) 1939–1949.

[293] I. Elizalde, J. Ancheyta, Modeling catalyst deactivation during hydrocracking of atmospheric residue by using the continuous kinetic lumping model, Fuel Process. Technol. 123 (2014) 114–121.

[294] C.S.L. Narasimhan, M. Sau, R.P. Verma, An integrated approach for hydrocracker modeling, Stud. Surf. Sci. Catal. 127 (1999) 297–306.

[295] K. Basak, M. Sau, U. Manna, R.P. Verma, Industrial hydrocracker model based on novel continuum lumping approach for optimization in petroleum refinery, Catal. Today. 98 (2004) 253–264.

[296] P.J.J. Becker, N. Serrand, B. Celse, D. Guillaume, H. Dulot, Comparing hydrocracking models: Continuous lumping vs. single events, Fuel. 165 (2016) 306–315.

[297] S. Sánchez, J. Ancheyta, W.C. McCaffrey, Comparison of probability distribution functions for fitting distillation curves of petroleum, Energy and Fuels. 21 (2007) 2955–2963.

[298] T.A. Osswald, G. Menges, Material science of polymers for engineers: Third edition, Hanser, Munich, 2012.

[299] J. Schneider, K. Walters, Interdisciplinary and experimental approach towards the teaching of materials science and engineering, in: Am. Soc. Eng. Educ., Virginia, 2010: pp. 1–10.

[300] E. Furimsky, Properties of catalysts for hydroprocessing of heavy feeds, in: Catal. Upgrad. Heavy Pet. Feed., Elsevier, Amsterdam, The Netherlands, 2007: pp. 23–41.

[301] A. Galarneau, D. Mehlhorn, F. Guenneau, B. Coasne, F. Villemot, D. Minoux, C. Aquino, J.P. Dath, Specific Surface Area Determination for Microporous/Mesoporous Materials: The Case of Mesoporous FAU-Y

Zeolites, Langmuir. 34 (2018) 14134–14142.

[302] A.G. Gayubo, P.L. Benito, A.T. Aguayo, M. Olazar, J. Bilbao, Relationship between Surface Aciditv and Activity of catalysts in the Transforhation of Methanol into Hydrocarbons, J. Chem. Tech. Biotechnol. 65 (1996) 186–192.

[303] A.T. Aguayo, J.M. Arandes, M. Olazar, J. Bilbao, A. T. Aguayo, J. M. Arandes, M. Olazar, J. Bilbao, A.T. Aguayo, J.M. Arandes, M. Olazar, J. Bilbao, Study of temperature-programmed desorption of tert-butylamine to measure the surface acidity of solid catalysts, Ind. Eng. Chem. Res. 29 (1990) 1621–1626.

[304] O.M. Busch, W. Brijoux, S. Thomson, F. Schüth, Spatially resolving infrared spectroscopy for parallelized characterization of acid sites of catalysts via pyridine sorption: Possibilities and limitations, J. Catal. 222 (2004) 174–179.

[305] I.S. Pieta, M. Ishaq, R.P.K. Wells, J.A. Anderson, Quantitative determination of acid sites on silica-alumina, Appl. Catal. A Gen. 390 (2010) 127–134.

[306] C.A.A. Emeis, Determination of Integrated Molar Extinction Coefficients for Infrared Absorption Bands of Pyridine Adsorbed on Solid Acid Catalysts, J. Catal. 141 (1993) 347–354.

[307] M. Jayamurthy, S. Vasudevan, Temperature programmed desorption studies on hydrodesulfurization catalysts, Catal. Letters. 23 (1994) 49–57.

[308] T.A. Al-Attas, M.H. Zahir, S.A. Ali, S.A. Al-Bogami, Z. Malaibari, S.A. Razzak, M.M. Hossain, Novel (Co-,Ni)- p - tert -Butylcalix[4]arenes as Dispersed Catalysts for Heavy Oil Upgrading: Synthesis, Characterization, and Performance Evaluation, Energy & Fuels. 33 (2019) 561–573.

[309] P.C. Anderson, J.M. Sharkey, R.P. Walsh, Calculation of the research octane number of motor gasolines from gas chromatographic data and a new approach to motor gasoline quality control, J Inst Pet. 58 (1972) 83–94.

[310] J. Shabtai, X. Xiao, W. Zmierczak, Depolymerization−Liquefaction of Plastics and Rubbers. 1. Polyethylene, Polypropylene, and Polybutadiene, Energy Fuels. 11 (1997) 76–87.

[311] T. Karayildirim, J. Yanik, S. Uçar, M. Sağlam, M. Yüksel, T. Karayıldırım, J. Yanik, S. Uçar, M. Sağlam, M. Yüksel, T. Karayildirim,

J. Yanik, S. Uçar, M. Sağlam, M. Yüksel, Conversion of plastics/HVGO mixtures to fuels by two-step processing, Fuel Process. Technol. 73 (2001) 23–35.

[312] M.F. Ali, M.N. Siddiqui, S.S.H.H. Redhwi, M. Nahid, S.S.H.H. Redhwi, M.F. Ali, Study on the conversion of waste plastics/petroleum resid mixtures to transportation fuels, J. Mater. Cycles Waste Manag. 6 (2004) 27–34.

[313] M.F. Ali, M.N. Siddiqui, Thermal and catalytic decomposition behavior of PVC mixed plastic waste with petroleum residue, J. Anal. Appl. Pyrolysis. 74 (2005) 282–289.

[314] E.G. Fuentes-Ordóñez, J.A. Salbidegoitia, J.L. Ayastuy, M.A. Gutiérrez-Ortiz, M.P. González-Marcos, J.R. González-Velasco, High external surface Pt/zeolite catalysts for improving polystyrene hydrocracking, Catal. Today. 227 (2014) 163–170.

[315] M. Thommes, K. Kaneko, A. V. Neimark, J.P. Olivier, F. Rodriguez-Reinoso, J. Rouquerol, K.S.W. Sing, Physisorption of gases, with special reference to the evaluation of surface area and pore size distribution (IUPAC Technical Report), Pure Appl. Chem. 87 (2015) 1051–1069.

[316] R.R. Chianelli, M.H. Siadati, M.P. De la Rosa, G. Berhault, J.P. Wilcoxon, R. Bearden, B.L. Abrams, Catalytic properties of single layers of transition metal sulfide catalytic materials, Catal. Rev. - Sci. Eng. 48 (2006) 1–41.

[317] H. Tops∅e, B.S. Clausen, H. TopsøE, B.S. Clausen, Importance of Co-Mo-S Type Structures in Hydrodesulfurization, Catal. Rev. 26 (1984) 395–420.

[318] T. Alphazan, A. Bonduelle-Skrzypczak, C. Legens, Z. Boudene, A.L. Taleb, A.S. Gay, O. Ersen, C. Copéret, P. Raybaud, Improved promoter effect in NiWS catalysts through a molecular approach and an optimized Ni edge decoration, J. Catal. 340 (2016) 60–65.

[319] D. Qi, A. Duan, Z. Zhao, H. Wu, H. Fan, H. Fang, J. Li, G. Jiang, J. Liu, Y. Wei, X. Zhang, Catalytic performance and sulfidation behaviors of CoMo/Beta-MCM-48 catalysts prepared with citric acid for FCC gasoline hydroupgrading, J. Porous Mater. 22 (2015) 127–135.

[320] J.N.D. de León, C.R. Kumar, J. Antúnez-García, S. Fuentes-Moyado, Recent insights in transition metal sulfide hydrodesulfurization catalysts for the production of ultra low sulfur diesel: A short review,

Catalysts. 9 (2019) 1–26.

[321] Y. V. Joshi, P. Ghosh, M. Daage, W.N. Delgass, Support effects in HDS catalysts: DFT analysis of thiolysis and hydrolysis energies of metal-support linkages, J. Catal. 257 (2008) 71–80.

[322] J.N. Díaz de León, L.A. Zavala-Sánchez, V.A. Suárez-Toriello, G. Alonso-Núñez, T.A. Zepeda, R.I. Yocupicio, J.A. de los Reyes, S. Fuentes, Support effects of NiW catalysts for highly selective sulfur removal from light hydrocarbons, Appl. Catal. B Environ. 213 (2017) 167–176.

[323] Y. Liu, Hydrocracking of Polyethylene to Jet Fuel Range Hydrocarbons over Bifunctional Catalysts Containing Pt- and Al-Modified MCM-48, Reactions. 1 (2020) 195–209.

[324] D.J. Rosenberg, J.A. Anderson, On determination of acid site densities on sulfated oxides, Catal. Letters. 83 (2002) 59–63.

[325] P.P. Dik, O. V. Klimov, G.I. Koryakina, K.A. Leonova, V.Y. Pereyma, S. V. Budukva, E.Y. Gerasimov, A.S. Noskov, Composition of stacked bed for VGO hydrocracking with maximum diesel yield, Catal. Today. 220–222 (2014) 124–132.

[326] M. Anilkumar, N. Loke, V. Patil, R. Panday, S. G, Hydrocracking of hydrotreated light cycle oil to mono aromatics over non-noble bi-functional (ni-w supported) zeolite catalysts, Catal. Today. 358 (2020) 221–227.

[327] M.C. Biesinger, B.P. Payne, A.P. Grosvenor, L.W.M. Lau, A.R. Gerson, R.S.C. Smart, Resolving surface chemical states in XPS analysis of first row transition metals, oxides and hydroxides: Cr, Mn, Fe, Co and Ni, Appl. Surf. Sci. 257 (2011) 2717–2730.

[328] M. Fantauzzi, F. Secci, M. Sanna Angotzi, C. Passiu, C. Cannas, A. Rossi, Nanostructured spinel cobalt ferrites: Fe and Co chemical state, cation distribution and size effects by X-ray photoelectron spectroscopy, RSC Adv. 9 (2019) 19171–19179.

[329] A.F.H. Sanders, A.M. De Jong, V.H.J. De Beer, J.A.R. Van Veen, J.W. Niemantsverdriet, Formation of cobalt-molybdenum sulfides in hydrotreating catalysts: A surface science approach, Appl. Surf. Sci. 144–145 (1999) 380–384.

[330] M. Rana, M.N. Islam, A. Agarwal, G. Taki, S.J. Park, S. Dong, Y.T. Jo, J.H. Park, Production of Phenol-Rich Monomers from Kraft Lignin Hydrothermolysates in Basic-Subcritical Water over MoO3/SBA-15

Catalyst, Energy and Fuels. 32 (2018) 11564–11575.

[331] M. Ponce-Mosso, M. Pérez-González, P.E. García-Tinoco, H. Crotte-Ledesma, M. Morales-Luna, S.A. Tomás, Enhanced photocatalytic activity of amorphous MoO3 thin films deposited by rf reactive magnetron sputtering, Catal. Today. 349 (2020) 150–158.

[332] A.P. Grosvenor, M.C. Biesinger, R.S.C. Smart, N.S. McIntyre, New interpretations of XPS spectra of nickel metal and oxides, Surf. Sci. 600 (2006) 1771–1779.

[333] S. Surendran, A. Sivanantham, S. Shanmugam, U. Sim, R.K. Selvan, Ni2P2O7 microsheets as efficient Bi-functional electrocatalysts for water splitting application, Sustain. Energy Fuels. 3 (2019) 2435–2446.

[334] X. Tao, Y. Zhou, Q. Wei, G. Yu, Q. Cui, J. Liu, T. Liu, Effect of morphology properties of NiW catalysts on hydrodesulfurization for individual sulfur compounds in fluid catalytic cracking diesel, Fuel Process. Technol. 118 (2014) 200–207.

[335] F.Y. Xie, L. Gong, X. Liu, Y.T. Tao, W.H. Zhang, S.H. Chen, H. Meng, J. Chen, XPS studies on surface reduction of tungsten oxide nanowire film by Ar + bombardment, J. Electron Spectros. Relat. Phenomena. 185 (2012) 112–118.

[336] P. Kumar, S.K. Maity, D. Shee, Role of NiMo Alloy and Ni Species in the Performance of NiMo/Alumina Catalysts for Hydrodeoxygenation of Stearic Acid: A Kinetic Study, ACS Omega. 4 (2019) 2833–2843.

[337] S. Damyanova, B. Pawelec, K. Arishtirova, J.L.G. Fierro, Ni-based catalysts for reforming of methane with CO2, Int. J. Hydrogen Energy. 37 (2012) 15966–15975.

[338] A. Alayat, E. Echeverria, F. Sotoudehniakarani, D.N. Mcllroy, A.G. McDonald, Alumina coated silica nanosprings (NS) support based cobalt catalysts for liquid hydrocarbon fuel production from syngas, Materials (Basel). 12 (2019) 1810.

[339] S. Rane, Ø. Borg, J. Yang, E. Rytter, A. Holmen, Effect of alumina phases on hydrocarbon selectivity in Fischer-Tropsch synthesis, Appl. Catal. A Gen. 388 (2010) 160–167.

[340] F.G. Botes, J.W. Niemantsverdriet, J. Van De Loosdrecht, A comparison of cobalt and iron based slurry phase Fischer-Tropsch synthesis, Catal. Today. 215 (2013) 112–120.

[341] A. Kostyniuk, D. Bajec, B. Likozar, Catalytic hydrogenation, hydrocracking and isomerization reactions of biomass tar model compound mixture over Ni-modified zeolite catalysts in packed bed reactor, Renew. Energy. 167 (2021) 409–424.

[342] A.J. Maia, B. Louis, Y.L. Lam, M.M. Pereira, Ni-ZSM-5 catalysts: Detailed characterization of metal sites for proper catalyst design, J. Catal. 269 (2010) 103–109.

[343] R.L. Tong, Y.G. Wang, X. Zhang, H.Y. Zhang, J.Z. Dai, X.C. Lin, D.P. Xu, Effect of phosphorus modification on the catalytic properties of NiW/γ-Al2O3 in the hydrogenation of aromatics from coal tar, Ranliao Huaxue Xuebao/Journal Fuel Chem. Technol. 43 (2015) 1461–1469.

[344] S. Chandra Shekar, J. Krishna Murthy, P. Kanta Rao, K.S. Rama Rao, Selective hydrogenolysis of dichlorodifluoromethane on carbon covered alumina supported palladium catalyst, J. Mol. Catal. A Chem. 191 (2003) 45–59.

[345] S. Bhogeswararao, D. Srinivas, Catalytic conversion of furfural to industrial chemicals over supported Pt and Pd catalysts, J. Catal. 327 (2015) 65–77.

[346] T. Romero, M. Esparragoza, R. Avila, L. Melo, L. García, G. Carruyo, A. Moronta, Conversion de Tolueno y de Metilciclohexano sobre catalizadorers bimetálicos PtPd/HY, 2008.

[347] R. Ramachandran, F.E. Massothm, Studies of Molybdena-Alumina Catalysts. Temperature Programmed Desorption of H2S and thiophene., Can. J. Chem. Eng. 60 (1982) 17–22.

[348] R. Burch, A. Collins, Chemisorption/catalytic activity correlations for sulphided Ni/Mo/Al2O3 hydrodesulphurisation catalysts, Appl. Catal. 17 (1985) 273–308.

[349] N.K. Nag, D. Fraenkel, J.A. Moulijn, B.C. Gates, Characterization of hydroprocessing catalysts by resolved temperature-programmed desorption, reduction and sulfiding, J. Catal. 66 (1980) 162–170.

[350] N.Y. Topsøe, H. Topsøe, F.E. Massoth, Evidence of Brønsted acidity on sulfided promoted and unpromoted Mo Al2O3 catalysts, J. Catal. 119 (1989) 252–255.

[351] J.M. Arandes, M.J. Azkoiti, I. Torre, M. Olazar, P. Castaño, Effect of HZSM-5 catalyst addition on the cracking of polyolefin pyrolysis waxes under FCC conditions, Chem. Eng. J. 132 (2007) 17–26.

[352] R. Ochoa, H. Van Woert, W.H. Lee, R. Subramanian, E. Kugler, P.C. Eklund, Catalytic degradation of medium density polyethylene over silica - Alumina supports, Fuel Process. Technol. 49 (1996) 119–136.

[353] J. Weitkamp, Catalytic hydrocracking - Mechanisms and versatility of the process, ChemCatChem. 4 (2012) 292–306.

[354] C. Li, T. Yang, W. Deng, H. Zhang, M. Cui, Effects of Iron(III) Dodecylbenzenesulfonate on the Slurry-Phase Hydrocracking of Venezuela Fuel Oil with an Oil-Soluble Mo Catalyst, Energy and Fuels. 30 (2016) 4710–4716.

[355] C. Li, H. Meng, T. Yang, J. Li, Y. Qin, Y. Huang, W. Deng, Study on catalytic performance of oil-soluble iron-nickel bimetallic catalyst in coal/oil co-processing, Fuel. 219 (2018) 30–36.

[356] M. Díaz, E. Epelde, A.T. Aguayo, J. Bilbao, Low-pressure oligomerization of 1-butene to liquid fuels on HZSM-5 zeolite catalysts: Effect of operating conditions, J. Ind. Eng. Chem. 87 (2020) 234–241.

[357] S.G.A. Ferraz, F.M.Z. Zotin, L.R.R. Araujo, J.L. Zotin, Influence of support acidity of NiMoS catalysts in the activity for hydrogenation and hydrocracking of tetralin, Appl. Catal. A Gen. 384 (2010) 51–57.

[358] Y. Duan, Y. Ren, H. Du, M. Li, D. Liu, Y. Ren, Y. Duan, Slurry-phase hydrocracking of heavy oil and model reactant: effect of dispersed Mo catalyst, Appl. Petrochemical Res. 5 (2015) 89–98.

[359] A.A. Lappas, S.S. Voutetakis, N. Drakaki, M. Papapetrou, I.A. Vasalos, Production of transportation fuels from biomass, in: Work. CPERI, Greece, 2004: pp. 23–26. https://www.researchgate.net/publication/268057018 (accessed February 12, 2021).

[360] C. Peng, Z. Zhou, Z. Cheng, X. Fang, Upgrading of Light Cycle Oil to High-Octane Gasoline through Selective Hydrocracking over Non-Noble Metal Bifunctional Catalysts, Energy and Fuels. 33 (2019) 1090–1097.

[361] P.J. Becker, N. Serrand, B. Celse, D. Guillaume, H. Dulot, A single events microkinetic model for hydrocracking of vacuum gas oil, Comput. Chem. Eng. 98 (2017) 70–79.

[362] M.A.B.A.B. Siddiqui, A.M.M. Aitani, M.R.R. Saeed, N. Al-Yassir, S. Al-Khattaf, Enhancing propylene production from catalytic cracking of Arabian Light VGO over novel zeolites as FCC catalyst additives, Fuel.

90 (2011) 459–466.

[363] H.S. Cerqueira, G. Caeiro, L. Costa, F. Ramôa Ribeiro, Deactivation of FCC catalysts, J. Mol. Catal. A Chem. 292 (2008) 1–13.

[364] M.E. Myers, J. Stollsteimer, A.M. Wims, Determination of gasoline octane numbers from chemical composition, Anal. Chem. 47 (1975) 2301–2304.

[365] K.H. Lee, Effects of the types of zeolites on catalytic upgrading of pyrolysis wax oil, J. Anal. Appl. Pyrolysis. 94 (2012) 209–214.

[366] F. Ding, C. Luo, H. Zhang, L. Xiong, X.D. Chen, Hydrocracking of Polyolefin Thermal Cracking Waxes over Ni-loaded Molecular Sieve Catalysts, Pet. Sci. Technol. 33 (2015) 1846–1852.

[367] C. Vasile, M.A. Brebu, T. Karayildirim, J. Yanik, H. Darie, Feedstock recycling from plastics and thermosets fractions of used computers. II. Pyrolysis oil upgrading, Fuel. 86 (2007) 477–485.

[368] F.J. Vela, R. Palos, J. Bilbao, J.M. Arandes, A. Gutiérrez, Effect of co-feeding HDPE on the product distribution in the hydrocracking of VGO, Catal. Today. 353 (2020) 197–203.

[369] J.S. Buchanan, J.G. Santiesteban, W.O. Haag, Mechanistic considerations in acid-catalyzed cracking of olefins, J. Catal. 158 (1996) 279–287.

[370] A. bin Jumah, A.A. Tedstone, A.A. Garforth, Hydrocracking of virgin and post-consumer polymers, Microporous Mesoporous Mater. 315 (2021) 110912.

[371] R.K. Singh, B. Ruj, A.K. Sadhukhan, P. Gupta, Thermal degradation of waste plastics under non-sweeping atmosphere: Part 2: Effect of process temperature on product characteristics and their future applications, J. Environ. Manage. 261 (2020) 110112.

[372] J.W. Thybaut, G.B. Marin, Multiscale Aspects in Hydrocracking: From Reaction Mechanism Over Catalysts to Kinetics and Industrial Application, 1st ed., Elsevier Inc., 2016.

[373] D. Munir, H. Amer, R. Aslam, M. Bououdina, M.R. Usman, Composite zeolite beta catalysts for catalytic hydrocracking of plastic waste to liquid fuels, Mater. Renew. Sustain. Energy. 9 (2020) 1–13.

[374] A. Quitian, Y. Fernández, J. Ancheyta, Viscosity Reduction of Heavy Oil during Slurry-Phase Hydrocracking, Chem. Eng. Technol. 42

(2019) 148–155. https://onlinelibrary.wiley.com/doi/full/10.1002/ceat.201800102 (accessed July 28, 2021).

[375] I.H. Metecan, A.R. Ozkan, R. Isler, J. Yanik, M. Saglam, M. Yuksel, Naphtha derived from polyolefins, Fuel. 84 (2005) 619–628.

[376] H.S. Joo, J.A. Guin, Continuous upgrading of a plastics pyrolysis liquid to an environmentally favorable gasoline range product, Fuel Process. Technol. 57 (1998) 25–40.

[377] K.H. Kang, N.T. Nguyen, P.W. Seo, H. Seo, G.T. Kim, N. Kang, C.W. Lee, S.J. Han, M.C. Chung, S. Park, Slurry-phase hydrocracking of heavy oil over Mo precursors: Effect of triphenylphosphine ligands, J. Catal. 384 (2020) 106–121.

[378] V.L. Mangesh, S. Padmanabhan, P. Tamizhdurai, S. Narayanan, A. Ramesh, Combustion and emission analysis of hydrogenated waste polypropylene pyrolysis oil blended with diesel, J. Hazard. Mater. 386 (2020) 121453.

[379] J.L. Agudelo, E.J.M. Hensen, S.A. Giraldo, L.J. Hoyos, Effect of USY Zeolite Chemical Treatment with Ammonium Nitrate on Its VGO Hydrocracking Performance, Energy and Fuels. 30 (2016) 616–625.

[380] K. Sato, Y. Nishimura, K. Honna, N. Matsubayashi, H. Shimada, Role of HY zeolite mesopores in hydrocracking of heavy oils, J. Catal. 200 (2001) 288–297.

[381] G. Elordi, M. Olazar, G. Lopez, M. Amutio, M. Artetxe, R. Aguado, J. Bilbao, Catalytic pyrolysis of HDPE in continuous mode over zeolite catalysts in a conical spouted bed reactor, J. Anal. Appl. Pyrolysis. 85 (2009) 345–351.

[382] M.G. Yang, I. Nakamura, K. Fujimoto, Hydro-thermal cracking of heavy oils and its model compound, Catal. Today. 43 (1998) 273–280.

[383] G. Escalona, A. Rai, P. Betancourt, A.K. Sinha, Selective poly-aromatics saturation and ring opening during hydroprocessing of light cycle oil over sulfided Ni-Mo/SiO2-Al2O3 catalyst, Fuel. 219 (2018) 270–278.

[384] J. Weitkamp, P.A. Jacobs, J.A. Martens, Isomerization and hydrocracking of C9 through C16 n-alkanes on Pt/HZSM-5 zeolite, Appl. Catal. 8 (1983) 123–141.

[385] J. Weitkamp, Isomerization of Long-Chain n-Alkanes on a Pt/CaY Zeolite Catalyst, Ind. Eng. Chem. Prod. Res. Dev. 21 (1982) 550–558.

[386] S. Bezergianni, A. Dimitriadis, G.C. Faussone, D. Karonis, Alternative diesel from waste plastics, Energies. 10 (2017) 1–12.

[387] M. Guisnet, P. Magnoux, Organic chemistry of coke formation, Appl. Catal. A Gen. 212 (2001) 83–96.

[388] Y.S. Kim, K.S. Cho, Y.K. Lee, Structure and activity of ni2p/desilicated zeolite β catalysts for hydrocracking of pyrolysis fuel oil into benzene, toluene, and xylene, Catalysts. 10 (2020) 47.

[389] E. Epelde, J.I. Santos, P. Florian, A.T. Aguayo, A.G. Gayubo, J. Bilbao, P. Castaño, Controlling coke deactivation and cracking selectivity of MFI zeolite by H3PO4 or KOH modification, Appl. Catal. A Gen. 505 (2015) 105–115.

[390] J.C. Groen, W. Zhu, S. Brouwer, S.J. Huynink, F. Kapteijn, J.A. Moulijn, J. Pérez-Ramírez, Direct demonstration of enhanced diffusion in mesoporous ZSM-5 zeolite obtained via controlled desilication, J. Am. Chem. Soc. 129 (2007) 355–360.

[391] B. Gil, Ł. Mokrzycki, B. Sulikowski, Z. Olejniczak, S. Walas, Desilication of ZSM-5 and ZSM-12 zeolites: Impact on textural, acidic and catalytic properties, Catal. Today. 152 (2010) 24–32.

[392] J. Ding, W. Chen, W. Wang, Production and carbon emission reduction decisions for remanufacturing firms under carbon tax and take-back legislation, Comput. Ind. Eng. 143 (2020) 106419.

[393] K.A. Tarach, K. Góra-Marek, J. Martinez-Triguero, I. Melián-Cabrera, Acidity and accessibility studies of desilicated ZSM-5 zeolites in terms of their effectiveness as catalysts in acid-catalyzed cracking processes, Catal. Sci. Technol. 7 (2017) 858–873.

[394] J.C. Groen, J.A. Moulijn, J. Pérez-Ramírez, Alkaline posttreatment of MFI zeolites. From accelerated screening to scale-up, Ind. Eng. Chem. Res. 46 (2007) 4193–4201.

[395] D. Verboekend, G. Vilé, J. Pérez-Ramírez, Mesopore formation in usy and beta zeolites by base leaching: Selection criteria and optimization of pore-directing agents, Cryst. Growth Des. 12 (2012) 3123–3132.

[396] Y. Li, S. Liu, Z. Zhang, S. Xie, X. Zhu, L. Xu, Aromatization and isomerization of 1-hexene over alkali-treated HZSM-5 zeolites: Improved reaction stability, Appl. Catal. A Gen. 338 (2008) 100–113.

[397] S. Abelló, A. Bonilla, J. Pérez-Ramírez, Mesoporous ZSM-5 zeolite catalysts prepared by desilication with organic hydroxides and

comparison with NaOH leaching, Appl. Catal. A Gen. 364 (2009) 191–198.

[398] M.S. Holm, M.K. Hansen, C.H. Christensen, "One-pot" Ion-exchange and mesopore formation during desilication, Eur. J. Inorg. Chem. 2009 (2009) 1194–1198.

[399] D. Verboekend, J. Pérez-Ramírez, Desilication mechanism revisited: Highly mesoporous all-silica zeolites enabled through pore-directing agents, Chem. - A Eur. J. 17 (2011) 1137–1147.

[400] J. Peréz-Ramírez, D. Verboekend, A. Bonilla, S. Abelló, Zeolite catalysts with tunable hierarchy factor by pore-growth moderators, Adv. Funct. Mater. 19 (2009) 3972–3979.

[401] H. Sammoury, J. Toufaily, K. Cherry, T. Hamieh, Y. Pouilloux, L. Pinard, Desilication of *BEA zeolites using different alkaline media: Impact on catalytic cracking of n-hexane, Microporous Mesoporous Mater. 267 (2018) 150–163.

[402] K. Tarach, K. Góra-Marek, J. Tekla, K. Brylewska, J. Datka, K. Mlekodaj, W. Makowski, M.C. Igualada López, J. Martínez Triguero, F. Rey, Catalytic cracking performance of alkaline-treated zeolite Beta in the terms of acid sites properties and their accessibility, J. Catal. 312 (2014) 46–57.

[403] H.J. Park, H.S. Heo, J.K. Jeon, J. Kim, R. Ryoo, K.E. Jeong, Y.K. Park, Highly valuable chemicals production from catalytic upgrading of radiata pine sawdust-derived pyrolytic vapors over mesoporous MFI zeolites, Appl. Catal. B Environ. 95 (2010) 365–373.

[404] J.C. Groen, L.A.A. Peffer, J.A. Moulijn, J. Pérez-Ramírez, Mesoporosity development in ZSM-5 zeolite upon optimized desilication conditions in alkaline medium, Colloids Surfaces A Physicochem. Eng. Asp. 241 (2004) 53–58.

[405] S. Yurdakal, C. Garlisi, L. Özcan, M. Bellardita, G. Palmisano, (Photo)catalyst characterization techniques: Adsorption isotherms and BET, SEM, FTIR, UV-Vis, photoluminescence, and electrochemical characterizations, in: Heterog. Photocatal. Relationships with Heterog. Catal. Perspect., Amsterdam, 2019: pp. 87–152.

[406] S.P. Sree, J. Dendooven, P.C.M.M. Magusin, K. Thomas, J.P. Gilson, F. Taulelle, C. Detavernier, J.A. Martens, Hydroisomerization and hydrocracking activity enhancement of a hierarchical ZSM-5 zeolite catalyst via atomic layer deposition of aluminium, Catal. Sci. Technol.

6 (2016) 6177–6186.

[407] A.G. Gayubo, A. Alonso, B. Valle, A.T. Aguayo, J. Bilbao, Selective production of olefins from bioethanol on HZSM-5 zeolite catalysts treated with NaOH, Appl. Catal. B Environ. 97 (2010) 299–306.

[408] Z. Qin, B. Shen, X. Gao, F. Lin, B. Wang, C. Xu, Mesoporous y zeolite with homogeneous aluminum distribution obtained by sequential desilication-dealumination and its performance in the catalytic cracking of cumene and 1,3,5-triisopropylbenzene, J. Catal. 278 (2011) 266–275.

[409] M. Gackowski, K. Tarach, Kuterasiński, J. Podobiński, S. Jarczewski, P. Kuśtrowski, J. Datka, Hierarchical zeolites Y obtained by desilication: Porosity, acidity and catalytic properties, Microporous Mesoporous Mater. 263 (2018) 282–288.

[410] K. Wojciechowska, The influence of desilication/dealumination processes on the physicochemical properties of clinoptilolite, Clay Miner. 54 (2019) 111–119.

[411] S. Ferdov, K. Tsuchiya, N. Tsunoji, T. Sano, Comparative study between high-silica faujasites (FAU) from organic-free system and the commercial zeolite Y, Microporous Mesoporous Mater. 276 (2019) 154–159.

[412] K.P. De Jong, J. Zečević, H. Friedrich, P.E. De Jongh, M. Bulut, S. Van Donk, R. Kenmogne, A. Finiels, V. Hulea, F. Fajula, Zeolite y crystals with trimodal porosity as ideal hydrocracking catalysts, Angew. Chemie - Int. Ed. 49 (2010) 10074–10078.

[413] J. Li, X. Li, G. Zhou, W. Wang, C. Wang, S. Komarneni, Y. Wang, Catalytic fast pyrolysis of biomass with mesoporous ZSM-5 zeolites prepared by desilication with NaOH solutions, Appl. Catal. A Gen. 470 (2014) 115–122.

[414] J. V. Milato, R.J. França, A.S. Rocha, M.R.C.M. Calderari, A. Sanches Rocha, M.R.C. Marques Calderari, Catalytic co-pyrolysis of oil sludge with HDPE to obtain paraffinic products over HUSY zeolites prepared by dealumination and desilication, J. Anal. Appl. Pyrolysis. 151 (2020) 104928. https://doi.org/10.1016/j.jaap.2020.104928 (accessed September 7, 2021).

[415] M.T. Nguyen, N.T. Nguyen, J. Cho, C. Park, S. Park, J. Jung, C.W. Lee, A review on the oil-soluble dispersed catalyst for slurry-phase hydrocracking of heavy oil, J. Ind. Eng. Chem. 43 (2016) 1–12.

[416] E. Karakhanov, A. Maximov, Y. Kardasheva, M. Vinnikova, L. Kulikov, Hydrotreating of light cycle oil over supported on porous aromatic framework catalysts, Catalysts. 8 (2018) 397.

[417] J.M. Escola, J. Aguado, D.P. Serrano, L. Briones, J.L. Díaz De Tuesta, R. Calvo, E. Fernandez, Conversion of polyethylene into transportation fuels by the combination of thermal cracking and catalytic hydroreforming over Ni-supported hierarchical beta zeolite, in: Energy and Fuels, American Chemical Society, 2012: pp. 3187–3195.

[418] P. Castaño, G. Elordi, M. Ibañez, M. Olazar, J. Bilbao, Pathways of coke formation on an MFI catalyst during the cracking of waste polyolefins, Catal. Sci. Technol. 2 (2012) 504–508.

[419] C. Le Minh, R.A. Jones, I.E. Craven, T.C. Brown, Temperature-programmed oxidation of coke deposited on cracking catalysts: Combustion mechanism dependence, Energy and Fuels. 11 (1997) 463–469.

[420] I. Sierra, J. Ereña, A.T. Aguayo, M. Olazar, J. Bilbao, Deactivation kinetics for direct dimethyl ether synthesis on a CuO-ZnO-Al2O3/γ-Al2O3 Catalyst, Ind. Eng. Chem. Res. 49 (2010) 481–489.

[421] A. Ochoa, B. Aramburu, B. Valle, D.E. Resasco, J. Bilbao, A.G. Gayubo, P. Castaño, Role of oxygenates and effect of operating conditions in the deactivation of a Ni supported catalyst during the steam reforming of bio-oil, Green Chem. 19 (2017) 4315–4333.

[422] B. Valle, P. Castaño, M. Olazar, J. Bilbao, A.G. Gayubo, Deactivating species in the transformation of crude bio-oil with methanol into hydrocarbons on a HZSM-5 catalyst, J. Catal. 285 (2012) 304–314.

[423] F. Bauer, H.G. Karge, Characterization of Coke on Zeolites, in: Mol. Sieve, Sci. Technol. Charact. II., Springer, Berlin, 2007: pp. 249–364.

[424] A. Ochoa, B. Valle, D.E. Resasco, J. Bilbao, A.G. Gayubo, P. Castaño, Temperature Programmed Oxidation Coupled with In Situ Techniques Reveal the Nature and Location of Coke Deposited on a Ni/La2O3-αAl2O3 Catalyst in the Steam Reforming of Bio-oil, ChemCatChem. 10 (2018) 2311–2321.

[425] G. Elordi, M. Olazar, G. Lopez, P. Castaño, J. Bilbao, Role of pore structure in the deactivation of zeolites (HZSM-5, Hβ and HY) by coke in the pyrolysis of polyethylene in a conical spouted bed reactor, Appl. Catal. B Environ. 102 (2011) 224–231.

[426] P. Castaño, G. Elordi, M. Olazar, A.T. Aguayo, B. Pawelec, J. Bilbao,

Insights into the coke deposited on HZSM-5, Hβ and HY zeolites during the cracking of polyethylene, Appl. Catal. B Environ. 104 (2011) 91–100.

[427] P. Dufresne, A. Quesada, S. Mignard, Influence of Nitrogen Feed Content On The Performances of A Zeolite Hydrocracking Catalyst, Stud. Surf. Sci. Catal. 53 (1989) 301–315.

[428] J. Leglise, J.M. Manoli, C. Potvin, G. Djega-Mariadassou, D. Cornet, The nature of NiMo phases encaged in HY zeolites, J. Catal. 152 (1995) 275–290.

[429] R. Cid, J. Neira, J. Godoy, J.M. Palacios, A. López Agudo, Thiophene hydrodesulfurization on sulfided nickel-exchanged USY zeolites. Effect of the pH of the catalyst preparation, Appl. Catal. A, Gen. 125 (1995) 169–183.

[430] W.J.J. Welters, G. Vorbeck, H.W. Zandbergen, J.W. Dehaan, V.H.J. de beer, R.A. van santen, HDS activity and characterization of zeolite-supported nickel sulfide catalysts, J. Catal. 150 (1994) 155–169.

[431] Z. Pan, X. Xue, C. Zhang, D. Wang, Y. Xie, R. Zhang, Evaluation of process parameters on high-density polyethylene hydro-liquefaction products, J. Anal. Appl. Pyrolysis. 136 (2018) 146–152.

[432] H.K. Joo, C.W. Curtis, Effect of reaction time on the coprocessing of low-density polyethylene with coal and petroleum resid, Energy and Fuels. 11 (1997) 801–810.

[433] M. Artetxe, G. Lopez, M. Amutio, G. Elordi, J. Bilbao, M. Olazar, Cracking of high density polyethylene pyrolysis waxes on HZSM-5 catalysts of different acidity, Ind. Eng. Chem. Res. 52 (2013) 10637–10645.

[434] E. Stauffer, J. A.Dolan, R. Newman, Flammable and Combustible Liquids, in: Handb. Saf. Heal. Serv. Ind. - 4 Vol. Set, CRC Press, London, 2020: pp. 199–233.

[435] X. Zhang, H. Lei, G. Yadavalli, L. Zhu, Y. Wei, Y. Liu, Gasoline-range hydrocarbons produced from microwave-induced pyrolysis of low-density polyethylene over ZSM-5, Fuel. 144 (2015) 33–42.

[436] Z. Pan, X. Xue, C. Zhang, D. Wang, Y. Xie, R. Zhang, Production of aromatic hydrocarbons by hydro-liquefaction of high-density polyethylene (HDPE) over Ni/HZSM-5, J. Anal. Appl. Pyrolysis. 136 (2018) 208–214.

[437] W. Wang, X. Cai, H. Hou, M. Dong, Z. Li, F. Liu, Z. Liu, S. Tian, J. Long, Different Mechanisms of Coke Precursor Formation in Thermal Conversion and Deep Hydroprocessing of Vacuum Residue, Energy and Fuels. 30 (2016) 8171–8176.

[438] C. Montero, A. Ochoa, P. Castaño, J. Bilbao, A.G. Gayubo, Monitoring Ni0 and coke evolution during the deactivation of a Ni/La2O3-αAl2O3 catalyst in ethanol steam reforming in a fluidized bed, J. Catal. 331 (2015) 181–192.

[439] P. Castaño, A. Gutiérrez, M.J. Azkoiti, J. Bilbao, J.M. Arandes, Deactivation of Pt-Pd/zeolite catalysts during the hydroprocessing of LCO for the production of ultraclean fuels, in: ACS Natl. Meet. B. Abstr., 2011.

[440] S. Uçar, S. Karagöz, T. Karayildirim, J. Yanik, Conversion of polymers to fuels in a refinery stream, Polym. Degrad. Stab. 75 (2002) 161–171.

[441] I. Barbarias, M. Artetxe, G. Lopez, A. Arregi, J. Bilbao, M. Olazar, Influence of the conditions for reforming HDPE pyrolysis volatiles on the catalyst deactivation by coke, Fuel Process. Technol. 171 (2018) 100–109.

[442] N. Martín, M. Viniegra, E. Lima, G. Espinosa, Coke Characterization on Pt/Al2O3-β-Zeolite Reforming Catalysts, Ind. Eng. Chem. Res. 43 (2004) 1206–1210.

[443] D. Munir, M.R. Usman, Catalytic hydropyrolysis of a model municipal waste plastic mixture over composite USY/SBA-16 catalysts, J. Anal. Appl. Pyrolysis. 135 (2018) 44–53.

[444] W. Ding, J. Liang, L.L. Anderson, Hydrocracking and hydroisomerization of high-density polyethylene and waste plastic over zeolite and silica - Alumina-supported Ni and Ni-Mo sulfides, Energy and Fuels. 11 (1997) 1219–1223.

[445] D.P. Serrano, J. Aguado, J.M. Escola, J.M. Rodríguez, G. San Miguel, An investigation into the catalytic cracking of LDPE using Py-GC/MS, J. Anal. Appl. Pyrolysis. 74 (2005) 370–378.

[446] G. Elordi, M. Olazar, M. Artetxe, P. Castaño, J. Bilbao, Effect of the acidity of the HZSM-5 zeolite catalyst on the cracking of high density polyethylene in a conical spouted bed reactor, Appl. Catal. A Gen. 415–416 (2012) 89–95.

[447] A. Ochoa, I. Barbarias, M. Artetxe, A.G. Gayubo, M. Olazar, J. Bilbao, P. Castaño, Deactivation dynamics of a Ni supported catalyst during

the steam reforming of volatiles from waste polyethylene pyrolysis, Appl. Catal. B Environ. 209 (2017) 554–565.

[448] M. Guisnet, L. Costa, F.R. Ribeiro, Prevention of zeolite deactivation by coking, J. Mol. Catal. A Chem. 305 (2009) 69–83.

[449] A. Akah, J. Hernandez-Martinez, C. Rallan, A.A. Garforth, Enhanced feedstock recycling of post-consumer plastic waste, Chem. Eng. Trans. 43 (2015) 2395–2400.

[450] I. Morawski, J. Mosio-Mosiewski, Effects of parameters in Ni-Mo catalysed hydrocracking of vacuum residue on composition and quality of obtained products, Fuel Process. Technol. 87 (2006) 659–669.

[451] S.C. Chapra, R.P. Canale, Multidimensional unconstrained optimization, in: Numer. Methods Eng., 6th ed., McGraw-Hill, México D. F., 2010: pp. 352–353.

[452] J. Ancheyta, R. Sotelo-Boyás, J. Ancheyta-Juárez, R. Sotelo-Boyás, Estimation of kinetic constants of a five-lump model for fluid catalytic cracking process using simpler sub-models, Energy and Fuels. 14 (2000) 1226–1231.

[453] J. Ancheyta, Reactor modeling in the petroleum refining industry, in: J. Ancheyta (Ed.), Model. Simul. Catal. React. Pet. Refin., 1st ed., John Wiley & Sons., Hoboken, NJ, 2011: pp. 177–178.

[454] M. Al-Sabawi, J.A. Atias, H. De Lasa, Kinetic modeling of catalytic cracking of gas oil feedstocks: Reaction and diffusion phenomena, Ind. Eng. Chem. Res. 45 (2006) 1583–1593.

[455] G. Valavarasu, B. Sairam, Hydrocracking of vacuum gas oil: Conversion, product yields, and product quality over an industrial hydrocracking catalyst system, Pet. Sci. Technol. 31 (2013) 551–562.

[456] M. Artetxe, G. Lopez, M. Amutio, G. Elordi, J. Bilbao, M. Olazar, Light olefins from HDPE cracking in a two-step thermal and catalytic process, Chem. Eng. J. 207–208 (2012) 27–34.

[457] H. Hassanzadeh, J. Abedi, Modelling and parameter estimation of ultra-dispersed in situ catalytic upgrading experiments in a batch reactor, Fuel. 89 (2010) 2822–2828.

[458] G. Félix, J. Ancheyta, F. Trejo, Sensitivity analysis of kinetic parameters for heavy oil hydrocracking, Fuel. 241 (2019) 836–844.

CHAPTER 11

DISSEMINATION OF RESULTS

11 DISSEMINATION OF RESULTS

This PhD Thesis has led to the publication of 3 papers in international journals of renowned prestige (Table 11.1), as well as 18 contributions (mainly oral) to national and international congresses (Table 11.2). Moreover, the writing of 2 more papers as the first author is also in progress.

11.1 PUBLICATIONS

Table 11.1 Papers derived from the Thesis published in international journals.

Authors: Vela F.J., Palos R., Bilbao J., Arandes J.M., Gutierrez A.

Title: Effect of co-feeding HDPE on the product distribution in the hydrocracking of VGO

Catal. Today, 353, 197-203 (2020)

Impact factor (JCT, 2020): **6.766**

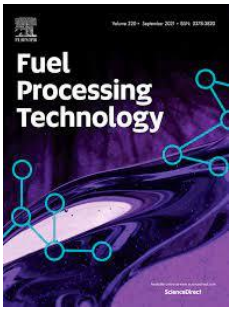

Authors: Vela F.J., Palos R., Trueba D., Bilbao J., Arandes J.M., Gutierrez A.

Title: Different approaches to convert waste polyolefins into automotive fuels via hydrocracking with a NiW/HY catalyst

Fuel Process. Technol., 220, 106891 (2021)

Impact factor (JCT, 2020): **7.033**

Authors: Palos R., Gutierrez A., Vela F.J., Olazar M., Arandes J.M., Bilbao J.

Title: Waste Refinery: The Valorization of Waste Plastics and End-of-Life Tires in Refinery Units. A Review

Energy & Fuels, 35, 3529-3557 (2021)

Impact factor (JCT, 2020): **3.605**

11.2 CONTRIBUTION TO CONGRESS

Table 11.2 Oral and poster contribution in national and international congresses.

SECAT'17 Oviedo, 26-28 junio	**Reunión de la Sociedad Española de Catálisis**, **SECAT'17**, Catálisis para un mundo más sostenible. Oviedo, España, 2017. **Oral** communication. **Title:** Efecto de la coalimentación de HDPE con VGO sobre los rendimientos y propiedades de la fracción gasolina en el craqueo catalítico en condiciones de FCC. **Authors:** E. Rodríguez, A. Ibarra, R. Palos, F.J. Vela, J. Bilbao, J.M. Arandes.
CHISA 2018 PRAGUE	**23rd International Congress of Chemical and Process Engineering (CHISA 2018)**, Prague, Czech Republic, 2018. **Oral** communication. **Title:** Effect of tire pyrolysis oil co-feeding on the product distribution of vacuum gasoil catalytic cracking. **Authors:** E. Rodríguez, F.J. Vela, A. Ibarra, J. Bilbao, J.M. Arandes
CHISA 2018 PRAGUE	**23rd International Congress of Chemical and Process Engineering (CHISA)**, Prague, Czech Republic, 2018. **Oral** communication. **Title:** Scrap tire oil (STO) and light cycle oil (LCO) blend hydrotreatment. **Authors:** R. Palos, F.J. Vela, A. Gutiérrez, J. Bilbao, J.M. Arandes.
CICAT 50 Aniversario	**XXVI Congreso Ibero-americano de Catálise (CICAT)**, Coimbra, Portugal, 2018. **Oral** communication. **Title:** Craqueo catalítico de líquido de pirolisis de neumáticos en condiciones de FCC. Análisis de catalizadores. **Authors:** E. Rodríguez, F.J. Vela, M. J. Azkoiti, J. Bilbao, J. M. Arandes.
CICAT 50 Aniversario	**XXVI Congreso Ibero-americano de Catálise (CICAT)**, Coimbra, Portugal, 2018. **Poster** communication. **Title:** Hidrodesulfuración de líquido de pirólisis de neumáticos fuera de uso (STPO): condiciones de operación y cinética. **Authors:** R. Palos, F. J. Vela, I. Hita, A. Gutiérrez, J. Bilbao, J. M. Arandes.
ANQUE-ICCE 2019 3rd International Congress of Chemical Engineering Santander, SPAIN June 19-21, 2019 "Building bridges in Chemical Engineering"	**3rd International Congress of Chemical Engineering (ICCE)**, Santander, Spain, 2019. **Oral** communication. **Title:** Valorization of a hydrotreated light cycle oil through a second hydrocracking stage over PtPd-based catalysts. **Authors:** D. Trueba, I. Hita, R. Palos, F. J. Vela, A. Gutiérrez, J. M. Arandes.

Table 11.2 (Continuation).

	**12th European Congress of Chemical Engineering (ECCE),** Florence, Italy, 2019. **Oral** communication. **Title:** Enhancement of hydrocracking activity of discarded fcc catalyst by means of acidity modification. **Authors:** A. Gutierrez, I Hita, R. Palos, F. J. Vela, J. M. Arandes.
	**12th European Congress of Chemical Engineering (ECCE),** Florence, Italy, 2019. **Poster** communication. **Title:** Zeolite-supported FEMOP catalysts for the hydrodeoxygenation of a raw black poplar bio-oil towards hydrocarbons. **Authors:** I. Hita, T. Cordero-Lanzac, G. Bonura, C. Cannilla, F. J. Vela, J. M. Arandes, F. Frusteri, J. Bilbao.
	**International Symposium of Advanced Hydrocracking Oil Fraction (ISAHOF)**, Mazatlan, Mexico, 2019. **Oral** communication. **Title:** Effect of the co-feeding of HDPE on the product distribution in the hydrocracking of VGO. **Authors:** F. J. Vela, R. Palos, A. Gutiérrez, J. M. Arandes.
	**International Symposium on Feedstock Recycling of Polymeric Materials (ISFRPM)**, Online, 2019. **Oral** communication. **Title:** Yield and nature of the products obtained in pyrolysis of waste plastic. **Authors:** R. Palos, F. J. Vela, A. Gutiérrez, J. Bilbao, J. M. Arandes.
	**Reunión de la Sociedad Española de Catálisis**, (**SECAT)**, Catálisis para un mundo más sostenible. Cordoba, España, 2019. **Oral** communication. **Title:** Producción de combustibles mediante el hidrocraqueo de ceras de pirólisis. **Authors:** F. J. Vela-Diaz, R. Palos, A. Gutiérrez, I. Hita, J. M. Arandes.
	**XXIV International Congress of Chemical and Process Engineering (CHEMREACTOR-24)**, Online, 2021. **Oral** communication. **Title:** An innovative kinetic modeling of the hydrocraking of a HDPE/VGO blend. **Authors:** F.J. Vela, D. Trueba, G. Lezcano, R. Palos, J.M. Arandes, A. Gutiérrez.

Table 11.2 (Continuation).

CONGRESO IBEROAMERICANO DE CATÁLISIS 2020	**XXVII Congreso Iberoamericano de Catálisis (CICAT)**, Online, 2020. **Oral** communication. **Title:** Valorización conjunta de residuos plásticos, su aceite de pirólisis y gasóleo de vacío mediante hidrocraqueo. **Authors:** F. J. Vela, R. Palos, D. Trueba, M. J. Azkoiti, J. M. Arandes, A. Gutiérrez.
CONGRESO IBEROAMERICANO DE CATÁLISIS 2020	**XXVII Congreso Iberoamericano de Catálisis (CICAT)**, Online, 2020. **Oral** communication. **Title:** Optimización de la configuración del lecho en la hidrogenólisis de glicerol en fase gas. **Authors:** R. Palos, F. J. Vela, D. Trueba, J. M. Arandes, A. Gutiérrez.
STS HydroCat 2020	**IV Scientific-Technological Symposium of Catalytic Hydroprocessing in Oil Refining (STS-HydroCat),** Online, 2021. **Oral** communication. Title: Fuels obtained from hydrocracking of different blends of VGO and polyolefinic wastes. Authors: Francisco J. Vela, David Trueba, Roberto Palos, José M. Arandes, Alazne Gutiérrez.
CAMURE-11 21-24 March, 2021 ISMR-10	**11th International Symposium in Multiphase Reactors (ISMR),** Online, 2021. **Oral** communication. **Title:** Avoiding over-cracking reactions in hydrocracking processes by means of desilication treatment of zeolites. **Authors:** David Trueba, Roberto Palos, Juan Rafael García, Francisco J. Vela, Javier Ereña, Alazne Gutiérrez.
SECAT 2021	**Reunión de la Sociedad Española de Catálisis**, (**SECAT)**, Catálisis para un mundo más sostenible. Valencia, España, 2021. **Oral** communication. **Title:** Assessing the production of fuels in the hydrocracking of polyolefins blended with VGO. **Authors:** F. J. Vela, S. Rodríguez, D. Trueba, R. Palos, A. Gutiérrez, J. M. Arandes.
CHISA 2021 VIRTUALLY	**24rd International Congress of Chemical and Process Engineering (CHISA)**, Online, 2018. **Oral** communication. **Title:** Tuning the operating conditions in the hydrocracking of a blend of HDPE and VGO to promote the formation of automotive-fuel like hydrocarbons. **Authors:** F.J. Vela, G. Lezcano, D. Trueba, R. Palos, M.J. Azkoiti, A. Gutiérrez.